Mechanisms of fibrous filtration

To Pat

MECHANISMS OF FIBROUS FILTRATION

by

J.I.T. STENHOUSE

Submitted for the degree of Doctor
of Philosophy of Loughborough University
of Technology

MARCH 1973

Department of Chemical Engineering
Director of research: Prof. D.C. Freshwater

SUMMARY

This thesis is concerned with the removal of particulate material from gases using fibrous filters. The work is described under three headings:-

(a) The Collision Efficiency : The particle fibre collision efficiency is calculated by computing trajectories in the Davies and Kuwabara flow fields. Electrostatic and gravitational field forces are taken into account. The influence of fibre Knudsen number and Reynolds number on inertial interception is predicted.

A model is described which takes into account a log normal distribution of fibre spacing in a filter. It is used to predict the pressure drop across a random fibre mat and its mean efficiency of inertial interception both of which are a factor of two or three less than predicted by the simple Kuwabara model.

(b) Particle Retention Mechanisms : It is shown that bounce is the only significant mechanism responsible for particle non-adhesion in fibrous filters. An equilibrium model is used to predict the critical particle size above which adhesion fails.

The behaviour of filters in the low adhesion region is examined by measuring the collection efficiency of model filters using narrow sized fractions of dust. The efficiency

is a decreasing function of particle size and velocity, trends which agree with the equilibrium model.

(c) Non-stationary Filtration : The behaviour of filters under load is examined experimentally. The efficiency may either increase or decrease initially with loading, the characteristics depending on the same factors which influence the single fibre efficiency.

Finally recommendations are made for future work in the field.

CONTENTS

INTRODUCTION

Fibrous filtration is one of several techniques for removing fine particles (solid or liquid) from a gas stream in which they are suspended. Among the most important applications of the technique are the removal of particles in the respiratory size range (0.1 - 5 μm diameter) using face masks and gas masks, and in the maintenance of clean rooms. Larger particles ($>$ 2-3 μm) must be removed from engine intakes because they can cause mechanical damage.

The capture of such particles by fibrous filters has been the subject of a large number of theoretical and experimental studies which have been well reviewed by Davies (1). It is normal to consider the behaviour of particles with respect to a single ideal fibre i.e. infinite cylinder normal to flow, within the depth of a filter and to relate this to the overall behaviour of the filter using an expression such as that developed by Wong and Johnstone (2):

$$\eta = 1 - \exp\left(\frac{-4\alpha L \eta_s}{(1-\alpha)\pi d_f}\right)$$

where η represents the particle retention efficiency of the filter. η_s is the single fibre efficiency which is the ratio of the volume of air cleaned by the fibre to the fibre swept volume.

There are four principal mechanisms which cause particles to collide with fibres of which the first two are self explanatory. These are Brownian diffusion, electrostatic attraction, interception or inertia. Interception occurs when a massless particle touches a fibre, which is placed normal to the direction of flow, purely because of its size. The inertia of a particle may cause it to cut across the fluid streamlines and impinge on a fibre.

In the vast amount of work in the field it has generally been assumed that once a particle touches a fibre it will adhere

to its surface. Whilst this is undoubtedly true in the case of particles which have been collected by one of the first two mechanisms mentioned above it is certainly not always the case with particles which have been collected by one of the second two mechanisms. Thus a better way of expressing filter efficiency would be

$$\eta_s = \eta_c \cdot \eta_A$$

where η_s is the single fibre efficiency, η_c is the collision efficiency and η_A is the retention efficiency. The characteristics of η_c , η_A and hence η_s are shown diagramatically below.

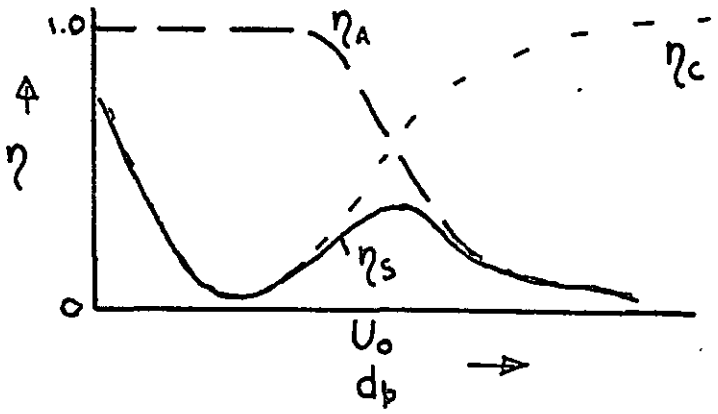

Chapter 1 of this thesis is concerned with the collision efficiency (η_c). A cellular model of the flow field is applied to describe theoretically the efficiency due to a number of mechanisms both indvidually and in combination. A theoretical model which takes filter structure into account is described.

In Chapter 2 the mechanisms which control the retention efficiency are described, a model is developed which is based on these mechanisms and experiments on the low adhesion regime are described.

The behaviour of filters under load is described in Chapter 3. The behaviour of filters in the low adhesion regime is explored experimentally. The results are shown and discussed.

Chapter 4 contains recommendations for future work.

NOMENCLATURE

A	Constant in flow equations	
A_1	Constant (equation 1.8)	
A_c	Total area of contact	m^2
A_H	Hamaker van der Waals constant	J
A_i	Face area of filter associated with packing density α_i	m^2
A_o	Total face area of filter	m^2
B	Constant in flow equations	
B_1	Constant (equation 1.8)	
C	Constant in flow equations	
C_D	Particle drag coefficient	
C_M	Cunningham slip correction factor	
D	Constant in flow equations	
D_B	Diffusion coefficient	$m^2 s^{-1}$
E	Young's modulus of elasticity	Nm^{-2}
$\overset{o}{E}_a$	Energy of adhesion between undeformed particle and half space	J
E_{ad}	Additional adhesion energy due to deformation	J
$E_{adhesion}$	Adhesion energy between deformed particle and half space	J
E_{ki}	Kinetic energy of particle at impact	J
F	Attraction force	N
$\overset{o}{F}$	Force of adhesion between undeformed particle and half space	N
F^*	Dimensionless drag (equation 1.)	
$F_{adhesion}$	Force of adhesion between deformed particle and half space	N
$\overline{F}_{r,p}$	Radial or planar field force	N
H	Coefficient, shadow effect (equation 1.39)	

$H(t)$	Hardness	
I	Parameter (equation 1.26)	
J	Parameter in flow equations	
K	Bessel function	
L	Filter depth	m
$\underline{L}$	Lift force	N
L^1	Dimensionless lift force, table 1.4	
N	Ratio of cell to fibre diameters	
N_{Kn}	Knudsen number, λ/r_f	
N_p	Sedimentation parameter, $\rho_p d_p^2 g/18\mu U_o$	
N_{pe}	Peclet number, $U_o d_f/D_B$	
N_R	Interception parameter, $\frac{dp}{df}$	
N_{Re}	Fibre Reynolds number, $\frac{\rho U_o d_f}{\mu}$	
N_{St}	Stokes number or inertia parameter, $\frac{\rho_p U_o d_p^2}{9\mu d_f}$	
P	Filter penetration $(1 - \eta)$	
P_o	Filter penetration at zero dust load	
P^-	Attraction force per unit adhesion area	Nm^{-2}
P_M	Number of grids in a model filter	
Q	Charge on fibre per unit length	Coulomb m^{-1}
R	Particle radius of curvature at contact	m
T	Filtration time	s
U	Contact potential	$J\ s^{-1}$
U^1	Dimensionless velocity, u/U_o	
U_o	Velocity of filtration (interstitial velocity)	ms^{-1}
$\underline{U}_{rel}$	Relative velocity between particle and fluid	ms^{-1}
V	Filter volume	m^3
V^1	Dimensionless velocity, v/U_o	
$V(\alpha)$	Volume distribution of packing densities	
W	Parameter (equation 1.35), x_p/x_u	
X^1	Dimensionless x co-ordinate, x/r_f	

X_p	Measured resistivity of filter (equation 1.32)	
X_T	Predicted resistivity of filter	
$X_u = X_T$	For uniform packing density	
Y^1	Dimensionless y co-ordinate, y/r_f	
Y_i	Parameter, equation 1.31, A_i/A_o	
a^1	Effective area of unit deposit, equation 3.1	m^{-1}
c	Aerosol concentration	
c_o	Initial aerosol concentration	
c_1	Coefficient, equation 3.2	
c^1	Relative concentration, equation 1.19, c/c_o	
d_c	Cell diameter (Happel-Kuwabara flow model)	m
d_f	Fibre diameter	m
d_p	Particle diameter	m
$\bar{d}_p$	Mass median particle diameter	m
$\bar{d}_e$	Equivalent fibre diameter	m
d_{pcrit}	Critical particle diameter above which adhesion fails	m
d_i	Distance between fibres in model filter	m
e	Coefficient of restitution	
e_i	Electronic charge, esn (1.602×10^{-19}C)	
f^1	Parameter, equation 2.23	
f_c	Maximum normal stress on contact	Nm^{-2}
f_p	Planar field force	N
$f_p{}^1$	Dimensionless planar field force	
f_r	Radial field force	N
$f_r{}^1$	Dimensionless field force	
g	Gravitational acceleration (9.81 ms^{-2})	ms^{-2}
g_1	Coefficient, equation 2.2	

h	Separation distance	m
k	Constants or coefficients in various equations	
$\bar{k}$	Coefficients, equations 3.7 and 3.8	
l	Distance between charge centres	m
l_1	Distance between particle and substrate	m
m	Mass of particle	Kgm
n	Number of basic charges	
p	Gas pressure	Nm^{-2}
Δp	Pressure drop across filter	Nm^{-2}
Δp_o	Initial pressure drop across filter	Nm^{-2}
q	Particle charge	C
r	Cylindrical polar co-ordinate	m
r^1	Dimensionless radial position, r/r_f	
r_1	Radius of curvature of meniscus	m
r_c	Radius of contact area	m
t	Time	s
t_c	Time of contact	s
u	Gas velocity (x resolute)	ms^{-1}
u_g	Particle terminal velocity	ms^{-1}
u_i	Particle impact velocity	ms^{-1}
u_p	Particle velocity	ms^{-1}
u_{pr}	Particle impact velocity normal to fibre surface	ms^{-1}
u^1_p	u_{pr}/U_o	
$u^1_{p_o}$	$\left(\frac{u_{pr}}{U_o}\right)_{y_o=0}$	
$u^1_{p_{50}}$	$\left(\frac{u_{pr}}{U_o}\right)\left(\frac{y_o}{\eta_c}\right)=0.5$	
u_{pi}	Particle impact velocity	ms^{-1}
u^1_{pi}	u_{pi}/U_o	
$u^1_{pi_{50}}$	$\left(\frac{u_{pi}}{U_o}\right)\left(\frac{y_o}{\eta_c}\right)=0.5$	

v	Gas velocity (y resolute)	ms^{-1}
v_r,	Gas velocity (polar co-ordinates)	ms^{-1}
x_i	Weight fraction of the i th component in a multicomponent filter	
x^*_i	x_i correction for "shadow" effect	
y_o	Y^1 co-ordinate of trajectory starting point	
z_o	Coefficient, equation 2.2	
α	Filter packing density (volume fibres/volume total filter)	
α_1	Clogging parameter, equation 3.5	
γ	Parameter, equation 1.36	
γ_1	Eule. constant	
γ_2	Particle collection efficiency, equation 3.1	
γ_3	Clogging parameter, equation 3.5	
δ	Dirac delta function	
δ_1	Thickness of space charge layer	m
ε_a	Adhesion energy per unit contact area	Jm^{-2}
ε_o	Permittivity of free space (8.85×10^{-12})	Farrads m^{-1}
ε_1	Dielectric constant of particle	
ε_2	Dielectric constant of fibre	
ξ, ξ', ξ''	Packing functions in flow equations	
η	Overall filter efficiency	
η_A	Single fibre adhesion efficiency	
η_c	Single fibre collision efficiency	
η_D	Single fibre collision efficiency, diffusion mechanism	
η_I	Single fibre collision efficiency, inertia mechanism.	
η_P	Single fibre collision efficiency, sedimentation mechanism	
η_R	Single fibre collision efficiency, interception mechanism	

η_{Qq}	Single fibre collision efficiency, electrostatic mechanism Where Q is the particle charge and q is the fibre charge.	
$\eta\_$	Single fibre collision efficiency, combined mechanisms	
η_S	Single fibre efficiency ($\eta_c \cdot \eta_A$)	
η_{Si}	Single fibre efficiency at zero loading - determined by extrapolation	
η_{DR}	Parameter, equation 1.30	
$\bar{\eta}$	Average single fibre efficiency (equation 1.51)	
θ	Cylindrical polar co-ordinate	
K	Velocity gradient	s^{-1}
λ	Mean free path of gas molecules	m
χ	Volume collection efficiency for a filter, equation 3.2	
ρ	Density of gas	Kgm m^{-3}
ρ_p	Density of particle	Kgm m^{-3}
σ	Surface tension	Jm^{-2}
σ_g	Geometric standard deviation of cell, or pore sizes	
σ_s	Particle deposite within a filter (volume particles/ volume filter)	
σ_c	Critical deposite within the filter at maximum load	
$\sigma_{m,M}$	Constants, equation 3.10	
τ	Dimensionless time,	
$\Delta\tau$	Dimensionless time interval used in trajectory calculations	
ϕ	Velocity potential	
χ	Vorticity	
ψ	Stream function	
$h\omega$	Lifschitz van der Waals constant	J

CHAPTER 1

The Collision Efficiency

1. Literature review

1.1 Flow field

1.1.1 Isolated cylinder

1.1.2 Fibre interference

1.2 Collision mechanisms

1.2.1 Brownian diffusion

1.2.2 Electrostatic attraction

1.2.3 Inertial interception

1.2.4 Sedimentation

1.2.5 Filtration in rarefied systems

1.2.6 Combination of mechanisms

1.3 Filter configuration

Summary

2. Application of cell model

2.1 Trajectory calculations

2.2 Inertial interception

2.3 Radial field forces

2.4 Planar field forces

2.5 Fibre Knudsen number

2.6 Generalisation

2.7 Distribution of fibre spacing

2.8 Filter resistance

2.9 Discussion and conclusions

CHAPTER I

THE COLLISION EFFICIENCY

The literature on this subject has been very well reviewed by Pich (3), Harrop (4) and Davies (1) so it will only be briefly described here. The present work which is concerned with the theoretical predictions of collision efficiencies using the cellular model of the flow field is described in section 2. A model in which the distribution of fibre spacing is taken into account is also described.

1.1 Literature Review

1.1.1 Flow Field

A pre-requisite of any particle-fibre collision theory is a description of the fluid flow field within a filter. The problem is to describe the flow field in the proximity of a circular fibre which is placed normal to the direction of flow. The true flow field within a filter is extremely complex due to random orientation of the fibres and defies analytical description. Consequently a mathematical model must be used. The simplest model is that of an isolated cylinder in an infinite medium. Using this type of model the influence of fibre Reynolds number can be taken into account but the effect of neighbouring fibres is ignored. The model has application in the case of relatively

open filters which are operated with high face velocities and in which the fibre Reynolds number may reach 10 or higher.

With compact filters which are operated with a low face velocity and low Reynolds number (inertial interception may be the main capture mechanism with a fibre Reynolds number as low as 0.01) the effect of fibre interference in the filter is more significant than that of fibre Reynolds number. Models of the field have been developed which describe the effect of filter packing density (ratio of fibre to filter volume) under conditions of zero fluid inertia. Unfortunately no model has been published which describes the combined effect of packing density and Reynolds number.

Isolated Cylinder

The fluid behaviour will satisfy the Navier-Stokes equation and the equation of continuity.

$$\underline{u} \cdot \nabla \underline{u} = -\frac{\nabla p}{\rho} + \nu \nabla^2 \underline{u} \qquad 1.1$$

$$\nabla \cdot \underline{u} = 0 \qquad 1.2$$

Oseen (5) approximated the non-linear term by:-

$$U_o \cdot \nabla \underline{u} = -\frac{\nabla p}{\rho} + \nu \nabla^2 \underline{u} \qquad 1.3$$

If we put $k = U_o / 2\nu$

equations 1.2 and 1.3 are satisfied by

$$u = -\frac{\partial \varphi}{\partial x} + \frac{1}{2k}\frac{\partial \chi}{\partial x} - \chi$$

$$v = -\frac{\partial \varphi}{\partial y} + \frac{1}{2k}\frac{\partial \chi}{\partial y} \qquad 1.4\text{-}5$$

Provided that

$$\left(\nabla^2 - 2k\frac{\partial}{\partial x}\right)\chi = 0 \qquad 1.6$$

and

$$\nabla^2 \varphi = 0 \qquad 1.7$$

where χ and φ are the vorticity and velocity potential.

General solutions in cylindrical polar co-ordinates to equations 1.6 and 1.7 are

$$\chi = e^{kx}\sum B_n \frac{\partial^n K_0(kr)}{\partial x^n} \; ; \; \varphi = \sum A_m \frac{\partial^m \ln r}{\partial x^m} \qquad 1.8$$

where A and B are constants and Ko is a Bessel function of the second kind.

The boundary conditions are those of undisturbed fluid at infinity and zero slip at the cylinder surface. The accuracy of the solution will depend on the number of terms taken in 1.8.

Lamb (6) in 1932 obtained a solution by using an approximation for the first term in χ and the first two terms in φ. After further simplification the field normally used and referred to as that of Lamb is obtained. Unfortunately this solution is only valid close to the cylinder surface.

Tomotika and Aoi (7) used the first term completely in χ and the first three terms in φ. Davies (8) used again the first term in χ and the first 5 terms in φ. Claiming that Davies' solution was incompatable, Natanson (9) used the first two terms in χ and the first three terms in φ.

Because of the limitations imposed by using the Oseen approximation any solution to equations 1.2 and 1.3 will become less valid as the cylinder Reynolds number is increased. 0.5 is generally taken as the maximum value at which such theories can be used.

To examine the fields proposed by the various authors, the velocity resolutes along the x and y axis (taking the cylinder centre as the origin) perpendicular and normal to the direction of flow, were computed. The results for the Lamb field, and those of Davies and Natanson are shown in figs 1.1 and 1.2. It will be seen that in front of the cylinder the Davies and Natanson fields are almost identical (in fact they differ only in the fourth decimal place at a Reynolds number of 0.2) whilst the approximate field of Lamb is widely in error, the velocity tending to infinity with distance upstream. It can be seen that the velocity profile predicted by Davies becomes somewhat eratic at large distances downstream.

Computation of the velocity profile close to the cylinder shows that the Davies and Natanson fields are again indistinguishable at low Reynolds number, but a slight discrepency begins to

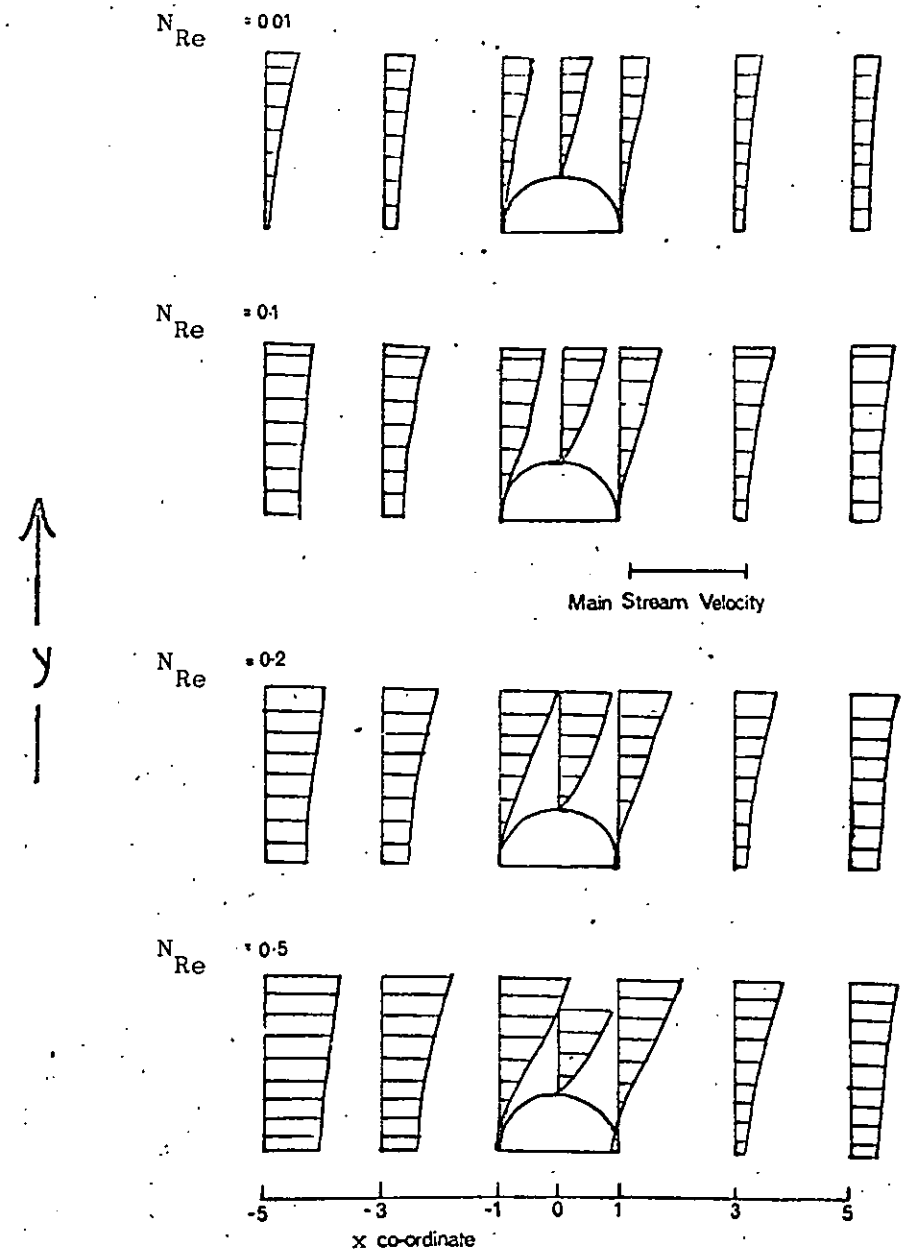

Values of x component of velocity in Davies field.

Fig. 1.1

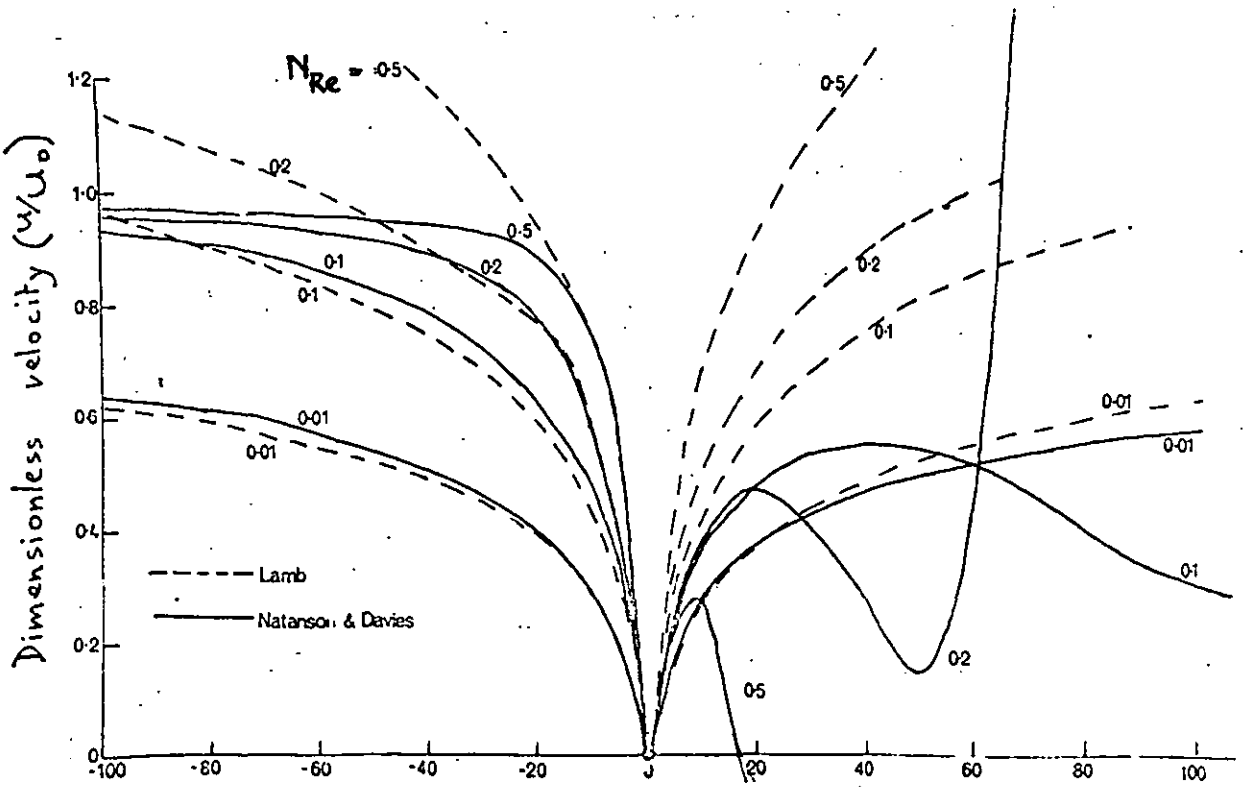

Dimensionless x component of velocity along X axis.

Fig. 1.2

show itself at higher values of N_{Re}. An interesting feature is that both theories predict a wake behind the cylinder at relatively low values of N_{Re}, certainly those encountered in fibrous filtration.

The solutions of Davies and Natanson are probably as accurate as can be obtained to equations 1.2 and 1.3. Any further improvement must come, by taking the non-linear terms in the Navier-Stokes equation into account at higher Reynolds numbers. The Oseen equation is a good approximation to the flow at distances from the cylinder where $\underline{u}$ is close to U_o and at low values of N_{Re} where the inertia terms are not too important. However, as N_{Re} is increased the Oseen approximation becomes less accurate close to the cylinder, where a Stokes solution would be more appropriate.

The technique of matched asymptotic expansions (10) in which both an "inner" and "outer" solution to the flow equations is obtained, allows the non-linear terms in the Navier-Stokes equations to be taken into account. Kaplun (11) has applied the method to the present problem to obtain a solution which is valid at higher Reynolds numbers than those described above. His solution is not, however, so readily amenable to calculation.

Thom (12) obtained a numerical solution for the flow round a cylinder with a Reynolds number of 10.

1.2 Fibre Interference

Five different approaches have been made to bring the

influence of fibre interference into account.

(a) Kovasznay (13) considered the flow close behind a two dimensional grid. Although his model predicts the effect of filter packing density on wake formation and the laws of decay of individual wakes it is of limited use in filtration and can only be used to obtain an estimate of the packing effect.

(b) Tamada and Fujikawa (14) and Miyagi (15) considered the Oseen flow past an infinite row of cylinders. They predicted the drag directly proportional to the velocity of flow as is found in practice. The isolated cylinder theories do not predict this dependence because of the discrepency in boundary conditions. The solutions to this model take the form of expansion series and are consequently cumbersome and difficult to apply.

(c) Happel (16) and Kuwabara (17) published a cellular model to describe the flow through banks of parallel cylinders. A filter may be considered to consist of a number of cells, each cell comprising a single fibre surrounded by a concentric envelope of fluid. The diameter of the cell is determined by the proximity of neighbouring fibres and is thus related to the filter packing density. The flow pattern within the cell is related to the cell diameter. Thus a model may be set up which in its fundamental concept takes account of the effect of neighbouring fibres. However, each cell may be considered as an independent entity and

the field inside may be considered in isolation from the rest of the filter.

The physical basis for the model as suggested by Kuwabara is to consider an assemblage of cylinders moving from right to left in a fluid; the fluid will be displaced above and below the cylinder as shown in Fig.1.3. Due to the opposite directions of neighbouring zones of fluid displacement the boundaries indicated will approximate to conditions of zero shear stress.

From this physical model both Happel and Kuwabara postulated the mathematical model shown in Fig.1.4. The cylinder, moving from right to left, is surrounded by a concentric cell of fluid, such that the ratio of fluid to solid in the cell is the same as the relative volume in the whole assemblage of cylinders. Thus the cell diameter is a measure of the packing in the system.

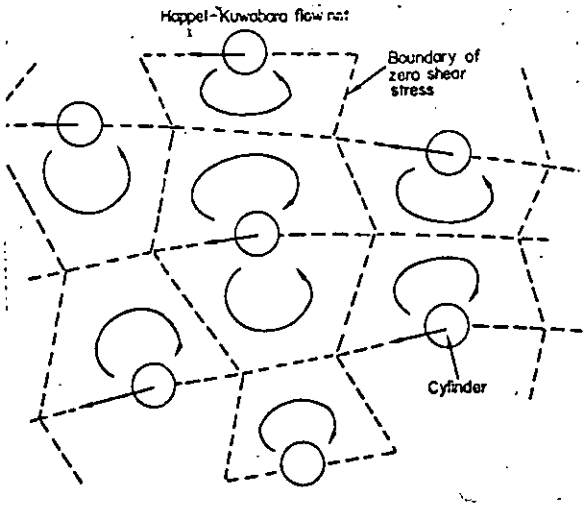

Cellular flow net.
Fig.1.3

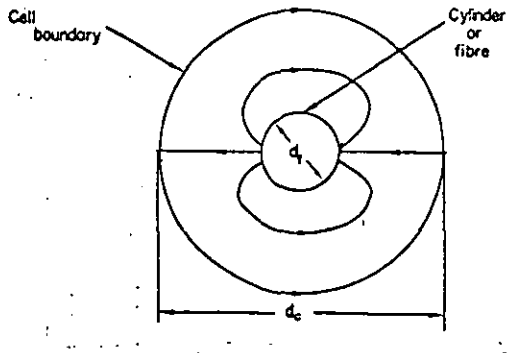

Mathematical model
Fig. 1.4

A general solution of the creeping motion equation in cylindrical polar co-ordinates (r, θ) is given by both Happel and

Kuwabara as

$$\psi = \left(\frac{A}{r} + Br + Cr\ln r + Dr^3\right)\sin\theta \qquad 1.10$$

where the polar velocities (u_r, u_θ) are:

$$u_r = \frac{1}{r}\frac{\partial\psi}{\partial\theta} \qquad u_\theta = -\frac{\partial\psi}{\partial r} \qquad 1.11$$

As the inertia forces in the fluid are assumed negligible and omitted from the Navier-Stokes equation to obtain the creeping motion equation, the model suffers from the disadvantage that it is only applicable at low Reynolds numbers.

To solve the general solution for the constants A, B, C and D, Kuwabara postulated four boundary conditions in a reference system in which the cylinders are at rest and the cell moving from left to right with mainstream velocity Uo.

$$\begin{aligned} u_\theta = u_r = 0 \quad &\text{for} \quad r = d_f/2 \\ u_r = U_o\cos\theta \quad &\text{for} \quad r = d_c/2 \\ \text{zero vorticity} \quad &\text{for} \quad r = d_c/2 \end{aligned} \qquad 1.12$$

The boundary conditions suggested by Happel are

$$\left.\begin{aligned} u_r &= -U_o\cos\theta \\ u_\theta &= U_o\sin\theta \end{aligned}\right\} \text{for} \quad r = d_f/2$$

$$u_r = 0 \qquad \text{for} \quad r = d_c/2 \qquad 1.13$$

$$\text{zero shear stress} \qquad \text{for} \quad r = d_c/2$$

In this case the cell is stationary and the cylinder is moving across its diameter from right to left with the mainstream velocity Uo.

Using the Happel boundary conditions the resolutes of velocity in the x and y directions are found when the cylinder is moving. The fluid velocity resolutes, with the cylinder stationary, are obtained by superimposing the main stream velocity on the resolutes calculated.

Expressions for A, B, C, D, u and v are given in Table 1.1.

The ratio of cell to cylinder radius (N) is related to α, the volume fraction of fibres, or packing density, of the filter mat. As α is increased N decreases and the extent to which the streamlines diverge is accentuated this effect being similar to that caused by an increase in Reynolds number. For a real filter the relationship between α and N is complex but for an array of equidistant parallel cylinders the packing density is given by:

$$\alpha = \pi / 4 N^2 \qquad 1.14$$

TABLE 1.1

Flow Field Solutions

Happel

$$A = N^4 d_f^3 U_0/4J$$

$$B = \{[1 - 2\ln(d_f/2) - N^4(1 + 2\ln(d_f/2))]U_0/J\} - U_0$$

$$C = [2(N^4+1)]\,U_0/J$$

$$D = -4U_0/Jd_f^2$$

where $J = 1 + 2\ln N - N^4(1 - 2\ln N)$

$$u = \frac{A}{r^2}\left(1 - \frac{2y^2}{r^2}\right) + B + C\left(\frac{y^2}{r^2} + \ln r\right) + Dr^2\left(\frac{2y^2}{r^2} + 1\right) + U_0$$

$$v = \left(\frac{xy}{r^2}\right)\left(\frac{2A}{r^2} - C - 2Dr^2\right)$$

where $r^2 = x^2 + y^2$

Kuwabara

$$u = \frac{A}{r^2}\left(1 - \frac{2y^2}{r^2}\right) + B + c\left(\frac{y^2}{r^2} + \ln r\right) + Dr^2\left(\frac{2y^2}{r^2} + 1\right.$$

$$v = \left(\frac{xy}{r^2}\right)\left(\frac{2A}{r^2} - c - 2Dr^2\right)$$

Where $r^2 = x^2 + y^2$

$A = (1 - 2N^2)r_f^2 U_0/J$

$B = (4N^2 \ln r_f + 2N^2 - 2)U_0/J$

$C = -4N^2 U_0/J$

$D = U_0/Jr_f^2$

$J = 1/N^2 + 3N^2 - 4 - 4N^2 \ln N.$

Solutions for the cellular flow field.

The flow lines of the two models practically coincide but the resistance predicted by the Kuwabara model is greater than that of Happel due to energy dissipation at the outer fluid envelope. Kirsch and Fuches (18) showed that the Kuwabara model was the more realistic of the two in predicting the flow through a regular array of cylinders in an hydraulic analogue. In their work α was defined as $1/N^2$ and not $\pi/4N^2$ as above. It is likely that $1/N^2$ will be closer to the truth with real filters of random array or with closely packed banks of cylinders, but $\pi/4N^2$ is a better approximation for model grid filters, which are widely spaced grids (see fig. 2.39).

The cellular model has been extended by Masliyah and Epstein (19) to a study of the behaviour of banks of elliptical cylinders.

(d) Brinkman (20) proposed that Darcy's law be incorporated in the equation of creeping motion to describe the flow field in

a sedimenting system:

$$\frac{\partial \underline{u}}{k_1} = -\frac{\nabla p}{\rho} + \nu \nabla^2 \underline{u}$$

where k_1 is related to the concentration (it is in face the permeability). This equation was recently solved by Spielman and Goren (21) to describe the influence of packing density in a filter. The essence of the model is that a body damping force which is proportional to the velocity and related to the permeability is introduced. Hence the packing effect is introduced without the often embarassing presence of an outer cell boundary. For the same value of α the flow lines are less tortuous and the resistance is less than in the cell model.

The general solution for the field is

$$\psi = U_o \sin\theta \left[-\frac{A k_1}{\mu U_o r} + \frac{B k_1 r}{\mu U_o} + C K_1 (k_1^{-1/2} r) \right]$$

1.16

where A $$\frac{\mu U_o r_f^2}{k_1} \left[1 + \frac{2 K_1 (k_1^{-1/2} r_f)}{k_1^{-1/2} r_f K_o (k_1^{-1/2} r_f)} \right]$$

B $$k_1 / \mu U_o$$

C $$-2 / k_1^{-1/2} K_o (k_1^{-1/2} r_f)$$

where K_o and K_1 are Bessel functions of zero and first order.

(e) Hasimoto (22) considered the Stokes flow through a

square array of cylinders. He used a point force technique so that his solution is applicable only in very dilute systems. He obtained a periodic solution to the following expression

$$\underline{F} \sum_{n_1} \sum_{n_2} \delta(r - r_n) = -\frac{\nabla p}{\rho} + \nu \nabla^2 \underline{u} \qquad 1.17$$

where δ is the Dirac delta function.

Simplified expressions which are valid close to the fibre surface are available for a number of flow fields. These may be summarised by:-

$$\psi = \frac{r_f \, U_o \sin\theta}{2\xi} \left\{ \frac{r_f}{r} - \frac{r}{r_f} + 2 \frac{r}{r_f} \ln\left(\frac{r}{r_f}\right) \right\} \qquad 1.18$$

Some expressions for ξ are given in table 1.2. The similarity between the influence of N_{Re} and α in these solutions is worthy of note.

TABLE 1.2

Expressions for ξ in equation 1.18

Field	ξ	ξ for very low α
Lamb	$2 - \ln N_{Re}$	
Happel	$-\frac{1}{2}\ln\alpha - \frac{1}{2} + \frac{\alpha^2}{2(1+\alpha^2)}$	$-\frac{1}{2}\ln\alpha - 1/2$
Kuwabara	$-\frac{1}{2}\ln\alpha - \frac{3}{4} + \alpha - \frac{\alpha^2}{4}$	$-\frac{1}{2}\ln\alpha - 3/4$
Spielman and Goren	$K_o(k_1^{1/2} r_f) / k_1^{1/2} r_f K_1(k_1^{1/2} r_f)$	$-\ln\left(\frac{1}{2} k_1^{1/2} r_f\right) - 0.5772$

The slip flow boundary condition has been applied to

most of the models described above (3,21) to extend their use to low Knudsen number systems.

1.1.2 Collision Mechanisms

Brownian Diffusion

Molecular bombardment causes random movement of small particles in a gas stream. If the stream is brought into close proximity of a solid surface a fraction of the particles will be deposited. Clearly the efficiency of deposition by this mechanism will be increased by an increase in the degree of Brownian motion (e.g. by a reduction in particle size) and by an increase in gas residence time close to the solid surface.

The behaviour of a diffusing aerosol is described in dimensionless form by

$$\frac{\partial c'}{\partial \tau} + \underline{u} \nabla c' = \frac{2}{N_{Pe}} \nabla^2 c' \qquad 1.19$$

where $c' = \frac{c}{c_o}$; $\tau = \frac{t U_o}{r_f}$

$$N_{Pe} = \frac{d_f U_o}{D_B}$$ Peclet No.

The diffusion coefficient, D_B , can be found from the Einstein (23) or Langmuir (24) equations. To determine the efficiency of diffusional deposition (η_D) it is necessary to solve 1.19 in conjunction with one of the flow fields. Obviously η_D will be strongly related to N_{Pe}.

Several methods of solution have been used. Langmuir (24) calculated the amount of deposition from a stagnant gas in time t: he then compared this with the residence time of gas close to the cylinder using the Lamb flow field. A more rigorous approach was applied by Natanson (25) using the same field. This technique has now been applied using the cellular model (26) and the Spielman and Goren field (21). The last three expressions are summarised by

$$\eta_D = 2 \cdot 9 \, f^{-1/3} N_{Pe}^{-2/3} \qquad 1.20$$

The form of this expression is in agreement with experimental data (21,26); the accuracy of the data is not, however, sufficiently high to confirm accurately the value of the constant or the form of f.

Electrostatic attraction

Four cases exist where electrostatic attraction may be important in fibrous filtration:-

(a) particle charged; fibre neutral - a charge is induced in the fibre which causes a polarization force.

(b) particle neutral; fibre charged.

(c) particle charged; fibre charged.

(d) externally induced electric field - polarization by the field causes the fibres to act as line dipoles.

The last case has been dealt with recently both

theoretically and experimentally (27,29); the results show that the technique is extremely promising as a high efficiency - low resistance method of filtration. However, since it is not relevant to the present work it will not be discussed further.

The R.M.S. charge value of naturally occuring aerosol clouds is low (30). Normally the charge on fibres is also low (31). However, artificially produced aerosols such as spray droplets (32) and dusts produced by dry drilling (29) may be highly charged and filters may be produced, such as the resin impregnated wool filter, in which the fibre charge is extremely high.

The particle fibre collision efficiency due to the mechanism is normally obtained by calculating particle trajectories in the neighbourhood of a fibre. The trajectory equations are obtained by equating the Stokes drag to the electrostatic attraction force:-

$$3\pi\mu d_p \underline{U_{rel}} + \underline{F_r(r)} = 0 \qquad 1.21$$

where $\underline{U_{rel}}$ is the relative velocity between the particle and the gas and $\underline{F_r(r)}$ is the electrostatic field force. One of the flow fields described in section 1.1 is used to describe the fluid velocity in equation 1.2 1. Expressions for the electrostatic force for cases a, b and c are given by Kraemer and Johnstone (33) and Natanson (34). The expressions are summarised in Table 1.3 where they are shown in dimensionless form and in terms of dimensionless force parameters.

TABLE 1.3

Kind of force	Coulombic	Induced	Image
electrostatic/fibre condition /particle	charged "	charged neutral	neutral charged
electrostatic parameter	N_{Qq}	N_{Qo}	N_{oq}
	$\frac{q\,Q}{\pi \varepsilon_0 B_1 d_f}$	$\left(\frac{\varepsilon_1 - 1}{\varepsilon_1 + 1}\right)\frac{Q^2 d_p^3}{\pi \varepsilon_0 d_f^3 B_1}$	$\left(\frac{\varepsilon_2 - 1}{\varepsilon_2 + 1}\right)\frac{q^2}{4\pi \varepsilon_0 d_f^2 B}$
$f_r'(r)$	$\frac{N_{Qq}}{r'}$	$\frac{N_{Qo}}{(r')^3}$	$\frac{N_{oq}}{(r'-1)^2}$

where $B_1 = 3\pi\mu U_0 d_p$; $r' = \frac{r}{r_f}$

Summary of electrostatic forces and parameters.

Theoretical expressions based on the above method are shown in Table 1.10. Experimental work has been confined to a study of case a. Lundgren (31) obtained the empirical expression

$$\eta_e = 1.5\, N_{oq}^{0.5} \qquad 1.22$$

but Yoshioka et al (34) using almost identical conditions concluded that the constant should be 2.3. The results were not sufficiently accurate to investigate the effect of Reynolds number or packing density. Good agreement can, however, be claimed between experiment and the theoretical work of Natanson.

Inertial interception

The inertial mechanism occurs when particles, because of their inertia, cross the fluid streamlines and impinge on the target. Interception occurs when a massless particle collides with the target purely because of its size. The inertial and interception mechanisms occur together so they are normally considered as a single mechanism. The interception mechanism alone is often calculated because it is a limiting case.

Theory.

The theories of inertial interception are obtained by computing particle trajectories in one of the flow fields. The trajectory equations which are described in detail in section 1.2.1 are given below in dimensionless form:-

$$N_{St}\frac{\partial^2 X'}{\partial \tau} + \frac{\partial X}{\partial \tau} - U' = 0 \qquad 1.23$$

$$N_{St}\frac{\partial^2 Y}{\partial \tau} + \frac{\partial Y}{\partial \tau} - V' = 0$$

where $N_{St} = \rho U_0 d_p^2 / 9 C_M d_f \mu = \frac{2X}{d_f} \cdot \frac{\rho V_0 d_p^2}{18 \mu}$

Equation 1.2 3 results from equating the particle inertia force to the Stokes drag based on its relative velocity. The inertia parameter or Stokes number N_{St} is the particle stop distance divided by the fibre radius. Other definitions of the inertia parameter have frequently been used including the ratio of the stop distance to the fibre diameter and $(N_{St})^{1/2}$. In this work N_{St} will be employed. There is some confusion concerning

the value of the velocity which should be used in N_{St}, several authors preferring the filter face velocity (U_o), some the mean interstitial velocity ($U_o/(1-\alpha)$) while Clarenburg and Van der Wal (36) advocate the use of an average velocity which is considerably modified due to the fibre arrangement within the filter ($1.5\ U_o/(1-\alpha)$).

Many theoretical predictions have been obtained by computing the critical particle trajectory i.e. that trajectory on which the particle just grazes the fibre. The efficiency is function of the following variables:-

$$\eta_{IR} = f^n\left(N_{St}, N_R, N_{Re}, \alpha\right) \qquad 1.25$$

where N_R is the interception parameter (d_p/d_f).

Since the results are dictated by the influence of the flow field the influence of N_{Re} and α must be considered separately.

(a) Isolated fibre

Figure 1.5 shows the calculated effect of N. on the single fibre efficiency as determined by a number of authors at different Reynolds numbers. The most useful and widely quoted of these curves is that due to Davies & Peetz (37) who employed the Davies solution of the Oseen equations - they performed the calculations for a fibre Reynolds number of 0.2. A more recent single fibre theory is that of Yoshioka et al (38). They used the Lamb solution and predicted a lower efficiency than that of Davies and Peetz. Recourse to fig. 1.1 will illustrate the danger of using the Lamb field. The particle trajectory starting point must be carefully chosen; at the same time the lower streamline

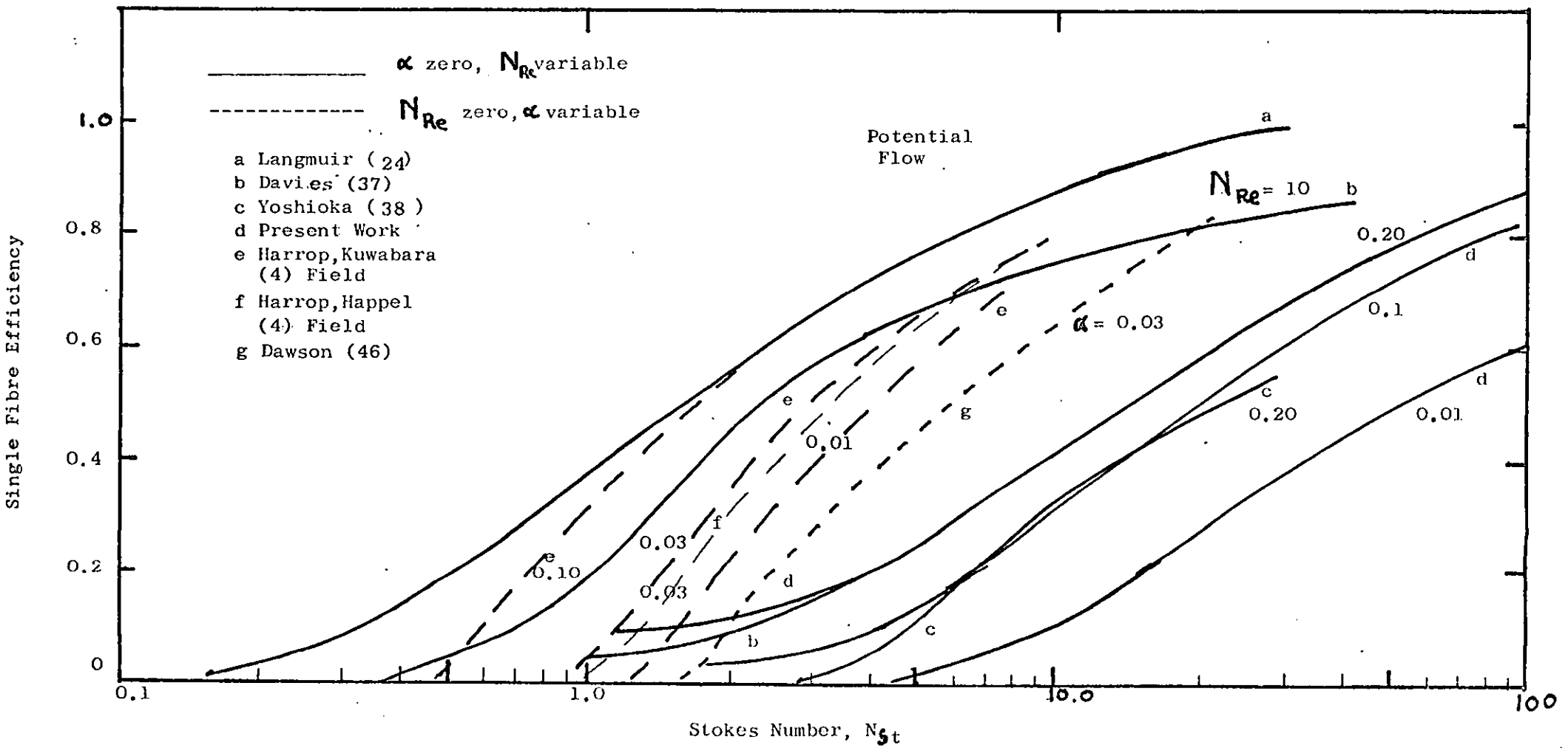

Efficiency of inertial collection - comparison of theories

Fig. 1.5

curvature of this field, which is less accurate than that of Davies, will result in the computation of a lower efficiency. It is interesting to note that Yoshioka predicts that the influence of Reynolds number on the efficiency is much more pronounced at low values of N_{St} than at higher values. It is logical that the influence of the fluid streamlines should become greater as a particle's ability to cross them is reduced.

Davies and Peetz used the Thom (12) model of the flow field to calculate the efficiency at a Reynolds number of 10. Loffler (39) has recently used boundary layer flow theory to obtain the efficiency characteristic at $N_{Re} = 50$.

Several expressions have been obtained by curve fitting, for the efficiency of intertial interception (3).

(b) Influence of filter packing density

The influence of filter packing density has been taken into account empirically by using an "apparent fibre diameter" which was determined using pressure drop measurements (40). Empirical expressions have been given by Chen (41) and Dorman (42) and Davies (43) has presented a semi-empirical approach.

Harrop and Stenhouse (4, 44, 45) used the Happel cellular field to investigate the influence of α on the efficiency of inertial interception. They compared the results obtained using the model with some obtained using the Kuwabara field and the simplified cellular field given in equation 1.18. They found only a slight variation between the results with the exception of those of the approximate Kuwabara field at high values of α. The Spielman and Goren field has been used by Dawson (46). His results are similar in form to those of Harrop and Stenhouse but predict lower efficiencies

(see fig. 1.5) over the entire range of variables considered.

There are three reasons for the discrepancy in results:-

(a) The cellular field is more tortuous than the Spielman and Goren field, hence a higher efficiency is predicted by Harrop and Stenhouse.

(b) The trajectory starting conditions in the work on the cellular model are likely to cause a higher efficiency prediction than those used by Dawson. The starting condition using the cell model was that of the main stream velocity at the outer boundary. Dawson was able to start his trajectories much further upstream.

(c) The relationship between α and the fields calculated is different for the two models.

The trajectory starting condition is important. Although it is theoretically correct to start a trajectory calculation for the case of an isolated cylinder at a position sufficiently far upstream (i.e. several hundred fibre diameters) for there to be no significant interference, it is not possible for this to occur in practice within a filter. In fact the fibre interference will not extend much upstream beyond what is accepted as a cell boundary: similarly it will not extend much further downstream than the boundary. Hence particles crossing a cell boundary are more likely to do so at the average flow conditions within the cell than in any other preconditioned state. The trajectory start conditions used with the cellular model are thus more realistic than a starting point much further upstream as is used by Dawson. Although inability to match neighbouring outer cell boundaries is a disadvantage the model is easily visualised.

Stechkina, Kirsch and Fuchs (47) derived an analytical expression for the efficiency of inertial interception for $N_{St} \ll 1.0$ using the Kuwabara model:

$$\eta_{IR}(N_R, N_{St}) = \eta_R + \frac{I}{4\xi^2} N_{St} \qquad 1.26$$

where $I = (29.6 - 28\,\alpha^{0.62})\,N_R - 27.5\,N_R^{2.8}$

Equation 1.26 was obtained by substituting a first order approximation for $\frac{\partial x}{\partial t}$ in terms of U' and N_{St} in equation 1.23 and solving for the total number of particles passing between the cylinder and $(1 + N_R)$ along the y axis:-

$$\eta_{IR} = \int_1^{1+N_R} \left(U_\theta, \frac{c}{c_o}\right)_{\theta=\frac{\pi}{2}} dr \qquad 1.27$$

At low values of N_{St} where 1.26 should be valid it predicts efficiencies which are much higher than those of Harrop and Stenhouse or Dawson.

The reason for the discrepancy is not clear but probably lies in the approximations made in deriving 1.26.

Experimental confirmation

The efficiency of inertial interception has been measured by several workers. The most reliable data, where monosized fibres and monosized particles have been used, is presented by Kumura and Iinoya (48) Wong et al (2) and Harrop (4); Gallily (49,50) and Harrop (4) have presented data on model filter systems. Dawson (46) carried out a thorough comparison of his work with that given in references 2, 48 and 49. He concluded that"the general trend of the comparison was that collection was often significantly under-predicted, but never significantly over-predicted without a particularly telling explanation".

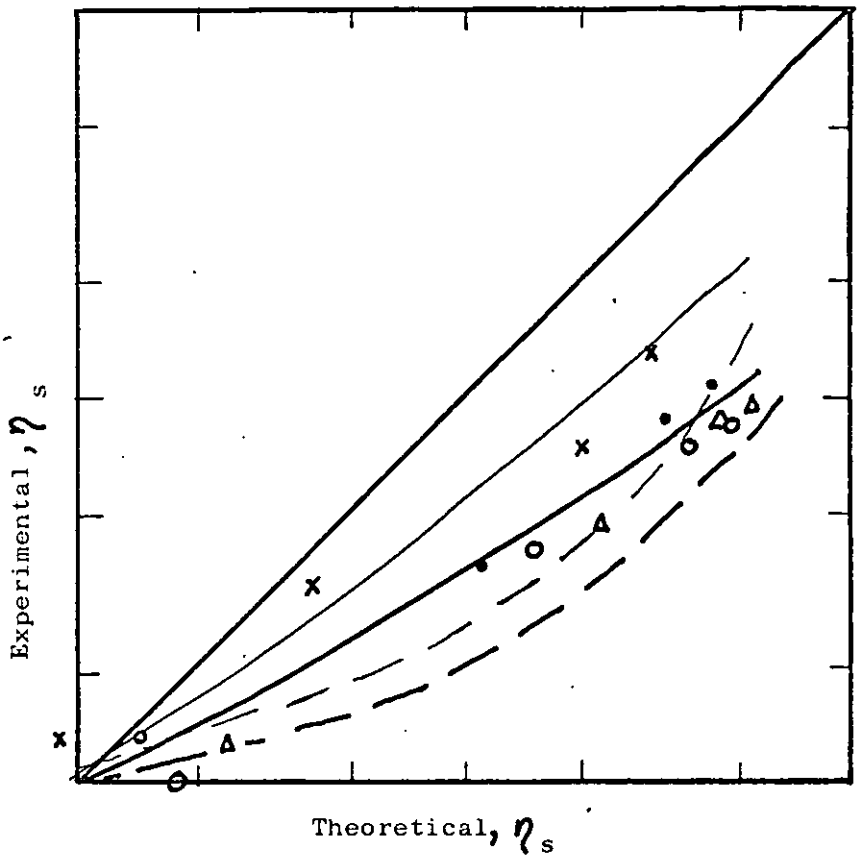

Comparison of theory and experimental results of Harrop (4).

x α = 0.03
• α = 0.06
⊙ α = 0.08
Δ α = 0.11

For real filter - Dawson comparison (——)

—— Real filter - Dawson
—— Model filter - Dawson
— — Real filter - Harrop and Stenhouse
— — Model filter - Harrop and Stenhouse

Fig. 1.6

Harrop compared his results using the cellular model with his own experimental data. He measured the filtration efficiency of 1.2 - 3.4μm monosized particles of sodium chloride using model and real filters. The model filters consisted of a series of grids of 50μm parallel stainless steel fibres. "Real" filters were constructed from monosized glass fibres. Packing densities in the range 0.01 - 0.11 were used and flame photometry was used as the method of concentration detection. He found that the cellular model significantly overestimated the experimental results.

A comparison between Dawson's theory and Harrop's experimental data is given in figure 1.6. Dawson's theory predicts a closer fit to the experimental results but still overestimates the efficiencies. Clearly the experimental data of Harrop is in conflict with that given in references 2, 48 and 49, the earlier workers obtaining much higher efficiencies. The cellular model gives closer agreement with the data in references 2, 48 and 49, whilst the Dawson model is in better agreement with Harrop's data.

No obvious reason can be found for the differences in experimental data. It is concluded, therefore, that further practical work is necessary before we can decide which of the two models of the flow field is most suitable. Both theories suffer from the assumptions of zero Reynolds Number and uniform filter packing density (which will have a cancelling effect - but will probably lead to an overestimate of efficiency).

The limiting case of interception only has been studied by numerous authors. The theory consists of solving equation 1.27

for one of the flow fields. Such solutions have been obtained for the cellular field (47) and that of Spielman and Goren (21).

Sedimentation

Stechkina et al (47) have shown that the contribution to the single fibre efficiency due to sedimentation during gas downflow and upflow is:-

$$\eta_p = (1 + N_R) N_p \qquad 1.27$$

for small values of N_p, which is the ratio of the sedimentation velocity (u_g) to U_o (positive for downflow and negative for upflow).

Thomas, Rimberg and Miller (51) compared upflow and downflow efficiencies experimentally. They showed that gravity is a contributory mechanism, the penetration (P) ratio being:-

$$\ln\left(\frac{P_{upflow}}{P_{downflow}}\right) \propto N_p^k \qquad 1.28$$

For the filters tested by them k had the value 0.71 - 0.85. It is not possible to extract the single fibre efficiencies from their data (they used a wide distribution of fibre sizes) to compare this with 1.27. However, they showed that if 1.27 is valid then

$$\ln\left(\frac{P_{upflow}}{P_{downflow}}\right) \propto (1 + N_R) N_p \qquad 1.29$$

Since other mechanisms, such as interception, must have contributed to capture it is not surprising that k is less than 1.0.

Filtration in rarefied systems.

The introduction of ultra-thin fibres in the manufacture of high efficiency filters and the necessity of filtering particulate material at high altitude, particularly radioactive dusts, makes the study of the effect of fibre Knudsen number $N_{Kn} = \lambda/r_f$ on the filtration efficiency one of practical importance.

The subject has been well reviewed by Pich (3). The Lamb (52) cellular (47) and Spielman and Goren (21) fields have been extended to the low pressure ($N_{Kn} < 0.25$) region using the slip flow boundary condition. The Lamb model was extended by Velichko and Radushkevich (53) using free molecular theory within one mean free path of the cylinder and continuous theory outside this to apply to intermediate values of N_{Kn}.

The first three solutions to the flow field have been used to derive expressions for efficiency of diffusional capture and interception. The Velichko theory has been used to find the interception efficiency. By including the N_{Kn} effect in ξ (see table 1.2) its influence on filter resistance is obtained, and Stechkina et al (47) have used $\xi(N_{Kn})$ to find its effect on η_I at very low values of N_{St}. Pich (54) has recently reviewed both theoretical and experimental work on filter resistance over a wide range of N_{Kn} values.

Stern, Zeller and Schekman (55) showed experimentally that the diffusional efficiency increased with N_{Kn}. This in accordance with theory but the magnitude of the effect was much less than predicted.

Combination of Mechanisms.

In the region of minimum efficiency several mechanisms are

significant simultaneously. Although it is frequently assumed so (46) the contributions are not additive and the computation of the efficiency due to the combined mechanisms presents a formidable mathematical problem. The only semi theoretical approach is that due to Stechkina et al (47) who considered the efficiency due to the combination of diffusion, interception, inertia and gravity:-

$$\eta_{DRIP} = \eta_D + \eta_{DR} + \eta_R + \eta_I + \eta_P$$

where

$$\eta_D = 2.9\,\xi^{-1/3} N_{Pe}^{-2/3} + 0.62\, N_{Pe}^{-1}$$

$$\eta_R = (2\xi)^{-1}\left[(1+N_R)^{-1} - (1+N_R) + 2(1+N_R)(1+2N_{Kn})\ln(1+N_R)\right] \qquad 1.30$$

$$\eta_{DR} = 1.24\,\xi^{-1/2} N_{Re}^{-1/2} N_R^{2/3}$$

$$\xi = -\tfrac{1}{2}\ln\alpha - \tfrac{3}{4} + 2N_{Kn}\left(-\tfrac{1}{2}\ln\alpha - \tfrac{1}{4}\right)$$

η_I and η_P are given by equations 1.26 and 1.27 respectively which are valid only for low N_{St}. The Kuwabara field was used to find 1.30.

Davies (43) and Torgeson (56) and Dorman (57) have produced expressions for η_{DRI}. Davies applied a theoretical approach assuming the efficiencies to be additive but the second two authors used semi-empirical methods.

1.1.3 Filter Configuration

This section is concerned with the way the configuration of fibres within a filter effect its performance. There are three levels of examining these effects, namely:

(a) the bulk effect of packing density

(b) the influence of fibre distribution in filters constructed of monosized fibres.

(c) the effect of mixing two or more fibre sizes in the filter.

The influence of α on filter behaviour has been reviewed well in reference (4). There are several empirical correlations, notably by Chen (41) and Dorman (42) and Davies (43) has produced a semi-empirical expression. The flow field descriptions which have been used to take α into account are designed to be used with regular systems of uniform packing density.

Dawson (46) has attempted a completely theoretical description of the influence of fibre distribution effects (mono sized systems) and Clarenburg and his co-workers (36,58-62) have introduced semi-empirical methods to describe the behaviour of filters consisting of different sized fibres.

i) Monosized fibres.

Dawson used a parallel flow model in which a filter consists of deep zones each of a uniform but different packing density.

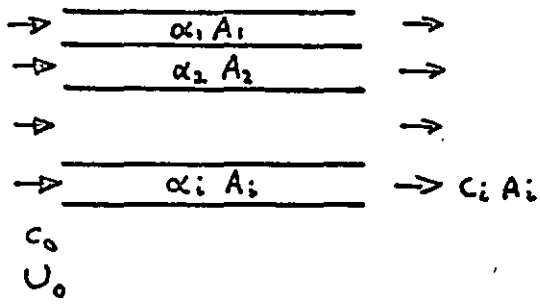

By using relatively large zones of different packing density instead of individual fibre spacings, the problem of matching boundary conditions is avoided.

He defines the distribution of packing densities as:-

$$\alpha = \sum Y_i \alpha_i \qquad 1.31$$

where $Y_i = A_i / A_{Total}$

and a resistivity (X_T) of the filter where

$$\frac{1}{X_T} = \frac{U_0 \mu L}{r_f^2 \Delta p} \qquad 1.32$$

Using the Darcy equation to describe the flow through the system the total resistivity is obtained in accordance with Ohm's law as

$$\frac{1}{X_T} = \sum \frac{Y_i}{X_i} \qquad 1.33$$

By considering a filter of two packing densities he shows how the resistivity is lower than that of a filter with the same mean but uniform packing density.

The average penetration of such a filter was obtained by assuming an exponential decay in aerosol concentration through each channel as is normal, and summing the efflux from the whole filter:-

$$\frac{c}{c_o} = 1 - \eta = X_p \sum \left(\frac{Y_i}{X_i} \exp\left(\frac{-4\alpha_i \eta_i L}{\pi d_f}\right)\right) \qquad 1.34$$

where X_p is the measured resistivity of the filter (theoretically the same as X_T) and η_i the single fibre efficiency in channel i. Hence he was able to calculate the reduction in pressure drop and filtration efficiency due to non-uniformity.

A description of non-uniformity even for a model with two packing densities requires the use of two parameters. This was reduced to one by including the constraint that the difference in the two packing densities should be a minimum. The following ratio then defines the uniformity of a filter:-

$$W = \frac{X_p}{X_u} \qquad 1.35$$

Dawson calculated the reduction in the efficiency of inertial interception in terms of W and filter depth. Clarenburg and Van der Wal (36) used a parallel capillary model to obtain a value for the volume average velocity. They included a log normal distribution of pore sizes. Using a σ_g of about 2.0 they showed that the volume average velocity is approximately 50% greater than the average interstitial velocity. This velocity was used to calculate the inertia parameter in Davies (43) equation to obtain the efficiency,

$$-\ln P = \gamma \frac{L}{\bar{d}_e^2} \frac{\alpha^2}{(1-\alpha)} \qquad 1.36$$

where $\gamma = 13.9\, d_f \left[1 + \left(0.75/N_R + 1.2\right) N_{St} - 0.236\, N_{St}^2\right]$

A large value of σ_g will increase γ and hence the calculated efficiency. This is in conflict with Dawson's work which predicts a reduction in efficiency. The method takes into account the increase in η_x or γ in lightly packed sections of a filter due to the increased velocity; this effect may, however, be more than compensated for by the reduction in number of targets in such a zone - i.e. the variation in $\frac{\alpha^2}{(1-\alpha)}$ from place to place in 1.36 should be taken into account. It is concluded, therefore, that 1.36 is invalid.

ii) Multisized fibres.

Clarenburg (60) described an empirical equation for the pressure drop across a filter consisting of multisized fibres:-

$$\ln \Delta p = \sum x_i^* \ln \Delta p_i \qquad 1.37$$

where x_i^* refers to corrected fractional composition.

The contributions of individual fibres to the pressure drop and efficiency are not additive. This is due to the configuration effect which is described as the combination of two separate effects, namely those of structure and shadow.

The structure effect leads to a reduction in resistance and efficiency. Presence of large fibres in a filter cause a widening in the pore size distribution of the fine fibres. The effect increases with increasing ratio of fibre sizes.

The shadow effect is a screening of coarse fibres by fine. The flow pattern imposed by the coarse fibres causes an increase in η_I of the fine fibres the efficiency of which are higher in any case. This results in an overall increase in efficiency and resistance.

The shadow effect is normally stronger than that due to structure. The influence of both effects on resistance is given by equation 1.37 which is purely empirical but in which the structure effect may be considered to be included in the logarithmic summation. The shadow effect is included in X_i^* where

$$X_i^* = x_i + (1 - x_i) H \qquad 1.38$$

where H is a correction factor due to shadow.

By analogy with equation 1.37 the penetration (P) for a filter consisting of multisized fibres was expressed as:-

$$\ln(-\ln P) = \sum X_i^* \ln(-\ln P) \qquad 1.39$$

Clarenburg's work explains his experimental findings that a quantity of fines in a filter greatly enhance its collection efficiency.

Summary

All the mechanisms of filtration have been described theoretically but quantitatively that description depends on the flow field used. The most satisfactory fields to date are those of Kuwabara and Spielman and Goren which take the influence of neighbouring fibres into account. Both fields have been applied to a study of the major mechanisms and both result from idealistic models. Experimental results are not sufficiently accurate to ascertain which model provides the best fit of practical data.

There are obvious comparative advantages in determining the efficiency due to all mechanisms and combinations of mechanisms using one model of the flow field. This requires an extension of the theories using one of the existing fields. Of the two methods, the Kuwabara is considered more useful than that of Spielman and Goren because it is easier to visualise and simpler to use.

Work on the influence of filter configuration is at an early stage; it is worthy of extension.

1.2 Application of Cell Model

The theoretical efficiency of particle fibre collision (η_c) in the cellular field is described in this section. The problem is solved by computing particle trajectories in the field. Both radial and planar field forces are incorporated to describe the combined mechanisms of electrostatic attraction and inertial interception of fibre Knudsen number and the distribution of pore sizes in a filter are also described.

1.2.1 Trajectory calculations.

A force balance on a particle in a fluid results in the following equation:-

$$m\frac{d\underline{u}_p}{dt} = C_D\pi\frac{|\underline{u}-\underline{u}_p|(\underline{u}-\underline{u}_p)}{2}d_p^2\rho + \underline{f}_p + \underline{f}_r + \underline{L} \qquad 1.40$$

where $\underline{f}_{p,r}$ = planar, radial, field forces

$\underline{L}$ = lift forces

The particle is considered as a point mass in the fluid which does not interfere with the flow field. The influence of the finite size of the particle is taken into account in determining the drag and lift forces and the particle cylinder collision conditions.

If the particle is moving in the linear Stokes regime equation 1.40 can be resolved as follows:-

$$\frac{m}{3\pi\mu d_p}\frac{\partial^2 x}{\partial t^2} + \frac{\partial x}{\partial t} - u - f_{p,x} - f_{r,x} - L_x = 0$$

$$\frac{m}{3\pi\mu d_p}\frac{\partial^2 y}{\partial t^2} + \frac{\partial y}{\partial t} - v - f_{p,y} - f_{r,y} - L_y = 0 \qquad 1.41$$

where u and v are the fluid velocity x and y resolutes. Equations 1.41 may be reduced to their dimensionless form using the conversions shown in table 1.4. N_{St} is the particle stop distance divided by the target radius. Hence equations 1.41 become

$$N_{St}\frac{\partial^2 X}{\partial \tau^2} + \frac{\partial X}{\partial \tau} - U' - f'_{p,x} - f'_{r,x} - L'_x = 0$$

$$N_{St}\frac{\partial^2 Y}{\partial \tau^2} + \frac{\partial Y}{\partial \tau} - V' - f'_{p,y} - f'_{r,y} - L'_y = 0 \qquad 1.42$$

TABLE 1.4

Parameter	Symbol	Derivation
Velocity	U	u/U_o
	V	v/U_o
Co-ordinate	X	x/r_f
	Y	y/r_f
Time	τ	$t\,U_o/r_f$
Inertia	N_{St}	$2\rho U_o r_f^2/9\mu$
Field Force	f'	$f/6\pi\mu r_f U_o$
Lift	L^1	$L/6\pi\mu r_f U_o$

Conversions used in equation 1.42.

There are three kinds of lift force to consider:-

(i) Lift due to the particle moving relative to a liquid which is under shear. Saffman (64) predicts that this lift will act in such a way that particles will tend to move towards the cylinder surface, enhancing the collision efficiency. The lift force in a simple shearing field is given by:-

$$\underline{L}_1 = \frac{1.615 \mu \underline{U}_{rel} d_p^2 K^{1/2}}{\nu^{1/2}} \qquad 1.43$$

Where $\underline{U}_{rel}$ = particle velocity relative to fluid

K = magnitude of velocity gradient

(ii) The particle will experience a lift due to the presence of the solid boundary which will tend to reduce the efficiency. This lift has been studied theoretically by Evans (65) who showed that:-

$$L_2 = \frac{6\pi\mu U_{rel}^3 d_p^3}{8\nu l_1} f^n\left(\frac{U_{rel} l_1}{\nu}\right) \qquad 1.44$$

where U_{rel} = relative velocity of sphere

l_1 = distance between sphere and wall

$$f^n\left(\frac{U_{rel} l_1}{\nu}\right) = \frac{9}{32} - 0.37973\left(\frac{U_{rel} l_1}{\nu}\right) + 0.46003\left(\frac{U_{rel} l_1}{\nu}\right)$$

$$- 0.23574\left(\frac{U_{rel} l_1}{\nu}\right) + 0.044238\left(\frac{U_{rel} l_1}{\nu}\right)$$

It is due to second order terms in the Navier-Stokes equation so it is significant in systems of high fluid inertia.

(iii) The particle will experience a drag in a direction which is parallel to the wall (65).

$$L_3 = 3\pi d_p \mu v_{pr} \left(\frac{9\, d_p}{32 l_1}\right) \qquad 1.45$$

In the absence of information to the contrary it is assumed that each of these forces can be simply resolved and that they are additive. L_1 L_2 and L_3 are considered only in the close proximity of the cylinder.

Examination of forces L_1 and L_2 shows that they are most significant in high shearing fields and in high particle inertia systems. The forces are in fact important in such systems, where potential theory can be applied to describe the flow field. However, a computer study using the Kuwabara field has shown that they have no effect beyond the second significant figure on the single fibre efficiency computed over a range of Stokes numbers up to 5.0 ($N_R = 0.05$).

Equations 1.39 must be solved using an iterative procedure. In the present work they were simply expressed in finite difference form using a Taylor expansion to yield:-

$$X_2 = \frac{1}{(2N_{St} + \Delta\tau)}\left[2U'(\Delta\tau)^2 + 4N_{St}X_1 - (2N_{St} - \Delta\tau)X_0\right]$$

$$Y_2 = \frac{1}{(2N_{St} + \Delta\tau)}\left[2V'(\Delta\tau)^2 + 4N_{St}Y_1 - (2N_{St} - \Delta\tau)Y_0\right] \qquad 1.46$$

where $X_{0,\,1,\,2}$ and $Y_{0,\,1,\,2}$ represent respective positions on the trajectory. $\Delta\tau$ is the time between each computed position. These expressions were solved using a digital computer.

A flow diagram of the computer program used is shown in fig. 1.7. Successive trajectories were calculated until the critical trajectory was obtained. Normally about 250 points were calculated on each trajectory, tests on the time interval used showed that the accuracy was within the second significant figure. The results agreed with those of Harrop (4) when the Happel model was used and with those of Davies (37) when his equation 25 in reference 8 (Davies flow field) was employed at values of N_{St} above 1.0. The latter calculation is in agreement with that of Dawson (46).

The influence of field and lift forces was included by adding their x and y resolutes in dimensionless form to U' and V' in equation 1.46. In the case of lift forces which are velocity dependent it was assumed that a linear resolution was adequate for the order of magnitude calculations which were made; when it was found that they were not important these terms were dropped from the calculations.

1.2.2. Efficiency of inertial interception

Further results using the Kuwabara field were obtained and are shown in table 1.5. In all the calculations described below the trajectory starting point was taken as the main stream velocity at the cell boundary. However, at the outside surface of the cell the y velocity resolute is not zero. The effect of using the theoretical outer boundary velocity instead of the main stream velocity as the trajectory starting condition is shown in table 1.5. With a packing density of 0.03 the effect is not severe for values of N_{St} below 5.0. At $N_{St} = 5.0$ and $\alpha = 0.03$ the effect is to reduce η_{IR} from 0.67 to 0.53; this may be compared with 0.41 which is the

efficiency predicted by Dawson for the same conditions (but using the Spielman and Goren field). Since a filter consists of a random array of fibres and not a regular array as is visualised as the concept of the cellular model the entry condition of the particle in the present work is taken as the average velocity (U_o) and not that of the fluid at the edge of the cell.

At high Reynolds numbers the influence of the fibre wake on the particle trajectories is interesting. Collision efficiencies were determined in the Davies field under a range of Reynolds numbers and inertia levels. The starting point for the trajectories was 100 diameters upstream and approximately 5000 points on each were calculated. Some typical trajectories are shown in figs. 1.8 and 1.9 where it is shown that the efficiency is considerably enhanced by particles being captured in the fibre wake and colliding with the rear of the fibre. In some cases the particle went as far as 5 diameters downstream before being returned in the wake. These calculations are, of course, highly dependent on the accuracy of the flow field used, and this must be suspect especially at the rear of the fibre, however, they do show that the mechanism of wake capture may be significant.

The predicted effect of Reynolds number and inertia is shown in fig. 1.10 and table 1.6. The influence of Reynolds number alone is shown in fig. 1.11. The results coincide exactly with those of Davies (see fig. 1.5) above an inertia parameter of 5, but at lower values of N_{St} wake capture is important. This phenomenon was not reported by Davies.

Wake capture has not been confirmed experimentally. The light particle deposites at the rear of fibres observed by microscope by the author and by Gillespie (75) could have resulted from either diffusional or electrostatic deposition. Neighbouring fibres will

Computer program flow sheet

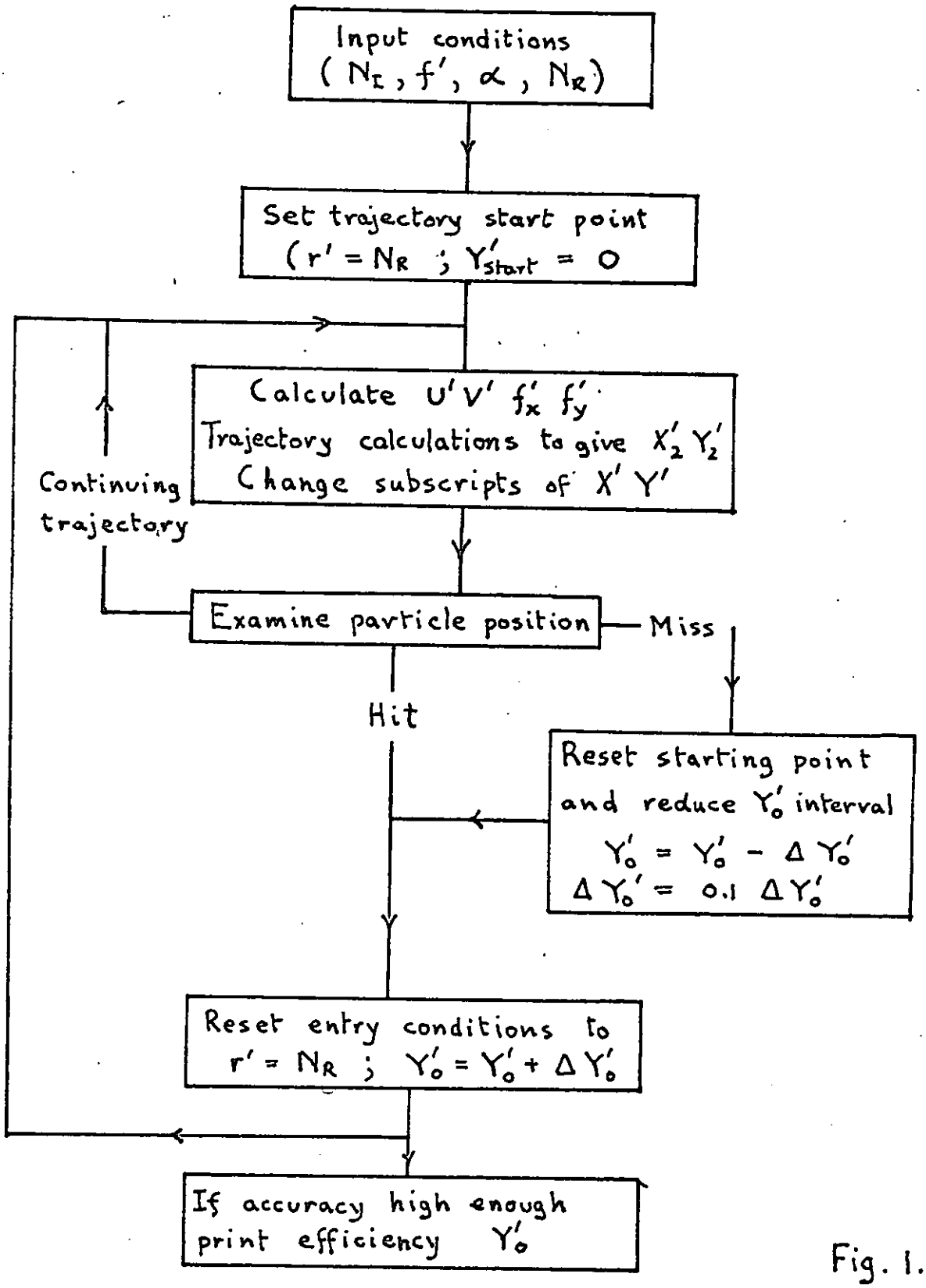

Fig. 1.7

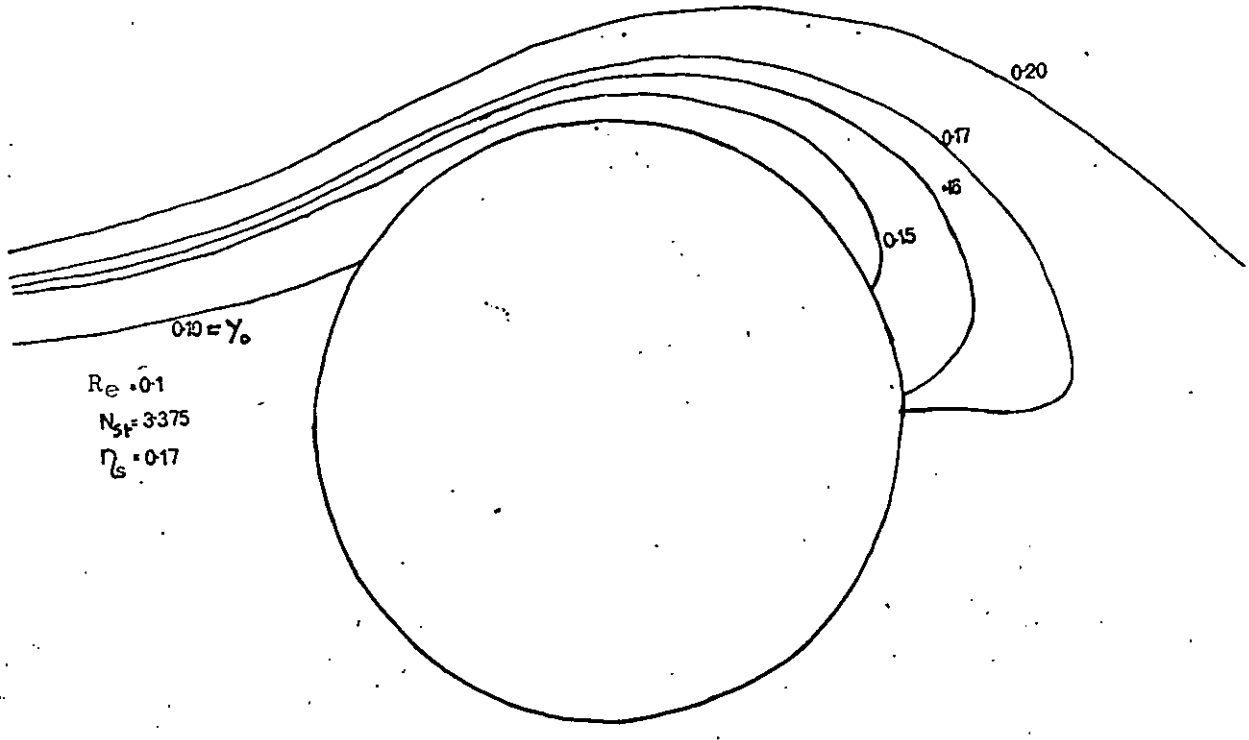

Particle trajectories in Davies field.
Fig. 1.8

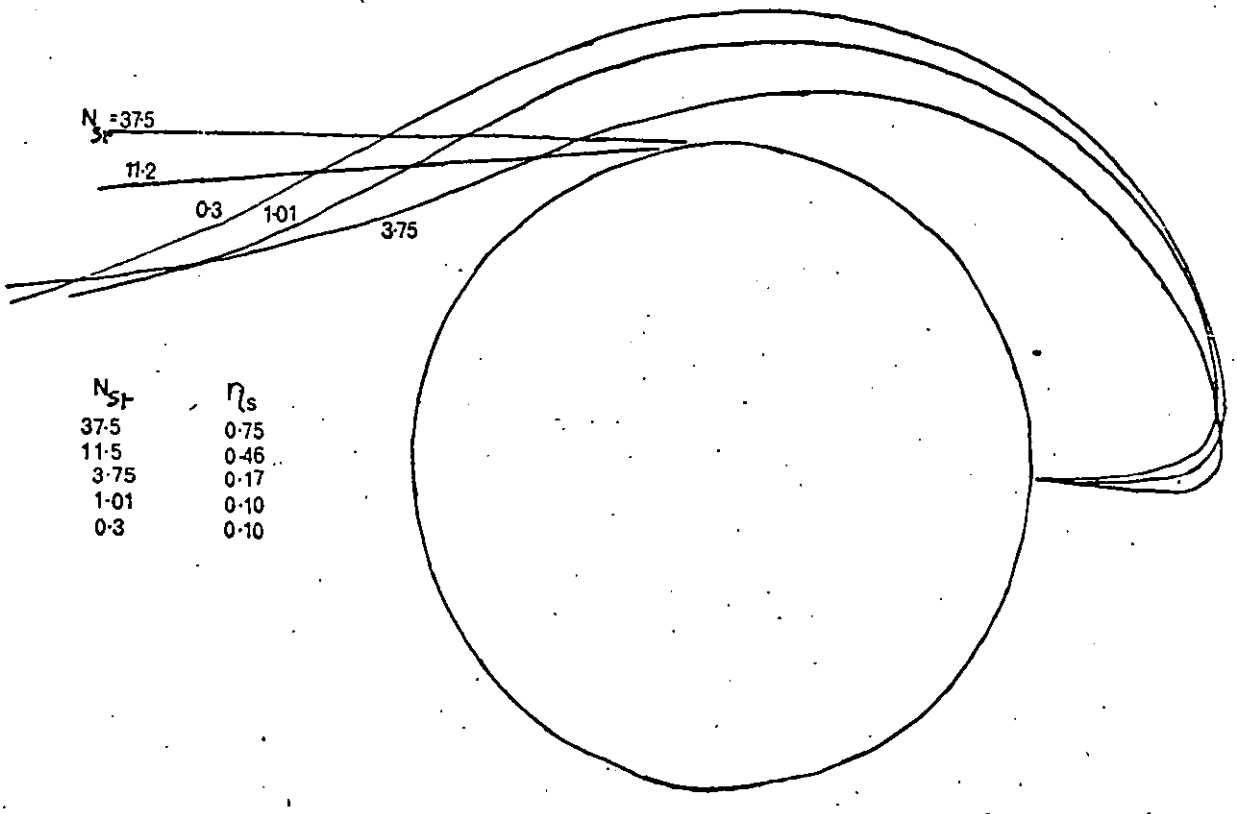

Particle trajectories in Davies field.
Fig. 1.9

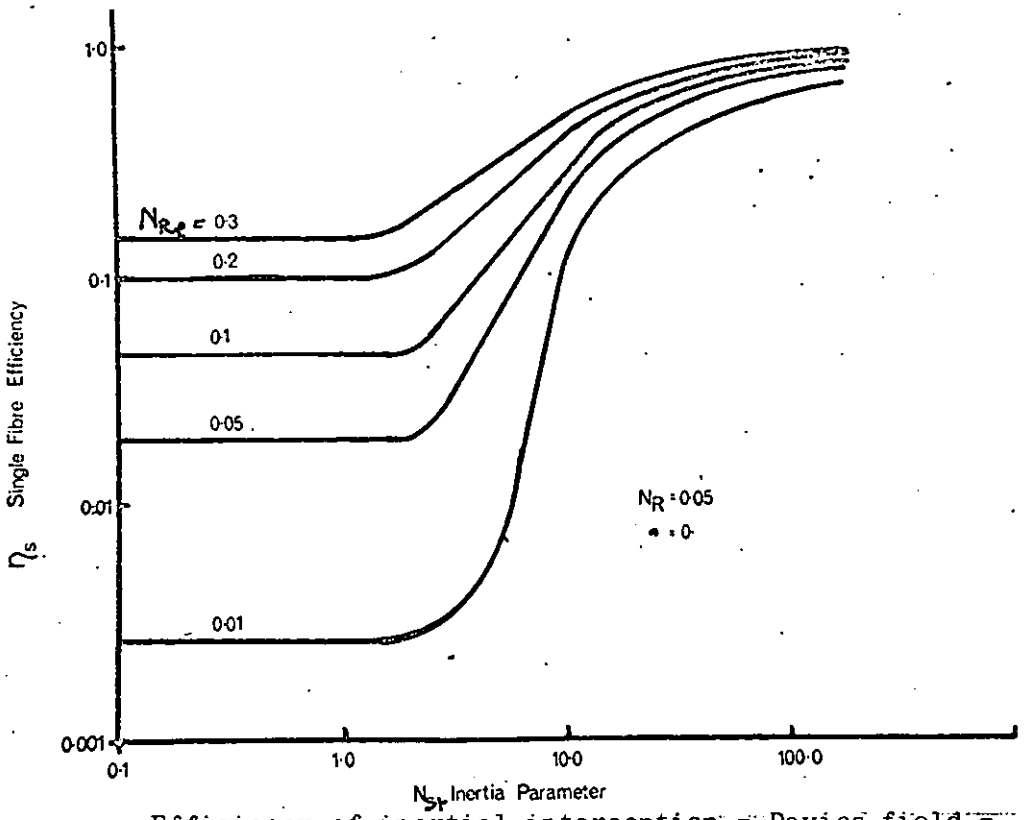

Efficiency of inertial interception - Davies field - wake capture included.

Fig. 1.10

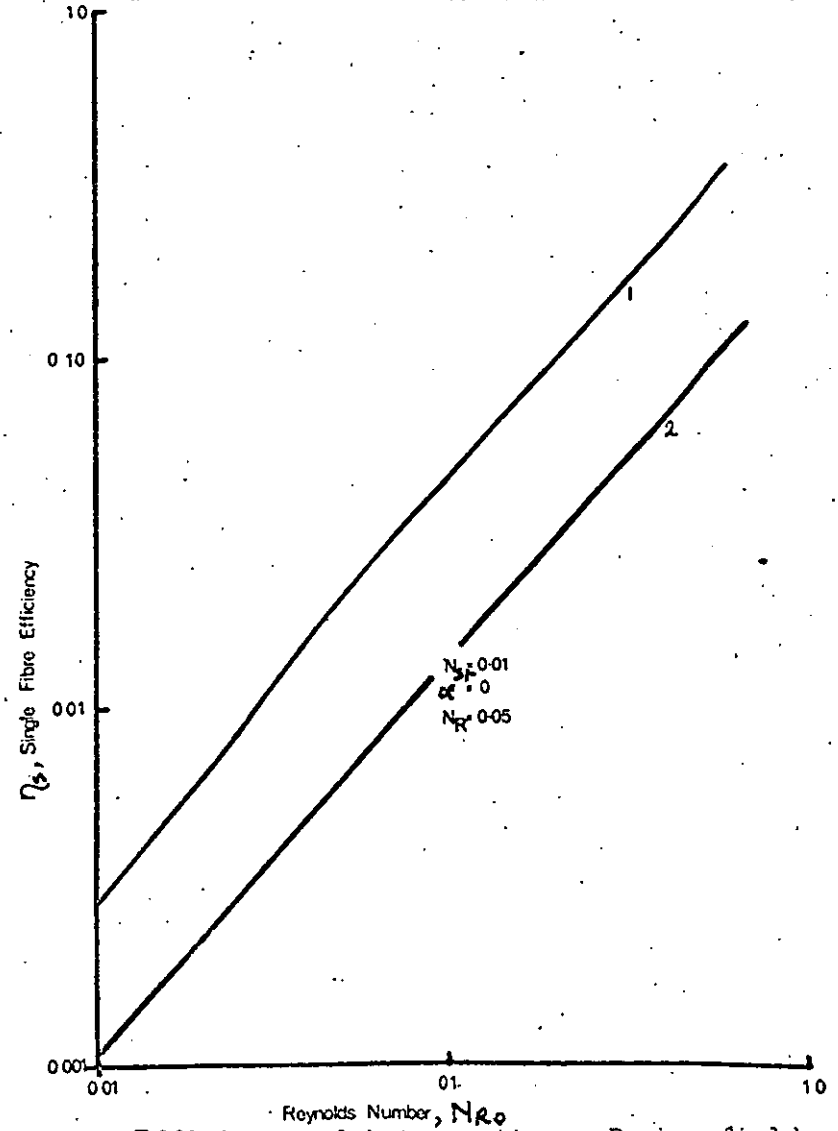

Efficiency of interception - Davies field.
1. Wake capture assumed; 2. No wake capture.

Fig. 1.11

TABLE 1.5

N_R	N_{St}	α					
		0.01	0.03	0.06	0.11	0.15	0.03*
0.05	50	0.97	1.00	1.01	1.01	1.02	
	10	0.75	0.83	0.88	0.91	0.93	
	5	0.55	0.67	0.75	0.81	0.83	0.53
	2.5	0.277	0.450	.553	.642	.687	0.38
	1.25	0.0104	0.142	.291	.416	.469	0.12
	.63	.0029	.0066	.0182	.125	.219	0.0062
	0.31	0.0019	.0033	.0056	.0115	.0204	0.0032
	0.16	0.0017	.0027	.0040	.0064	.0092	0.0026
	0.08	.0016	.0024	.0036	.0054	.0072	0.0024
	0.04	.0016	.0024	.0035	.0053	.0069	0.0024
	0.02	.0016	.0024	.0036	.0054	.0070	0.0024
0.02	50	0.95	0.97	0.98	0.98	0.99	
	10	0.73	0.81	0.85	0.88	0.90	
	5	0.53	0.65	0.72	0.77	0.80	
0.10	50	1.02	1.04	1.06	1.06	1.07	
	10	0.79	0.87	0.92	0.95	0.98	
	5	0.58	0.71	0.79	0.84	0.88	

Values of single fibre efficiency computed using the Kuwabara field

* particle entry condition is gas velocity at outer cell boundary.

TABLE 1.5a

α	N_R	N_{st} 0.01	0.1	0.5	1	2	5	10	20
0.01	0.01	.0000	.0000	.0001	.0002	.1500	.5200	.7200	.8400
0.03		.0001	.0001	.0002	.0016	.3300	.6400	.8000	.8900
0.06		.0001	.0001	.0004	.1500	.4500	.7100	.8400	.9200
0.10		.0002	.0002	.0013	.2700	.5200	.7600	.8700	.9300
0.15		.0002	.0003	.0350	.3600	.5800	.7900	.8900	.9400
0.01	0.05	.0016	.0016	.0024	.0055	.1700	.5500	.7500	.8800
0.03		.0025	.0025	.0048	.0340	.3600	.6700	.8300	.9300
0.06		.0035	.0036	.0100	.1800	.4700	.7400	.8700	.9500
0.10		.0050	.0051	.0280	.3000	.5500	.7900	.9000	.9700
0.15		.0070	.0075	.1200	.3900	.6200	.8300	.9300	.9800
0.01	0.10	.0063	.0064	.0090	.0190	.1900	.5800	.7900	.9200
0.03		.0090	.0090	.0170	.0850	.3900	.7100	.8700	.9700
0.06		.0130	.0140	.0350	.2200	.5100	.7900	.9200	1.0000
0.10		.0190	.0190	.0850	.3400	.6000	.8400	.9500	1.0200
0.15		.0270	.0280	.1800	.4400	.6700	.8800	.9800	1.0300
0.01	0.20	.0240	.0240	.0320	.0620	.2500	.6400	.8600	1.0100
0.03		.0360	.0360	.0600	.1600	.4500	.7900	.9600	1.0700
0.06		.0520	.0520	.1100	.3100	.5900	.8700	1.0100	1.1000
0.10		.0720	.0730	.1900	.4400	.6900	.9300	1.0500	1.1200
0.15		.1000	.1000	.3100	.5500	.7700	.9800	1.0800	1.1300
0.01	0.30	.0510	.0510	.0660	.1100	.3100	.7100	.9400	1.1000
0.03		.0770	.0780	.1100	.2400	.5300	.8700	1.0500	1.1600
0.06		.1100	.1100	.1900	.4000	.6700	.9700	1.1100	1.2000
0.10		.1500	.1500	.3100	.5400	.7900	1.0400	1.1500	1.2200
0.15		.2100	.2100	.4400	.6700	.8900	1.0900	1.1800	1.2400
0.01	0.50	.1200	.1300	.1500	.2200	.4400	.8500	1.1100	1.2800
0.03		.1900	.1900	.2600	.4100	.6900	1.0400	1.2300	1.3500
0.06		.2700	.2700	.3900	.6000	.8700	1.1600	1.3100	1.3900
0.10		.3800	.3700	.5600	.7800	1.0100	1.2500	1.3600	1.4200
0.15		.5200	.5000	.7500	.9600	1.1500	1.3300	1.4000	1.4500

Values of single fibre efficiency computed in Kuwabara field - particle entry condition is that of main stream velocity, U_o, parallel to x axis at entrance to cell surface.

TABLE 1.6.

N_{Re} / N_{St}	0.01	0.05	0.10	0.20	0.30
125	0.66	.75	.81	.90	.93
37.5	.43	.57	.65	.75	.80
10	.11	.23	.32	.44	.52
5	.01	.07	.13	.23	.32
3.8	.0038	.04	.07	.17	.26
3.0	.0035	.029	.046	.15	.23
1.0	.0026	.020	.046	.10	.15
0.6	.0026	.020	.046	.10	.15
0.01	.0026	.020	.046	.10	.15

$N_R = 0.05$

Davies flow field (eqn. 25 ref. 8)

$\eta_{IR} = 0.7\ N_{Re}^{1.2}$ at $N_{St} = 0.01$

Values of single fibre efficiency computed using Davies field (wake effects taken into account).

probably dampen wake formation within a filter so the effect will have less practical significance than the above results suggest. For comparison the efficiencies without wake capture (i.e. trajectory calculation stopped at x = o) have been computed and are shown in table 1.6a.

1.2.3 Radial Field Forces

No work could be found in the literature on the combined mechanisms of electrostatics and inertial interception, although this is important in practice. Neither could work be found on the influence of packing density on the electrostatic mechanisms alone.

The influence of radial field forces i.e. electrostatics was calculated from expression 1.42. The three cases a - c described in section 1.2 were examined. Expressions for the dimensionless force used in 1.42 and for the electrostatic force parameters are given in table 1.3.

The Kuwabara flow field was used to include the effect of packing density on the flow pattern. The influence of packing density on the electrostatic field must also be included. Application of Gauss' theorem to a regular system of parallel cylinders shows that the contribution of neighbouring cylinders to the field inside the cell is zero. The field inside the cell is, therefore, the same as that of an isolated cylinder but will not extend beyond the cell boundary. Consequently, the influence of filter packing density on the electrostatic force is included if the equations 1.42 are solved in the normal manner, taking the trajectory starting point as the outside surface of the cell.

The influence of electrostatics and N_{St} on the efficiency for a packing density of 0.03 and interception parameter of 0.05 is shown in tables 1.7 and 1.8 and figs. 1.12-14. Table 1.9 shows the effect of filter packing density and the electrostatic

TABLE 1.6a

N_{St}	N_R	N_{Re} .05	.20	.30	.50	1.0
125	0.01	.7500	.860	.890	.910	.94
37.5		.5700	.740	.780	.820	.88
11.3		.2500	.480	.530	.620	.73
3.4		.0270	.140	.210	.310	.49
1.0		.0100	.056	.089	.150	.31
.303		.0077	.042	.067	.120	.26
.091		.0071	.038	.061	.110	.24
1.5	.05	.780	.900	.920	.950	.98
37.5		.590	.770	.810	.860	.91
11.3		.260	.480	.550	.670	.76
3.4		.032	.150	.220	.330	.51
1.0		.012	.059	.090	.160	.32
.303		.009	.045	.071	.120	.26
.091		.009	.041	.065	.110	.25
.027		.009	.040	.064	.110	.24
125	.10	.820	.940	.970	.990	1.02
37.5		.620	.800	.850	.900	.96
11.3		.270	.500	.580	.670	.79
3.4		.039	.160	.230	.350	.54
1.0		.016	.066	.100	.170	.33
.303		.012	.050	.077	.130	.27
.071		.012	.046	.071	.120	.26
.027		.012	.046	.070	.120	.25
125	0.20	.890	1.030	1.050	1.090	1.12
37.5		.670	.880	.930	.980	1.04
11.3		.300	.550	.630	.740	.87
3.4		.056	.190	.260	.390	.60
1.0		.025	.082	.120	.190	.37
.303		.021	.064	.090	.150	.30
.091		.020	.060	.087	.140	.28
.027		.020	.059	.086	.140	.28
125	0.50	1.120	1.290	1.320	1.360	1.40
37.5		.850	1.100	1.160	1.231	1.31
11.3		.400	.700	.810	.940	1.10
3.4		.120	.280	.380	.530	.77
1.0		.067	.140	.200	.290	.51
.303		.059	.120	.160	.240	.42
.091		.058	.110	.150	.220	.40
.027		.057	.110	.150	.220	.39

Davies flow field (eqn 25 reference 8)

Influence of fibre Reynolds number on η_{IR} (wake effects not taken into account).

TABLE 1.7

	N_{Qq}	0	0.0001	0.001	0.01	0.05	0.10	0.50	1.0
α	N_{St}								
0.01	5	.55		.55	.55		.59		1.03
	2.5	.27		.27	.29		.42		1.52
	1.25	.010		.017	.069		.30		1.94
	0.63	.0028		.0053	.034		.27		2.29
	0.31	.0019		.0038	.029		.27		2.53
	0.16	.0017		.0035	.029		.29		2.67
	0.01	.0016		.0034	.030		.30		2.79
0.03	5	.67	.67	.67	.68	.69	.70	.82	0.95
	2.5	.45	.45	.45	.45	.48	.51	.82	1.21
	1.25	.14	.14	.14	.17	.27	.36	.91	1.54
	0.63	.0065	.0069	.0090	.043	.15	.27	1.03	1.89
	0.31	.0033	.035	..0052	.030	.13	.26	1.17	2.20
	0.16	.0026	.0038	.0043	.028	.14	.27	1.28	2.39
	0.01	.0024	.0026	.0042	.030	.15	.30	1.40	2.57

$N_R = 0.05$; Kuwabara field
Particle and Fibre charged

Influence of electrostatics on inertial interception.

TABLE 1.8

N_{Qo}	0.	0.001	0.001	0.05	0.1	.50	1.0
N_{St}							
5	.67	.67	.67	.68	.70	.72	.77
2.5	.45	.45	.45	.46	.47	.61	.74
1.25	.14	.14	.14	.23	.28	.51	.68
0.62	.0066	.0068	.0090	.10	.16	.44	.65
0.31	.0033	.0034	.0049	.086	.14	.43	.67
0.16	.0026	.0027	.0041	.084	.14	.45	.71
0.01	.0024	.0025	.0039	.090	.15	.49	.74

N_{Oa}	0.	0.001	0.001	.01	.10	.50	1.0
N_{St}							
5	.67	.67	.68	.72	.88	1.12	1.29
2.5	.45	.45	.47	.55	.75	1.05	1.26
1.25	.14	.17	.23	.34	.60	.97	1.23
0.62	.0065	.035	.089	.21	.50	.93	1.24
0.31	.0033	.021	.062	.17	.47	1.00	1.30
0.16	.0026	.019	.057	.16	.48	1.02	1.36
0.01	.0024	.019	.059	.17	.51	1.05	

N_R = 0.05; α = 0.03; Kuwabara field.

Influence of electrostatics on inertial interception.

TABLE 1.9

N_{Qq_v} / α	0	0.001	0.01	0.1	1.0
.01	.0016	.0034	.031	.30	2.79
.03	.0024	.0042	.030	.30	2.57
.06	.0035	.0053	.030	.30	2.38
.10	.0050	.0066	.030	.29	2.20
.15	.0071	.0086	.029	.28	2.01
N_{Qo} / α	0	0.001	0.01	0.1	1.0
.01	.0016	.0031	.022	.14	.67
.03	.0024	.0039	.023	.15	.77
.06	.0035	.0050	.024	.16	.86
.10	.0050	.0064	.024	.17	.94
.15	.0071	.0084	.024	.18	1.01
N_{oq_v} / α	0	0.0001	0.001	0.05	0.50
.01	.0016	.015	.048	.30	.86
.03	.0024	.019	.059	.37	1.05
.06	.0035	.023	.071	.45	1.27
.10	.0050	.027	.084	.53	–
.15	.0071	.032	.090	.62	–

$N_{St} = 0.01$; $N_R = 0.05$
Kuwabara flow field

Efficiency of electrostatic attraction.

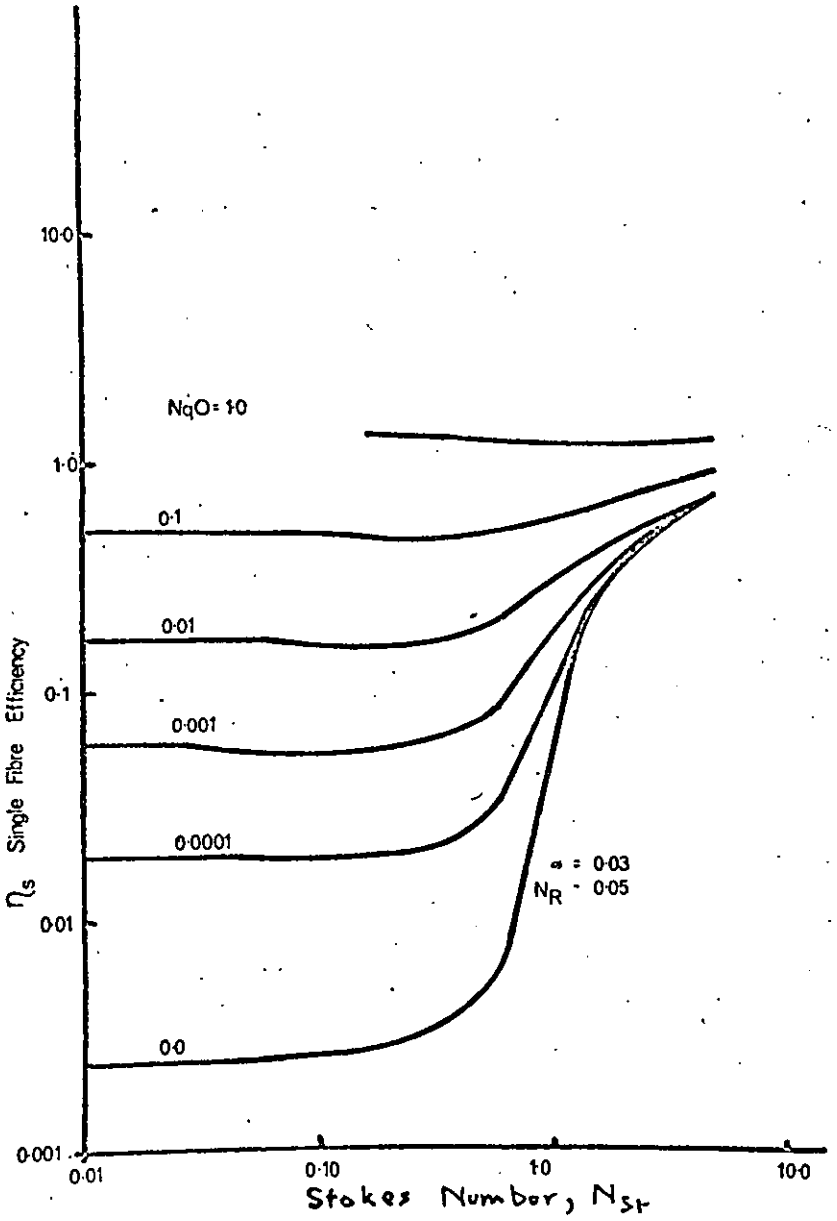

Efficiency of intertial interception and electrostatics.
Fig. 1.13

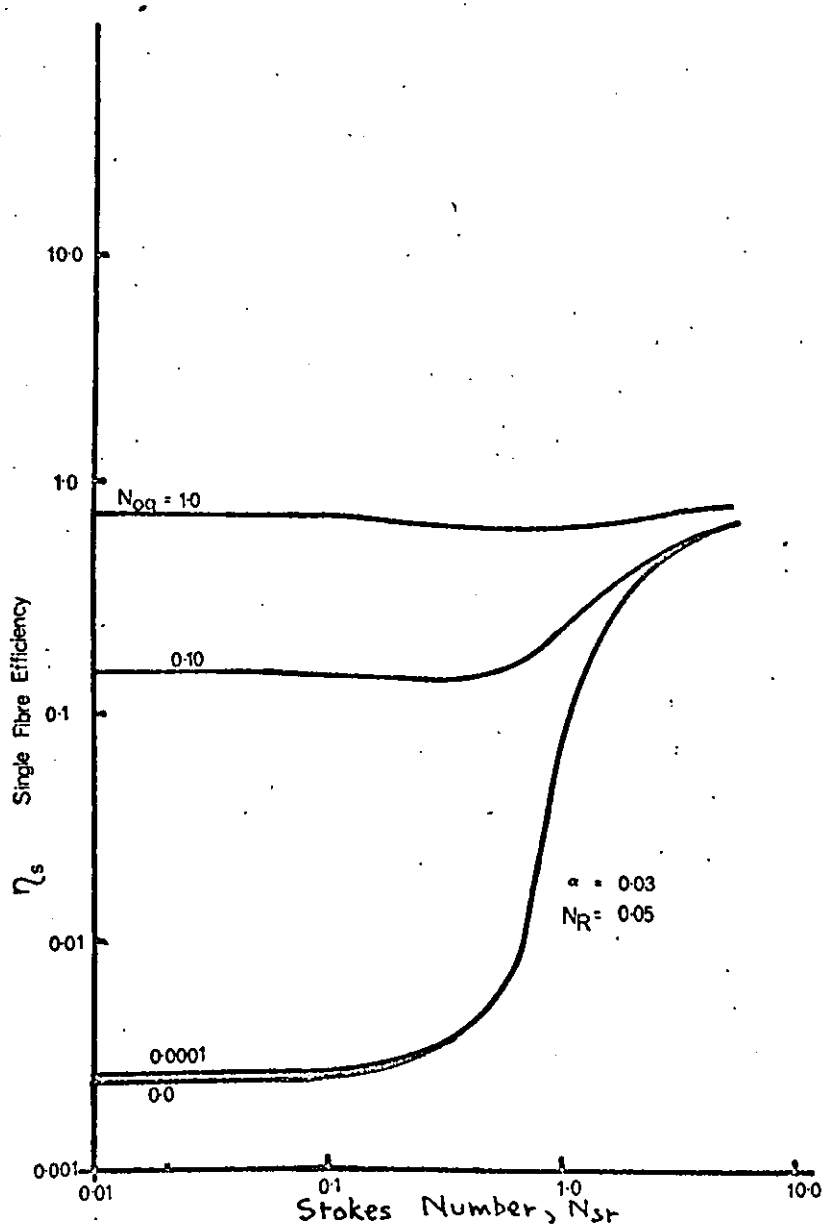

Efficiency of inertial interception and electrostatics.
Fig. 1.12

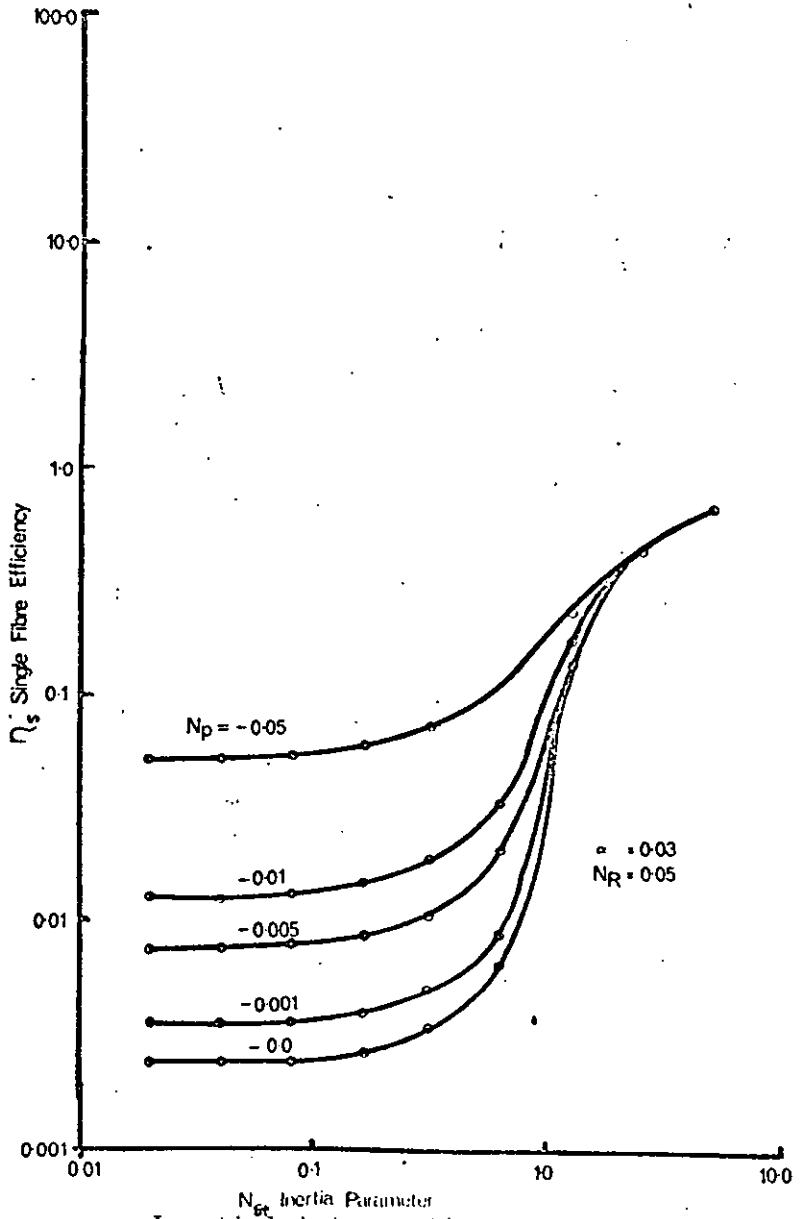

Inertial interception and planar field forces.

Fig. 1.15

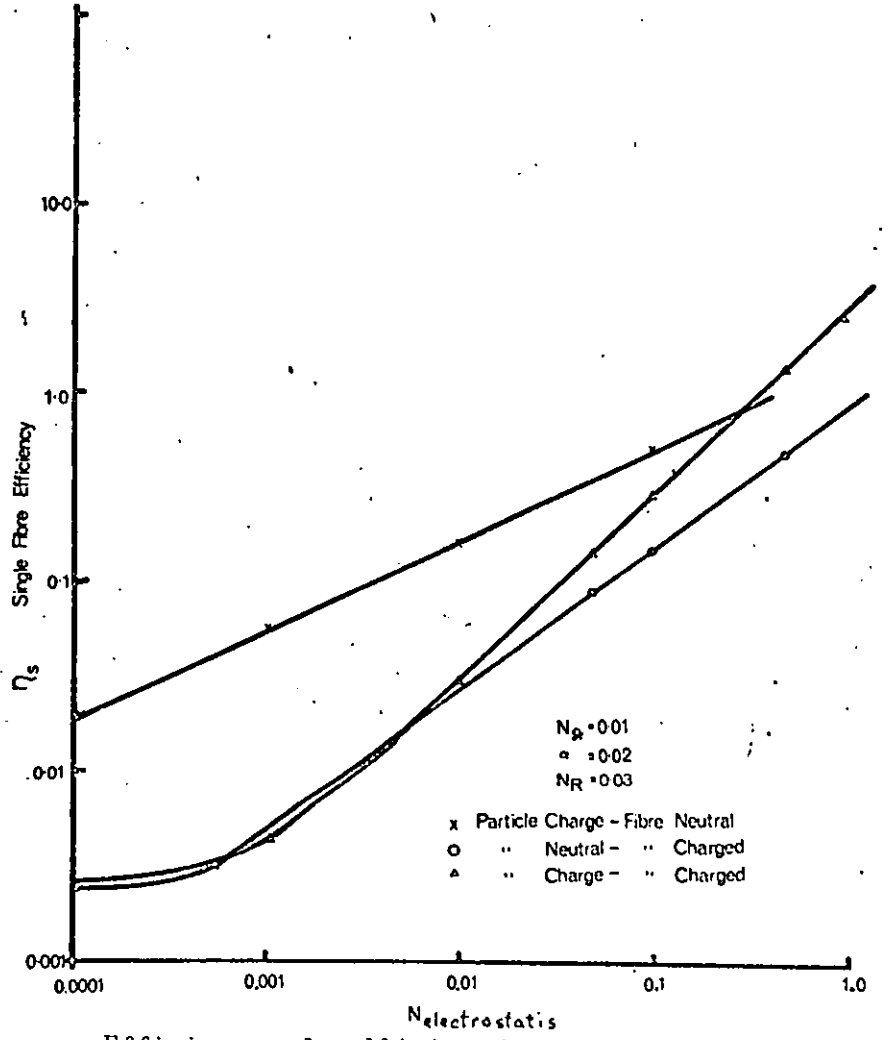

Efficiency of collision due to electrostatics.

Fig. 1.14

parameter for zero inertia particles. At low levels of electrostatic attraction an increase in packing density will increase the filter efficiency due to the interception mechanisms. At higher levels of electrostatic attraction the tendency will be for the efficiency to be reduced in tightly packed filters. This is because the range of influence of the field force is reduced. The effect will, of course, be most significant where the attractive force is most long ranging, i.e. in the case where both the particle and fibre are charged.

It is interesting to compare the results obtained at zero inertia (see fig.1.14) with those obtained by other methods. The curves for a packing density of 0.03 are closely approximated by the expressions shown in table 1.10 where it can be seen that they agree closely with previously published data, both experimental and theoretical, in every case except where the fibre only is charged. In that case the exponent is found to be 0.75 and not 1.0 as predicted by Natanson. Even then, however, the absolute values do not differ by more than 50% over the entire range.

1.2.4. Planar Field

Planar (i.e. gravitational) field forces may be important especially at low levels of particle inertia. The system was analysed in accordance with equation 1.42 and the results are shown in table 1.11 and fig. 1.15 - 1.17. In these calculations the value of the velocity used in N_{St} is that of the gas but the boundary condition approach velocity of the particle to the Kuwabara cell is takes as the actual particle approach velocity. The case of downward flow (N_G + ve) is simple to analyse, the capture efficiency being enhanced by the field force. In upward flow, however, the

TABLE 1.10.

Electrostatic condition	Particle Fibre	Charged Neutral	Neutral Charged	Charged Charged
Comment				
Kraemer & Johnstone (33) - theory		–	$\frac{3\pi}{2} N_{Oq}^{0.23}$	πN_{Qq}
Natanson (34) - theory		$2 N_{Qo}^{0.5}$	πN_{Oq}	–
Lundgren & Whitby (31) - expt.		$(2 - N_{Re})^{0.5}$	–	–
Yoshioka (35) - expt.		$1.5 N_{Qo}^{0.5}$	–	–
Present work (α = 0.03)		$2.3 N_{Qo}^{0.5}$	$0.84 N_{Oq}^{0.75}$	$2.8 N_{Qq}$
		$1.5 N_{Qo}^{0.5}$		

Single fibre efficiency due to electrostatics.

TABLE 1.11

N_R	N_{St}	N_p								
		-.05	-.01	-.005	-.001	0	+.001	+.005	+.01	+.05
0.05	5.0	0.67	.67	.67	.67	.67	.67	.67	.67	.67
	2.5	0.47	.45	.45	.45	.45	.45	.45	.44	.42
	1.25	.24	.17	.15	.15	.14	.14	.12	.10	0.157
	0.63	.11	.035	.021	.0090	.0066	0.063	0.092	0.107	0.274
	0.31	.074	.020	.011	.0050	.0033	0.063	0.093	0.107	0.276
	0.16	.062	.015	.0090	.0039	.0026	0.063	0.094	0.107	0.276
	0.08	.057	.014	.0084	.0036	.0024	0.064	0.094	0.107	0.276
	0.01	.050	.013	.0078	.0035	.0024	0.065	0.094	0.107	0.276
0.20	5.0		.79			.79		.79		.79
	2.5		.55			.55		.54		.52
	1.25		.27			.25		.24		.12
	0.63		.090			.077		.054		0.274
	0.31		.060			.045		.030		
	0.16		.051			.038		.025		
	0.08		.048			.037		.024		
	0.01		.048			.036		.024		

α = 0.03; Kuwabara field; negative figures refer to fluidisation

Influence of gravity on inertial interception.

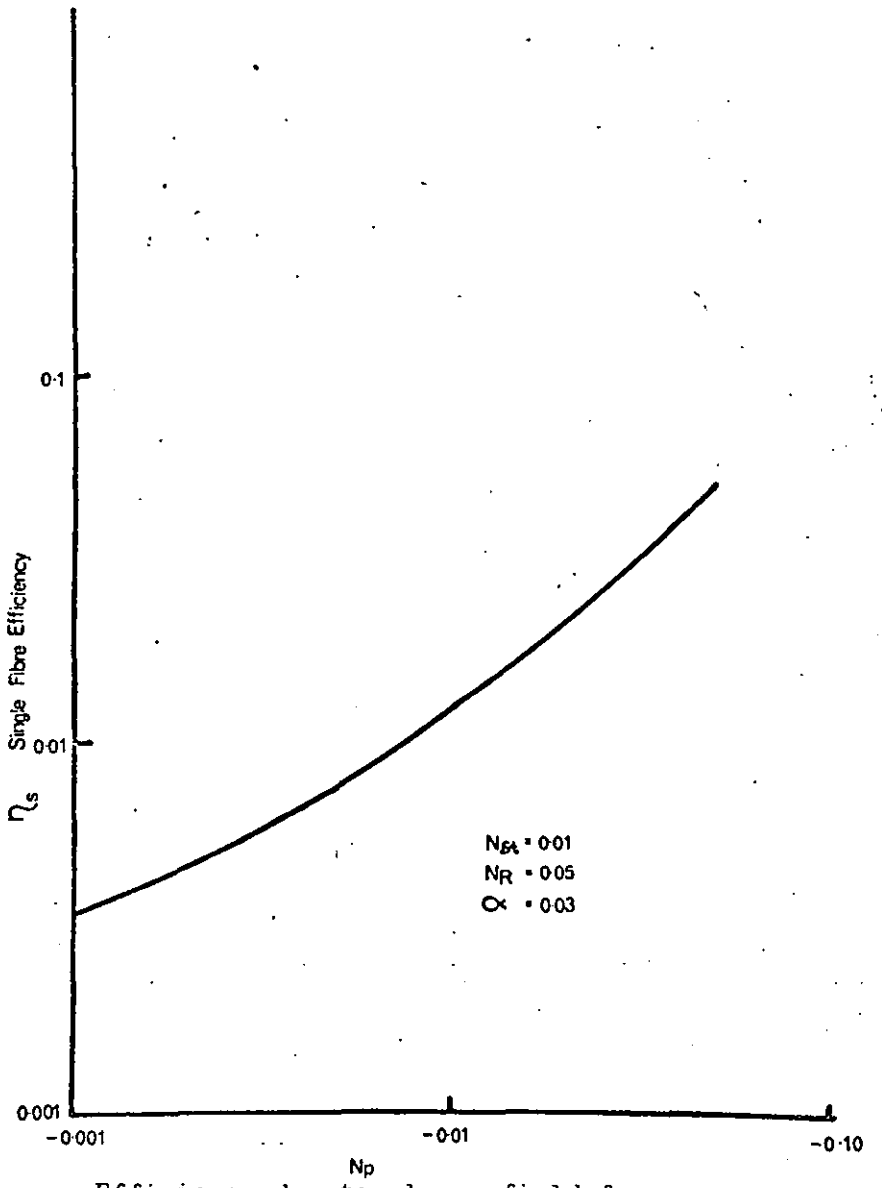

Efficiency due to planar field force.

Fig. 1.17

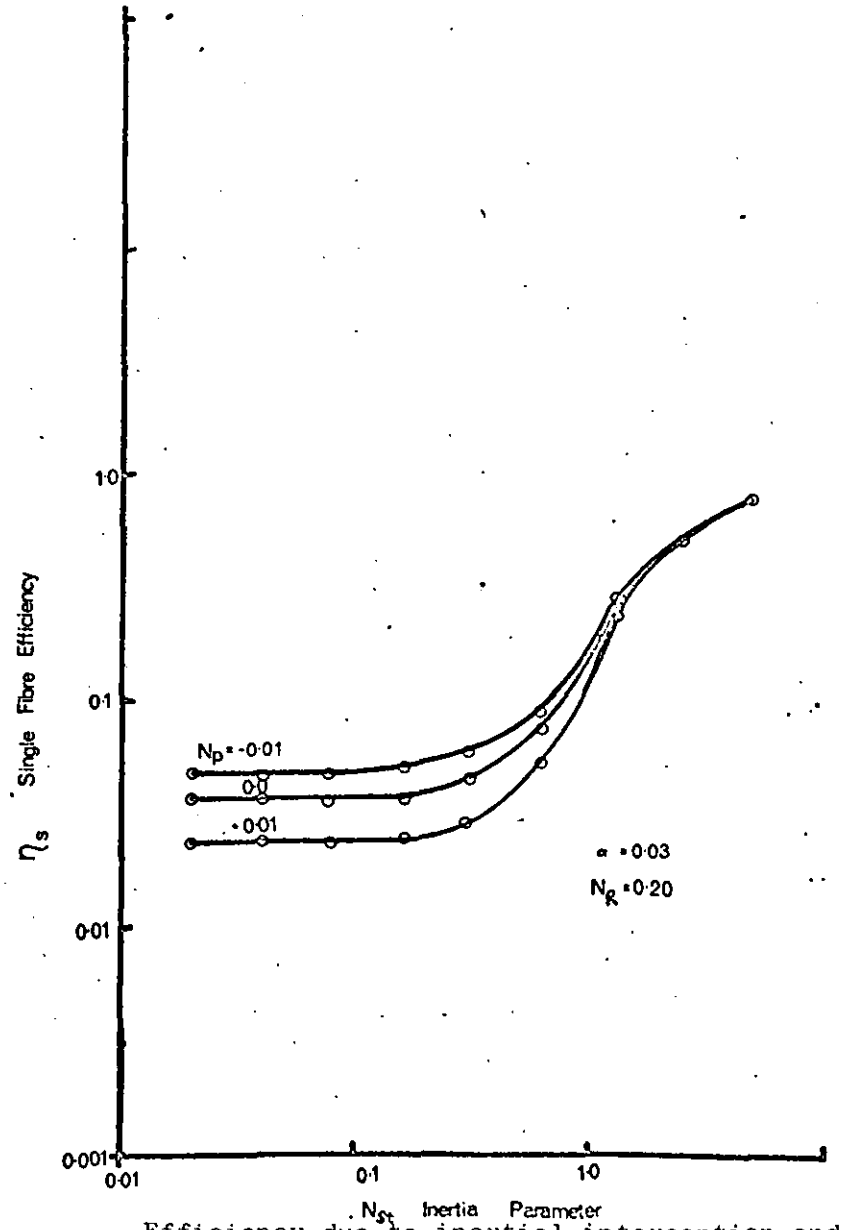

Efficiency due to inertial interception and planar field force.

Fig.1.16

particle may reach an equilibrium position from which it cannot theoretically escape. The capture efficiency of such particles is theoretically zero. The fluidisation position is also in table 1.11. In practice wake capture, enhanced by sedimentation, will be an important mechanism in such systems.

The increase in η for downward flow is much greater than would be predicted by using the actual particle velocity in the inertia parameter rather than the gas velocity. This is because the relative magnitudes of the particle and gas velocities is much higher near the fibre where the gas velocity is greatly reduced.

The collection efficiency for downward flow in the absence of inertia is shown in fig.1.17. Subtracting the efficiency due to interception a value of η_p was found for the contribution due to the field force. The values obtained are compared with those predicted by equation 1.27 in table 1.11. The agreement is almost exact.

1.2.5. Fibre Knudsen Number

Using the slip flow boundary condition Pich (3) obtained a solution to the Kuwabara flow field applicable for $N_{Kn} < 0.25$. Particle trajectories were calculated in this field to find the influence of fibre Knudsen number on the efficiency of inertial interception. The results are shown in tables 1.12 and 1.13 and figures 1.18 and 1.19. It can be seen that N_{Kn} is important only at low levels of inertia.

The collision efficiency due to pure interception is easily found analytically using the same technique as Stechkina et al (47). The stream function at its central plain of the fibre is equated to that at some distance upstream - in this case the cell boundary. The expression (eqn 1.30) for η_R was obtained by

TABLE 1.12

N_{Kn}		α 0.01	.03	.06	.11	.15
0.01	5	.554	.679	.750	.809	.838
	2.5	.280	.452	.556	.644	.607
	1.25	.014	.149	.296	.419	.482
	.63	.0039	.0090	.0245	.135	.225
	.31	.0027	.0046	.0077	.015	.027
	.16	.0023	.0036	.0054	.009	.012
	.04	.0023	.0034	.0049	.007	.009
	.01	.0023	.0034	.0049	.007	.010
0.10	5	.567	.690	.761	.819	.848
	2.5	.303	.469	.522	.660	.705
	1.25	.044	.188	.322	.442	.505
	.63	.0108	.0244	.064	.183	.263
	.31	.0072	.0121	.020	.038	.063
	.16	.0064	.0097	.014	.022	.030
	.04	.0065	.0095	.013	.019	.024
	.01	.0067	.0095	.014	.020	.025
0.25	5	.580	.701	.770	.828	.856
	2.5	.325	.487	.587	.673	.718
	1.25	.077	.220	.346	.463	.524
	.63	.018	.041	.100	.216	.291
	.31	.011	.019	.031	.058	.093
	.16	.010	.015	.021	.032	.043
	.04	.011	.015	.020	.027	.034
	.01	.011	.015	.021	.030	.036

N_R = 0.05; Kuwabara field

Influence of fibre Knudsen number on η_s.

TABLE 1.13

α	N_{Kn}	Eqn.1.47	Eqn.1.30	Computer Solution $N_{St} = 0.01$
0.01	0.00	0.001434	0.001690	.00164
0.01	0.01	0.001989	0.002343	0.00228
0.01	0.10	0.005962	0.006966	.00672
0.01	0.25	0.010088	0.011692	.0111
0.03	0.00	0.002002	0.002742	.00250
0.03	0.01	0.003909	0.003785	.00345
0.03	0.10	0.008569	0.010929	.00993
0.03	0.25	0.014247	0.017814	.0160
0.06	0.00	0.002937	0.004516	.00359
0.06	0.10	0.004053	0.006188	.00494
0.06	0.10	0.011714	0.017045	.01380
0.06	0.25	0.019109	0.026602	.0217
0.11	0.00	0.004377	0.010394	.00546
0.11	0.01	0.006017	0.013918	.00747
0.11	0.10	0.016900	0.033383	.0200
0.11	0.25	0.026846	0.046781	.0303
0.15	0.00	0.005718	0.031118	.00715
0.15	0.01	0.007832	0.038562	.00975
0.15	0.10	0.021511	0.065516	.0252
0.15	0.25	0.033488	0.076460	.0372

Comparison between computer solution and equations 1.30 and 1.47.

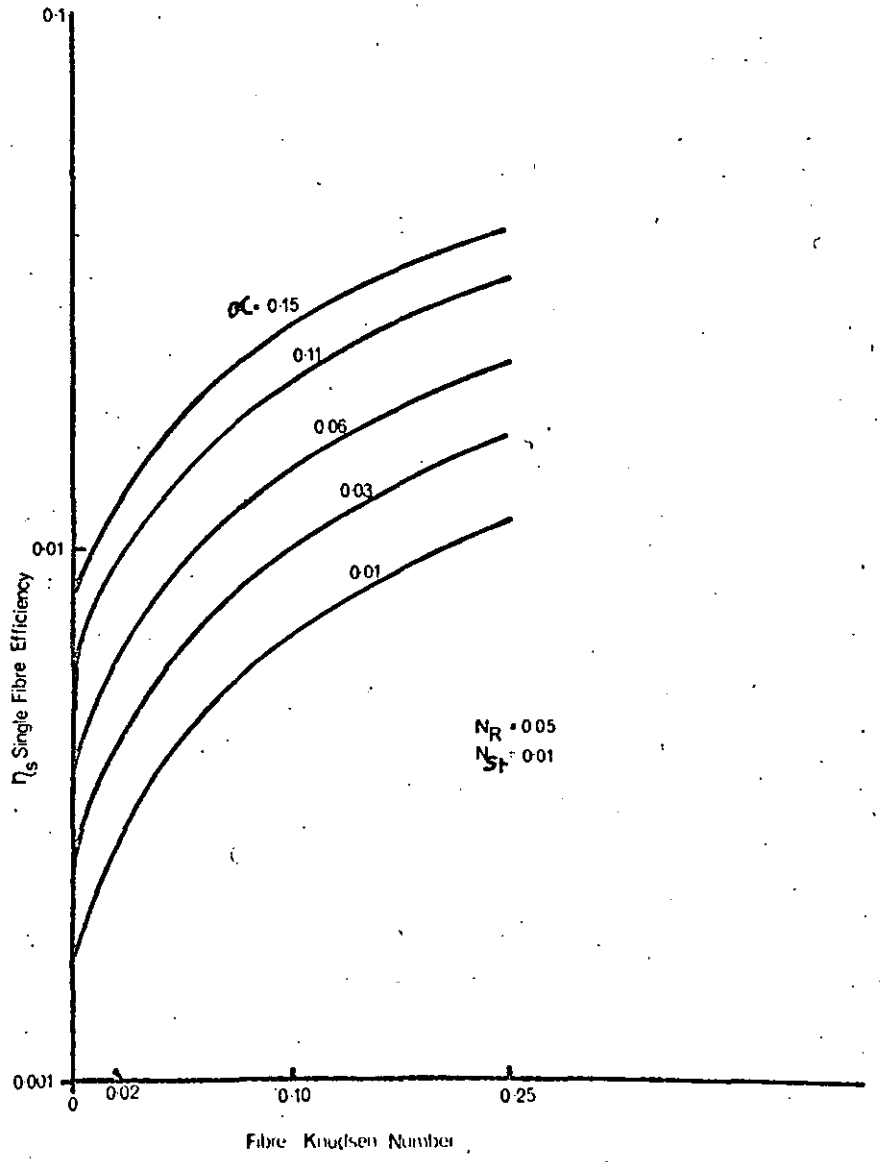

Interception efficiency in rarefied systems.

Fig. 1.19

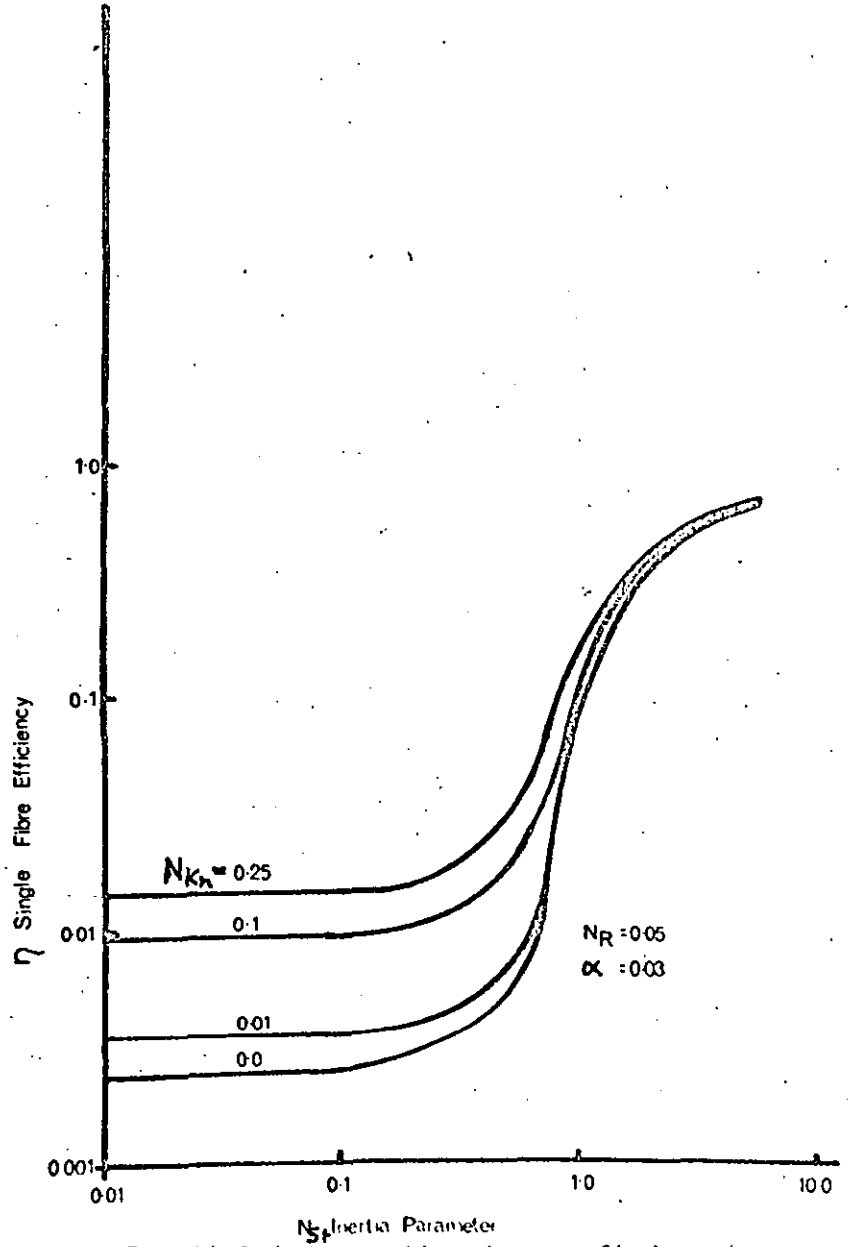

Inertial interception in rarefied systems.

Fig. 1.18

Stechkina (47). This expression is, however, a simplification; a more exact solution is obtained by replacing ξ' by ξ'' where

$$\xi'' = \left[\frac{1}{N^2} - 1 + 2(1+2N_{Kn}) \ln N \right]^{-1} \qquad 1.47$$

A comparison between equations 1.30, 1.47 and the computer solution for $N_{St} = 0.01$ is shown in table 1.13. At high values N_{Kn} and α the discrepency between equation 1.30 and the other two methods is severe. Although this is partly due to the use of $(\pi/4\alpha)^{1/2}$ for N in the computer solution and equation 1.47 and $(1/\alpha)^{1/2}$ in equation 1.30 the main reason is the simplifications made in deriving ξ'.

It is clear that the influence of N_{Kn} is not strong for N_{St} values above 0.1. However, in a rarefied system the particle Knudsen number will be significant. This influence is taken into account in the inertia parameter which includes the Cunningham correction.

1.2.6. Generalisation

This section has been concerned primarily with the combined mechanisms of inertial interception and field forces. The procedure which has been adopted by many authors (46) to describe the effect of these combined mechanisms is to assume that the contributions due to the individual mechanisms are additive, so that

$$\eta = \eta_{IR} + \eta_F \qquad 1.49$$

This assumption was tested by determining the value of K in the equation

$$\eta = \eta_{IR} + K\eta_F \qquad 1.50$$

as a function of N_{St}. The results are shown in fig. 1.20. The scatter is large, but K is constant up to a value of N_{St} of about 0.5; therefater it reduces to zero approaching that value when N_{St} is about 8.0. Obviously as the particle inertia is increased this mechanism becomes sufficiently strong to override any other. It is obvious then that the mechanisms are not additive and that the single fibre efficiency will be more correctly represented by equation 1.49 where K has the value shown in fig. 1.20.

Where there are no field forces the computed data shown in table 1.5 are well fitted by the following expression:-

$$\eta_{IR} = \eta_R + (1 + N_R - \eta_R)\left\{1 - \frac{1}{0.45 + 1.4\alpha + (1.3 + 0.5\log_{10}\alpha)N_{St}}\right\}$$

$$\text{for} \quad 0.45 + 1.4\alpha + (1.3 + 0.5\log_{10}\alpha)N_{St} \geq 1.0 \qquad 1.50$$

$$\eta_{IR} = \eta_R$$

$$\text{for} \quad 0.45 + 1.4\alpha + (1.3 + 0.5\log_{10}\alpha)N_{St} < 1.0$$

where η_R is given by equation 1.47.

It is convenient to use the Happel-Kuwabara flow field in this study since expressions for the collection efficiency due to each of the collision mechanisms and for combined mechanisms can now be expressed using the same field. These expressions are summarised.

1.2.7 Distribution of Fibre Spacing

The flow model used hitherto is that of a cell which is

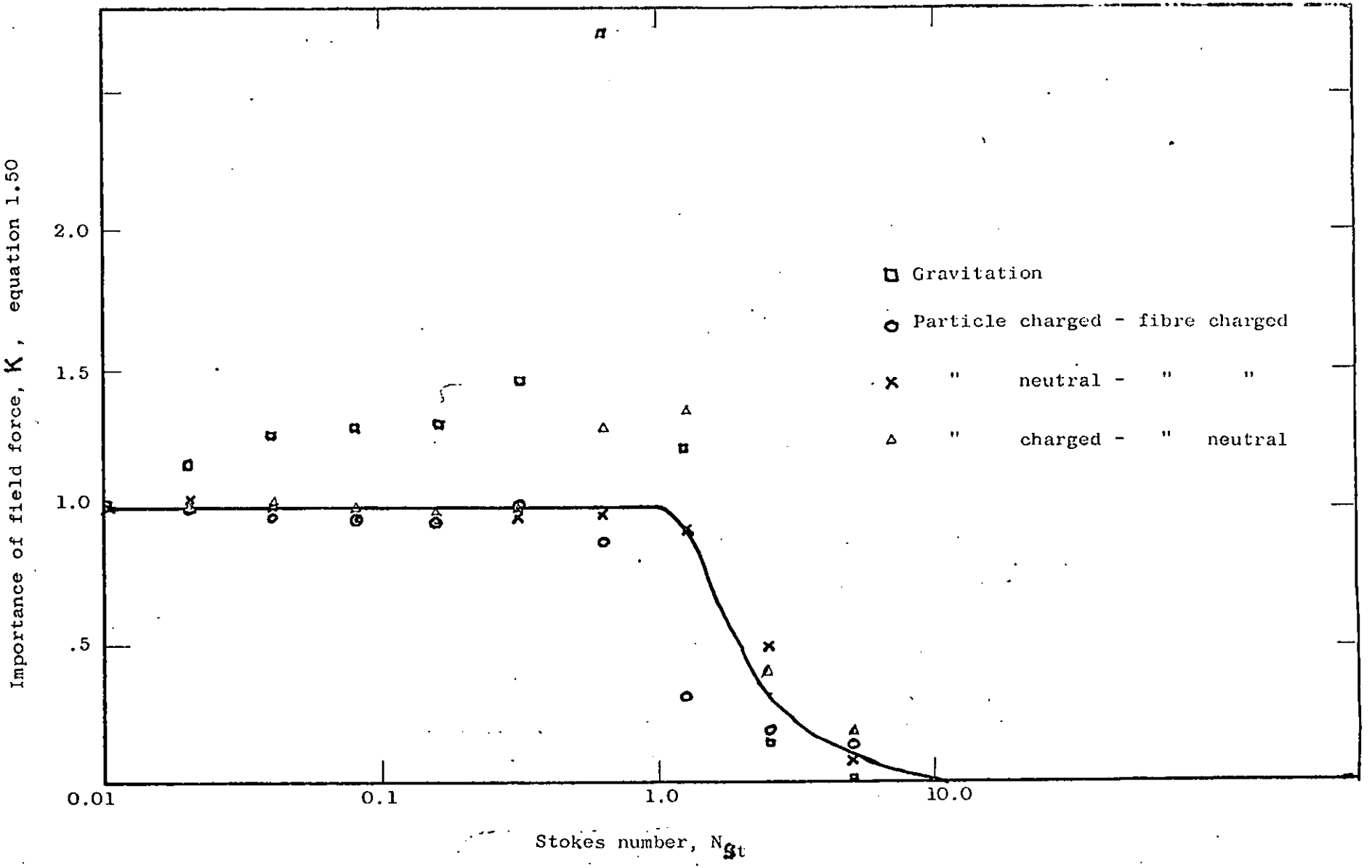

Influence of field forces on inertial interception.

Fig. 1.20

taken to represent the average properties of the filter so that:-

$$\bar{\eta} = f^{n}(\alpha, \bar{U}_0) \qquad 1.51$$

for the cell.

In fact there will be a wide distribution of fibre spacing which will cause the true efficiency normally to be less than that calculated. The model described below is designed to take this into account by introducing a distribution of cell sizes.

Assumptions:-

(i) Each cell can be treated as a single entity in all aspects except that the velocity through the cell is effected by the distribution of cell sizes. The zero shear stress boundary condition still applies. This is an oversimplification and highlights one of the basic faults of cell models.

(ii) The pressure gradient through each cell is constant.

(iii) The filter can be represented in depth as a series of thin filter zones interspersed by mixing zones as shown below.

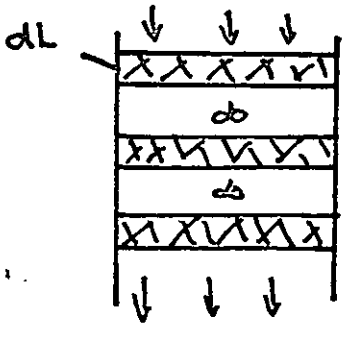

fig.1.21

dL is the volume of filter (unit cross sectional area) containing length of fibre

(iv) The fibres are monosized.

(v) The volume distribution of packing densities, $V(\alpha)$, in the filter is log normal.

This model will not predict the influence of pore size distribution on the behaviour of a filter with depth.

Consider a uniform filter in which the average efficiency, critical trajectory start point, interstitial velocity and packing density are $\bar{\eta}$, $\bar{y}_o$, $\bar{U}_o$ and $\bar{\alpha}$. Then the length of fibre, l, in a filter of volume dL is $\frac{\bar{\alpha}\, dL}{\pi r_f^2}$.

Hence volume of air filtered, $dc = 2\bar{y}_o \bar{U}_o l = \frac{2\bar{y}_o \bar{U}_o \bar{\alpha}\, dL}{\pi r_f^2}$

Volume air passing through filter (since $\bar{U}_o = \frac{Q}{(1-\bar{\alpha})}$ by definition)

$$= \bar{U}_o(1-\bar{\alpha})$$

$\therefore$ Fraction of particles removed

$$= -\frac{dc}{c} = \frac{2\bar{y}_o \bar{U}_o \bar{\alpha}\, dL}{\pi r_f^2 \bar{U}_o (1-\bar{\alpha})} = \frac{2\bar{\eta}\,\bar{\alpha}\, dL}{\pi r_f (1-\bar{\alpha})}$$

This expression may be used as a definition of the average efficiency, $\bar{\eta}$.

Consider now a distribution of packing densities, $l(\alpha)$ along the length of the fibre. The fraction of length having a density between α and $\alpha+d\alpha$ is $l(\alpha)\,d\alpha$, consequently the volume of air filtered with density between α and $\alpha+d\alpha$ is $2y_o(\alpha)U_o(\alpha)l.l(\alpha)\,d\alpha$

and
$$-dc = \int_0^1 \frac{2 y_o(\alpha)\, U_o(\alpha)\, l(\alpha)\, \bar{\alpha}\, dL}{\pi r_f^2}\, d\alpha \qquad 1.53$$

Hence
$$-\frac{dc}{c} = \frac{2\bar{\alpha}\, dL}{\pi r_f^2 \bar{U}_o(1-\bar{\alpha})} \int_0^1 \eta(\alpha)\, U_o(\alpha)\, l(\alpha)\, d\alpha \qquad 1.54$$

Comparing 1.52 and 1.54 :-

$$\bar{\eta} = \frac{1}{\bar{U}_o} \int_0^1 \eta(\alpha)\, U_o(\alpha)\, l(\alpha)\, d\alpha \qquad 1.55$$

A volume distribution of packing densities, $V(\alpha)$, in a filter is now defined such that the fraction of volume of the filter having a packing density between α and $\alpha+d\alpha$ is $V(\alpha)\,d\alpha$. Since the length of fibre contained in the volume $V(\alpha_i)$ of filter is $4\alpha_i V(\alpha_i)/\pi d_f^2$ it follows that for a filter containing single sized fibres

$$l(\alpha) = \frac{\alpha}{\bar{\alpha}} V(\alpha) \qquad 1.56$$

The average packing density, $\bar{\alpha}$, used in the above and in the description of filter properties is the volume average density so it is more convenient to express 1.55 in terms of $V(\alpha)$ rather than $l(\alpha)$:-

$$\bar{\eta} = \frac{1}{\bar{\alpha}\,\bar{U}_0} \int_0^1 \alpha\, \eta(\alpha).\, U_0(\alpha).\, V(\alpha)\, d\alpha \qquad 1.57$$

An alternative derivation of 1.57 is given in appendix I. To obtain a solution of equation 1.57 $\eta(\alpha)$, $U_0(\alpha)$ and $V(\alpha)$ must be expressed in terms of the mean values and some distribution function of α.

(a) Single fibre efficiency, $\eta(\alpha)$

Equation 1.50 is used to describe $\eta = f^n(N_{St}, N_R, \alpha)$ where N_{St} is given by

$$N_{St} = \frac{U_0(\alpha)}{\bar{U}_0} \bar{N}_{St} \qquad 1.58$$

(b) Velocity, U_o

It is now assumed that the flow rate through a cell is such that the pressure gradient in the main direction of flow is the same for each cell. This assumption is equivalent to using a parallel flow model like that of Dawson (see section 1.1.3) between each mixing stage. Hence for each cell, or zone of uniform packing density, the drag force per unit cell volume is constant or

$$\text{Pressure gradient} \propto \left(\frac{\alpha U_o}{\xi}\right) = \left(\frac{\alpha U_o}{\xi}\right)_i = \overline{\left(\frac{\alpha U_o}{\xi}\right)} \qquad 1.59$$

The flow rate, Q, is given by

$$Q = \bar{U}_o A(1-\bar{\alpha}) = U_o \frac{V(1-\bar{\alpha})}{dL} = \int_A (1-\alpha) U_o \, dA = \frac{1}{dL}\int_0^1 U_o (1-\alpha) V . V(\alpha)\, d\alpha \qquad 1.60$$

$$\therefore \bar{U}_o = \frac{1}{(1-\bar{\alpha})}\int_0^1 (1-\alpha) U_o . V(\alpha)\, d\alpha = \left(\frac{\alpha U_o}{\xi}\right)\frac{1}{(1-\bar{\alpha})}\int \frac{(1-\alpha)\xi V(\alpha)\, d\alpha}{\alpha} \qquad 1.61$$

$$\therefore \frac{U_o}{\bar{U}_o} = \frac{(1-\bar{\alpha})\xi}{\alpha\int_0^1 \frac{(1-\alpha)\xi . V(\alpha)\, d\alpha}{\alpha}} = \frac{\xi}{\alpha} C(\bar{\alpha}, \sigma_g) \qquad 1.62$$

The value of ξ for the Kuwabara field is used.

(c) Packing density distribution, $V(\alpha)$

For the purpose of this calculation it is assumed that the distribution of $V(\alpha)$ is log normal:-

$$V(\alpha)\,d\alpha = \frac{1}{\sqrt{2\pi}\ln\sigma_g}\exp\left\{-\left(\frac{\ln\alpha + \ln\bar{\alpha} - 0.5\ln^2\sigma_g}{2\ln^2\sigma_g}\right)^2\right\}\frac{d\alpha}{\alpha} \qquad 1.63$$

since by (67), the geometric mean, $\bar{\alpha}_g$, is related to the arithmetic mean, $\bar{\alpha}$, by

$$\ln\bar{\alpha}_g = 0.5\ln^2\sigma_g - \ln\bar{\alpha} \qquad 1.64$$

Theoretical work on the structure of random fibrous beds by Piekaar and Clarenburg (62) and Corte (68) indicates that the distribution of fibre spacing (fibres per unit volume, which is proportional to α), $V(\alpha)$, and of the hydraulic radius of the pores, $V(p)$, is log normal. It was further shown (68) that the geometric standard deviation of the pore size, σ_{gp}, is independent of the mean. If the packing density is small, then it can be related to the pore size, p, by $\alpha = \text{const}/p^2$ and it can be shown that if $V(p)$ is log normal, then $V(\alpha)$ is log normal.

Shirato et al (69) determined the pore size distribution of paper using mercury porosimetry. Log probability plots of the volume fraction oversize against pore size using their data show a linear relationship above 20%; below this the log normal function underestimated the fraction of small pores. Since the flow through the smallest pores is only an extremely small fraction of the total the deviation is unimportant. Hence the use of a log normal function for $V(\alpha)$ is in agreement with their experimental data as well as existing theoretical work.

The photographs in fig 1.22 illustrate the randomness of the structure of a real filter. A packed bed of black fibres (1 mm diameter and 4 cm long) was constructed by throwing them at

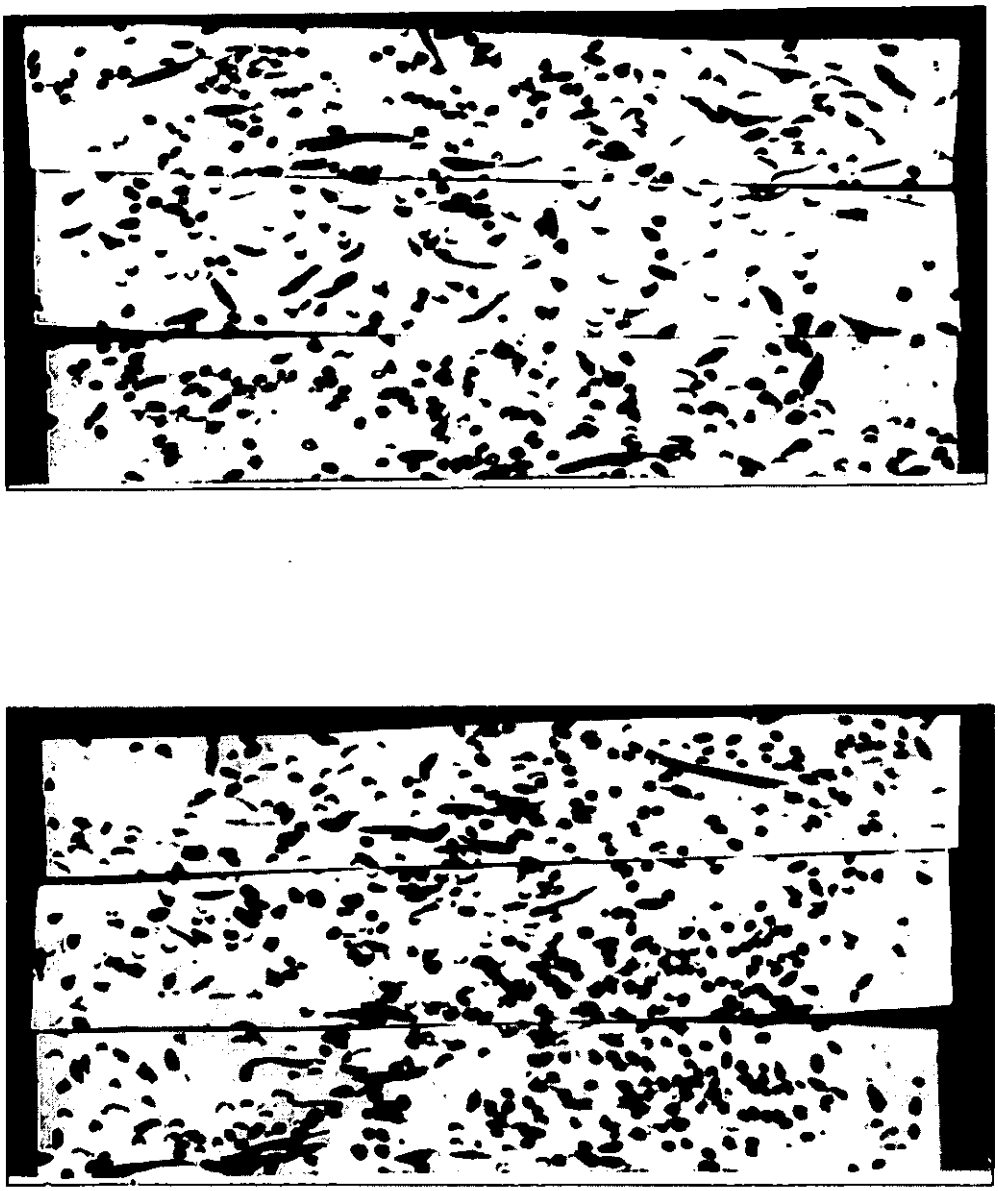

Photographs of sections of filter.

Figure 1.22

random into a 10 cm diameter container. The bed was compressed using a top plate and impregnated with hot Araldite to which had been added TiO_2 pigment. After coding the bed was disected and the sections polished and photographed. A convenient method of measuring the uniformity of packing from section photographs is to measure the area density (1- area porosity) as a function of the sample size. The area density and distribution of area densities measured using this technique will be the same as the packing density, α, and $V(\alpha)$ if the fibres are randomly arranged in the horizontal plain. The area densities were measured using a line scanning analyser (the Quantinet 740). The average area packing density of each sample is shown in fig. 1.22. The σ_g of the packing densities is shown in table 1.14 below as a function of the area sample size.

TABLE 1.14

σ_g of area densities	1.0	1.45	1.77	2.05	2.15
No. of sub areas	1.0	24	48	96	-
No. of fibres per sub area (average)	125	5.2	2.6	1.3	1.0

Measure of structure uniformity - sample 1.

A σ_g of 2.15 is obtained for a sample area which is large enough on average to contain one fibre. Analysis of the work of Shirato et al (69) suggests that σ_g is in the range 1.6 - 2.3. Defining the hydraulic radius as the ratio of the surface area and the perimeter of a polygon in a theoretically simulated random filter Piekaar and Clarenburg (61) used a σ_{gf} of 1.9 in their work which is

equivalent to a σ_g of 3.3.

To obtain a useful measure of σ_g as a function of α, using the above technique the length to diameter ratio of the fibres, fibre strength, position in the bed and other variables should be taken into account. A large number of samples would have to be prepared to obtain statistically significant results. The photographs in fig. 1.22 are typical examples; they show clearly the shortcomings of using a cellular model, even with a distribution of cell sizes, in a description of the system. However, there is no better method at present available.

Results

The above expressions were integrated numerically to obtain an estimate of the effect of σ_g on the efficiency of inertial interception in a filter. The results for an interception parameter of 0.05 are given in table 1.15 and in figures 1.23 and 1.24. Figure 1.24 shows the effect of σ_g on the efficiency for three values of N_{st}.

At high ($>$ 10.) and low ($<$ 0.5) values of N_{st}, where the efficiency is not sensitive to changes in velocity, the efficiency must be reduced by increasing σ_g. This is because most of the flow passes through zones of low packing density in the filter and the number of fibres effectively exposed to aerosol flow is reduced. At intermediate values of N_{st} it is possible for $\bar{\eta}$ to increase with σ_g as is shown in fig. 1.24. Here, when a low density zone of the filter is exposed to a higher than average gas velocity, the filtration efficiency may be greatly increased due to an increase in Stokes number. This increase may be sufficient to outweigh any decrease due to a reduction in number of fibres exposed to the flow. An example of this behaviour is shown in fig. 1.24.

TABLE 1.15

σ_g	α	N_{St} 0.1	0.5	1.0	2.5	5.0	10.0	50.0
1.0	0.01	.0014	.0014	.0014	.1867	.5164	.7475	.9822
1.1		.0014	.0014	.0014	.1807	.5042	.7312	.9622
1.2		.0014	.0014	.0014	.1557	.4759	.7033	.9370
1.5		.0011	.0011	.0011	.0657	.3295	.5440	.7771
2.0		.0007	.0007	.0007	.0007	.0847	.2445	.4750
2.5		.0004	.0004	.0004	.0004	.0004	.0446	.2063
5.0		.0002	.0002	.0002	.0002	.0002	.0002	.0342
1.0	0.03	.0021	.0021	.0333	.4801	.7211	.8718	1.0118
1.1		.0021	.0012	.0375	.4696	.7084	.8583	.9979
1.2		.0020	.0020	.0455	.4427	.6758	.8234	.9621
1.5		.0016	.0016	.0456	.3215	.5237	.6586	.7913
2.0		.0010	.0010	.0151	.1498	.2828	.3870	.5024
2.5		.0006	.0006	.0006	.0464	.1274	.2023	.2984
5.0		.0001	.0001	.0001	.0001	.0001	.0030	.0310
1.0	0.06	.0029	.0029	.1940	.5861	.7869	.9090	1.0201
1.1		.0029	.0029	.1877	.5737	.7724	.8937	1.0045
1.2		.0028	.0046	.1733	.5422	.7354	.8546	.9645
1.5		.0022	.0145	.1285	.4028	.5672	.6741	.7781
2.0		.0013	.0103	.0648	.2075	.3149	.3937	.4798
2.5		.0007	.0010	.0234	.0993	.1658	.2206	.2877
5.0		.0001	.0001	.0009	.0001	.0010	.0080	.0287
1.0	.10	.0041	.0041	.2976	.6462	.8222	.9283	1.0242
1.1		.0040	.0177	.2897	.6318	.8054	.9107	1.0064
1.2		.0038	.0308	.2700	.5954	.7632	.8863	.9611
1.5		.0029	.0435	.1928	.4399	.5782	.6682	.7566
2.0		.0016	.0280	.0967	.2291	.3178	.3808	.4502
2.5		.0009	.0113	.0445	.1159	.1706	.2137	.2654
5.0		.0001	.0001	.0001	.0001	.0038	.0115	.0262
1.0	.15	.0057	.1042	.3755	.6874	.8453	.3406	1.0268
1.1		.0056	.1016	.3658	.6705	.8258	.9201	1.0061
1.2		.0052	.0978	.3419	.6284	.7770	.8688	.9537
1.5		.0038	.0819	.2424	.4562	.5733	.6504	.7277
2.0		.0022	.0450	.1179	.2358	.3081	.3590	.4160
2.5		.0011	.0207	.0562	.1203	.1657	.1998	.2406
5.0		.0001	.0001	.0001	.0014	.0065	.0128	.0237

Influence of distribution of fibre spacing on average single fibre efficiency, $\bar{\eta}_{IR}$ ($N_R = 0.05$)

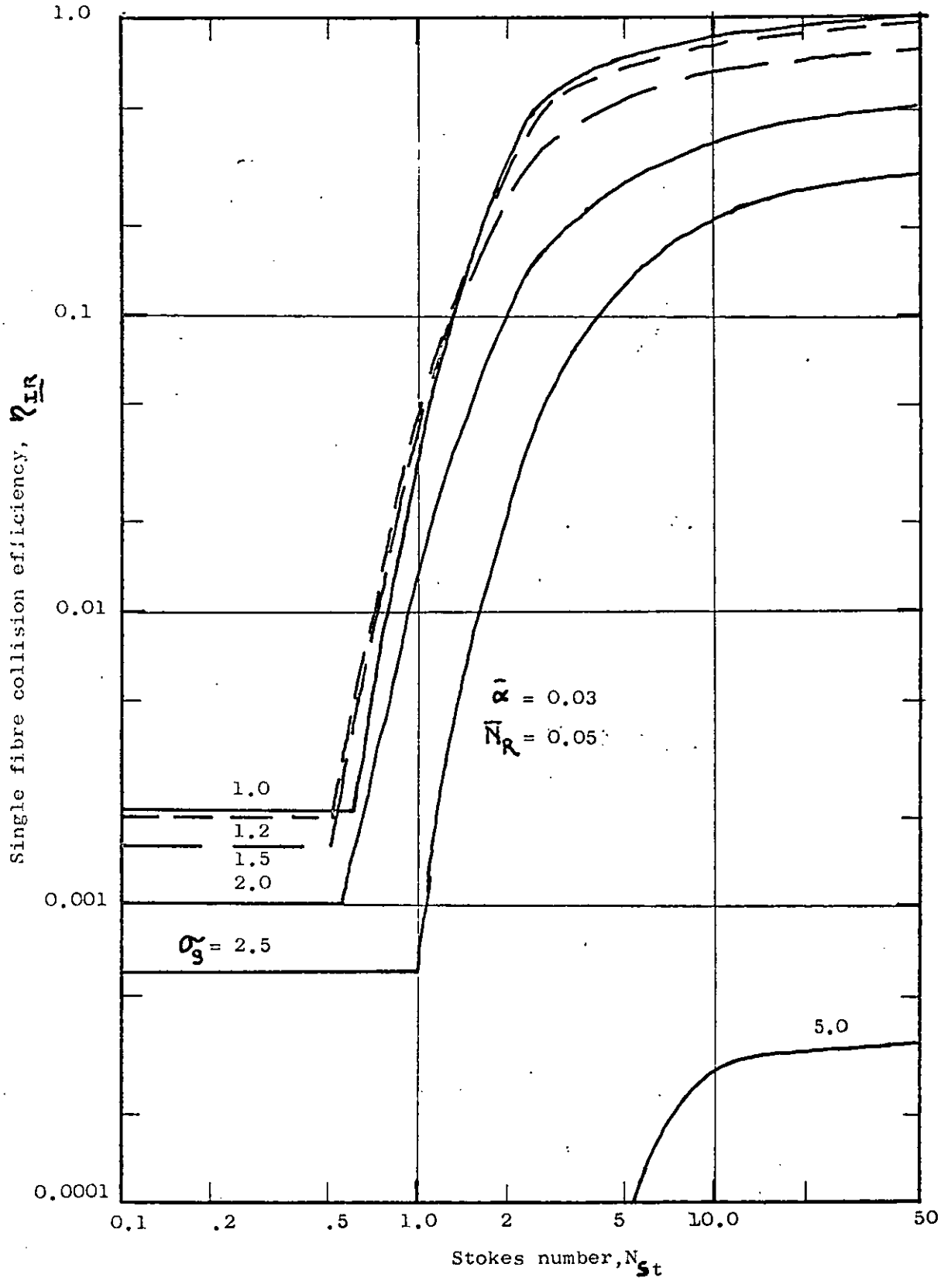

Influence of distribution of packing density on efficiency.

Fig. 1.23

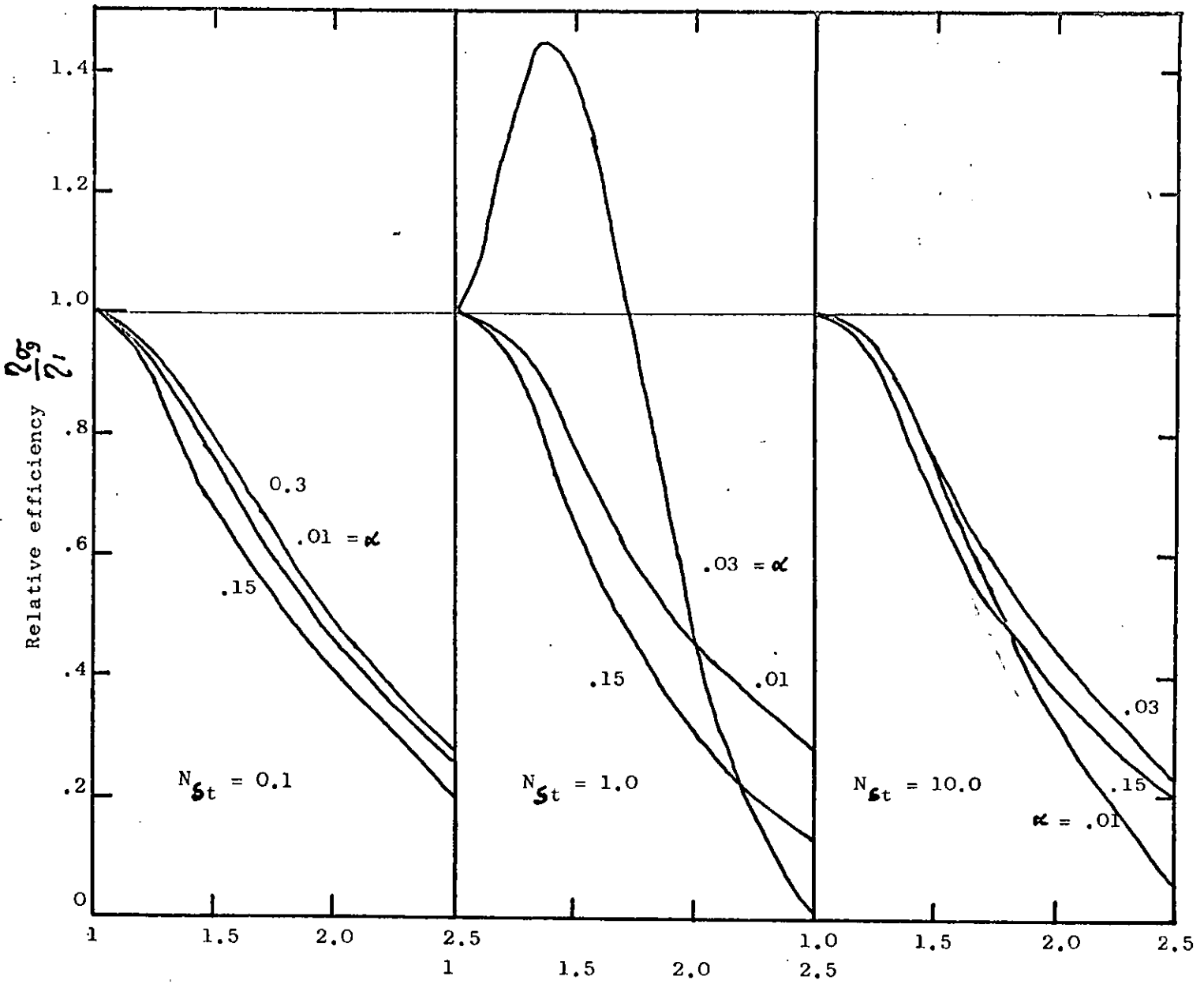

Geometric standard deviation, σ_g

Influence of distribution of packing density on efficiency.

Fig. 1.24

The numerical value of σ_g which should be used is difficult to determine directly. It will be a function of the physical properties of the fibres constituting the filter (i.e. length, flexibility etc) as well as the manner in which the filter is constructed. The experimental determinations described above indicate a value in the region of 1.6 - 2.3. An indirect, but simple method of measuring σ_g is to measure the filter pressure drop.

The pressure drop across a filter relative to that with a uniform packing density is given by the ratio

$$\frac{\Delta p_{\sigma_g}}{\Delta p_1} = \frac{c(\bar{\alpha}, \sigma_g)}{c(\bar{\alpha}, 1)} \qquad 1.65$$

Computed values of this ratio are shown in table 1.16 and figure 1.25. It can be seen that the pressure drop ratio falls off with σ_g at approximately the same rate as the efficiency ratio. These results will be discussed further in section 1.2.8.

In the above theory it is assumed that all the fibres have their axes normal to the direction of flow but, of course, in practice this is not the case. These fibres which are in line with the flow will contribute less than those normal to the flow to the pressure drop and will not contribute at all to the efficiency of collection in the inertia region. Hence in the worst possible case, that of an isotropic structure, the efficiency will be reduced to

TABLE 1.16

σ_g	α				
	.01	.03	.06	.10	.15
1.1	.9911	.9847	.9823	.97931	.9753
1.2	.9524	.9454	.9372	.9269	.9135
1.5	.7871	.7609	.7315	.6968	.6548
2.0	.5059	.4624	.4202	.3753	.3272
2.5	.2756	.2689	.2358	.2008	.1663
5.0	.1210	.0457	.0270	.0182	.0127

Influence of filter uniformity on pressure drop, $\Delta p_{\sigma_g} / \Delta p_1$.

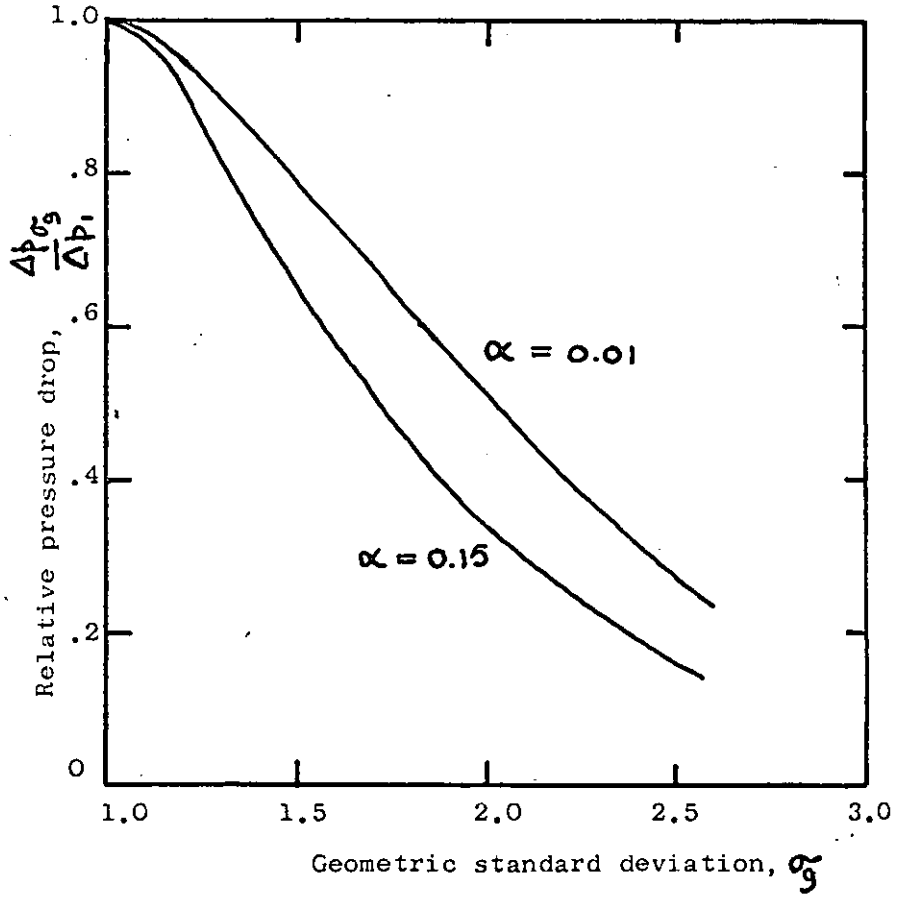

Influence of distribution of fibre spacing on pressure drop.

Fig. 1.25

two thirds of that described above.

Unlike Dawson's theory which is based on the idea that channels of constant packing density extend through the depth of the filter, it is assumed above that there is perfect mixing of the gas stream after it has passed through each of a series of thin strips. Clearly these two models represent limiting cases and the truth will lie between them. Nevertheless it is considered that the present model is the more realistic because constant density channels are not common in a filter, as is supported by the photographs in fig.1.22, and the present model retains the concept of a single fibre efficiency which does not vary with depth. This concept is extremely useful and is in agreement with experimental findings.

The only experimental work on the effect of filter uniformity on efficiency is that of Harrop (4) who showed (see fig. 1.6) that lack of uniformity reduces the efficiency in the inertial region by a factor of about 2.0. Comparing this result with the above theory (see fig. 1.24) it suggests a σ_g of about 1.8-2.0 for Harrops "real" filters.

1.2.8 Filter Pressure Drop

The pressure drop across a filter is easy to determine and provides an excellent measure of the applicability of a flow field. The results of many measurements of the influence of packing density and Reynolds number are available.

A suitable method of comparing results of low Reynolds number systems is to use the dimensionless drag for unit fibre length, F_f^* defined by Fuchs and Kirsch (70):-

$$F^* = \frac{\Delta p}{U_0 \mu l} = \frac{\Delta p \, \pi d_f^2}{4 U_0 \mu \alpha L} = \frac{4\pi}{\xi} \qquad 1.66$$

where l is the length of fibre and L the filter depth. Experiment and theory are compared in terms of filter packing density in table 1.17 below. The ratio of drag to that predicted from the Kuwabara model is used. The experimental values used are those of Harrop (4) who used monosized glass fibres (20 μm diameter) (the results were extrapolated to zero Reynolds number), and those of Kimura et al (71) who also used filters of very narrow fibre size distribution. The table shows that not only does theory overestimate the drag by a factor of 2-3, but it overestimates the effect of α on the results.

In fig. 1.26 the Kuwabara predictions corrected for cell size distribution effects are compared with experimental results. The results are consistent with a σ_g of about 2.0 which is in agreement with other observations. More significantly, the behaviour with respect to packing density is in agreement with experiment.

TABLE 1.17

Filter Resistance (F^* /F^* Kuwabara)

Filter packing density (α)		0.03	.06	.08	.11	.15
Happel	Theoretical	.82	.79	.78	.76	.75
Spielman and Goren (21)	Theoretical	.74	.74	.67	.73	.75
Tomatiki and Aoi (7)	Theoretical	.91	.85	.85	.81	-
Harrop (4)	Experimental	.61	.46	.45	.38	.31
Kimura et al (71)	Experimental	.43	.40	.38	.32	.27

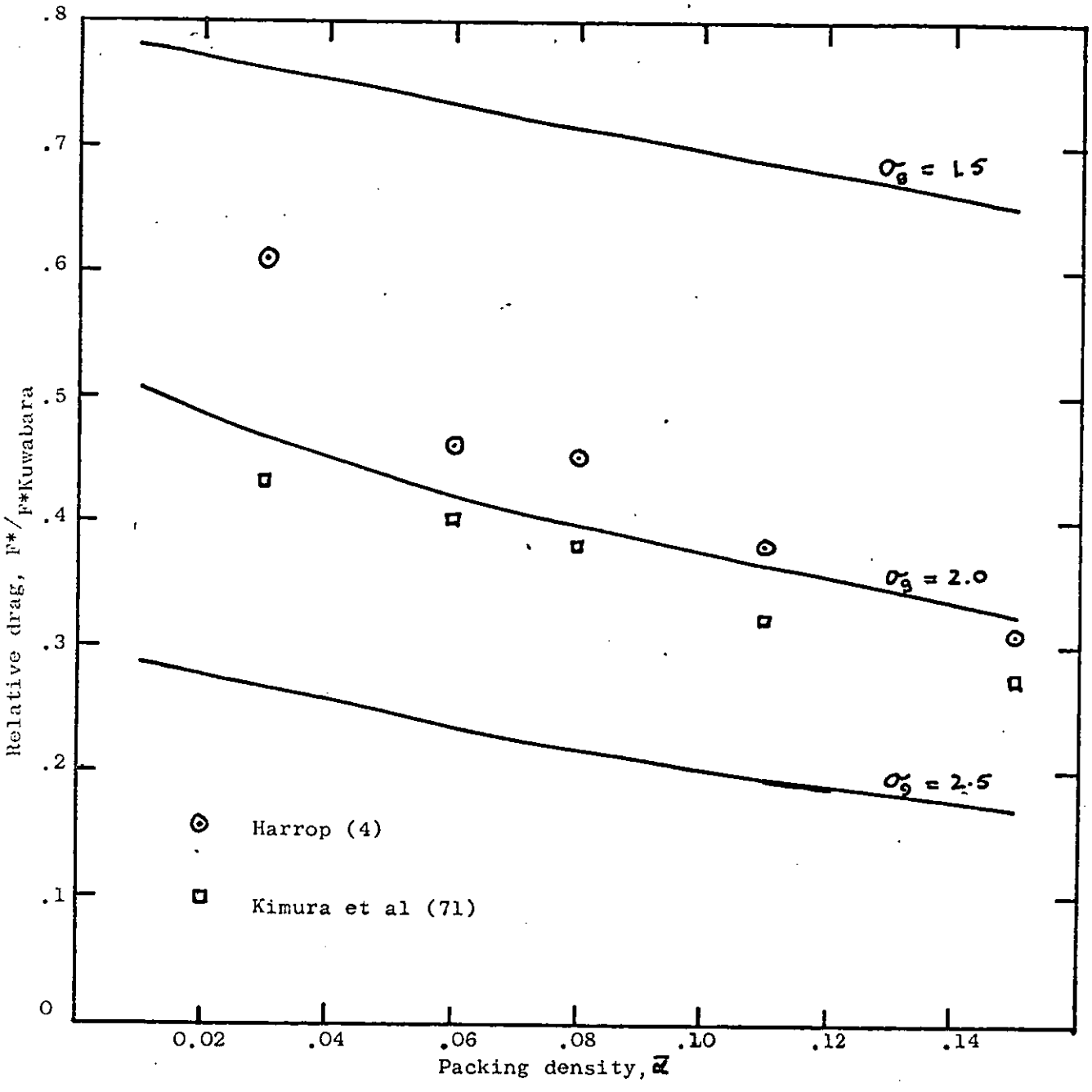

Influence of packing density on relative pressure drop.

Fig. 1.26

The results of Werner and Clarenburg (63) have not been used in the present analysis; they found a 5 fold increase in pressure drop but used filters consisting of very wide distributions of fibre size.

The influence of fibre Reynolds number on resistance provides a guide to the range of conditions under which the laminar flow assumption is applicable. The results of Kimura et al (71) show a linear relationship between drag and velocity up to a Reynolds number of at least 1.0. Harrop's (4) measurements of the resistance of real and model filters confirms that the linear relationship exists up to a Reynolds number of 1.5 for a 3% packing density: the range is extended for higher packing densities as would be expected.

1.2.9 Conclusions

The theory of fibrous filtration has been extended mainly by the calculation of particle trajectories in the cellular flow field. A model which takes into account the distribution of fibre spacing within a filter has been described. The following conclusions arise from the work:-

(i) The influence of fibre Reynolds number on inertial interception has been investigated using the Davies flow field.

(ii) Use of the cell model gives a convenient method of examining the influence of packing density on collision efficiency. However, it introduces a dilemma as to which particle trajectory starting condition to use (i.e. main stream or outer cell boundary velocity). The effect is not very important for systems where N_{st} is not large (< 5).

(iii) The results for interception only agree with the theory of

Kirsch provided a modified value of f' is used in his equation.

(iv) The collision efficiency due to electrostatics is calculated using the cell model. For the case of charged particle - neutral fibre the results agree with published experimental data. No data is available on the other cases studied. An increase in packing density may lead to a reduction in efficiency due to electrostatics.

(v) The results agree with existing theories for the effect of sedimentation and fibre Knudsen number on interception.

(vi) The efficiency due to the combined mechanisms of inertial interception and electrostatics and inertial interception and gravitation have been calculated. The effect of fibre Knudsen number on inertial interception has been calculated. The contributions due to the individual mechanisms are not additive.

(vii) A theory which takes into account variations in local packing density with a filter is presented. It predicts a reduction in pressure drop due to filter non uniformity. It is shown that an increase in the geometric standard deviation, σ_g, of packing density normally causes a reduction in filtration efficiency although in some cases (intermediate values of N_{st}) an increase can result.

CHAPTER 2

Particle Retention Efficiency

1. Removal Froces

1.1 Mechanisms

2. Adhesion Forces

2.1 London van der Waal forces

2.2 Electrostatics

2.3 Capillary forces

2.4 Relative magnitude of adhesion forces

2.5 Influence of process variables on adhesion forces

3. Equilibrium Theory

4. Experimental

4.1 Photographic analysis

4.2 Quantitative analysis

5. Results and discussion

6. Conclusions

CHAPTER 2

PARTICLE RETENTION EFFICIENCY

For a fibrous filter to be effective the particles which touch the fibres must adhere subsequently. The efficiency of particle adhesion decreases with increasing particle size and velocity and falls with reduction in fibre size. The object of the study reported in chapter 2 is to investigate the efficiency of particle retention in clean filters i.e. in the regime in which the probability of particle adhesion is low. The mechanisms of particle removal and adhesion are reviewed. The energies of removal and adhesion for the predominant mechanisms are then equated to obtain theoretical values for the critical conditions under which adhesion will fail. These results are used to interpret experimental data obtained by operating filters in the low adhesion regime.

The decrease in filtration efficiency at high particle inertia has been observed by many authors. Becker (72), Whitby (40) and Loffler (73) noted this with particles above 2 μm and velocities above 2 ms^{-1}. Harrop (4) observed the phenomenon with 3 μm particles and velocities of 1 ms^{-1}. Davies (74) has stated that adhesion is not certain with particles above 0.5 μm.

Using a simple microscope technique, Gillespie (75) investigated the influence of filtration velocity (0.05 - 0.26 ms^{-1}) on the efficiency of collection of 2.2 μm and 3.6 μm particles of stearic acid and paraffin wax. He defined a slippage coefficient

which is $(1 - \eta_A)$ and claimed that a minimum in the overall efficiency was due to lack of adhesion, the slippage coefficient going through a maximum. His results could equally be interpreted in terms of a minimum in the collision efficiency. Since the inertia parameter of the system is in the range 0.05 - 0.25 this is possible.

Recently Stenhouse (76) and Freshwater and Stenhouse (77) described the important mechanisms in the "low adhesion" region and reported some preliminary experiments on the influence of the main parameters on filter performance. Walkenhorst (115) showed experimentally that 1 μm particles of coal dust failed to adhere to 300 μm steel fibre at a velocity of 4 ms^{-1}. Loffler (78) has attributed the removal mechanism to bounce and Dahneke (79) and Loffler (39) have equated the adhesion and bounce energies to obtain a particle size at which bounce first takes place.

2.1 Removal Forces

2.1.1 Mechanisms

Removal forces are as follows:-

(i) Forces applied during impact - normal rebound force
- tangential impulse force

(ii) Continuously applied forces - vibration
- drag
- aerodynamic lift
- particle impact
- gravity

Gillespie (75) and Jordan (80) considered two mechanisms of particle removal from filters, namely normal bounce off due to the recovery of normal elastic energy and peel off due to aerodynamic drag. Larsen (81) studied the effect of vibration and found it to be a minor force. Vidal (82) considered that aerodynamic lift was important. The lift force used was

$$L_r = 0.375 \frac{\rho}{2} U_0^2 \pi r_p^2 \qquad 2.1$$

Corn (83) contends that particles are retained on filters in aerodynamically stable positions.

Both Larsen (81) and Loffler (73) report that the velocity of air required to remove deposited particles from a fibre is at least an order of magnitude higher than used in practice, where it is known that particles fail to adhere on first contact.

Impact theory has been well reviewed by Goldsmith (84). The dynamics of normal impact was first analysed for elastic bodies by Hertz (85) who showed that for a sphere colliding with a flat surface,

$$r_c^2 = R Z_0$$

$$t_c = 2.94 Z_0 / U_{pr} \qquad 2.2$$

where $$Z_0 = \left\{\frac{15}{16} m g\right\}^{0.4} R^{-0.2} U_{pr}^{0.8}$$

$$g_1 = (1-\nu_1)/E_1 + (1-\nu_2)/E_2$$

for quartz/steel systems, these expressions simplify to:

$$r_c^2 = 2.05 \times 10^{-3} r_p^{1.2} R^{0.8} U_{pr}^{0.8}$$

$$t_c = 6.05 \times 10^{-3} r_p^{1.2} R^{-0.2} U_{pr}^{-0.2}$$

Table 2.1

Particle Removal Forces ($Nx10^{-5}$) (quartz-steel)

Particle Size, d_p (μm)		1			10			20		
Impact angle, u_r/u_e		0	1	10	0	1	10	0	1	10
Impact velocity	Force									
0.1 m/s	normal impulse	$6x10^{-2}$	$4.6x10^{-2}$	$9.6x10^{-3}$	2.42	1.84	.385	7.5	5.7	1.2
	tangential "	0	$2.3x10^{-2}$	$4.8x10^{-2}$	0	.92	1.92	0	2.85	5.95
	drag	0	10^{-6}	$1.4x10^{-5}$	0	10^{-5}	$1.4x10^{-5}$	0	$2x10^{-5}$	$2.8x10^{-5}$
1.0 m/s	normal impulse	.385	.30	.60	15.4	12.0	2.5	48	37	8
	tangential "	0	.15	.30	0	6.0	12.0	0	19	57
	drag	0	10^{-5}	$1.4x10^{-5}$	0	10^{-4}	$1.4x10^{-4}$	0	$2x10^{-4}$	$2.8x10^{-4}$
10.0 m/s	normal impulse	2.4	2.0	.4	96	80	39	300	250	52
	tangential "	0	1.0	1.9	0	40	76	0	125	235
	drag	0	10^{-4}	$1.4x10^{-4}$	0	10^{-3}	$2.3x10^{-3}$	0	2.10^{-3}	$6.2x10^{-3}$

The oblique impact of macroscopic ellipsoidal particles was studied theoretically by Matsumoto (86) by considering only the overall mechanics of the system. The effect of angle of impact and velocity on the angle of bounce of particles has been determined experimentally by Muschelknautz (87) but no analysis has been undertaken of the detailed physical processes involved in oblique impact or in its significance in particle adhesion or removal.

A detailed theoretical analysis of the physical behaviour of particles during impact is not feasible because the stress distribution in a sphere during oblique impact is not known. Hence only an estimate of the magnitude of the forces acting on particles has been attempted. The results are shown in table 2.1.

In determining the tangential impulse force, it was assumed that all the tangential momentum of the particles was adsorbed in the contact time as calculated from the Hertz theory. This was in the range 10^{-7} to 10^{-8} secs, during which time a particle travelling at the tangential impact speed would travel 10^{-1} - 10^{-2} microns. In each case the calculated lift force is negligible and the drag is less than the impulse force by a factor of 10^{6}. The gravitational force on a micron particles is 5×10^{-5} dynes. These calculations confirm the

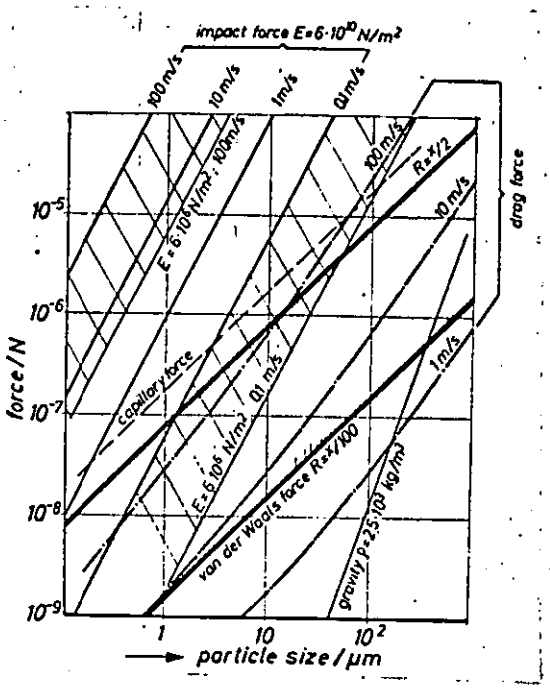

Forces acting between particles and surfaces (87)

Fig. 2.1

estimates of Loffler (88) shown in fig. 2.1. It is feasible that drag forces are important with extremely light particles. Gillespie illustrated this by blowing all the deposited lycopodium spores from a fibre at 3 times the deposition speed. Hence it is concluded that the only forces of any consequence with particles of normal density are these due to the kinetic energy of the particles on impact.

2.2 Adhesion Forces

The three forces responsible for particle adhesion in fibrous filters are van der Waals, electrostatic and capillaric forces. The subject has been well reviewed by Corn (89) and Zimon (90) so it will only be briefly discussed below. Those aspects of the subject which are especially relevant to filtration will be discussed.

2.2.1 London van der Waal forces

The London van der Waal dispersion forces are significant adhesion forces in "dry" filters.

For an undeformed spherical particle adhering to a flat smooth surface, Hamaker (91) and Bradley (92) showed that the adhesion force pressure and energy are:-

$$\overset{\circ}{F} = \frac{A_H R}{6 h^2} \quad ; \quad \bar{p} = \frac{A_H}{6\pi h_o^3} \quad ; \quad \overset{\circ}{E}_a = -\frac{A_H R}{3h} \qquad 2.3$$

where A_H is the Hamaker van der Waals constant and h is the separation distance. This constant lies in the range 10^{-18} -

10^{-20} J (A_H for quartz (4) = 2.2×10^{-19}). Gregory (93) has recently reviewed methods of calculating A_H. In the derivation of these expressions no account was taken of electromagnetic lagging, or retardation, an omission which limits their use to small values of h. Lifshitz (94) extended the theory to allow for this and his expressions tend to 2.3 as h is reduced. A is then related to the Lifshitz van der Waal constant, $\hbar\omega$ by

$$A_H = \frac{3\,\hbar\omega}{4\pi} \qquad 2.4$$

It has been shown experimentally that "non retardation" theories are valid up to a separation of 100Å (95). The Lifshitz theory has been extended by Langbein (96) to include the effect of surface adsorbed layers.

Particle deformation causes an increase in the adhesion force given by 2.3. For smooth particles which have been flattened by impact Gillespie (75) intengrated the London forces to shown that

$$F = 6\pi\epsilon_a R\left[1 + \frac{r_c^2}{3Rh}\right] \; ; \; E_{adhesion} = 6\pi\epsilon_a h R + \pi\epsilon_a r_c^2$$

where

$$\epsilon_a = A_H/36\pi h^2 \qquad 2.5$$

Krupp (97) allowed for local surface deformation, due to creep caused by adhesion forces by adding the undeformed force and the force acting over the contact area:-

$$F = \overset{\circ}{F} + \pi r_c^2 \bar{P} \qquad 2.6$$

He introduced the Hertz theory and creep properties of

the material to obtain an expression for the adhesion force as a function of time. For small particles this reduces to

$$F = \overset{o}{F}\left[1 + \frac{\bar{P}}{H(t)} + \begin{Bmatrix} 0.04 \\ -0.085 \end{Bmatrix} r_p \times 10^{-6}\right] \qquad 2.7$$

for either elastic or non-elastic recovery on particle removal. For values of $r_p < 10\mu m$ the last term is not important. The hardness, H is a reducing function of time so the second term looses its significance as the loading time is reduced. Measurements of H (98) indicate that creep is unimportant during the very short period of contact during filtration.

Deryagin (99) and Sperling (100) have described the process thermodynamically and find that the force is proportional to the radius of curvature. However, shortage of adequate data on surface energies renders their theory of little immediate value.

The van der Waals force acts normal to the surface; Polke (101) measured the normal and tengential force required to remove particles and found that the tangential force was about 1/30th of the normal force.

2.2.2 Electrostatics

Adhesion forces are caused by a difference in potential between the particle and substrate. The particles may already posses a charge before impact or they may acquire a charge on contact.

Adhesion of charged particles

Although an aerosol cloud is neutral individual particles may be quite highly charged. If a particle carries n

electron units, then the adhesion force will be

$$\overset{o}{F} = \frac{n^2 e_1^2}{l^2} \times 10^{-9} = \frac{1}{4\pi\varepsilon_o}\frac{q^2}{l^2} \qquad 2.8$$

where l is the distance between charge centres.

Kunkel (30) measured the charge distribution on artificially dispersed mica and showed that the rms charge may be as high as 600 esu on a 10 μm particle. Jordan (80) showed that for the electrostatic adhesion force on such a particle to be the same as the calculated van der Waals force the charge would have to be concentrated within 0.01 μm of the contact. A number of particles in a cloud may have extremely high charges, in the order of several thousand e.s.u; in such cases electrostatic adhesion may be important. In normal filtration, however, these forces will not be significant.

Contact charging

Two surfaces which are placed together will undergo contact charging which may cause large electric double layer forces. Such forces have been studied by Krupp (97) who showed that

$$\overset{o}{F} = \frac{q^2 \ln\left(1 + \delta_1/h\right)}{16\pi\varepsilon_o r_p \delta_1 \left\{\gamma_1 + \frac{1}{2}\ln\left(\frac{2r_p}{h}\right)\right\}\left\{\gamma_1 + \frac{1}{2}\ln\left(\frac{2r_p}{h+\delta_1}\right)\right\}} \qquad 2.9$$

where δ_1 ranges between 0 for a conductor to 1 μm for an insulater. Krupp showed that in the case of very high (although realistic) contact potentials the electrostatic force could be much higher than the van der Waals force for particles with surface asperities. The adhesion energy for conducting systems is

$$\mathring{E} = 2\pi\varepsilon_0 r_p U^2 \left[\gamma + \tfrac{1}{2}\ln\left(\frac{2r_p}{h}\right)\right] \qquad 2.10$$

where U is the contact potential, the difference in work functions of the two materials. With a metal/metal contact a double layer will be set up almost instantly, but with a metal/semi-conductor the time required for an electron flow to be set up may be very long (102). With an insulator (such as silica) an electron flow will not be set up.

2.2.3 Capillary Forces

Surface tension forces may be responsible for very large adhesion forces in filters, particularly where the fibre is coated with a light oil or where there is a high relative humidity.

In the case of a sphere touching a flat plate the adhesion force is (103, 104).

$$\mathring{F} = 4\pi\sigma R \qquad 2.11$$

where σ is the surface tension. For two spheres, the force is $2\pi\sigma R$. Experimentally the force is found to be only slightly lower than this (90). The energy of adhesion is simply given by:

$$\mathring{E}_{adhesion} = A_c\sigma \qquad 2.12$$

where A_c is the total area of contact. This reduces to

$$\mathring{E}_{adhesion} = 4\pi\sigma r_1 R \qquad 2.13$$

where r_1 and R are the radii of curvature of the meniscus and particle.

In the case of a particle which is flattened on contact, simple geometrical reasoning shows that the contact area will be given by

$$A_c = \pi r_c^2 + 4\pi r_1 \left(R - r_c^2/4R \right) \qquad 2.14.$$

where r_c is the radius of contact in the absence of liquid.

Capillary condensation is not instantaneous; hence in this case the adhesion force is time dependent (90) it requiring about 30 minutes for equilibrium to be attained. It is significant at relative humidities in excess of 65% but Zimon (90) is of the opinion that at lower humidities capillary condensation plays no part in adhesion.

Zimon (90) has studied the influence of depth of oil coating on the adhesion force. He identified three zones; the force initially increases rapidly with depth, the depth has no effect and finally when the depth is of the same order as the particle radius, there is a slight reduction in force. For thin layers on fibres, the influence was studied theoretically by Larsen (81) who confirmed his results experimentally for spherical particles of size greater than 100 μm.

$$F = 4\pi k \sigma r_p$$

$$\text{where} \quad k = \left[k_d / (k_c^2 + k_d^2)^{\frac{1}{2}} + 1/(k_c^2+1)^{\frac{1}{2}} \right] \Big/ \left[2/k_d + 2 \right]$$

$$k_c = \frac{\text{liquid contact diameter}}{\text{sphere diameter}} \qquad 2.15$$

$$k_d = \frac{\text{fibre diameter}}{\text{sphere diameter}}$$

Zimon studied the influence of impact velocity on the adhesion force with a thick (10 μm) layer of oil. He used a wide particle size distribution so his results are of little value except that

they show that the force varies with velocity to a power less than one fifth.

2.2.4 Relative magnitude of adhesion forces

It is pertinent at this stage to consider the magnitude of adhesion forces arising from the various mechanisms. Theoretical values of the forces for quartz particles and a steel plate are shown as a function of particle size in Table 2.2. These calculations are in general agreement with the estimates of Loffler (73) (see fig. 2.1). It can be seen that capillary forces are most significant and will outweigh all others when the surface is coated or at high relative humidities. In dry systems van der Waal forces will generally be much more significant than electrostatic forces which are only important in the following cases:-

(a) Very large difference in work functions between the solids - this will not normally occur.

(b) Very high individual particle charges - the charges assumed to obtain the values in table 2.2 are much higher than those normally obtained in practice.

(c) The particles have surface asperities - the van der Waals forces are short range compared with electrostatic forces. Van der Waals forces will, therefore, be highly dependent on the radius of curvature at the contact, whilst the electrostatic forces will remain dependent on the particle size.

In his work on adhesion in fibrous filters, Loffler (73) concluded that van der Waals forces were responsible for the adhesion between quartz particles and polyester fibres. Larsen (81) and Gillespie (75) also concluded that molecular forces were predominant in their experiments. However, in the work reported by Kordecki and Orr (105) it is obvious that electrostatic forces are highly

significant.

TABLE 2.2

THEORETICAL ADHESION FORCES DUE TO VARIOUS MECHANISMS ($N \times 10^{-5}$)

Force	1μm	10μm	20μm
Van der Waals $R = r_p$ $R = 0.1\mu m$	0.021 .002	0.21 .002	0.42 .002
Electrostatic (i) Coulomb Force (charge density of 1 esu on a 1 μm particle) $l^2 = r_p^2$ $l^2 = h r_p$	 7×10^{-11} 1.2×10^{-8}	 7×10^{-7} 5×10^{-3}	 3.8×10^{-5} 1.9×10^{-2}
(ii) Contact charging maximum quartz-steel	10^{-3} -	10^{-2} negligible	2×10^{-2} -
Capillaric forces water $R = r_p$ $R = 0.1\mu m$	4.6×10^{-2} 9.2×10^{-3}	4.6×10^{-1} 0.2×10^{-3}	9.2×10^{-1} 9.2×10^{-3}

In ideal systems i.e. spherical particles and smooth surfaces, the calculation of the magnitude of adhesion forces is complex and frequently impossible due to lack of physical data, the presence of adsorbed layers etc. The calculation of the magnitude of the force in a real system where particles have complex shapes probably micro asperities and the "flat" surface is in fact rough, is obviously out of the question. There will be a wide range of adhesion forces for each particle size. Once the particular adhesion mechanism has been ascertained, however, the

theories may be applied to estimate the effect of a number of variables on the mean force or energy of adhesion.

TABLE 2.3

PARTICLE - FIBRE ADHESION FORCES

Experimentally measured adhesion forces (73) ($Nx10^{-9}$) for quartz particles and 50 μm polyester fibres.

Collection velocity (ms^{-1})	particle size (dp) (μm) 5	10	15
0	8	5	20
0.28	8	14	30
0.42	10	24	58
0.63	12	35	100
0.84	14	42	-

For any given condition, particularly in the case of real systems, there will be a wide range of adhesion forces. The number distribution of adhesion forces measured by Loffler is log-normal, 68% of the particles lying within a range of about 1.5 orders of magnitude (the figures referred to in table 2.3 are the median values).

2.2.5 Influence of process variables on adhesion forces

Particle size

The dependence of the force on particle size for zero impact velocity is shown in Table 2.4.

The molecular and capillaric forces are dependent on particle size only in as much as this influences the radius of curvature at the contact point; hence for smooth spheres $R = r_p$. Obviously the force is so dependant on the nature of the surface

that no conclusions can be drawn on the effect of size. In the case of quartz particles Krupp (97) states that surface asperities in the order of 0.2 μm are observed on ground quartz (figures 2.21-24 confirm this with AC dust) and with irregular quartz particles adhering to a hard metal surface the force was approximately proportional to $r_p^{0.5}$. Krupp concluded - "Hence the adhesion is very sensitive to surface asperities whose effect can only be estimated more or less crudely".

TABLE 2.4

DEPENDENCE OF ADHESION FORCE ON PARTICLE SIZE

Force	Molecular	Coulombic	Contact Potential	Capillaric
Dependence on size	R	$1/r_p^{0-2}$	$r_p^{1/3}$	R

Impact velocity

The velocity of impact affects the contact area and separation at the moment of maximum stress. Since molecular and Coulombic forces are instantaneous this will influence the adhesion force and energy in these cases.

Capillary forces are time dependent and although these may be partially effective during impact it is impossible to say to what extent. One of the main effects of a coating is undoubtedly to cause dissipation of kinetic energy during impact through viscous shear.

Gillespie (75) incorporated the Hertz theory to describe the effect of normal impact velocity on the van der Waals force.

Substituting equation 2.1 into 2.5 yields

$$E = 6\pi\varepsilon_a h R + \pi\varepsilon_a k r_p^{1.2} R^{0.8} u_{pr}^{0.8} \qquad 2.16$$

where $k = 2.07 \times 10^{-3}$ for quartz-steel

After Bowden and Tabor's observations (106) on the behaviour of "large" static systems Gillespie postulates that the real contact area is the product of the "apparent" area and maximum normal force. (Although Bowden and Tabor's results actually indicate that the real area is proportional to the applied force to the power 1.3). Gillespie thus concludes that the real contact area varies with R^4 and u_{pr}^2 . However, with smaller particles where the surface roughness is not so important it is likely that the real area of contact is better approximated by the apparent area; this has been used in evaluating expression 2.16.

Relative humidity

Zimon (90) observed that adhesion increased with relative humidity(fig.2.2) and that a plateau existed between 30 and 60% RH approximately. A similar characteristic has been observed with the shearing stress of powders by Topper (107). The strength of pellets is high at zero humidity but falls to a steady value as the relative humidity is increased beyond 1-2% RH. Kordecki and Orr (105) observed a fall in adhesion force in the range 25-75% R.H. Loffler (73) observed an increase in this range and Harrop observed an

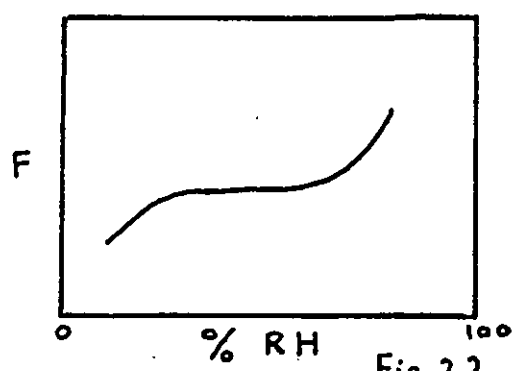

Fig 2.2

increase in filtration efficiency in the range 8-90% R.H. using particles of sodium chloride; he also obtained a plateau similar to that of Zimon.

These observations may be explained by recourse to the mechanisms of adhesion as follows:-

(a) Van der Waals force : The presence of water molecules on a surface causes a masking of the molecular forces - hence the rapid fall in pellet strength with % R.H. at low values. The presence of moisture may influence surface micro-hardness or cause swelling, leading to a larger contact area. According to Krupp (97) this is even significant on glass surfaces. Both Loffler and Harrop attribute their results to this phenomenon.

(b) Electrostatics : Electrostatic adhesion forces will be reduced by the presence of moisture which will increase the rate of charge neutralization - this explains the results of Kordecki and Orr.

(c) Capillary adhesion : Above 65% R.H. the adhesion force rises due to capillary adhesion (90, 109) with hydrophillic surfaces, but only attains that given by equation 2.3 at 100% R.H. in a static system. Only an extremely fine layer of moisture in the region of 100 molecules thick is required to provide a normal surface tension (109). With hydrophillic surfaces the depth of moisture increases rapidly above about 70% R.H. This phenomenon probably explains the rapid rise in adhesion strengths above 65% R.H. observed by Zimon and rise in filtration efficiency observed by Harrop.

Condition of Substrate

The condition of the fibre surface is obviously of major importance, it may be dry, coated with grease, oil or particles. The influence of a coating of oil or grease has already been dealt with. Zimon (90) describes briefly the influence of surface

roughness on the adhesion force. The presence of a coating of particles will change the impact angle, the adhesion force and the number of point contacts also physical blocking may occur. In studying this region of filtration, therefore, it is important to investigate the influence of dust loading, particularly in the initial stages.

2.3 Equilibrium Theory.

A particle will be retained by a filter if the energy of adhesion exceeds the energy of removal. The conditions effecting the particle size ($d_{p_{crit}}$) at which adhesion fails in filters have been studied by Gillespie (75), Jordan (80) and Harrop (4) briefly and in more detail by Dahneke (79) and Loffler (39). The theories are applicable to normal impact and are based on a simple energy balance.

It is necessary to distinguish two particle adhesion energies namely that of the incident undeformed particle as seen by the surface just before impact, $\overset{\circ}{E}_a$, and the additional adhesion energy during contact due to deformation, E_{ad}. The bounce, or removal energy will then be

$$E_{removal} = e^2 (E_{ki} + \overset{\circ}{E}_a) \qquad 2.17$$

where E_{ki} is the normal particle kinetic energy at impact unaffected by adhesion attraction forces. The total adhesion energy is

$$E_{adhesion} = \overset{\circ}{E}_a + E_{ad} \qquad 2.18$$

The removal and adhesion energies will be equal at the critical particle size, so

$$\overset{\circ}{E}_a + E_{ad} = e^2 E_{ki} + e^2 \overset{\circ}{E}_a \qquad 2.19$$

Hence

$$\frac{1}{2} m v_i^2 = E_{ki} = \frac{1}{e^2}\left[\overset{\circ}{E}_a (1 - e^2) + E_{ad} \right] \qquad 2.20$$

Two extreme cases of 2.20 have been considered. Jordan and Dahneke assumed that E_{ad} is negligible. This assumption is not valid but Dahneke's results are useful in that they illustrate the importance of the coefficient of restitution, e. He examined the influence which the various components of energy dissipation have on e. He showed that the coefficient of restitution of small particles colliding on a large surface (polystyrene spheres) is about 0.99. However, flexural work reduces the value of e when a particle collides with a thin body with a thickness of the same order of magnitude as the particle. He presented a theory to take this into account and used equation 2.20, ignoring E_{ad} and particle retardation due to air drag as it approaches the fibre, to calculate $d_{p_{crit}}$ as a function of v_0 and d_f. As would be expected his values were much too low. The effect of d_f on e was, however, such that a minimum appeared on a plot of $d_{p_{crit}}$ against v_0. The effect is only apparent when $d_f < d_p$.

Loffler (39) assumed that the first term in brackets in 2.20 was negligible and used Krupp's theory of adhesion to find E_{ad}. This was achieved by integrating the second term in expression 2.7:

$$E_{ad} = \int_{h_0}^{\infty} \frac{\overset{\circ}{F}\,\bar{P}}{H(t)}\, dh \qquad 2.21$$

A value of 3×10^7 N m^{-2} was taken for H (t) for a quartz-polyamide system. Hence Loffler included the effect of creep on particle deformation but like Dahneke he ignored particle retardation due to air drag on approaching the fibre. Values of $d_{p_{crit}}$ were calculated using this theory but again the predictions are extremely low.

In each of the above theories no account was taken of viscous dissipation due to air drag. Particle deformation due to impact and its influence on E_{ad} has been ignored. Creep will play only a very minor part during the very short period of contact ($\approx 10^{-7}$ secs).

The above theories are applicable to normal impact and are intended to give a measure of the value of $d_{p_{crit}}$ and influence of the major parameters. However, particles greater than $d_{p_{crit}}$ do adhere to fibres during filtration and some smaller particles fail to adhere for the following reasons:-

(a) Particle impact normal to the fibre occurs only at the stagnation point. Particles on trajectories beyond the centre line will collide at an angle and have a lower probability of capture. The tangential impulse force is now significant and the contact area is reduced.

(b) The angle of impact of an irregularly shaped particle will affect its probability of adhesion. This is also affected by the nature of surface at the contact point - radius of curvature of proturberences, number of proturberances and hardness of the micro surface.

An equilibrium theory is presented below which takes into account some of the shortcomings of existing theories. The

impact and adhesion energies are described separately before using them in 2.20.

(a) Impact energy: The following section refers to the total particle impact energy rather than the normal component of that energy.

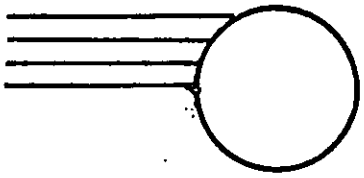

Fig. 2.3a
infinite inertia
system

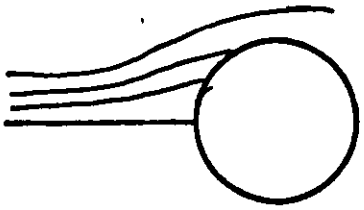

Fig. 2.3b
finite inertia
system

With infinite inertia systems (fig.2.3a) all particles which collide with a fibre will have an impact energy of $\frac{1}{2}m\ U_o^2$. However, the impact velocity of particles in the intermediate region (fig. 2.3b) will be only a fraction of that of the main stream. The energy is a function of the initial starting point and the inertial properties of the system. Hence it is necessary to obtain the dimensionless velocity of impact as a function of the starting point (takes as a fraction of the single fibre efficiency) as follows:-

$$u'_{pi} = \frac{u_{pi}}{U_o} = f^n\left[\left(y/\eta_c\right), N_{St}, N_R, N_{Re}, \alpha\right] \qquad 2.22$$

These values were determined using the technique described in Chapter I. Typical results are shown in figs. 2.4 and 2.5. The influence of the main parameters on the median value of the dimensionless impact velocity is summarised in figs 2.6 and

TABLE 2.5

Dimensionless impact velocity of particle trajectory normal to fibre (u'_{p_0}) (Kuwabara field).

N_R	α	N_{St} 0.01	0.1	0.5	1.0	5.0	10.0
0.02	.01	.0003	.0003	.0003	.00027	.5230	.7400
	.03	.0004	.0004	.0004	.0004	.6860	.8370
	.06	.0005	.0005	.0006	.1030	.7790	.8870
	.10	.0008	.0008	.0009	.2780	.8340	.9170
	.15	.0012	.0012	.0194	.4310	.8760	.9380
0.05	.07	.0016	.0016	.0016	.0018	.5270	.7450
	.03	.0024	.0024	.0025	.0029	.6950	.8400
	.06	.0035	.0035	.0038	.1340	.7840	.8900
	.10	.0051	.0051	.0056	.3100	.8400	.9210
	.15	.0072	.0072	.0756	.4810	.8820	.9410
0.10	.07	.0058	.0059	.0061	.0068	.5370	.7500
	.03	.0089	.0090	.0098	.0318	.7040	.8450
	.06	.0128	.0131	.0152	.1781	.7950	.8930
	.10	.0182	.0189	.0380	.3490	.8510	.9230
	.15	.0263	.0276	.1610	.5070	.8940	.9440
0.20	.01	.0201	.0205	.0220	.0286	.5590	.7590
	.03	.0308	.0314	.0370	.1041	.7230	.8560
	.06	.0445	.0458	.0660	.2690	.8100	.9040
	.10	.0620	.0660	.1530	.4450	.8680	.9330
	.15	.0900	.0970	.3190	.5890	.9110	.9530

2.7. As would be expected these figures are almost identical to those of the single fibre efficiency. The existence of a minimum is caused by alteration of the position of the critical trajectory and not the change in impact velocity at any given position on the cylinder. Using the Spielman and Goren field, Dawson (46) calculated relative grazing speeds; he obtained a diagram which is similar in form to fig.2.6.

The correct energy of impact is thus $\frac{1}{2} m U_0^2 u_{pi}'^2$ which may be expressed as

$$\frac{1}{2} m U_0^2 (u_{pi}')^2 = \frac{81\pi}{12} \mu^2 d_p \rho_p \left(\frac{N_{St}}{N_R}\right)^2 (u_{pi}')^2$$

$$= f' d_p \qquad 2.23$$

where $$f' = 13.8 \times 10^{-15} \left(\frac{N_{St}}{N_R}\right)^2 (u_{pi}')^2$$

for quartz in air at N.T.P.

f' for quartz in air is shown as a function of N_{St} and N_R in fig. 2.7. The sudden increase in the median value of f', f'_{50}, - hence impact (or removal) energy is most obvious. In the range $1.0 < N_{St} < 10.0$ the impact energy is most sensitive to variation in operating conditions.

From the data shown above it is possible to calculate the energy of impact in a filter. An example of this is shown in figs. 2.8 and 2.9 for particles at 0.2 and 1.0 ms^{-1} colliding with a 50 μm fibre but with particle sizes ranging from 1 to 10 μm. Here the total impact energy is shown as a function of the relative starting point.

Where $d_f > d_p$ e is close to unity so the removal energy

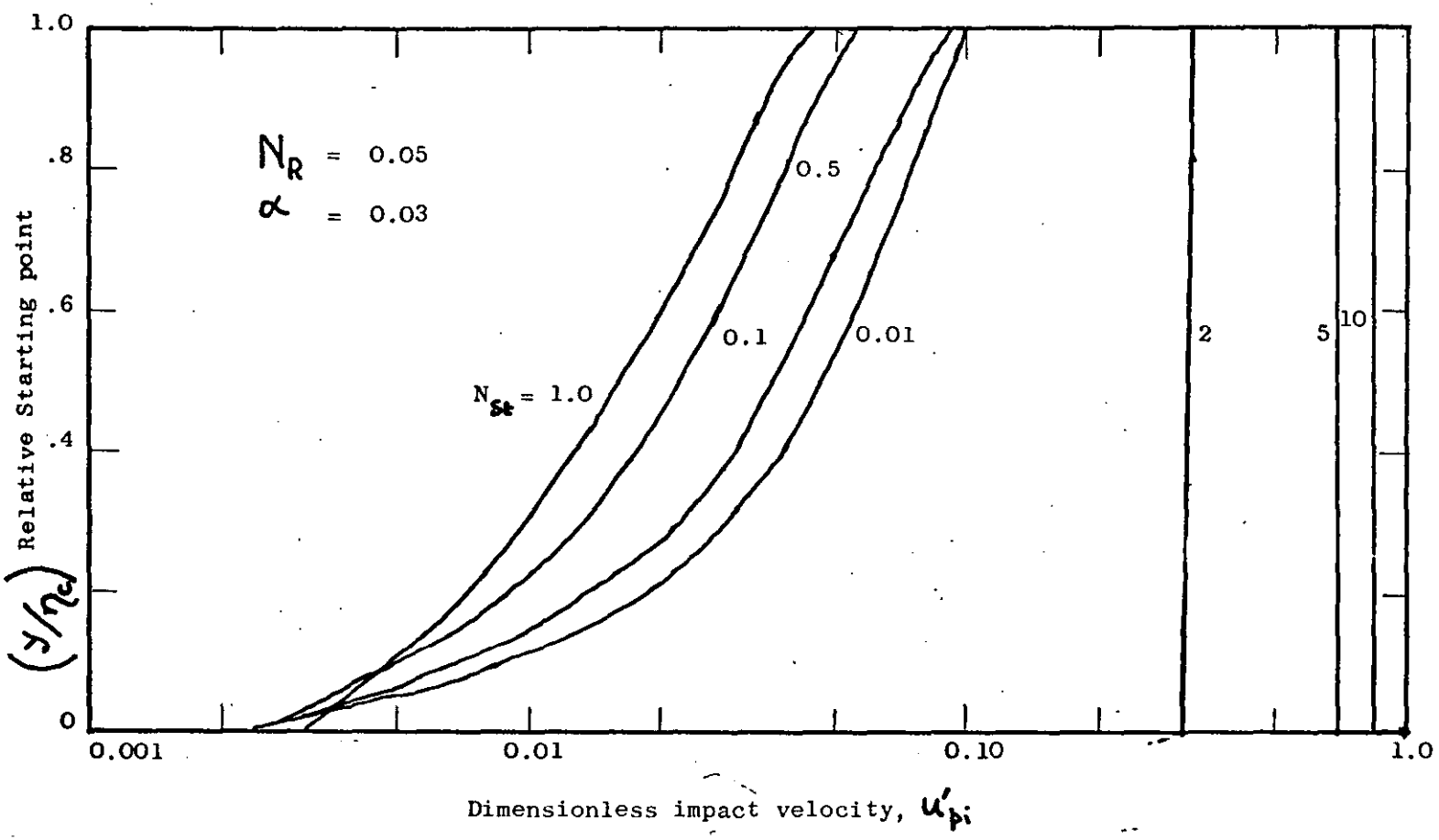

Fig. 2.4 Influence of relative trajectory starting point on impact velocity.

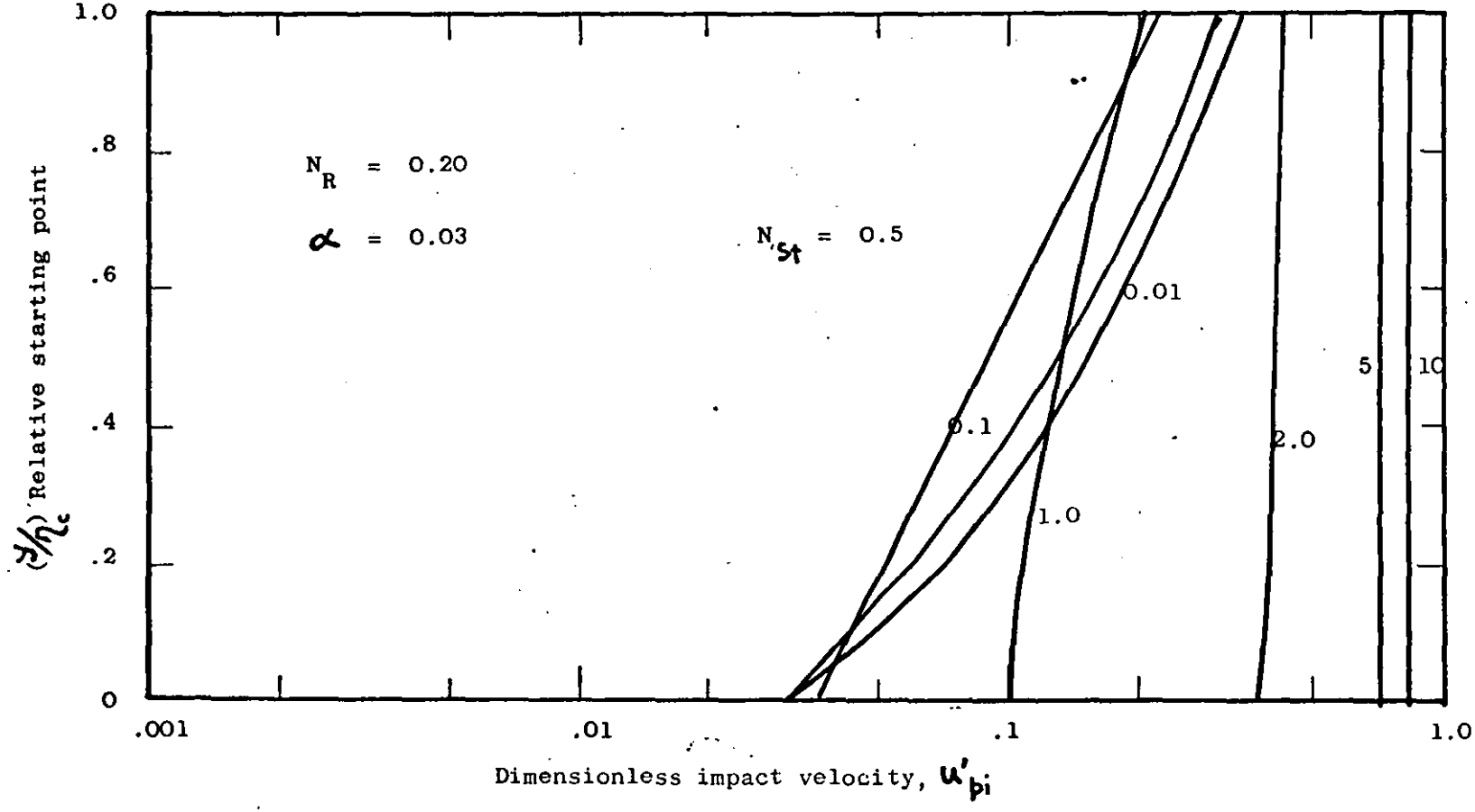

Fig. 2.5 Influence of relative trajectory starting point on impact velocity.

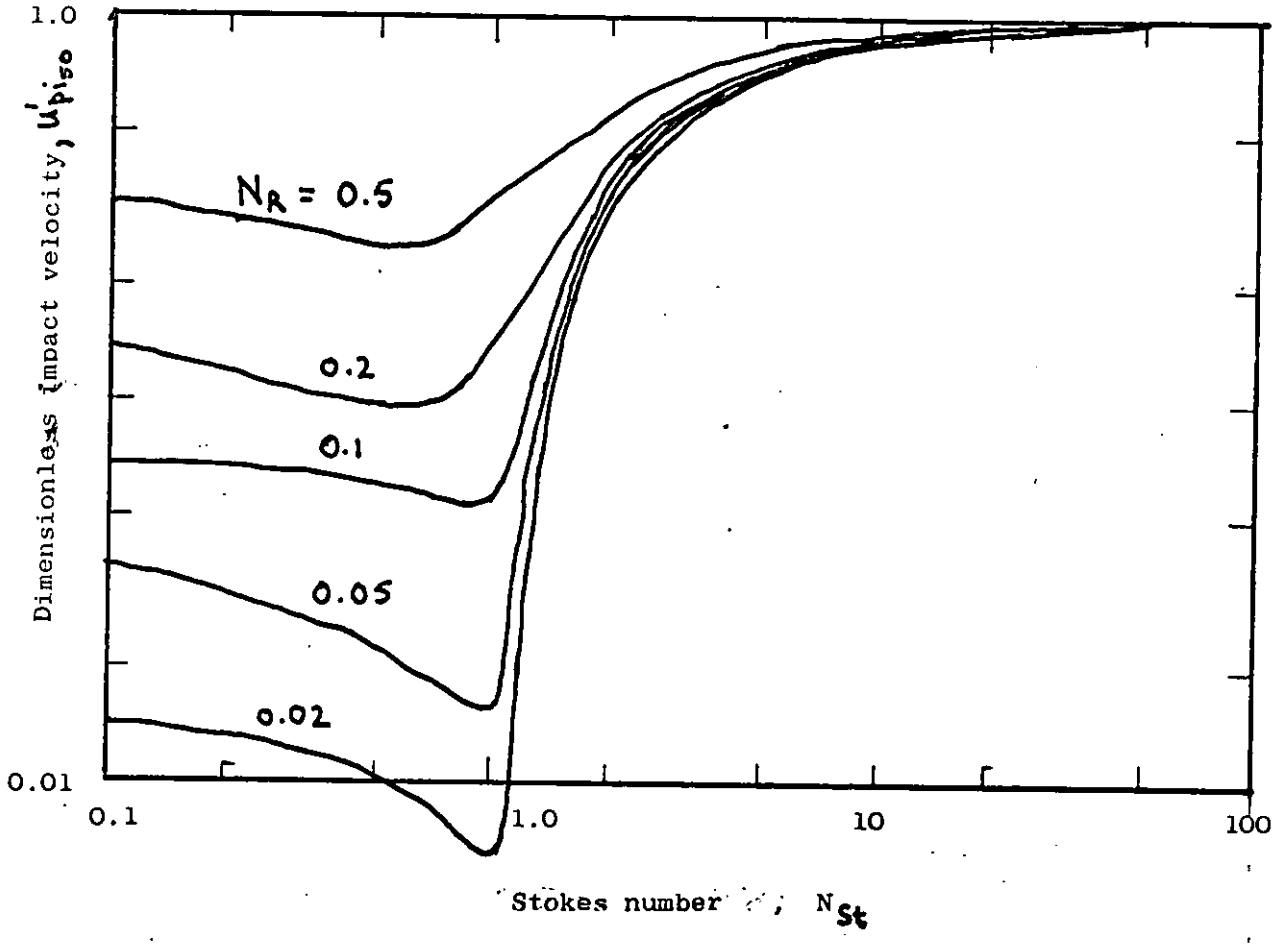

Dimensionless impact velocity.

FIGURE 2.6

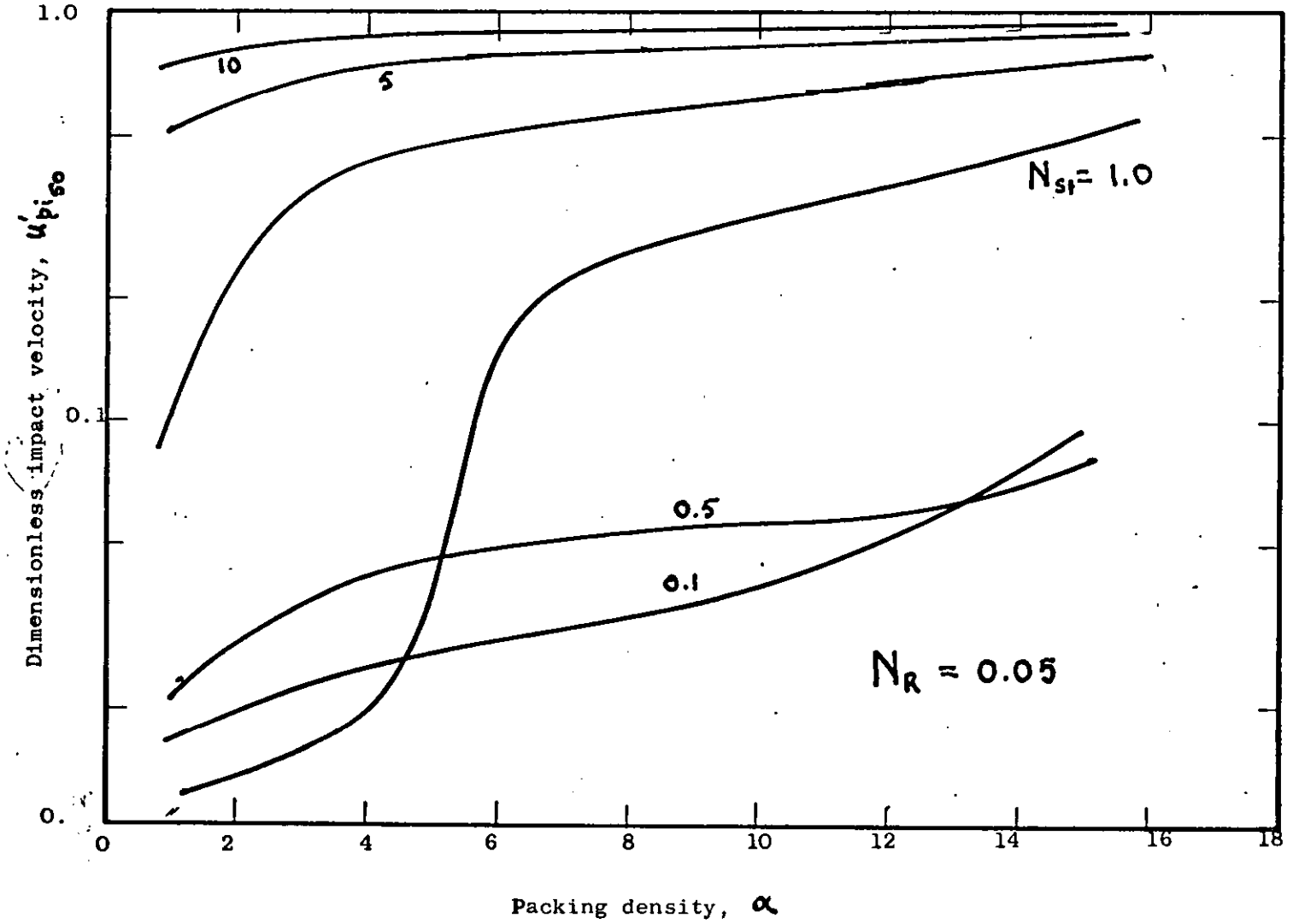

Fig. 2.7 Influence of packing density on impact velocity.

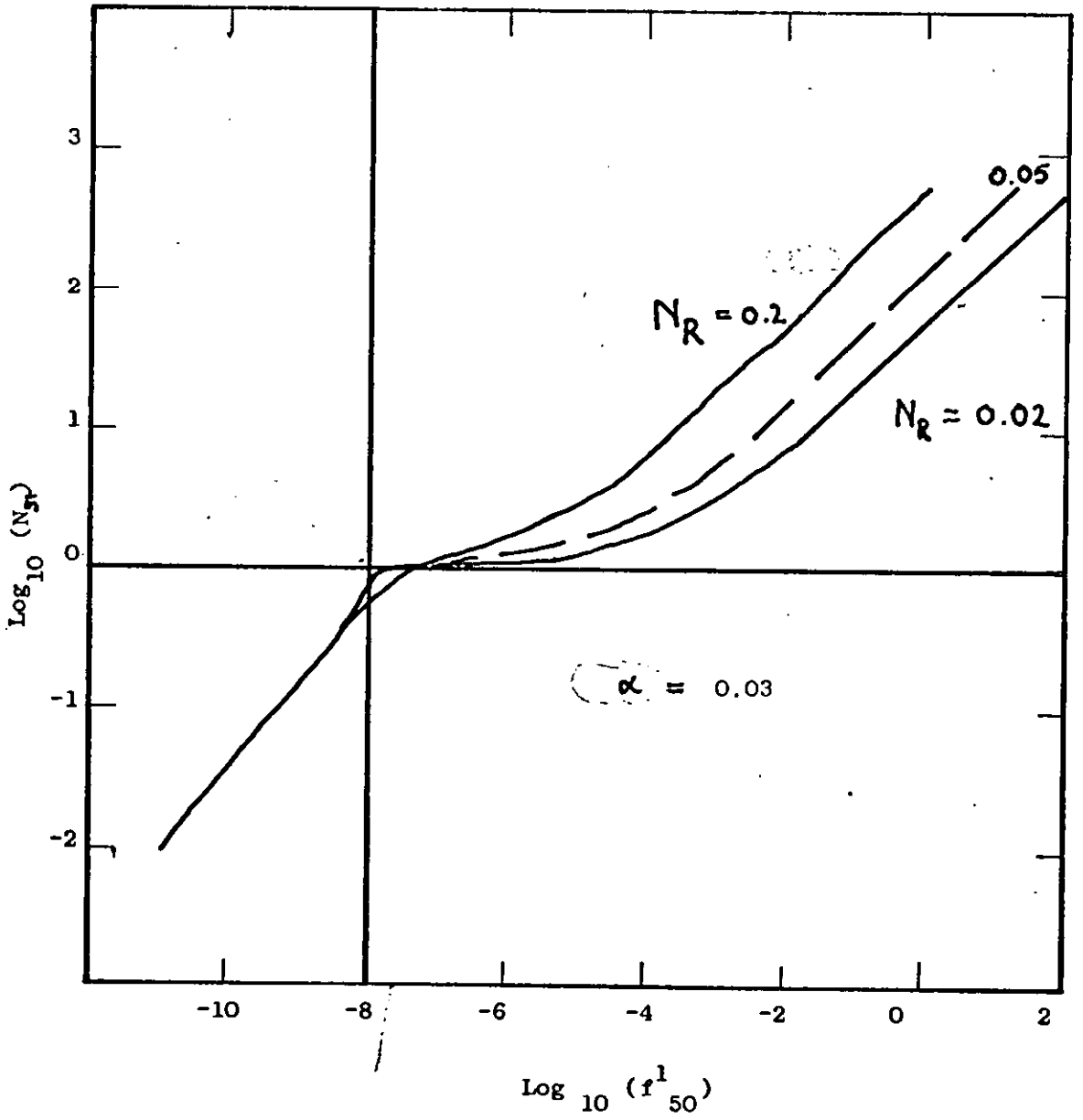

Fig. 2.8. Influence of N_{St} on impact (or escape) energy.

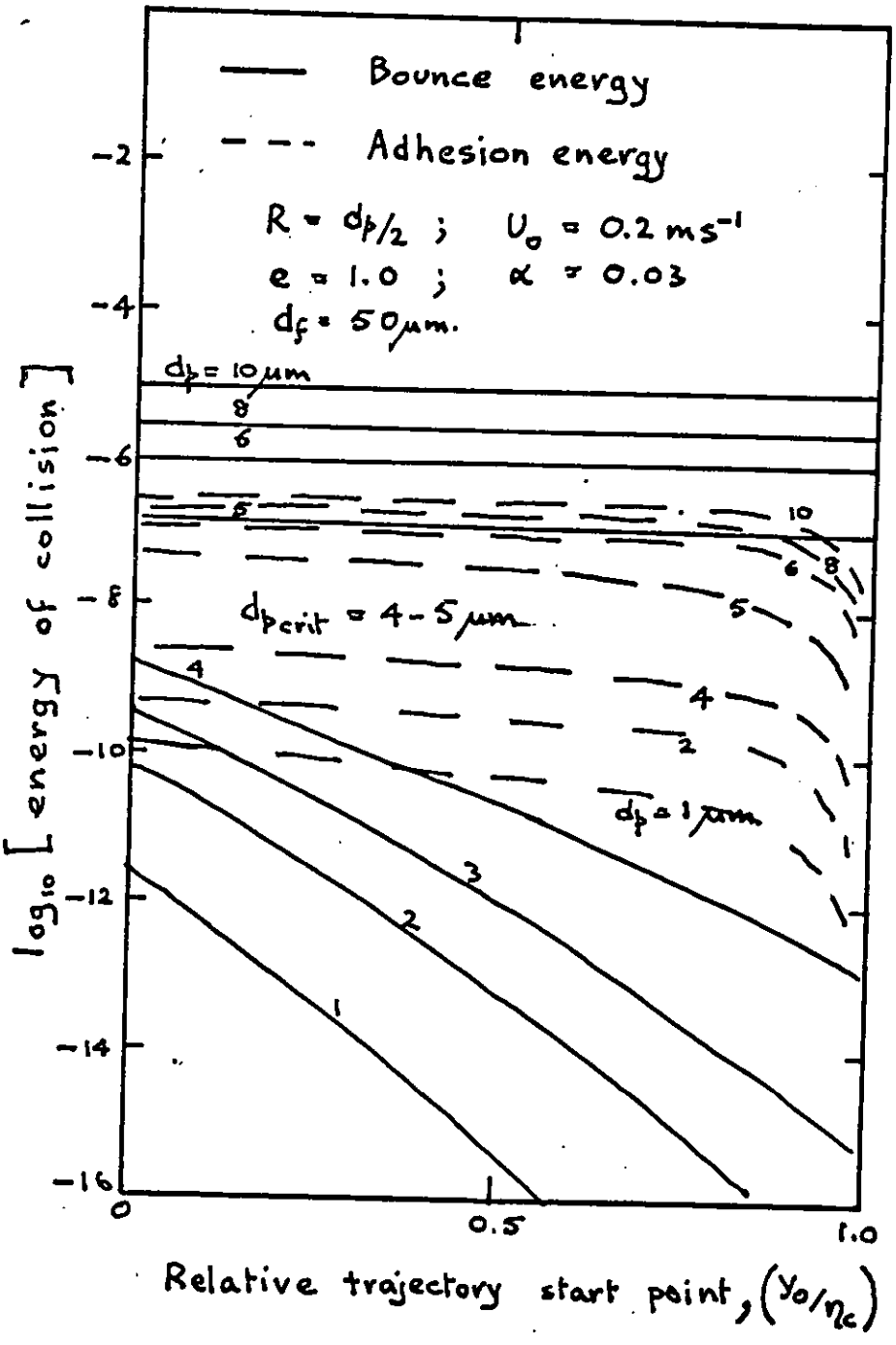

Figure 2.8 Energy spectra

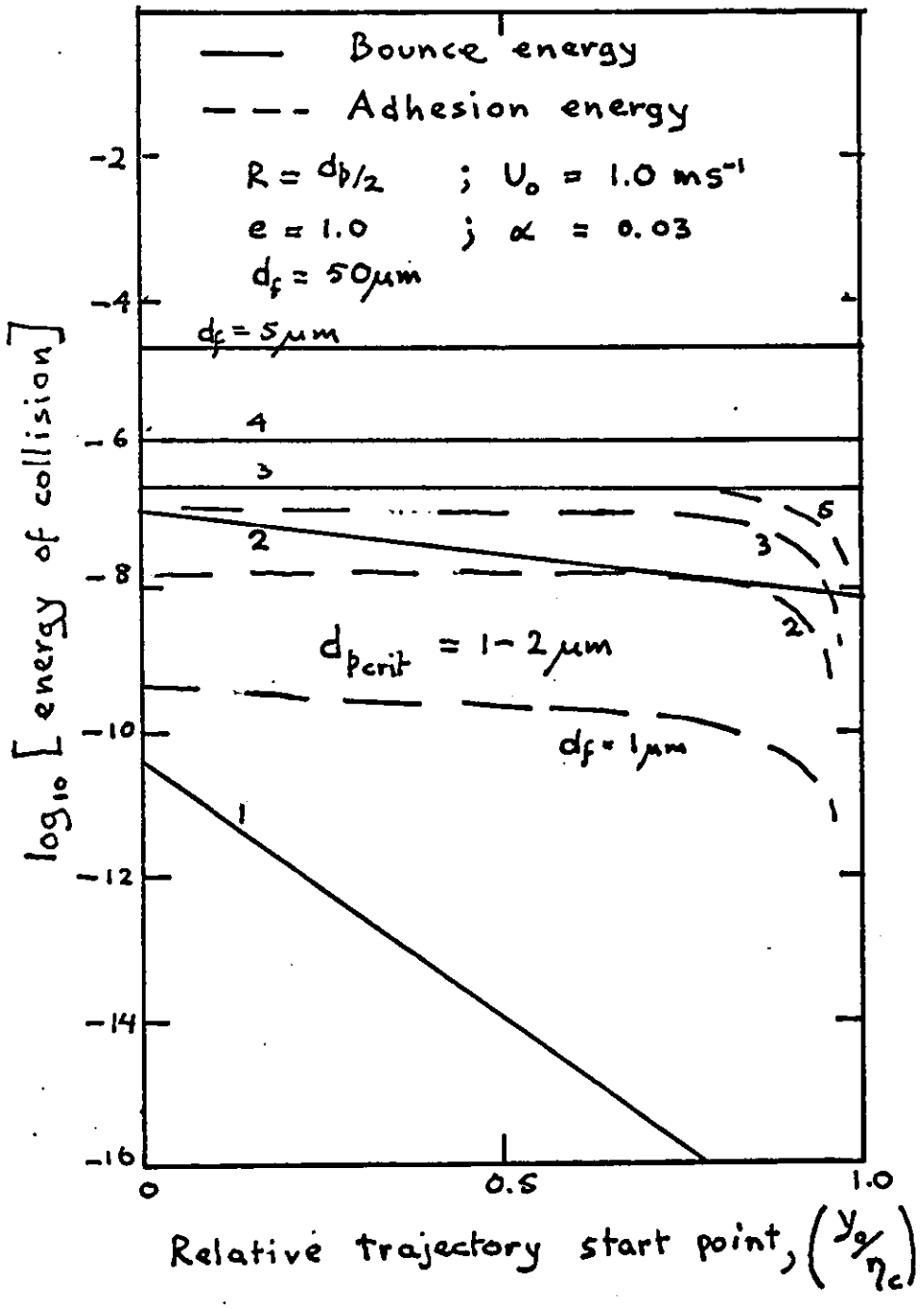

Figure 2.9 Energy spectra

can be equated to the impact energy.

(b) Adhesion energy : The undeformed and the additional adhesion energy due to flattening on impact are given by the first and second terms in equation 2.16 for a quartz-steel system. The velocity of impact normal to the fibre surface was calculated as a function of N_{St}, N_R and α using the Kuwabara model as described above. In each case it was found that good approximation to u_{pr} is given by

$$u_{pr} = U_o u'_{po} \left[1 - \left(\frac{y}{\eta_c} \right) \right]^{1/2} \qquad 2.24$$

where values of u'_{po}, the dimensionless impact velocity are given in table 2.5.

Values of the energy spectra (E_{ad} only) for particles in the size range 1-10 μm impinging on a 50 μm stainless steel fibre are given in figs. 2.8-9 for main stream velocities of 0.20 and 1.0 ms^{-1}. In this model h was assumed to be 4Å and the particles were taken to be round ($R = r_p$).

Construction of η_A characteristic

There is a distribution of adhesion and removal energies for the same size of particles because of the different trajectory starting points for any given condition as shown in fig. 2.11.

Recourse to figs 2.8 and 2.9 shows how the diagram can be constructed from theory. For a main stream velocity of 0.20 ms^{-1} and 1.0 ms^{-1} the particles size at which adhesion fails is about 4-5 μm and 1-2 μm respectively. The particle size for adhesion failure is in the right order thus providing confirmation of the mechanisms assumed. An extremely rapid fall off in efficiency is however predicted. The distribution of removal

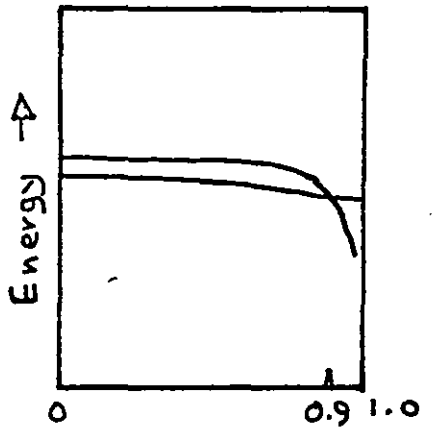

Relative particle starting point (here $\eta_A = 0.9$) fig. 2.11

energies may be easily estimated but our knowledge of adhesion is such that an estimate of the distribution of adhesion energies is out of the question. The adhesion energies in figs 2.8 and 2.9 are based on the assumption that each impact condition provides a specific adhesion energy; however, there will be a wide distribution for any given impact condition. This will increase with the width of the adhesion energy spectra causing a more gradual fall off in efficiency with particle size as is found in practice.

From a knowledge of the mechanisms concerned it is possible to predict qualitatively the influence of almost all operating and design parameters on fig. 2.11. However, the quantitative behaviour of the system can only be determined experimentally.

Value of d_{pcrit}

Since the fall of in η_A with d_p is very rapid it is convenient to examine the influence of a number of parameters on the values of the critical particle size. This was done using equation 2.20 in which the following were applied.

$$U_i = U_o u'_{pi}$$

$$E_{ad} = \pi \epsilon_a k r_p^{1.2} R^{0.8} u_{pr}^{0.8} \qquad 2.25$$

$$= 2.07 \times 10^{-3} \pi \epsilon_a r_p^{1.2} R^{0.8} u_{pr}^{0.8}$$

$$e = 1.0 \; ; \quad \text{for } u_{pr} \text{ see eqn 2.24}$$

The computed values of u'_{p_o} and $u'_{pi_{so}}$ are well approximated for the Kuwabara field, where $\alpha = 0.03$, by:-

$$u'_{p_o} = 0.7\,N_R + (1 - 0.7\,N_R)(1 - {}^{1}/_{0.9\,N_{St}})$$

$$u'_{pi_{so}} = 0.52\,N_R^2 + (1 - 0.52\,N_R^2)(1 - {}^{1}/_{N_{St}}) \qquad 2.26$$

$$\text{for } N_{St} > 1.0$$

$$u'_{p_o} = 0.7\,N_R \quad ; \quad u'_{pi_{so}} = 0.52\,N_R^2$$

$$\text{for } N_{St} < 1.0$$

By including equation 2.24 with the above all the particle impact velocities required to solve 2.20, for particles whose relative trajectory start point is either 0 or $(\gamma_o/\eta_c) = 0.5$, are available. Hence it is possible to calculate the critical particle size at which adhesion ceases, $d_{p_{crit}}$, for the conditions $(\gamma_o/\eta_c) = 0$ and $(\gamma_o/\eta_c) = 0.5$ over a wide range of conditions. Using this simple theory the influence of fibre size, approach velocity and radius of curvature at the point of contact have been investigated. The results are shown in table 2.6 and figs. 2.12 and 2.13. The computations are all for the quartz-stainless steel system. Each of the sub-tables consists of a 10 x 10 matrix of values of $d_{p_{crit}}$. In each column the fibre size is increased from 10 μm to 1000 μm (10, 25, 50, 100, 150, 200, 300, 500, 750 and 1000 μm) and each row represents an increase in approach velocity from 0.1 to 10.0 ms^{-1} (0.1, 0.25, 0.5, 1.0, 1.5, 2.0, 3.0, 5.0, 7.5 and 10.0 ms^{-1}).

The results for perfectly elastic spheres in the Kuwabara field for the $(\gamma_o/\eta_c) = 0.5$ condition are shown in table 2.6.1 and figure 2.12. The $(\gamma_o/\eta_c) = 0.5$ condition was used because it most closely represents the behaviour of the average

particle. The influence of fibre size and approach velocity are as expected, the bounce energy increasing with velocity and the dissipation of kinetic energy increasing with fibre size.

Table 2.6.2 shows the results of an "asperity" model in which the radius of curvature at contact was taken to be a constant. That particles have a large number of asperities or surface protuberances in the order of 0.2 μm in size is in accordance with the evidence of Krupp (97) and Fuchs (110) together with photographic evidence described below. The radius of the asperity, or point of contact, R, was taken as 0.1 μm in the construction of table 2.6.2. The difference between tables 2.6.1 and 2.6.2 is extremely small as is shown graphically in fig. 2.13. A small reduction in the coefficient of restitution is also of little significance as is shown in table 2.6.3.

Table 2.6.4 shows that use of the collision conditions of particles on the $(Y_o/\eta_c) = 0$ trajectory has a negligible effect on the results.

Measurements of filter resistance show that the assumption of laminar flow is a close approximation up to a fibre Reynolds number of 1.0. However, in the non adhesion region the Reynolds number is often in excess of this. Thom (12) used a relaxation technique to analyse the flow round an isolated cylinder with a Reynolds' number of 10. This field was later used by Davies (37) to calculate the efficiency of inertial interception. The data shown in Davies' paper has been analysed to obtain an expression for u'_{p_o} in the Thom field:-

$$u'_{p_o} = 1 - 1/\left[(0.53 + 0.34\, N_R)(N_{St} + 1.47 + 1.04\, N_R)\right] \quad 2.27$$

The lowest possible value of u'_{p_o} was taken to be $0.6\, N_R$

the impact velocity in a zero inertia system. Values of $u'_{pi_{so}}$ could not be obtained so it was necessary to use u'_{p_o} instead in the expression for U_i (equation 2.25). The effect of making this assumption using the Kuwabara field was marginal (table 2.6.4). Results using the Thom field are given in table 2.6.5. Again results do not differ substantially from those using the Kuwabara model. The theoretical efficiency characteristics obtained using the two fields are very close (fig. 1.5) suggesting that the impact conditions are similar, so it is to be expected that the values of $d_{p_{crit}}$ should be close.

That particle retardation prior to impact is important is shown in table 2.6.6. In calculating these values it was assumed that the impact velocity was the same as the main stream velocity. The substantial reduction in $d_{p_{crit}}$ is also shown in fig. 2.13.

In the derivation of equation 2.20 it was assumed that the "undeformed" adhesion energy is converted to kinetic energy which is almost completely recoverable as bounce energy at impact. If the particle inertia is such that this is not so the total adhesion energy will be greater than assumed. To test the numerical importance of this a series of values of $d_{p_{crit}}$ were calculated in which the total adhesion energy shown in equation 2.5 was equated to the impact energy of equation 2.23. The resultant values of $d_{p_{crit}}$ are shown in table 2.6.7 and fig. 2.13. $d_{p_{crit}}$ is higher but under the cond itions examined it is not significantly so.

The predictions of Dahneke and Loffler are shown in fig. 2.13 for comparison. There is a dearth of experimental information on the actu al values of $d_{p_{crit}}$ but those values which have been published suggest that the theory reported here

is realistic.

The region of filtration beyond $d_{p_{crit}}$ has been studied by Loffler (78) and the author (76, 77). Loffler (78) determined the retention efficiency by counting those particles which adhere on collision using high speed cine photography. He examined the influence of velocity on the retention efficiency of 5μm and 10μm quartz particles colliding on 19μm and 50μm fibres (fig. 2.15). Those factors which effect $d_{p_{crit}}$ would be expected to influence filtration in the same way in this region. The experimental results in references 76 and 77 are described and extended in section 2.4 below.

TABLE 2.6

Table 2.6.1 Kuwabara field; (eqn.2.26 for u'_{50}) $N_{Re}=0$; $\alpha=0.03$
$R = d_p/2$; e =1

3.08	1.80	1.22	0.84	0.68	0.58	0.47	0.36	0.29	0.25
4.60	2.74	1.88	1.31	1.06	0.91	0.74	0.57	0.46	0.40
6.29	3.80	2.63	1.83	1.49	1.28	1.04	0.80	0.65	0.56
8.66	5.29	3.68	2.57	2.09	1.81	1.47	1.13	0.92	0.80
10.48	6.44	4.49	3.14	2.56	2.21	1.80	1.39	1.13	0.98
12.01	7.40	5.17	3.62	2.95	2.55	2.07	1.60	1.31	1.13
14.57	9.01	6.31	4.43	3.60	3.12	2.54	1.96	1.60	1.38
18.62	11.57	8.11	5.70	4.65	4.02	3.27	2.53	2.06	1.79
22.66	14.12	9.91	6.97	5.68	4.91	4.01	3.10	2.53	2.19
26.06	16.26	11.43	8.05	6.56	5.67	4.62	3.58	2.92	2.53

Table 2.6.2 Kuwabara field (eqn.2.26 for u'_{50}); $N_{Re}=0$; $\alpha=0.03$;
$R = 0.1\ \mu m$; e = 1.

2.58	1.63	1.15	0.81	0.66	0.57	0.46	0.36	0.29	0.25
4.04	2.55	1.80	1.27	1.04	0.90	0.73	0.56	0.46	0.40
5.69	3.59	2.54	1.7	1.46	1.26	1.03	0.80	0.65	0.56
8.02	5.07	3.58	2.53	2.06	1.79	1.46	1.13	0.92	0.80
9.81	6.20	4.38	3.10	2.53	2.19	1.78	1.38	1.13	0.97
11.32	7.16	5.06	3.57	2.92	2.52	2.06	1.59	1.30	1.13
13.86	8.76	6.19	4.38	3.57	3.09	2.52	1.95	1.59	1.38
17.88	11.30	7.99	5.65	4.61	3.99	3.26	2.52	2.06	1.78
21.89	13.84	9.78	6.92	5.65	4.89	3.99	3.09	2.52	2.18
25.27	15.98	11.30	7.98	6.52	5.64	4.61	3.57	2.91	2.52

Table 2.6.3 Kuwabara field (eqn.2.26 for u'_{50}); $N_{Re}=0$; $\alpha=0.03$;
$R = d_p/2$; e = 0.75

3.54	1.95	1.29	0.87	0.70	0.59	0.48	0.36	0.29	0.25
5.06	2.90	1.95	1.34	1.08	0.93	0.75	0.57	0.46	0.40
6.75	3.96	2.70	1.87	1.51	1.30	1.05	0.81	0.66	0.57
9.13	5.46	3.76	2.61	2.11	1.82	1.48	1.14	0.93	0.80
10.95	6.60	4.57	3.18	2.58	2.23	1.81	1.39	1.13	0.98
12.48	7.57	5.25	3.66	2.97	2.56	2.09	1.61	1.31	1.13
15.05	9.19	6.39	4.47	3.63	3.13	2.55	1.97	1.60	1.39
19.12	11.75	8.20	5.74	4.67	4.04	3.29	2.54	2.07	1.79
23.17	14.30	10.00	7.01	5.71	4.93	4.02	3.11	2.53	2.19
26.58	16.45	11.52	8.09	6.58	5.69	4.64	3.58	2.92	2.53

Table 2.6.4 Kuwabara field (eqn.2.26 for u'_0); $N_{Re}=0$; $\alpha=0.03$
$R = d_p/2$; e = 1.0

3.46	2.08	1.42	0.97	0.78	0.67	0.53	0.41	0.33	0.28
4.76	2.92	2.02	1.40	1.13	0.97	0.79	0.60	0.49	0.42
6.30	3.90	2.72	1.90	1.54	1.33	1.08	0.83	0.67	0.58
8.53	5.33	3.73	2.62	2.13	1.84	1.50	1.15	0.94	0.81
10.28	6.44	4.52	3.18	2.59	2.24	1.82	1.41	1.14	0.99
11.76	7.38	5.19	3.65	2.97	2.57	2.09	1.62	1.32	1.14
14.25	8.96	6.31	4.45	3.62	3.13	2.55	1.97	1.61	1.39
18.22	11.48	8.09	5.71	4.65	4.03	3.28	2.54	2.07	1.79
22.20	14.00	9.88	6.97	5.69	4.92	4.01	3.11	2.53	2.19
25.56	16.12	11.38	8.04	6.56	5.67	4.63	3.58	2.92	2.53

Table 2.6.5 Thom field (eqn.2.27); N_{Re}=10; α =0; R = $d_p/2$; e=1.0

3.21	1.59	1.28	0.79	0.71	0.61	0.46	0.35	0.29	0.25
3.99	2.52	1.78	1.26	1.11	0.89	0.72	0.60	0.46	0.39
6.59	4.00	2.52	1.78	1.45	1.26	1.10	0.79	0.65	0.56
7.98	5.04	3.57	2.52	2.06	1.78	1.45	1.12	0.92	0.79
9.77	6.18	4.37	3.09	2.52	2.18	1.78	1.38	1.12	0.97
12.62	7.14	5.04	3.57	2.91	2.52	2.06	1.59	1.30	1.12
13.82	8.74	6.18	4.37	3.57	3.09	2.52	1.95	1.59	1.38
17.85	12.18	7.98	6.01	4.60	3.99	3.25	2.52	2.06	1.78
21.86	13.82	9.77	6.91	5.64	4.88	3.99	3.09	2.52	2.18
25.24	15.96	12.04	7.98	6.51	5.64	4.60	3.57	2.91	2.52

Table 2.6.6 $u'_0 = u'_{p50}$ = 1.0 N_{Re} = 0; α=0.03; R = $d_p/2$; e = 1.0

0.92	0.30	0.13	0.05	0.03	0.02	0.01
0.92	0.30	0.13	0.05	0.03	0.02	0.01
0.92	0.30	0.13	0.05	0.03	0.02	0.01
0.92	0.30	0.13	0.05	0.03	0.02	0.01
0.92	0.30	0.13	0.05	0.03	0.02	0.01
0.92	0.30	0.13	0.05	0.03	0.02	0.01
0.92	0.30	0.13	0.05	0.03	0.02	0.01
0.92	0.30	0.13	0.05	0.03	0.02	0.01
0.92	0.30	0.13	0.05	0.03	0.02	0.01
0.92	0.30	0.13	0.05	0.03	0.02	0.01

Table 2.6.7 Kuwabara field (eqn.2.27 for u'_{50}); N_{Re} =0; α =0.03; R = $d_p/2$; e = 1.0; eqn.2.5 used for adhesion force

5.23	2.59	1.60	1.02	0.79	0.67	0.53	0.39	0.31	0.27
6.55	3.47	2.23	1.48	1.17	0.99	0.79	0.60	0.48	0.41
8.11	4.49	2.96	2.00	1.59	1.36	1.10	0.83	0.67	0.58
10.37	5.95	4.00	2.73	2.20	1.89	1.52	1.17	0.94	0.81
12.13	7.08	4.80	3.30	2.66	2.29	1.85	1.42	1.15	0.99
13.63	8.03	5.48	3.78	3.05	2.62	2.13	1.63	1.33	1.14
16.14	9.63	6.61	4.58	3.71	3.19	2.59	1.99	1.62	1.40
20.15	12.17	8.41	5.85	4.75	4.09	3.32	2.56	2.08	1.80
24.15	14.71	10.21	7.12	5.78	4.99	4.06	3.13	2.55	2.20
27.53	16.85	11.72	8.19	6.66	5.75	4.67	3.61	2.94	2.54

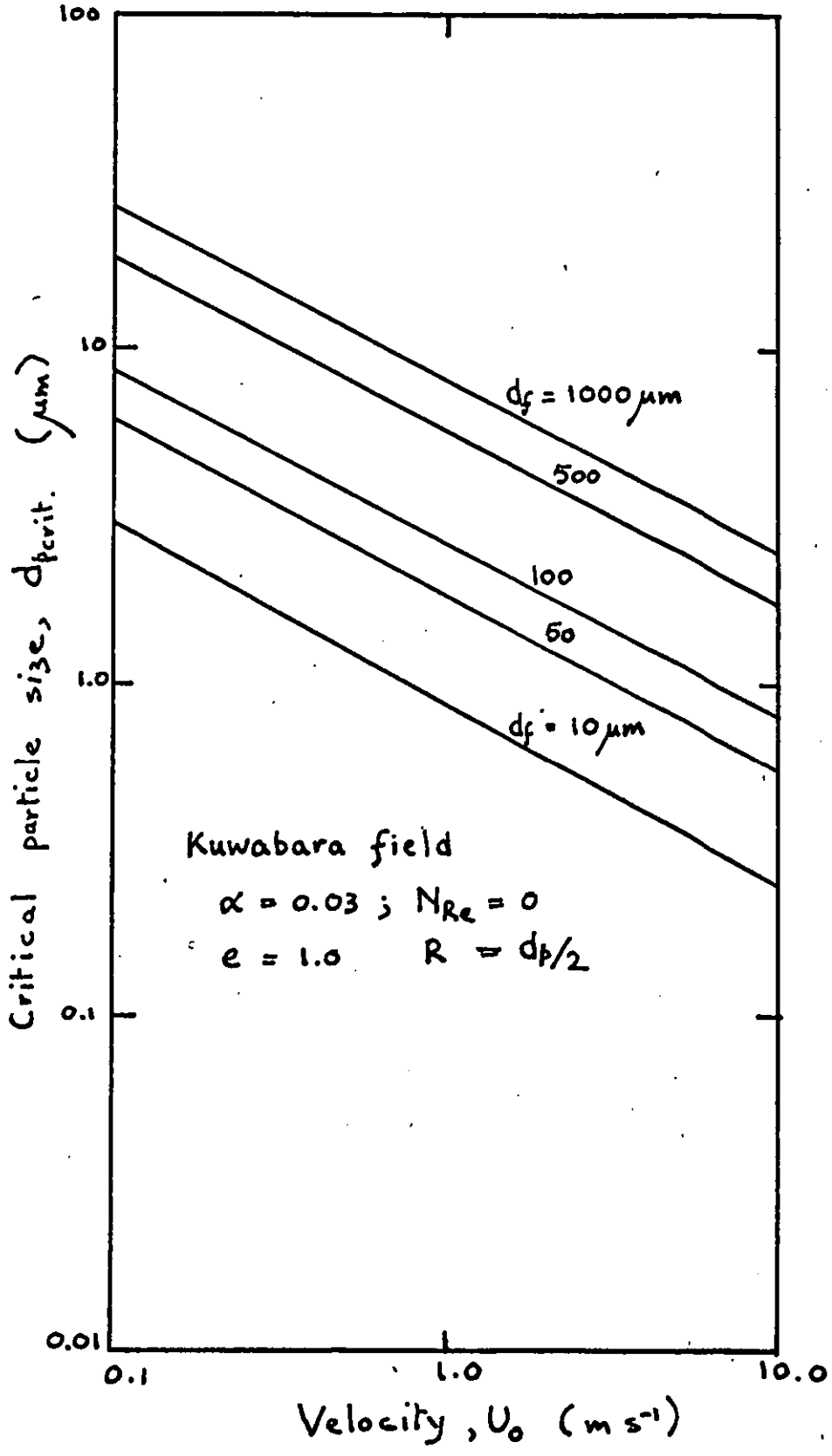

Figure 2.12 Critical particle size

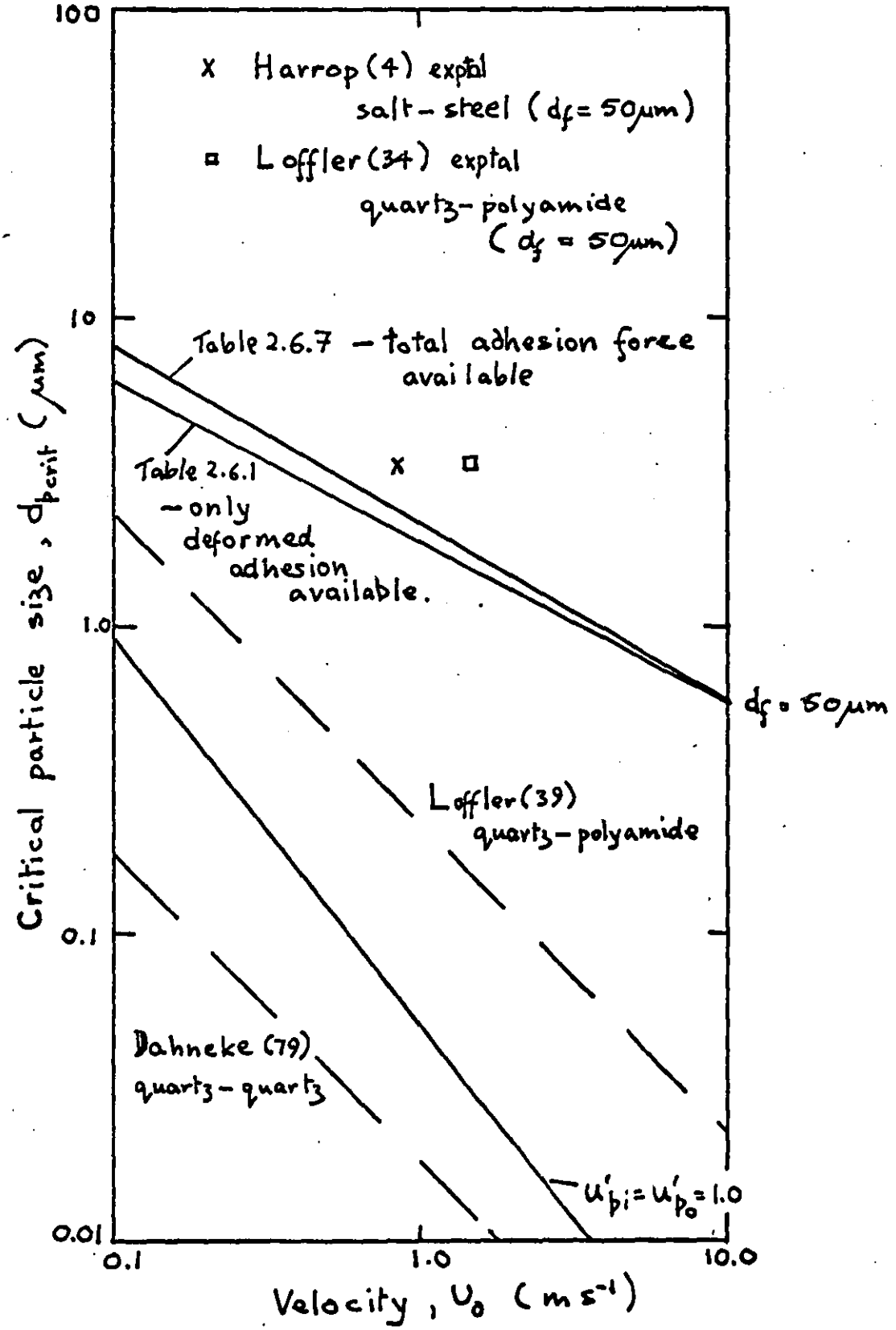

Figure 2.13 Critical particle size

2.4 Experimental

The object of this work is to examine the behaviour of fibrous filters in the non adhesion region to elucidate the mechanisms involved. To obtain a qualitative picture of the system, a photographic study was made. This was followed by an exploratory quantitative analysis.

2.4.1 Photographic Analysis

Three methods of photographic analysis were employed. Firstly a static study was made of particles which had been deposited on a fibre. This was followed by a 64 f.p.s. cine analysis of particle build up and finally by a high speed cine study of the collision mechanism.

Static analysis

Particles of AC test dust in the size range 5-10 μm were captured on a 50 μm diameter stainless steel fibre. The dust was dispersed in a shearing field as described in BS 1701 and the tests were performed under normal atmospheric conditions. The air velocity used was 2.5 ms^{-1}. At the end of the test the fibres were photographed using a scanning electron microscope.

Some typical S.E.M. photographs are shown in figs. 2.16 - 2.35. They illustrate the following aspects:-

(i) Orientation and surface coverage - Figs. 2.16 - 2.20 show the general arrangement of particles on a fibre. The contact area may be quite small (fig.2.20) or it maybe extremely large as is shown in figs 2.21 and 2.22. Clearly the surface coverage is relatively small when direct particle - fibre impact becomes a

virtual impossibility.

(ii) Surface protuburences - Figs. 2.18, 2.20, 2.21 and 2.22 clearly show the presence of small protuberances, in the order of 0.1-0.2 μm in size on the surface of the particles; fig.2.28 suggests that these are in fact fine particles of dust. They will cause the contact area to be extremely small and perhaps of a secondary nature, the ultra fine particles acting as an adhesion intermediary. It is possible, therefore, that the presence of such protuberances will be of major importance in filtration.

Washing the dust in water containing a dispersant apparently reduced the number of protuberances fig.2.22 and 2.23 and a fraction of these are likely to be surface asperities (such a surface has been reported on silica dust). Filtration tests showed that prior washing of the dust had only a negligibly small effect on the efficiency, showing that the presence of the fines on the particles is in fact of little importance.

(iii) Presence of soot - to examine further the influence of added fines on filtration, a quantity of soot was added to the test dust (fig.2.24 and 2.27. Soot was chosen because it is added to AC test dust in a widely used standard test procedure. The soot acts as a 'landing pad' for the coarser dust particles. Tests (fig.2.48) show that this is not a significant mechanism in the initial stages of filtration. However, once a coating of soot has been established within a filter, a substantial increase in efficiency will result.

(iv) Presence of an oil coating - two fibres, one coated with a fine layer of oil and the other washed in carbon tetrachloride to clean the surface were placed side by side (o.5 cm appart) in a stream of 5 μm particles. The influence of the oil is obvious (figs.2.28 and 2.29) and supported by efficiency tests.

(v) Effect of loading - particles were allowed to build up on

a lightly coated fibre. Theresults are shown in figs. 2.30 - 2.34. That particles may act efficiently as impact targets is shown in fig.2.30 where the presence of "trees" is illustrated. The small contact area required for efficient adhesion is again shown. Figs. 2.33 and 2.34 show multilayer packing. Obviously the filtration efficiency will change as the surface condition is changed.

(vi) Behaviour of thick oil coating - A fibre was coated with a thick layer of silicon oil (used because of its extremely low vapour pressure). Fig.2.35 was taken 30 minutes after impact. The fluid has crept round the particle, completely coating it. In such situations the influence of the oil must extend well beyond the first layer of particles.

Cine analysis (normal speed)

A 10 μm fraction of A.C. test dust was fed to a 200 μm stainless steel fibre. A Bolex 16 m.m. cine camera with a microscope attachment was used to photograph particle build up. The fibre was suspended in a perspex tube. The air velocity was 0.5 ms^{-1}.

The film (P.S.T.I.S. no. 10) clearly showed particle capture on the leading edge of the fibre (see also fig.2.36). On coating the fibre with adhesion assisting oil, oil creep round retained particles was visible and was complete in less than a second. This phenomenon continued even with a layer several particles deep.

It has been reported (83) that particle re-entrainment is severe on increasing the air velocity after deposition. To examine this particles were deposited at 0.5 ms^{-1} and the air rate immediately doubled. However, there was no visible re-entrainment

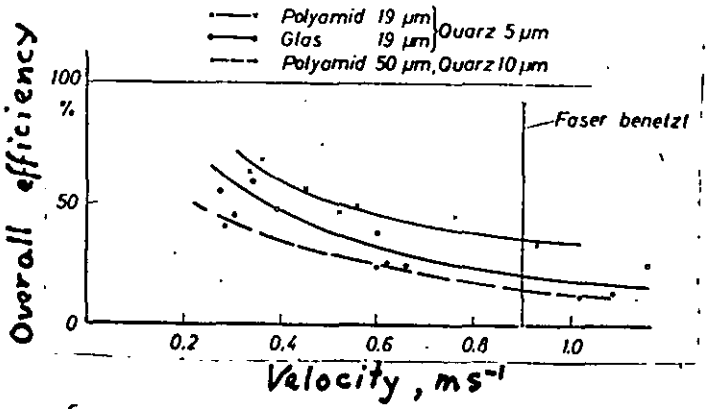

Fig.2.15. Influence of velocity, U_o, on η_A (after Loffler (78))

2.4.2 Quantitative Analysis

Two types of filter were tested, a woven wire filter and model filters. In each case the filters employed were 3.8 cm diameter. The dust consisted of fractions of either AC test or limestone. The efficiency of collection of AC dust was determined gravimetricallyand that of limestone titrametrically.

Gravimetric analysis

The gravimetric method was used because it is a convenient method for examining the effect of particle loading, a realistic test dust can be employed and the dust properties may be varied at will.

A diagram of the apparatus is shown in fig.2.37. A preweighed sample of dust was dispersed in a shearing field. The dispersal unit is a reduced version (fig.2.38) of that described in BS.1707. Following collection of particles on a coated microscope slide the degree of dispersion was considered satisfactory. Tests showed that over 99% of the dust fed to the unit reached the filter. Experimentally the reproducibility of efficiency measurements was found to be within ± 1%

Two test filters were employed:-

(a) A tightly packed section of woven stainless steel wire in a 1½ inch diameter perspex tube with an antistatic coating was

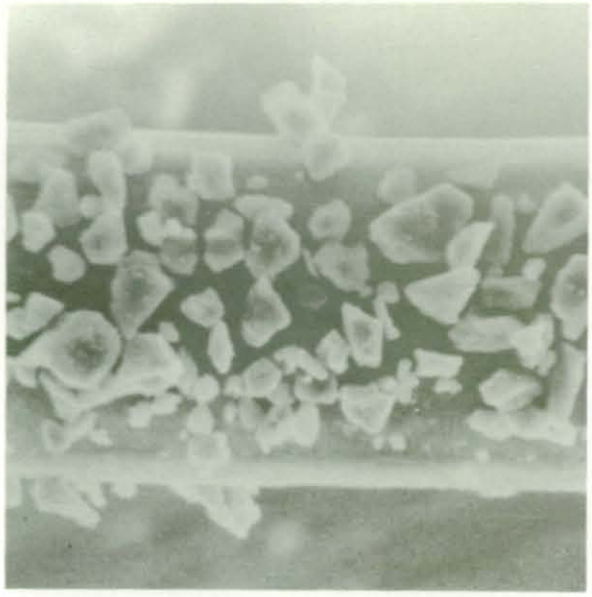

Fig.2.16
5-10μm particles of A.C. dust on 50μm stainless steel fibre

Fig.2.17
Close up of 5-10μm particles

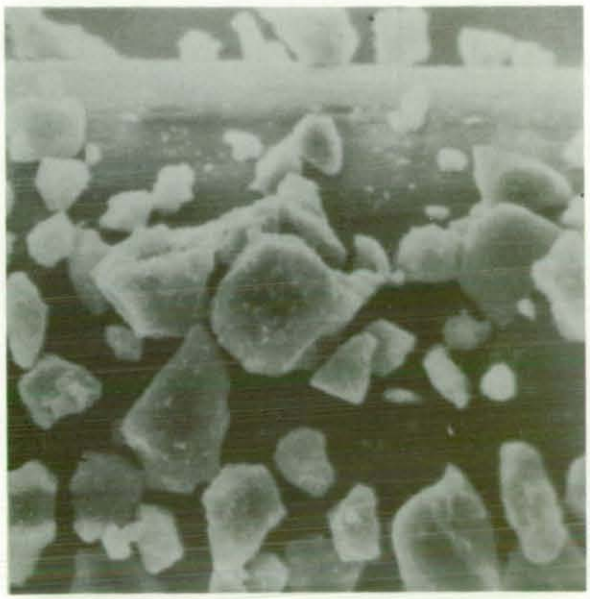

Fig.2.18
5-10μm particles of A.C. dust on 50μm stainless steel fibre

Fig.2.19
Close up of 5-10μm particles

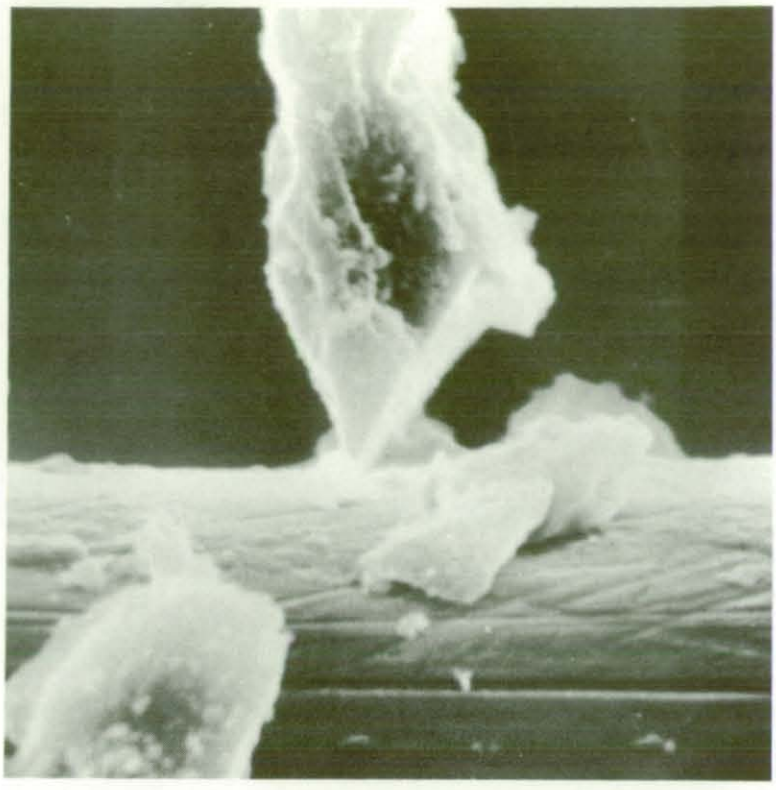

Fig. 2.20

Fig. 2.21

10μm particles on a stainless steel fibre

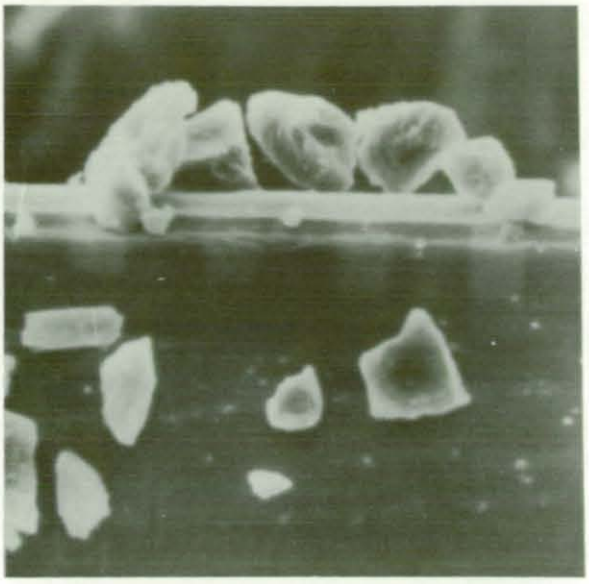

Fig.2.22

Fig.2.23

Test dust washed to remove fines

Fig.2.24
10µm particle on fibre

Fig.2.25
Effect of adding soot to test dust

Fig.2.26

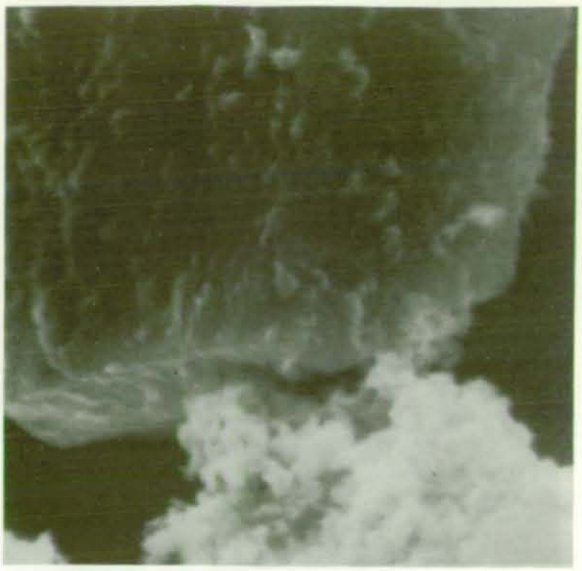

Fig.2.27

Effect of feeding AC dust and soot simultaneously to a filter

Fig.2.28

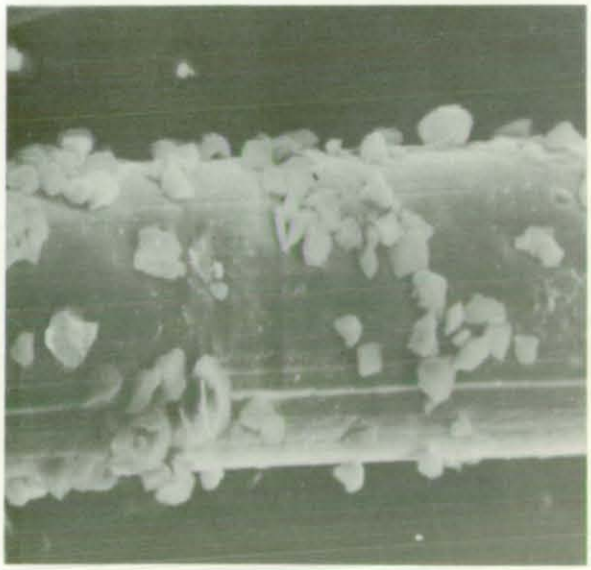

Fig.2.29

Influence of coating on collection of 5µm particles

Fig.2.30 Close up of partially loaded fibre

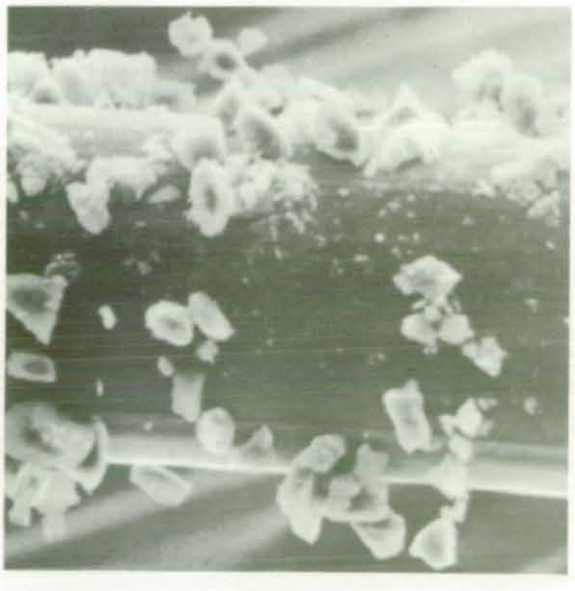

Fig.2.31

Fig.2.32

Tree formation

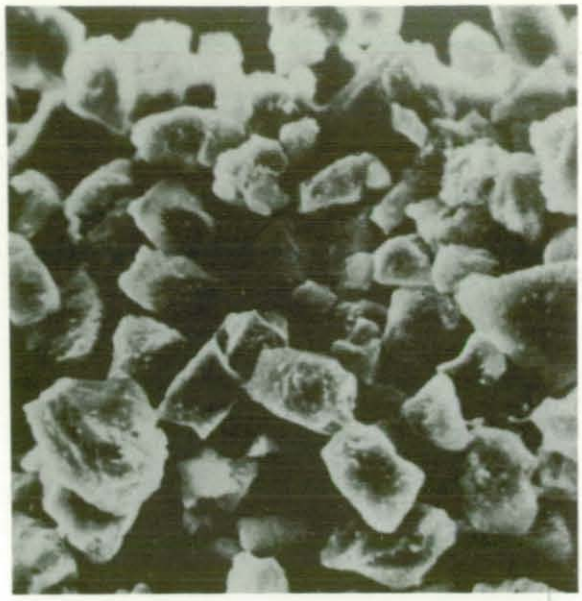

Fig.2.33

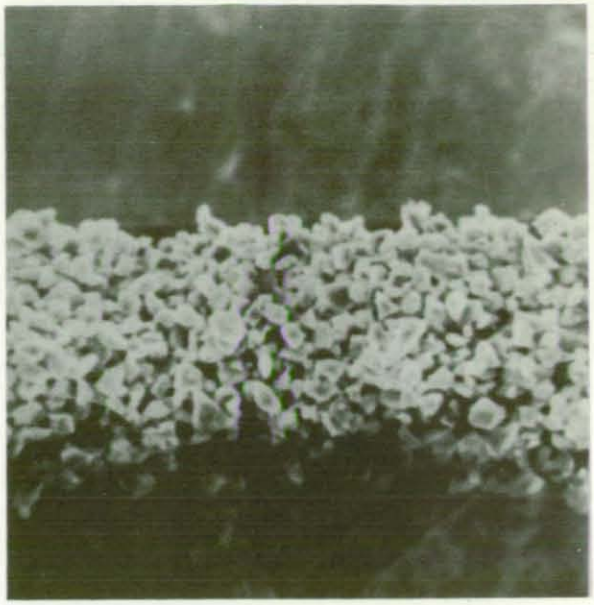

Fig.2.34

Fig.2.35
5µm particle adhering to fibre coated with a thick layer of oil (silicone fluid)

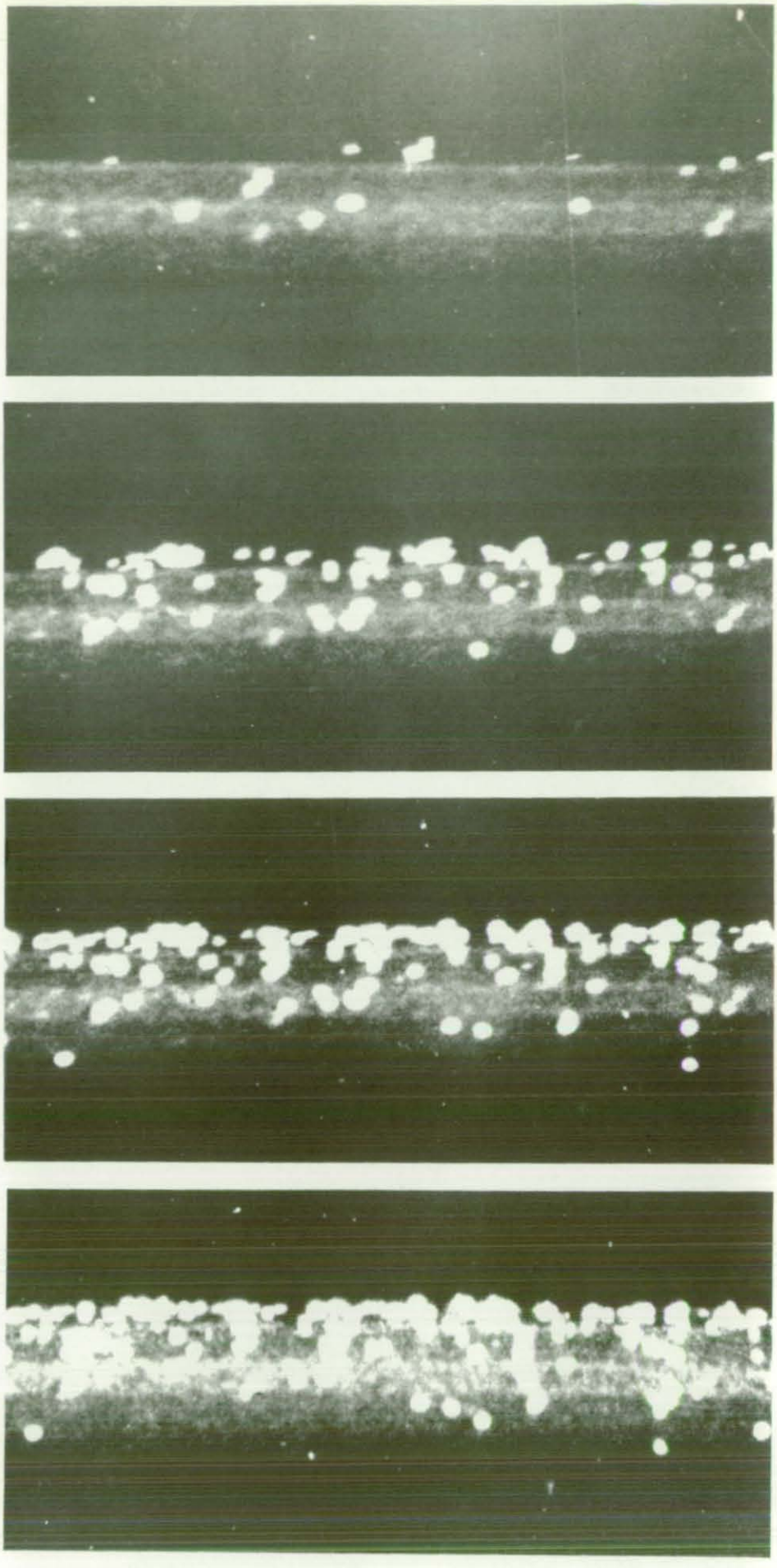

Fig. 2.36 Series of frames from cine film of 10μm particles accumulating on a 200 μm fibre

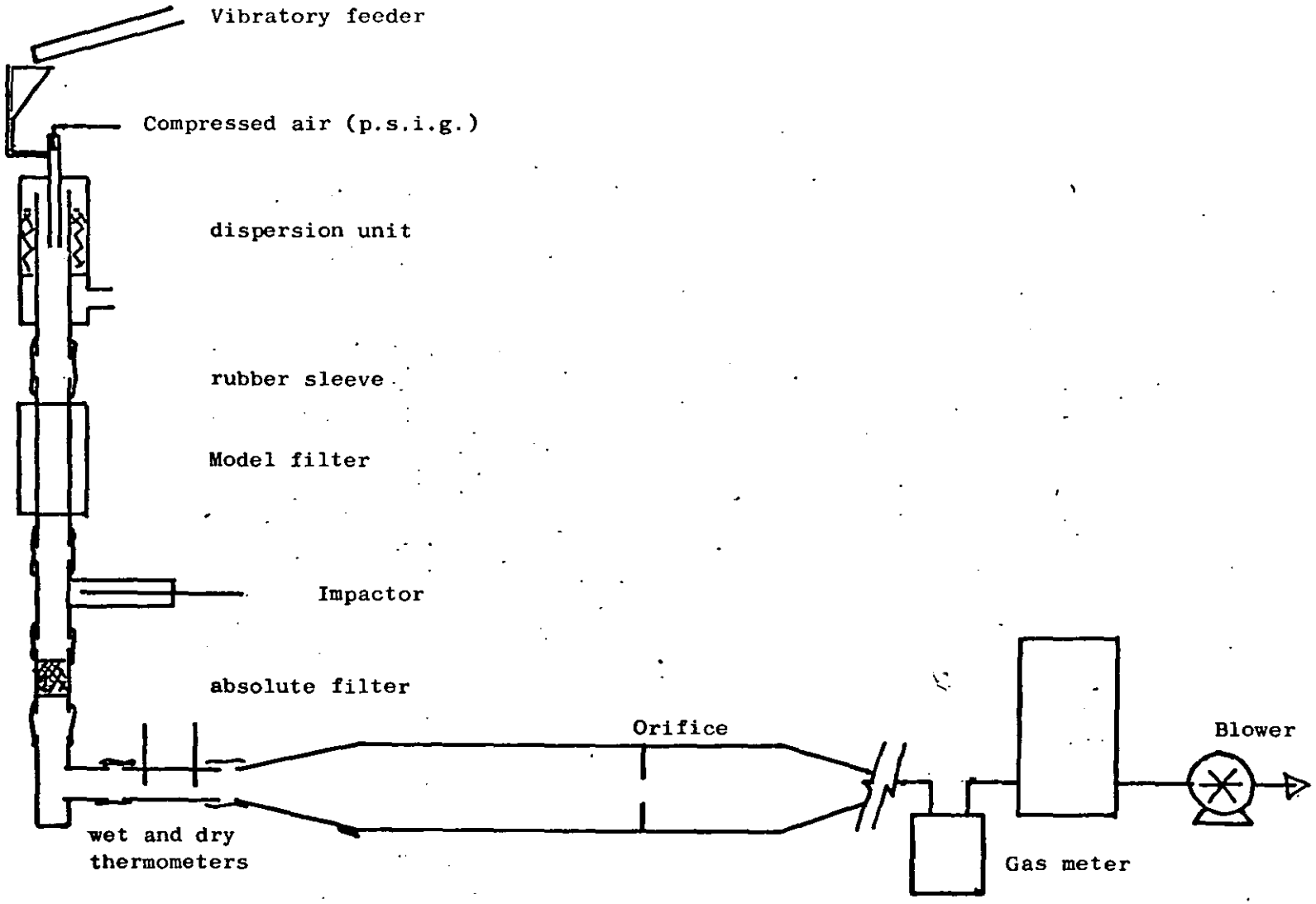

Fig. 2.37 Diagram of experimental rig.

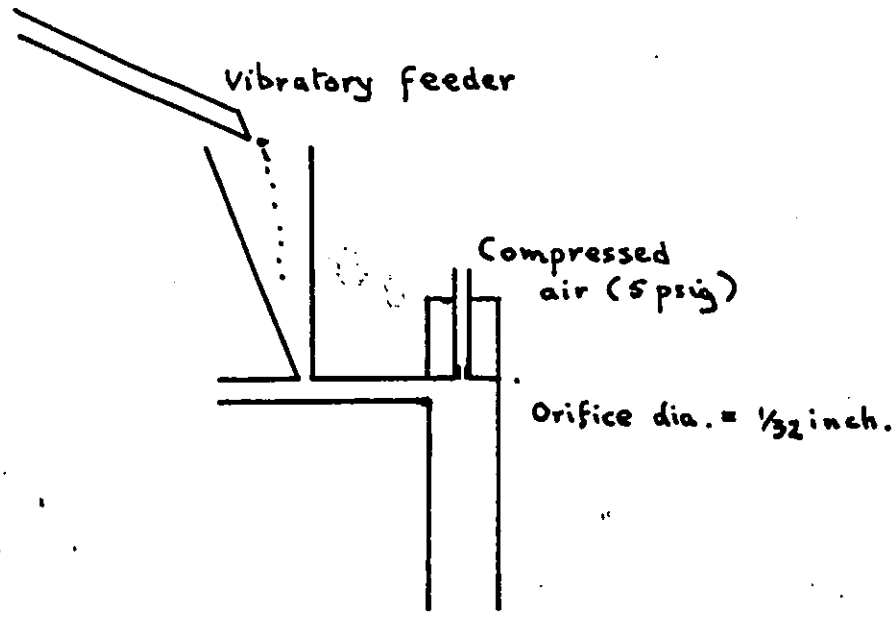

Figure 2.38 Dust dispersal unit.

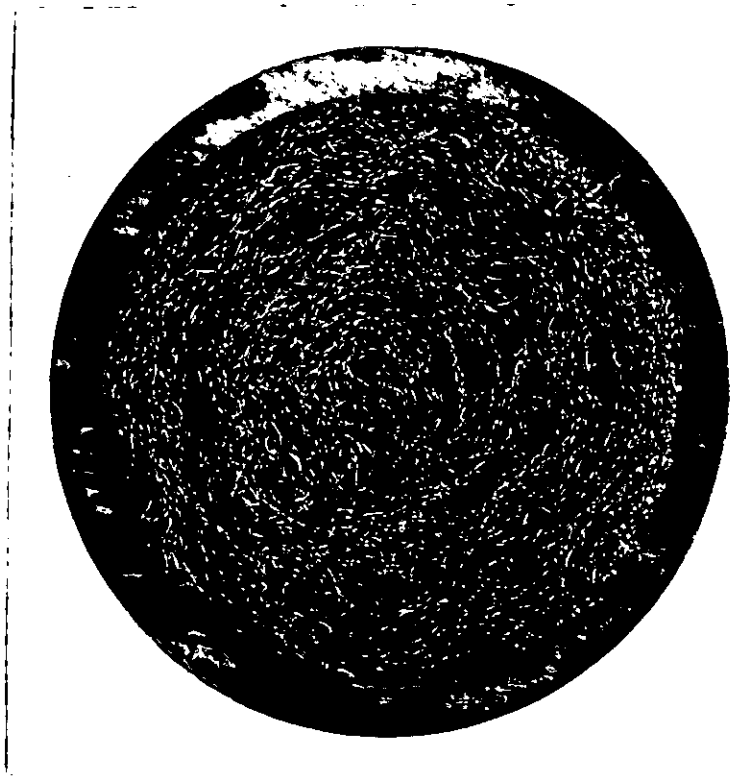

Figure 2.39. Knitmesh filter unit.

used. The properties of this filter together with the experimental conditions are summarised in table 2.6. A photograph of the filter unit is shown in fig.2.39. The filter is easy to use, can be cleaned and replaced without its structure changing and has monosized fibres.

TABLE 2.6

Experimental conditions

Velocity range (ms^{-1})	0.4 - 6.0
Particle size range (μm)	5-60
Particle density ($Kgm.m^{-3}$)	2.61×10^3
Relative humidity (%)	40 - 55
Woven wire filter	
Fibre diameter (μm)	145
Filter depth (m)	0.10
Packing density	0.10
Model filters	
Fibre diameter (μm)	50, 100
Filter depth (no of grid plates)	20
Packing density	0.03

(b) Model filters as described in references (4) and (111) were used. Theoretical analysis of filter behaviour must be in terms of the single fibre efficiency, η_s. The overall efficiency, η, which is obtained experimentally should, therefore, be related to η_s in some way which is reliable. Wong and Johnstone (2) derived two expressions.

Consideration of the efficiency of an increment of a fibre mat and integrating over the whole mat gave:

$$\eta = 1 - \exp\left[\frac{-4\alpha L}{(1-\alpha)\pi d_f}\eta_s\right] \qquad 2.28$$

Considering a fibre mat as a series of grids and considering one grid gave:

$$\eta = 1 - \left[1 - 2\eta_s\left(\frac{\alpha}{\pi}\right)^{1/2}\right]^{\left(\frac{2L}{d_f}\right)\left(\frac{\alpha}{\pi}\right)^{1/2}} \qquad 2.29$$

It can be shown that when $L^2 \gg d_f$ equations (2.9) and 2.10 give similar results. In their derivation the following assumptions were made:-

(a) Perfect uniformity of the filter.

(b) Mixing of the aerosol behind each fibre or grid.

(c) Fibres all perpendicular to the flow.

(d) Fibres ends have negligible effects.

(e) The configuration effects are negligible.

These conditions are not fulfilled in ordinary fibrous filters. However, theories of particle collection can be tested in a multiple fibre filter by constructing an idealised array of fibres or a model filter.

Model filters are constructed such that their packing, configuration and other effects are accurately definable. Work on such filters is limited, but has been carried out by Gallily (50) Fuchs and Stechkina (112), Radushkevich (113), Botterill and Aynsley (114) and by Harrop (4). Gallily (50) investigated filters made from 50 μm diameter wire, with a monodispersed d.o.p. aerosol. Radushkevich used a polydispersed aerosol of polystyrene, to investigate models made from methacrylate resin. Botterill and Aynsley investigated the effect of grids in causing particle aggregation.

Model filters offer the following advantages:-

(i) The wires in each grid are parallel to each other and normal to the direction of flow, enabling the flow through the filter to be described mathematically.

(ii) As the wire spacing is accurately known, the filter packing may be determined from the fibre geometry with confidence. The packing may be expressed as follows:-.

$$\alpha = (\pi/4)\left[d_f/(d_f + d_i)\right]^2 \qquad 2.30$$

(iii) The grids are known to be a finite distance apart, and mixing between each grid can be determined, consequently the relationship between single fibre efficiency and filter efficiency can be accurately determined from the filter geometry.

$$(1 - \eta) = \left[1 - \eta_s \left(d_f/(d_f + d_i)\right)\right]^{P_M} \qquad 2.40$$

A plate of a grid type model filter, used in this work, is shown diagrammatically in fig.2.40. The filter consists of a series of 2 inch plates separated by paper gaskets and bolted rigidly in a box. The "filter plates" are constructed of thin brass plates with a 3.8 cm hole stamped in the centre. The stainless steel wires are attached by mounting the plates on a boss and using a winding machine. Araldite was applied to fix the wire in the correct position. The wires were earthed. Details are given in table 2.6.

Two techniques of filter testing were used depending on the specific measurements to be made.

(i) The filter unit was simply weighed before and after filtration to ascertain the quantity of dust collected.

(ii) A master filter, consisting of a perspex tube tightly packed with glass wool was weighed before and after filtration.

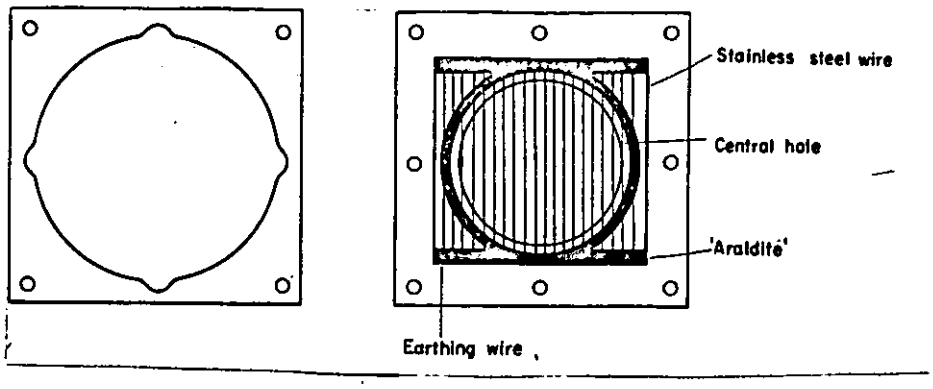

Figure 2.40 Filter plate and gasket.

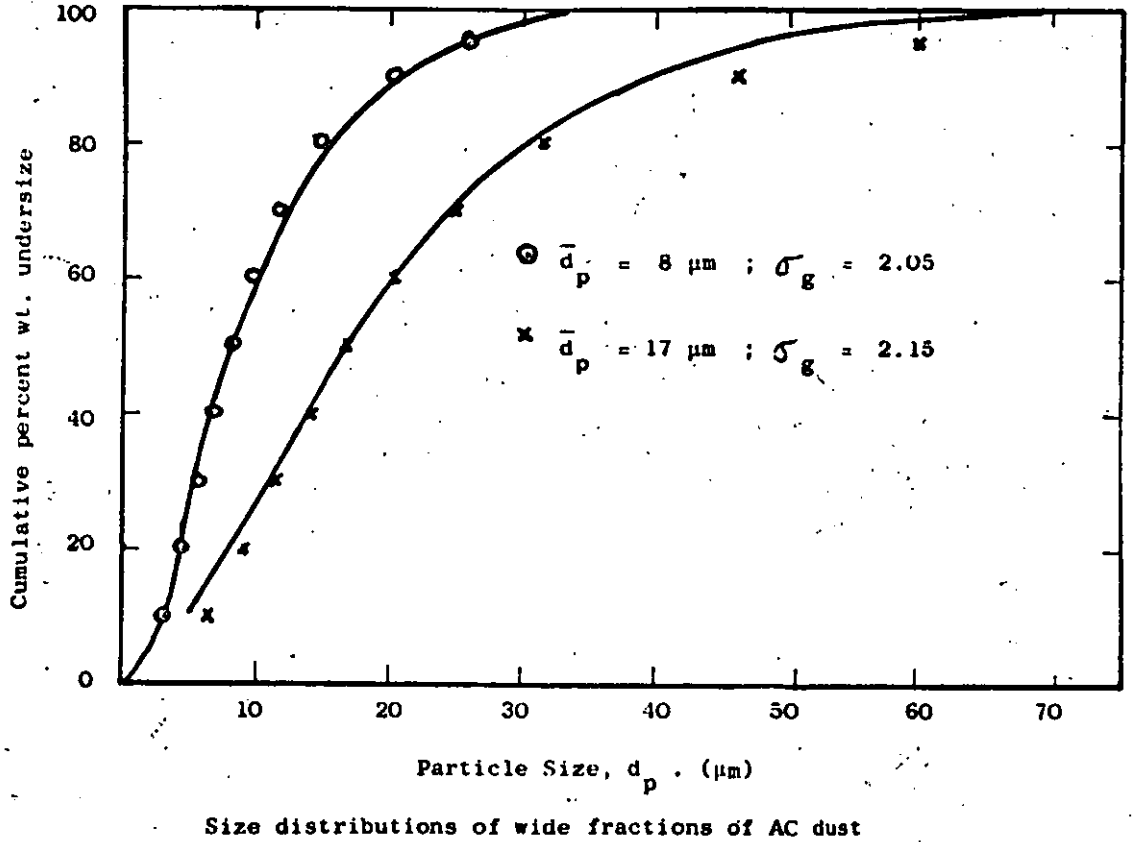

Size distributions of wide fractions of AC dust

Figure 2.41

This method was used to obtain increased sensitivity when a small quantity of dust was fed.

In these tests both narrow and wide fractions of AC test dust were used. The fractions were obtained using a Zig-Zag classifier and analysed by gravity sedimentation (Microscal technique). It was found that each fraction closely fitted a log-normal distribution (for an example see fig. 2.41 in which the distributions of 0-25 and 0-60 μm material are shown). The median values and geometric standard deviations of all the dust used in this work are shown in table 2.7.

Before application of the technique it was necessary to test it and the influence of a number of ancillary parameters. The results of these tests are described below:-

(a) Velocity Profile : The velocity profile immediately upstream of the filter was measured by performing a pitot traverse. The profile is shown in fig. 2.42 together with a profile measured behind a filter. The maximum velocity is approximately 20% greater than the average for an unimpeded pipe and 10-15% greater than the average behind a filter. It is considered that this is sufficiently close to plug flow for wall effects to be insignificant in the filtration tests. This was confirmed by microscope examination of the surface of filter elements which showed no detectable variation of deposition with position.

(b) Vibration : A microphone, inserted in the unit, detected a high frequency sonic vibration (30 ks/s) which was produced by the dust dispersion unit. To determine the relative importance of this phenomenon the entire filter unit was artificially subjected to an ultrasonic vibration of similar frequency but much higher intensity. This extreme measure did not produce a measurable reduction in efficiency. It is concluded, therefore, that vibrat-

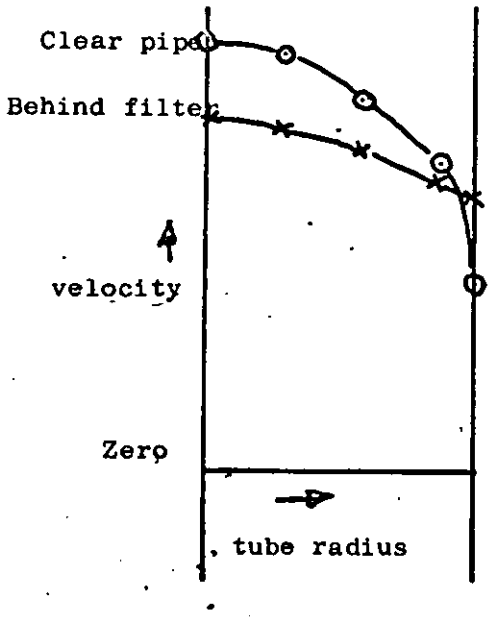

Velocity Profile in test unit

FIGURE 2.42

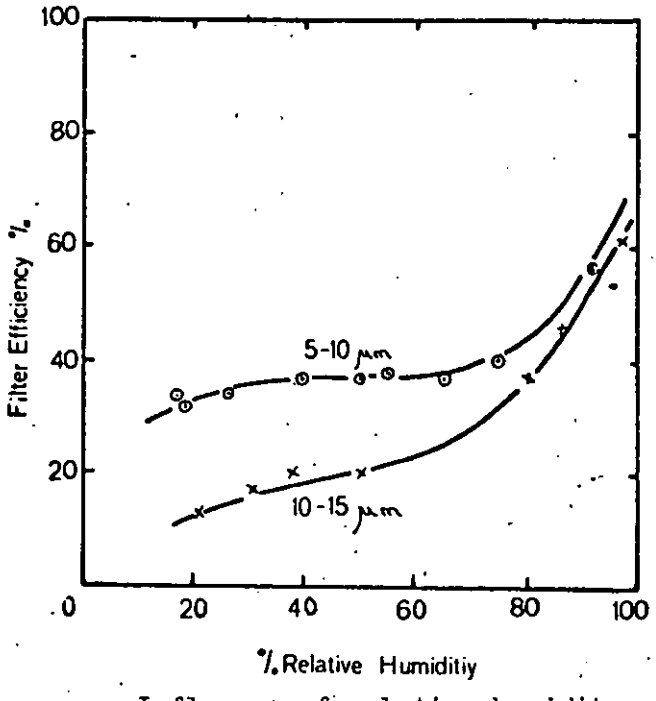

Influence of relative humidity on efficiency of filtration of AC dust.

Figure 2.43

ional effects of this nature do not have a significant influence on the results of tests made using this technique.

(c) Feed rate : Experiments showed that the feed rate did not affect the results significantly provided it was less than about 1 gm per minute. Consequently all experiments were conducted with a constant feed rate of 0.2 gm per minute.

(d) Relative humidity : Tests were performed using 5-10 μm and 10-15 μm fractions of AC dust to determine the influence of relative humidity. The results are shown in fig. 2.43. The effect on a dry fibre is identical to that observed by Zimon (90) and Harrop (4) as described above. Henceforth all tests were performed at 40-55% R.H.

(e) Dust loading : The efficiency is sensitive to this parameter, especially at low loadings. The results described immediately below were obtained on the addition of 1 gm of dust to the unit. The quantity of dust finally collected in the filter is equivalent to a uniformly distributed layer of dust approximately one particle diameter in depth where woven wire filters are used. Where model filters are used the final dust layer is deeper.

Titrametric Analysis

The apparatus described above was used to filter classified fractions of limestone. The quantity of dust collected on a cotton wool absolute filter was determined titrametrically. The limestone was removed from the cotton wool using .02$\bar{N}$ HCl which was subsequently back titrated with .005$\bar{N}$ Na_2CO_3. The accuracy of the method was found by determining the quantity of material retained in the absolute filter and a test filter and comparing this with the weight of limestone added; when a sample of 0.05 grams was added the error amounted to 4%. This compares with an error of 1-2% for a 0.25 gram feed and 6-8% for a 0.1 gram feed

when an absolute filter was used to measure the efficiency of collection of AC dust gravimetrically. Three test runs were performed, each measuring the efficiency at a series of different filter loadings, to illustrate the reproducibility of the method (see fig.2.44).

2.5 Results and Discussion

Upon conducting tests with narrow sized fractions of dust it became apparent that the efficiency of filtration was sensitive to loading in the initial stages. This effect, due to the rapidly changing nature of the fibre surface, is complex and will be different for different particle sizes. With a dust of wide size distribution, the effects with different particle sizes tend to cancel each other and the influence of loading on efficiency is not so pronounced. By using such wide distributions the overall effect of some of the main parameters may be observed. Some tests described below merely show trends and are not intended to give definite qualitative data which would be misleading.

(a) Velocity : One gram of AC test dust was fed to model and woven wire filters. The efficiency is clearly shown as a decreasing function of velocity in fig. 2.45.

(b) Particle size : Classified fractions of AC test dust were fed to the filters with the results shown in figs. 2.46-47. Again as expected the efficiency is a decreasing function of particle size. The single fibre efficiency was obtained from the results of tests using model filters and applying equation 2. The single fibre efficiencies shown in figs. 2.47 are low (the collision efficiency is close to 1.0) but these values were confirmed by counting particle concentration, under an optical microscope, on

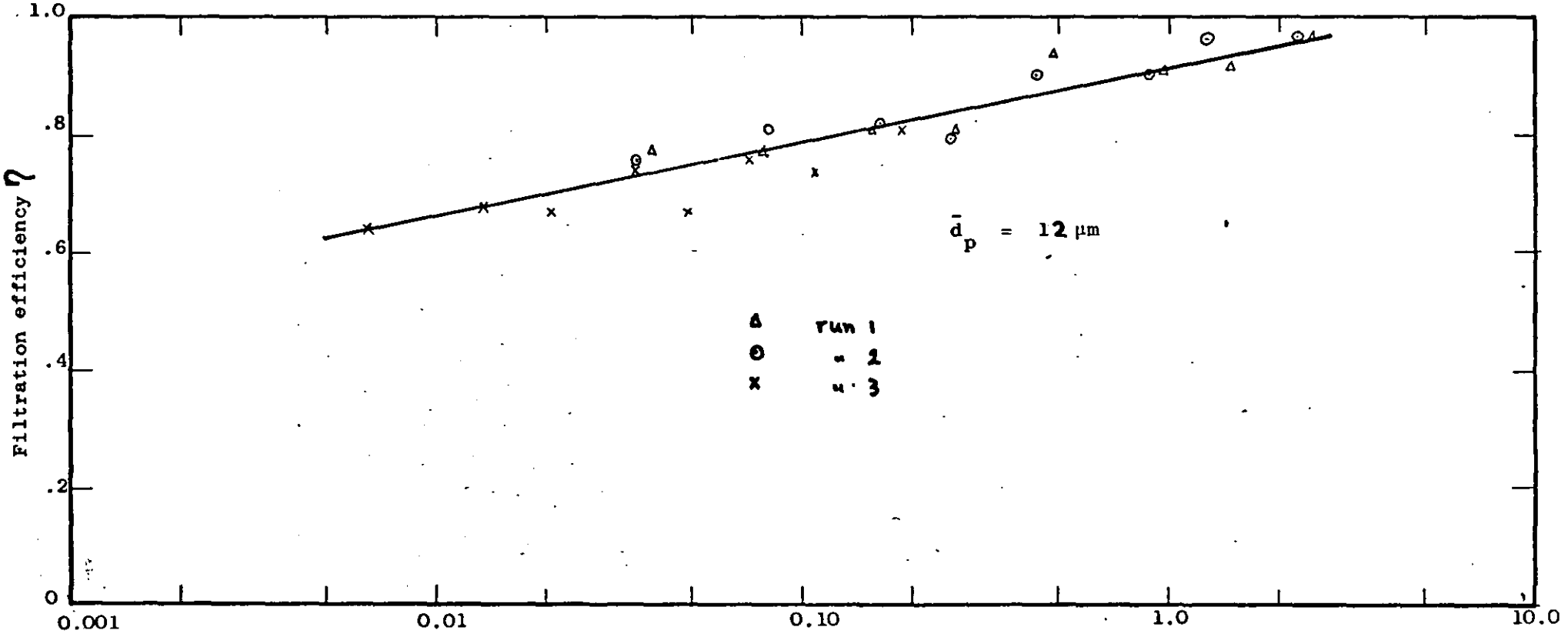

Fig. 2.44 Results of reproducibility tests.

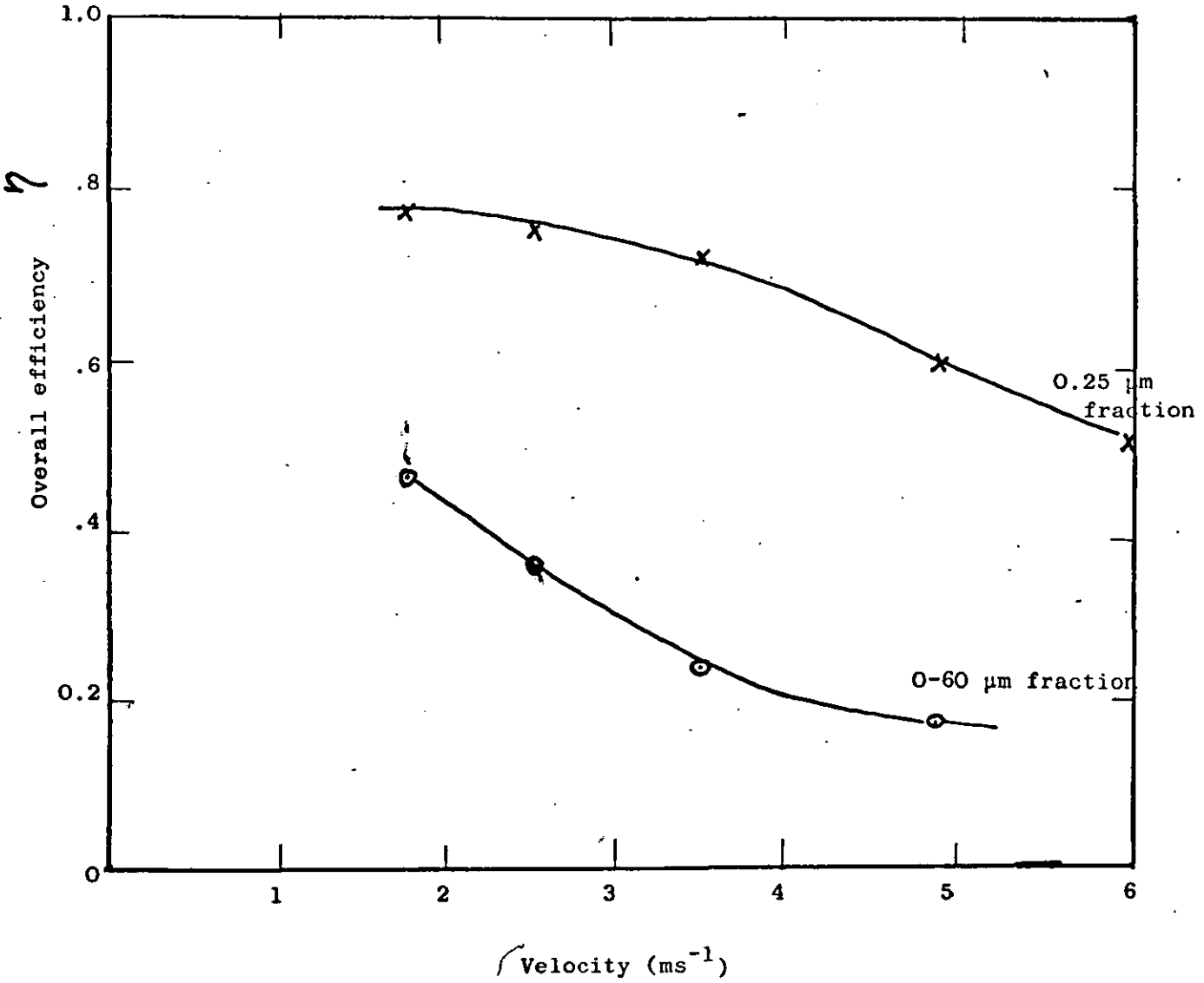

Fig. 2.45 Influence of velocity on filtration efficiency.

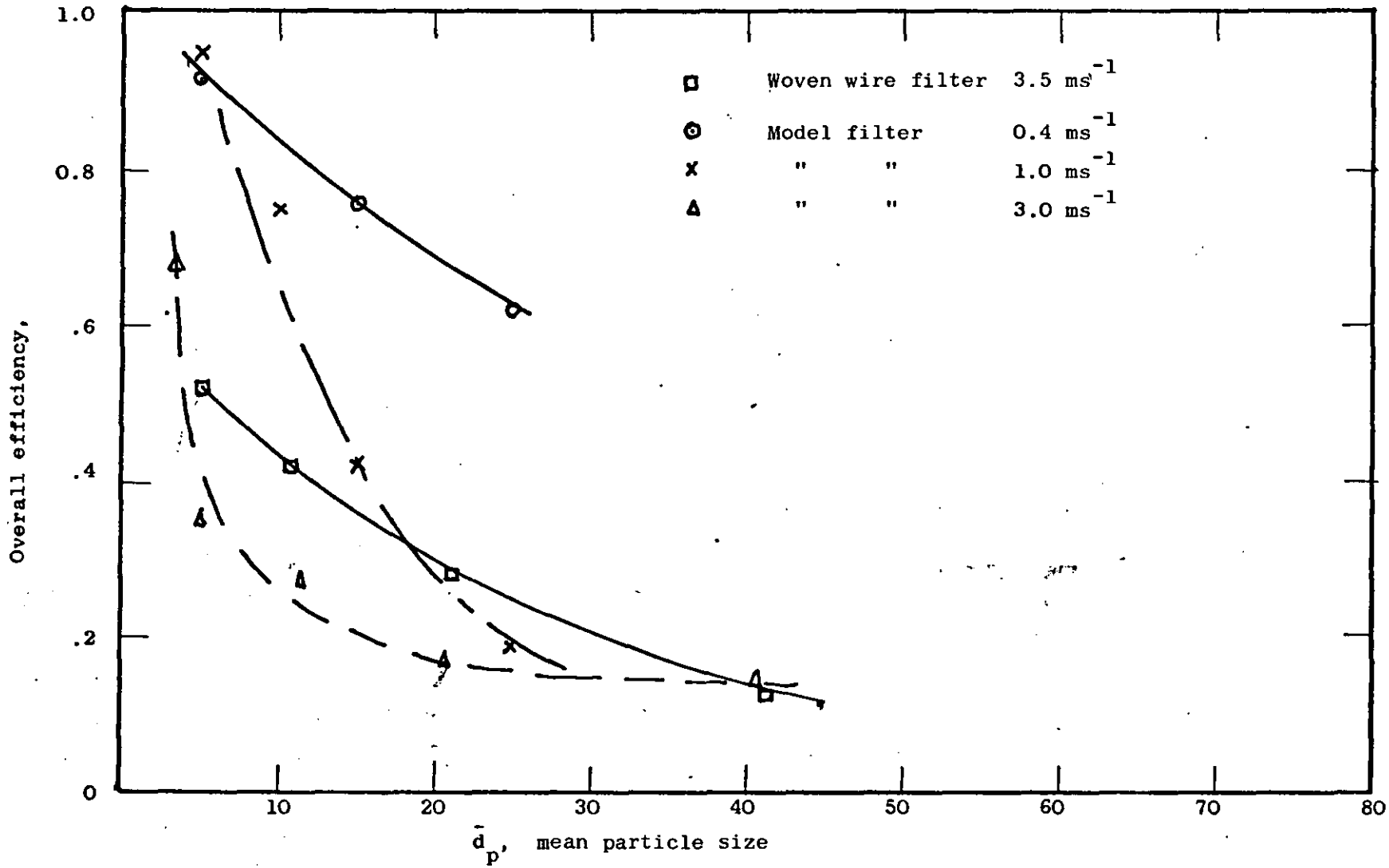

FIGURE 2.46 Influence of particle size on efficiency.

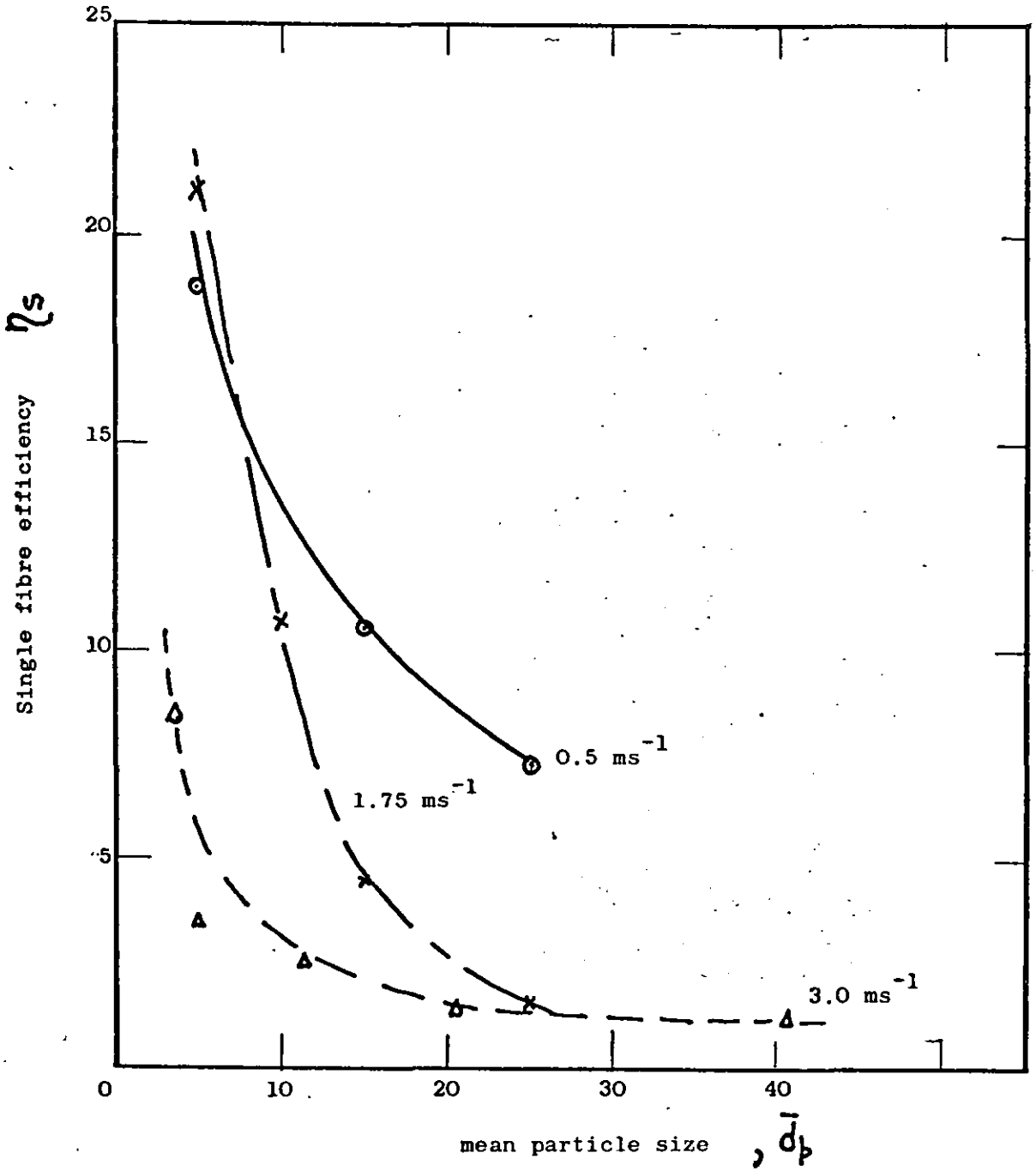

FIGURE 2.47 Influence of particle size on efficiency.

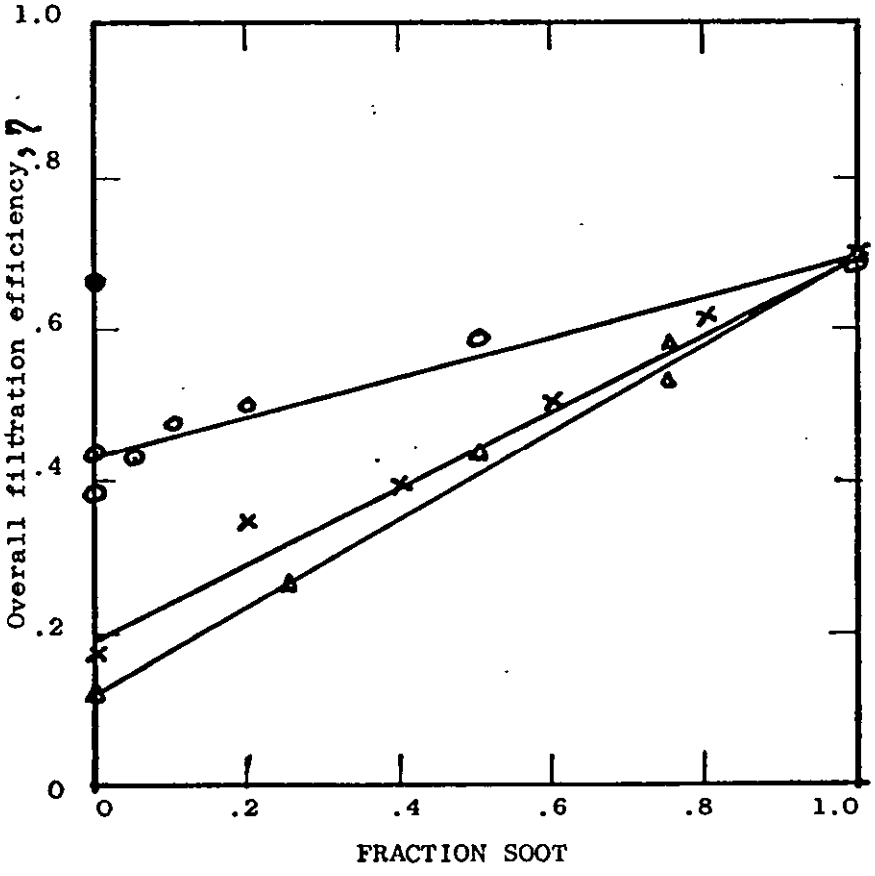

AC dust(fine)

Soot coated filter - efficiency of AC fine collection

0-60 μm fraction

AC coarse dust

Velocity, U_o = 3.5 m s^{-1}

Knitmesh filter

FIG. 2.48 Influence of dust/soot ratio on initial filtration efficiency

fibres of the model filter. Every third grid in the filter was adhesion coated with vaseline; the concentration on coated grids could then be compared with that on dry grids (see table 2.8).

The results contained in this section confirm that the efficiency in the low adhesion regime is a decreasing function of both the particle size and velocity. In all cases considered the critical particle size is below 5 microns, probably in the region 1-4 microns. Once the critical particle size is reached the single fibre efficiency decreases very rapidly as predicted in section 2.3. Since the efficiency in this region depends almost exclusively on the particle shape and orientation as well as the method of collision with surface irregularities, it is virtually impossible to concieve a theoretical description of this part of the characteristic. However, it should be possible to develop a semi-empirical extension of section 2.3. In section 2.3 only the mean adhesion energy of particles was considered; it is obvious, however, that any species of particle will have a distribution of adhesion energies on impact. A realistic model would, therefore, incorporate an energy distribution function into the theory and so describe the system behaviour in the region beyond d_{pcrit}.

Such a theory, the concept of which is supported by the above results, would incorporate the important physical properties of the system and, more significant from a practical point of view, be used to predict those properties of fibres which are most conducive to strong adhesion.

TABLE 2.7

Size analyses of dusts.

Material	Mass median size	Geometric standard deviation
AC dust	3.8	2.04
AC dust	4.9	1.29
AC dust	8.0	1.45
AC dust	10.0	1.14
AC dust	11.4	1.23
AC dust	19.0	1.15
AC dust	20.7	1.23
AC dust	28.0	1.17
AC dust	40.7	1.26
AC dust (0-25μm)	8.0	2.05
AC dust (0-60μm)	17.0	2.15
Limestone	4.0	2.00
"	12.0	1.28
"	26.0	1.34
AC Fine		
AC Coarse		

Note: All size analyses were obtained by sedimentation.

TABLE 2.8

Particle Counts on Model Filters.

Grid Plate No.	10	11	12	13	14	15	16	18
Number of particles	104	122	1032*	74	58	800*	50	706*
Relative efficiency			0.078			0.067		

Random particle counts on a total of 400 length of fibres in a model filter. Velocity 1 ms^{-1}, particle size 10μm.

* gridsadhesion coated

CHAPTER 3

Non Stationary Filtration

1. High Adhesion systems

2. Low Adhesion systems

2.1 Literature

2.2 Experimental

2.2.1 Influence of filter depth

2.2.2 General characteristics

2.2.3 Soot addition

2.3 Discussion of Results

2.4 Conclusions

CHAPTER 3

Non Stationary Filtration

This chapter is concerned with the behaviour of fibrous filters under load. The deposition of particles within a filter alters its collection efficiency so that the efficiency of an individual fibre varies both with position and age. Thus the behaviour of filters in a loaded condition is much more complex than that of "clean" filters; the subject has received comparatively little attention despite its obvious practical importance. In the following sections the literature on systems in which particle adhesion is complete is reviewed and some exploratory experimental work on the behaviour of filters in which adhesion is not complete are described and discussed.

3.1 High Adhesion Systems

Radushkevich (116) described the secondary processes of filtration qualitatively in four catagories:-

(i) Co-precipitation : As particles build up in a filter they act on efficient collision targets for further collection - trees of particles are formed. Eventually the front of the filter becomes clogged and seiving becomes the predominent collection mechanism leading to cake formation. A relatively low increase in resistance is followed by a rapid increase due to clogging.

(ii) Capillary phenomena : Capture of liquid droplets causes wetting of the filter material a change in its structure and reduction in efficiency.

(iii) Destruction of filter : Swelling due to moisture and chemical decay, particularly at high temperatures, may cause severe structural damage of a filter mat.

(iv) Loss of electric charge : Electrostatic filters loose their collection properties due to charge leakage and chemical decomposition of the resin layer.

Of these secondary processes the first is of most practical importance and is the only one to receive any research attention.

Radushkevich (116) considered that the rate of accumulation of particles in a filter is due both to collection on the clean filter and collection on deposited particles:-

$$\frac{\partial \sigma_s}{\partial t} = \frac{2 \eta_0 U_0 c \alpha}{\pi r_f} + \gamma_2 a' U_0 c \sigma_s \qquad 3.1$$

η_0 = single fibre efficiency

γ_2 = particle collection efficiency

c = concentration of air blown particles

σ_s = deposite within the filter

a' = effective area of unit deposite

By combining this with the continuity equation and solving he obtained an expression for the influence of depth and time on the overall efficiency:

$$\eta = 1 - \frac{c}{c_0} = 1 - \frac{1}{1 + e^{c_1 t}(e^{\lambda_0 L} - 1)} \qquad 3.2$$

where :-

$$c_1 = \frac{U_0 c_0 a' \gamma_2}{(1-\alpha)} \quad ; \quad \lambda_0 = \frac{2 \eta_0 \alpha}{(1-\alpha)\pi r_f}$$

Experimental results (117) in the diffusion region suggest that $a'\gamma_2$ is about the same order of magnitude as the cross sectional area of the particles. Equation 3.2 is applicable only in the early stages of filtration. By assuming that the single fibre efficiency, η_s, increases linearly with σ_s, Yoshioka and Sato (118) derived the same expression but using

$$a'\gamma_2 = \frac{\eta_0 2\alpha k_1}{\pi r_f}$$

where k_1 was found empirically to be 5.0. They confirmed the expression experimentally using particles in the inertia region.

Equation 3.1 can be simplified to

$$\frac{-1}{U_0(1-\alpha)}\frac{\partial \sigma_s}{\partial t} = \frac{\partial c}{\partial L} = \lambda_1(\lambda_0, \sigma_s)\, c \qquad 3.3$$

where the simple function

$$\lambda = \lambda_0(1 + k_1 \sigma_s) \qquad 3.4$$

is used.

λ_0 is a unit or volume collection efficiency for the clean filter which is given by $\frac{2\eta_0\alpha}{(1-\alpha)\pi r_f}$. Expressions for k_1 are given in table 3.1

TABLE 3.1

Values of k_1 suggested for equation 3.4

Radushkevich (general)(116)	$\frac{\gamma_2 a' \pi r_f}{2\eta_0\alpha}$
Radushkevich (diffusional region)(119)	$\frac{3 D_B^{2/3} \pi^2 d_p^{4/3} U_0^{-2/3} d_f}{16\eta_0\alpha}$
Yoshioka et al (inertial region)(118)	5.0
Kimura et al (inertial region)(120)	$\frac{12.5\mu}{d_p \rho_p \rho U_0 L}\left(\frac{\pi}{L}\right)^{\frac{1}{2}}$

Radushkevich attempted a theoretical description of k_1

by considering the kinetics of coprecipitation in the early stages of filtration. He showed the dependence of k_1 on d_p, U_o and D_B by considering the collection efficiency of single particles in a filter in the diffusion region (119); the influence of agglomerates on the course of filtration has not yet been determined. Kimura et al (120) applied dimensional analysis to previously published results (121,122) to obtain k_1 in the inertial region.

Davies (123) applied a different approach to the study of clogging filters. The resistance, R', to gas flow through a filter is related to the total aerosol penetration P. It was found experimentally that

$$P = P_o \gamma_3^{\left(\sqrt{R'/R_o} - 1\right)} \qquad 3.5$$

$$\text{and} \quad \frac{1}{R'} \frac{dR'}{dt} = \alpha_1$$

α_1 and γ_3 the clogging parameters, are related to the single fibre efficiencies by

$$\gamma_3 = e^{\frac{2\eta_o \alpha L}{(1-\alpha)\pi r_f}} = e^{\lambda_o L}$$

$$\alpha_1 = \frac{2}{t} \ln\left(\frac{\eta_s}{\eta_o}\right) = \frac{2}{t} \ln\left(\frac{\lambda_1}{\lambda_o}\right)$$

Expressions were derived to enable the mean efficiency and the quantity of deposite in a filter over a period of use to be calculated from the clogging parameters.

Several attempts have been made to obtain an expression for the increase in resistance due to dust loading. Yoshioka (124) derived a complex expression based on the Kozeny Carmen equation and the increase in surface area due to the presence of particles. The expression contains two constants which must be determined experimentally. Juda et al (125) used a model based on the

cellular flow field. As particles accumulate within the filter they build up to form a new equivalent fibre diameter; their presence is thereby taken into account in predicting the drag. The model is simpler and more elegant than that of Yoshioka but still requires the experimental determination of two constants. It is difficult to envisage how the density of particle packing on the fibre and the overall shape of the deposit could be determined other than empirically.

3.2 Low Adhesion Systems

3.2.1 Literature

Virtually nothing is published on the behaviour of low adhesion systems under load. Whereas with high adhesion systems dust builds up on the fibres until clogging occurs with low adhesion systems the dust builds up until a stage is reached where agglomerates break off. When this happens the unit will act as an agglomerator and eventually become completely ineffective as a filter. The critical conditions which cause a filter to behave in one way or the other are not known.

The primary mechanism of agglomerate removal have not yet been elucidated; it may be due to either air drag or particle bombardment or any of the other mechanisms mentioned in Chapter 2. Particle removal experiments by Corn (83) led him to conclude that air drag was responsible for non adhesion. However, Loffler (78) was able to show a non-compatability in Corn's reasoning. He showed that the blow off speed for both mono-layers of particles and "heaps" is well above that commonly used in practice and above which such mono-layers and heaps fail to form. He reported a factor of 10 for single particles and a factor of 4-5 for "heaps".

Just as bounce has been shown to be the main reason for non-adhesion of single particles it is obvious that bounce, or bombardment of agglomerates, is an extremely important force in the present case. On the other hand the blow off factor is reduced from 10 to 4-5 showing that blow off is becoming increasingly important as the size of agglomerate increases. This is obvious since the bombardment force does not change but the drag force increases with agglomerate size. As, therefore, the agglomerate size for dislodgement increases, air drag will become more important and particle bombardment less important.

A critical size of agglomerate will occur when further particle impact together with the existing air drag are sufficient to cause removal.

The rate of increase in collection efficiency with loading will be effected by the voidage of material collected. Lapple et al (126) showed that the velocity of particle collection had a strong influence on this, the particle voidage varying from 95-99% at 0.3 - 3 ms^{-1} to 60-80% for 10-30 ms^{-1} with 1.4 μm particles. Their experiments were conducted in the inertial regime in which the predominant mechanism was collision (although at the higher velocities there was evidence of non-adhesion) and their results support the validity of equation 3.4.

In complete adhesion systems as described in Radushkevich's first classification the efficiency of filtration increases with loading. However, in systems in which adhesion is not complete the filter behaviour may be much more complex. A number of phenomena can occur depending on the conditions prevailing; these may be calssified as follows:-

(i) The adhesion conditions between a particle and fibre surface are different from those between a particle and a surface coated

with particles. This will be affected by the increase in surface roughness, impact angles and particle and fibre adhesion strengths. Consequently the clean single fibre efficiency will change, either increasing or decreasing, to that of a fibre coated with a monolayer of particles. This will occur early in the filtration process.

(ii) If the layer of particles is cohesive material will accumulate on the fibre. Due to the increase in apparent cross sectional area of the fibre the efficiency will increase with loading until clogging occurs.

(iii) If the layer of particles is not cohesive agglomerates will be removed from the filter by increased drag and bombardment. The efficiency of removal will be continuously reduced to zero when the filter reaches maximum loading and acts only as an agglomerater. Depending on the cohesiveness of the particles adhering to the filter this may occur later in the life of the filter so that a maximum can occur.

Published quantitative experimental work on filtration efficiency in this regime is sparse. Kimura et al (127) examined urethane foam filters (which have non-circular fibres) using dust of average mass median size 3-5.5 μm, at 0.5-5.0 ms^{-1} to show that the cumulative collection efficiency goes through a maximum with loading. They gave the critical dust load at maximum efficiency for their systems as:

$$\bar{\sigma}_c = \frac{0.64\, d_p\, g_c}{\rho\, U_o^2} \left(\frac{\alpha}{d_f}\right)^2 L \qquad 3.6$$

Their results show that the degree of adhesion was very high in almost all of their experiments. It is difficult to

reconcile equation 3.6. with their graphed data (particularly with regard to the influence of fibre size) and to get a true measure of the effect of filter depth. Because of the very specific nature of the filter it would be wrong to apply their results to any other system. Qualitatively they are valuable showing that the critical load, before re-entrainment commences, is a reducing function of velocity.

The only other work that has been reported on the behaviour of large particles ($>5\mu m$) is on their removal from filters (81) and on the pressure drop across loaded filters. In their work on pressure drop Botterill and Aynsley (114) studied the factors which influence particle agglomeration but the quantity of dust retained on the filters was not measured in their experiments.

In view of the absence of experimental data on the loading behaviour of filters in the low adhesion region a series of exploratory experiments was performed. These are described below.

2.2. Experimental

The experimental methods used to determine the influence of loading on the behaviour of low adhesion systems are those described in section 2.4.2. Where a high loading (dust retained in filter $>$ 0.5gm or $\sigma_s > 0.02$ approx) of AC dust was used the filter under test was carefully removed from the system, weighed and replaced before the next run; this was continued until a high load was obtained. With low (dust retained < 0.5 gms or $\sigma_s < 0.02$ approximately) dust loads the quantity of dust retained in the master filter was ascertained periodically. The rate of dust feed and other conditions were constant throughout each test. The range of experimental conditions employed is shown in table 3.2. These

experiments were designed to examine the influence of the major physical parameters on both the filtration efficiency and pressure drop. The parameters investigated were particle size, size distribution, face velocity and fibre size and filter depth.

TABLE 3.2

Particle type	AC dust and Limestone
Particle sizes	See Table 2.7
Fibre type	Stainless steel
Fibre sizes	50 m and 100 m
Filter packing density	0.03 (model filters)
Particle density	2.6×10^{-3} Kgm m^{-3}
Range of loadings	0.05 gm - 10 gm
Range of specific loadings	0.0003 - 0.5
Face velocity	0.4 - 7.9 ms^{-1}
Reynolds number	2 - 20
Pressure drop	7.5×950 N m^{-2}

(A series of experiments using a mixture of AC coarse dust and soot was performed using a woven wire filter. The conditions of this experiment are described below).

Description of Experimental Conditions

The results are given in tables 3.3, 3.6, 3.8, 3.10, 3.12, 3.14 and 3.15 in which the pressure drop and overall efficiency are expressed in terms of the total dust fed to the filter. The incremental efficiency is the collection efficiency for each individual test during a run (i.e. in the case of the second test reported in table 3.3 for 5 grids, the efficiency of collection of the second quantity of dust added (0.05 gms) is 0.35). Figs. 3.3 - 3.8 show the results graphically in terms of dust actually retained in the filter. The pressure drop recorded is that at the end of each individual test.

The influence of relative humidity and reproducibility on the loading experiments when using limestone is shown in table 3.3 and fig. 3.1. The results of experiments performed at 35% and 45% relative humidity show no significant difference. All subsequent tests with limestone were performed within this range; some tests with AC dust were performed at conditions up to 55% R.H. since this was previously shown to be acceptable for that material.

In an attempt to obtain some measure of the change in efficiency and pressure drop with loading the factors shown in the following expressions were calculated:

$$\frac{\lambda}{\lambda_o} = \frac{\eta_s}{\eta_{si}} = 1 + \bar{k}_1 \sigma_s \qquad 3.7$$

$$\frac{\Delta p}{\Delta p_o} = 1 + \bar{k}_2 \sigma_s \qquad 3.8$$

The value of $\bar{k}_1$ thus obtained is not the same as k_1 in equation 3.4, but is the closest experimental determination of it.

Values of σ_s, $\Delta p/\Delta p_o$ and η_s are shown in tables 3.4, 3.5 3.7, 3.9, 3.11 and 3.13. The average values of $\bar{k}_1$ and $\bar{k}_2$ for each run are shown. $\bar{k}_1$ was obtained by plotting η_s as a function of σ_s. The slope of the resulting plot which was taken as linear was divided by its intercept, η_{si}.

Influence of Filter Depth

The single fibre efficiency is a function of loading and therefore depth. Hence it is necessary to examine the relationship between efficiency, depth and loading first. The initial loading region was studied using limestone dust and the high loading region using AC dust.

The results of a titrametric test on limestone dust are shown in tables 3.3-3.5 and figures 3.1 and 3.2. 12 μm limestone was fed to model filters of 4 depths. The efficiency was measured for dust feed loads between 0.001 and 0.22 gms (in a filter containing 5 grids with a particle voidage of 0.5, 0.01 gms is equivalent to a single layer of particles). Fig. 3.1 shows the influence of loading on the overall efficiency for each depth of filter. The 10 and 20 grid results, each at two different humidities, show that the relative humidity was maintained within sufficiently narrow limits not to influence the results. Figure 3.2 shows log (penetration) against depth. The single fibre efficiency is proportional to the slope of the curves. Even at the lowest loadings the efficiency decreases rapidly over the first 5 grids; thereafter it becomes reasonably constant. The reasons for this may be as follows:-

(i) The dust is not monosized and the particles which are most easily captured will be collected by the initial layers (i.e. η_c varies).

(ii) The efficiency of particle retention may vary substantially between particles which have the same Stokes diameter. This may be due to the availability of active adhesion on sites (particle shape will influence this).

(iii) The relatively large loading at the front of the filter (although it is only a monolayer of dust) may cause an increase in efficiency.

It is likely that each of these contributes towards the high efficiency in the initial layers. The polydispersity is not sufficient for (i) to be soully responsible and the results at higher loadings which show little evidence of an increased effic-

iency of the last 30 grids indicates that (iii) is not entirely responsible for the effect. Hence it is considered that (ii) is significant.

Tests performed with a wider size distribution using AC dust and with a much higher loading permitted the determination of the weight of dust deposited on each grid of a filter. The results of such tests for 3 loadings are shown in fig. 3.3. In fig. 3.3 the logorithm of each grid loading is plotted against depth. A linear relationship indicates a single fibre efficiency which does not vary with depth. With loading the concavity should increase but as the maximum loading is approached (as described in section 3.2.1) the curve will flatten out and become concave upwards until the maximum loading is achieved. Despite the wide scatter in the results it is obvious that the filter is approaching its maximum load. In the case of the highest load in which a high deposite was found on the first grid, clogging occurred.

These results confirm the reasoning in section 3.2.1 and show that accurate experimental quantitative data cannot be obtained by testing a filter of one fixed depth. This is shown in table 3.5 in which the values of F'', $\bar{k}_2$, η_{si}, $\bar{k}_1$ and the pack efficiencies are given. The pack efficiency is the single fibre efficiency based on the behaviour of the last section of the filter. However, it is possible to obtain information of a qualitative nature using a fixed depth filter. The results of such tests are described in the next two sections.

General Characteristics.

Initial Loading

The influence of particle size, velocity and fibre size on the initial loading characteristics of limestone are shown in tables 3.6-3.9 and figs. 3.4 and 3.5. The effect of velocity on

the behaviour of 12 μm particles (fig. 3.4) clearly shows that non-adhesion is the predominant mechanism, the efficiency reducing with gas velocity.

It was shown in the previous sections that the concept of the single fibre efficiency is of dubious value when attempting an accurate description of filter behaviour in this region. However, its application still provides the most fundamental measurement of capture efficiency. It has been used, in conjunction with equation 3.7 to give a comparative measure of the efficiency and the way in which it is effected by the main operating parameters.

A value for the initial single fibre efficiency, η_{si}, was obtained from these results by extrapolating a graph of η_s versus σ_s to zero loading. This procedure introduces inaccuracies but facilitates an estimate of η_{si} which can be compared with the theoretical collision efficiency to give a value for η_A. The values of η_A thus obtained are shown in tables 3.7 and 3.9; they show the same trend.

The effect of increasing the fibre size from 50 μm to 100 μm is shown in tables 3.8 and 3.9 and in fig. 3.5. Although the effect is not large an increase in overall efficiency with fibre size is shown for the 12 μm and 28 μm dust. However, the trend is reversed for the 4 μm dust. The overall inertial interception collision efficiencies of 4 μm dust calculated from the theoretical values in the Kuwabara field and equation 2.40 are 0.93 and 0.88 for 50 μm and 100 μm fibres respectively. These figures are in reasonably close agreement with the experimental results in all but the lowest loading test. It is likely, therefore, that the adhesion efficiency of the 4 μm dust is high and that the process is controlled in this case by the collision efficiency. The calculated values of the initial retention efficiency (table

3.9). The effect of this velocity change on efficiency was not large enough to provide conclusive evidence because of the confidence limits of the results. However, the results are in agreement with the above and suggest that 4 μm is the critical particle size with a velocity between 1.15 and 1.5 ms^{-1} and 100 μm fibres in the present system.

The results show that an increase in particle size and velocity cause a reduction in the rate of increase of efficiency ($\bar{k}_1$) with loading.

Intermediate Loading

These tests were conducted with narrow and wide fractions of AC dust using model filters. The influence of particle size and velocity was investigated. The results are shown in tables 3.10-3.13 and figs. 3.6 and 3.7.

The results with classified fractions are summarised in fig. 3.6. The collection efficiency of the 28 μm material is greatly reduced by increasing the velocity showing as expected that it is entirely dependent on the adhesion efficiency. As was found with the low loading tests with limestone the trend is reversed with smaller particle sizes, in this case 8 μm dust. However, inclusion of the theoretical collision efficiencies to calculate η_A (see table 3.11) does not support the argument that the system is controlled by the collision efficiency in this case. An explanation for this discrepancy is that the theory overestimates the collision efficiency at high levels of particle inertia. It was shown in section 1.2.2 that the theoretical efficiency is sensitive to the conditions used for particle entry to the Kuwabara cell at high levels of particle inertia. The efficiency of collection of a model filter, in which the particles approach from a

large distance upstream and have the y component of drag force acting on them for a long time, will be less than that predicted. This conclusion does not conflict with the reasoning given in the caseof limestone.

When particle adhesion is high (8μm) the efficiency is an increasing function of loading and where it is low (28μm) is a decreasing function. In the transition (10μm at 1.0 ms^{-1} and 28μm at 0.4 ms^{-1}) a maximum is observed. It is likely that at a critical loading the size of agglomerates adhering to the fibres is such that they are easily removed. The 19μm results are difficult to explain showing a minimum and extremely complex although reproducable (at 1.0 ms^{-1} and 2.0 ms^{-1}) behaviour. In the transition region several mechanisms will be effective.

The polydispersed material was fed at higher face velocities; the results clearly show that the filter behaviour is controlled by particle adhesion.

Both figures 3.6 and 3.7 show that the form of loading characteristic is dependent on the same factors which control the initial efficiency. It is reasonable, therefore, to express the loading characteristics in terms of the initial efficiency (as in equation 3.7).

High Loadings

At the relatively high velocity of 3.5 ms^{-1} and high loadings (table 3.14) a maximum is clearly shown in fig. 3.8. As expected, the loading at maximum efficiency is reduced with particle size; with 40μm dust a maximum could not be detected.

Expressions 3.7 and 3.8 were found to fit the results reasonable well for low loadings ($\sigma_s < 0.10$) for all but the initial tests with 4μm dust; even for this material the relationships apply in the range $5 \times 10^{-3} < \sigma_s < 0.1$. η_{si}, $\bar{k}_1$ and $\bar{k}_2$

are shown in tables 3.7, 3.9, 3.11 and 3.13.

The initial single fibre efficiencies are shown as a function of face velocityin fig. 3.9. These values are the same as those shown in the tables except for those of the 4 μm limestone. In this case a very rapid increase of efficiency with σ_s was observed at low values of σ_s. The values were obtained by extrapolating the early section of the curves to zero, rather than the linear sections as was used to obtain the tabulated values. Fig. 3.9 shows the same characteristics as described in Chapter 2. Fig. 3.10 shows the influence of particle size, again in agreement with the discussion in Chapter 2. It was not possible for these tests to distinguish between the adhesion efficiency of limestone and AC dust. The influence of fibre size is shown more clearly in fig. 3.5.

The influence of face velocity on $\bar{k}_1$ is similar to its effect on η_{si} (fig. 3.11). In general $\bar{k}_1$ is decreased with d_p but the results show a wide scatter.

Pressure drop.

The influence of fibre size, particle size and face velocityon $\bar{k}_2$are shown in figs. 3.12 and 3.13. Within the limits of the experiments, $\bar{k}_2$ is proportional to d_f (fig. 3.12) showing, as expected, that the increase in pressure drop is simply proportional to the total dust load. $\bar{k}_2$ is a decreasing function of d_p and U_o. Clearly the density of particle packing on the fibres is increased with both particle size and velocity. The influence of material type is shown in fig. 3.13 where AC dust is seen to cause more drag than limestone. Only the more tightly packed particles will be retained when the less cohesive AC dust is used, hence again, where a low efficiency is expected the rate of increase of pressure drop is less. Similarly high polydispersity increases $\bar{k}_2$ as

shown in fig. 3.11. Although the trends are similar no general correlation between $\bar{k}_2$ and η_{si} was found. An approximate empirical relationship is

$$\bar{k}_2 \propto d_f \, d_p^{-1/2} \, U_o^{-1}$$

Soot addition

It is common filter testing practice to add a quantity of soot to the test dust (130). This is claimed to simulate more closely actual conditions. It is known that the presence of soot increases filter dust holding capacity and it was shown in Chapter 2 that it increases collection efficiency.

Woven wire filters were used to examine the influence of soot content in AC coarse test dust. The filters were removed and weighed periodically to test the efficiency. The results, test conditions and filter properties are shown in table 3.15.

Filter clogging occurred during these tests, the more cohesive the material (i.e. the higher the soot content) the greater the tendency to clogg. This is illustrated in fig. 3.14 which shows the additional pressure drop due to deposited dust as a function of filter load for a range of compositions and for two face velocities. The sharp increase in pressure drop is obviously caused by clogging.

The variation of efficiency with filter load is shown in fig. 3.15. Clearly two mechanisms are in operation:-

(a) A decreasing efficiency characteristic

(b) Clogging, or bridging between fibres.

The controlling process changes from (a) to (b) as

clogging increases. The distribution of fibre spacing will strongly influence the rate of clogging.

The minimum in fig. 3.15 may be taken as a criterion of clogging to show the influence of soot content and face velocity. Such a omparison is shown in fig. 3.16 where the influence of soot content is seen to be large below 20%. The face velocity has comparatively little effect. The efficiency is a reducing function of velocity showing that the system is adhesion controlled. The factors which influence the first mechanism have already been discussed. Those which effect clogging are cohesiveness and impact conditions (which control particle packing density) and fibre spacing.

3.2.3 Discussion of Results

The influence of loading on the efficiency of filtration in the low adhesion region was the main purpose of the study reported in this Chapter. However, the results confirm those of Chapter 2 and lead to some interesting conclusions with respect to the single fibre efficiency.

(i) Single fibre efficiency

A quantitative description of the filtration efficiency in terms of the commonly accepted single fibre efficiency is of dubious value even in the case of a clean filter in the low adhesion region. Experiments on the effect of filter depth indicate that the retention efficiency of particles experiencing their first bounce is higher than that during subsequent impact. This suggests apparently equal particles have a distribution of "adhesive strengths". A complete description of the process, therefore, would require an estimate of this distribution function.

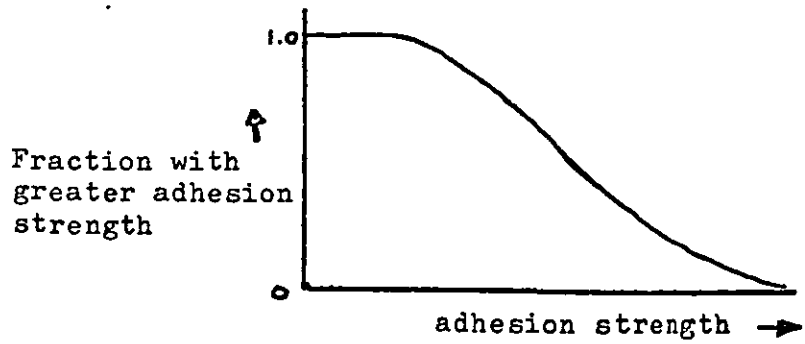

This type of function is already measured in adhesion experiments. The retio of adhesion to removal forces acting on the deposite will fall as build up proceeds. When the ratio is less than unity the deposite will be removed. If the gap between fibres is bridged before this point is reached then clogging will occur. Clearly filter packing density and density uniformity will have an important influence on whether a maximum or glogging will occur. A standardised single fibre efficiency for a given depth of filter may, however, be used comparatively to examine the influence of such parameters as d_p, U_o and d_f on the filter behaviour. These have been examined and the results found to be compatible with the reasoning on the mechanisms given earlier in the thesis.

ii) General Characteristics

The mechanisms of filtration that have been postulated have been illustrated experimentally. Initially the efficiency may be either an increasing or a decreasing function of loading. At higher loads either reduction in efficiency when the filter reaches its maximum load or clogging may occur.

iii) Initial Loading Characteristics.

Application of equation 3.7 in conuunction with 3.3 and the continuity equation to describe the overall behaviour of a

filter is only valid if η_s is not a function of depth. Such a condition can only be fulfilled for monosized particles where adhesion is complete. Where there is a distribution of particle sizes or adhesion strengths then a series of equations such as 3.7 would be required. Nevertheless, a linear relationship between η_s and σ_s provides a reasonable fit of the results suggesting that 3.7 is an adequate though approximate description of the process. The values of η_{si}, F_1^* $\bar{k}_1$ and $\bar{k}_2$ quoted here are average values over the first 20 grids so they can only be used to show the qualitative effect of the main parameters.

The change in pressure drop with loading is desdribed by equation 3.8 in which $\bar{k}_2$ varies as follows:

$$\bar{k}_2 \propto d_f\, d_p^{-1/2}\, U_o^{-1}$$

iv) High Loading Characteristics

At high loadings equation 3.7 is not adequate. An expression of the form

$$\frac{\lambda}{\lambda_o} = \frac{\eta_s}{\eta_o} = (1 + a\sigma_s + b\sigma_s^2) \qquad 3.9$$

would be more appropriate. Herzig et al (128) in a review on the theory of deep bed filtration describes such a function but express it in the form

$$\frac{\lambda}{\lambda_o} = \left(1 + \frac{\sigma_s}{\sigma_M}\right)\left(1 - \frac{\sigma_s}{\sigma_m}\right) \qquad 3.10$$

where σ_M and σ_m are constants. The solution of this in conjunction with 3.3 and the continuity equation is considered and a partial solution is given. Using this technique a complete description of a filter with respect to depth and age is possible provided η_s is independent of depth.

This is a semi-empirical approach to the subject but the two parameters required, a and b, together with λ_o or η_{si} could be determined by using relatively simple experiments and the entire filtration behaviour calculated.

A more fundamental approach to estimate the values of, a and b, could be attempted using the cellular model of a filter (the influence of packing density and distribution of fibre spacing could thus be taken into account in predicting the rate of clogging for example).

3.2.4 Conclusions

1. The mechanisms of filtration which have been postualted are confirmed by the experimental results.
2. The results indicate that in the low adhesion region the single fibre efficiency decreases with depth.
3. Equations 3.7 and 3.8 can be used as approximate descriptions of filter behaviour at low σ_s (< 0.10).
4. η_{si} and $\tilde{k}_1$ decrease with increase in d_p and U_o
5. The rate of change of pressure drop across a filter with loading can be expressed in terms of equation 3.8 using

$$\tilde{k}_2 \propto d_f\, d_p^{-\frac{1}{2}}\, U_o^{-1}$$

over the range of experimental conditions studied.

6. At high loading equation 3.7 is inadequate.

TABLE 3.3

Influence of Depth and Relative Humidity on Filtration of Limestone with Model Filters.

No.of grids	5		10		20		46	
% relative humidity	35		35		34		35	
Feed load (gms).	Δp	η	Δp	η	Δp	η	Δp	η
0.01	7.5	.25	13.5	.32	23.7	.46	52.5	.57
0.06	7.5	.35	14.5	.42	24.2	.49	53.7	.65
0.11	8.0	.39	15.5	.45	25.5	.50	54.7	.72
0.16	8.2	.37	16.2	.42	26.5	.53	56.2	.73
0.22	8.7	.37	17.0	.42	28.0	.55	57.5	.76
1.22							78.2	.94

No.of grids	10			20		
% relative humidity	44			45		
Feed load (gms)	Δp	η	Feed load (gms)	Δp	η	
0.050	13.5	.46	0.050	25.0	.52	
0.100	14.5	.43	0.103	26.2	.52	
0.151	15.5	.44	0.155	27.2	.52	
0.201	17.0	.44	0.209	28.0	.57	

$\bar{d}_p = 12\mu m$ $\quad \alpha = 0.03$

$d_f = 50\mu m$ $\quad U_o = 1\ ms^{-1}$

TABLE 3.4

Influence of depth on Filtration of Limestone with Model Filters - processed data.

No. of grids												
5			10			20			46			
$\sigma_s \times 10^3$	$\frac{\Delta p}{\Delta p_o}$	η_s	$\sigma_s \times 10^3$	$\frac{\Delta p}{\Delta p_o}$	η_s	$\sigma_s \times 10^3$	$\frac{\Delta p}{\Delta p_o}$	η_s	$\sigma_s \times 10^3$	$\frac{\Delta p}{\Delta p_o}$	η_s
0.8	1.0	.26	0.5	1.0	.20	0.43	1.0	.16	0.30	1.0	.10
5.7	1.0	.36	3.7	1.08	.27	2.25	1.03	.17	1.3	1.03	.12
11.4	1.07	.41	7.7	1.15	.30	4.13	1.08	.18	2.4	1.04	.14
17.0	1.10	.38	11.3	1.20	.27	6.2	1.12	.19	3.4	1.07	.14
23.0	1.16	.38	14.9	1.26	.27	8.4	1.18	.20	5.0	1.10	.16
									34.2	1.49	.26

TABLE 3.5

Effect of Filter depth.

No. of grids	F^*	$\bar{k}_2$	η_{si}	$\bar{k}_1$	Pack efficiency
5	22.1	6.0	.24	50	.24
10	19.6	18.0	.19	56	.09
20	17.3	18.0	.15	43	.12
46	16.6	18.0	.10	85	.04

TABLE 3.6

Influence of Velocity on Initial Loading Characteristics.

Velocity (ms^{-1})	0.7		1.0		1.6		2.9	
Feed load (gms)	Δp	η	Δp	η	Δp	η	Δp	η
0.	15.5		23.7		47.0		80.5	
0.014	15.5	.51	23.7	.46	47.0	.40	80.5	.26
0.065	16.2	.71	24.2	.49	48.0	.42	80.5	.40
0.12	17.2	.75	25.5	.50	49.0	.43	81.0	.37
0.17	18.7	.78	26.5	.53	50.2	.45	81.5	.30
0.22	20.2	.83	28.0	.55	51.5	.43	82.5	.38

Relative humidity = 35-38% α = 0.03

d_f = 50μm No.of grids = 20

Nominal particle size = 12μm Type of dust = Limestone

TABLE 3.7

Influence of Velocity on Filtration of Limestone with Model Filters.

	Face velocity (ms^{-1}); Fibre Reynolds No.											
	0.7 ; 2.07			1.0 ; 2.95			1.6 ; 4.70			2.9 ; 8.50		
	$\sigma_s \times 10^3$	$\frac{\Delta p}{\Delta p_o}$	η_{si}	$\sigma_s \times 10^3$	$\frac{\Delta p}{\Delta p_o}$	η_{si}	$\sigma_s \times 10^3$	$\frac{\Delta p}{\Delta p_o}$	η_{si}	$\sigma_s \times 10^3$	$\frac{\Delta p}{\Delta p_o}$	η_{si}
	0.52	1.0	.18	0.43	1.0	.16	0.41	1.0	.13	0.29	1.0	.08
	3.08	1.05	.31	2.25	1.03	.17	1.96	1.02	.14	1.77	1.0	.13
	5.90	1.13	.35	4.13	1.08	.18	3.58	1.04	.14	3.10	1.01	.12
	8.90	1.21	.38	6.20	1.12	.19	5.35	1.07	.15	4.20	1.01	.08
	12.10	1.31	.43	8.40	1.18	.20	7.05	1.10	.14	5.70	1.03	.12
$\bar{k}_2$		20			18			13			5	
η_{si}		0.28			0.15			0.13			0.10	
$\bar{k}_1$		46			38			19			11	
η_{cm}		1.07			1.14			1.18			1.22	
η_A		0.26			0.13			0.11			0.08	

TABLE 3.8

Influence on Particle and Fibre Size on Filtration of Limestone with Model Filters.

Particle Size (μm) $\bar{d}_p$			4		12		26	
Feed load (gms)	Fibre size (μm)	Face Velocity (ms^{-1})	Δp	η	Δp	η	Δp	η
0.	50	1.0	23.7		23.7		23.7	
	100	1.0	12.5		12.5		12.5	
	100	1.15	14.9		14.9		14.9	
	100	1.50	20.9					
0.012	50	1.0	23.7	.79	23.7	.46	23.7	.41
	100	1.0	12.7	.80	12.5	.51	12.5	.47
	100	1.15	14.9	.82	14.9	.45	14.9	.36
	100	1.50	20.9	.71				
0.065	50	1.0	25.4	.93	24.2	.49	24.1	
	100	1.0	13.5	.87	12.9	.56	12.9	.43
	100	1.15	16.7	.90	15.4	.61	15.2	.40
	100	1.50	22.4	.84				
0.120	50	1.0	29.4	.95	25.5	.50	24.6	.39
	100	1.0	14.7	.87	13.7	.61	13.2	.42
	100	1.15	18.2	.92	16.2	.53	15.7	.39
	100	1.50	23.4	.89				
0.170	50	1.0	31.9	.94	26.5	.53	25.4	.38
	100	1.0	15.7	.88	14.7	.57	13.7	.40
	100	1.15	19.2	.92	16.9	.55	16.2	.38
	100	1.50	24.4	.89				
0.220	50	1.0	35.1	.96	28.0	.55	26.1	.44
	100	1.0	16.7	.88	15.4	.62	14.2	.41
	100	1.15	20.4	.94	17.7	.55	16.7	.45
	100	1.50	25.4	.87				

No. of grids = 20 α = 0.03 Relative humidity = 35-40%

TABLE 3.9

Influence of Particle & Fibre Size on Filtration of Limestone with Model Filters.

Nominal Particle Size (μm)		4			12			28		
Fibre size (μm)	Fibre Reynolds No.	$\sigma_s \times 10^3$	$\frac{\Delta p}{\Delta p_o}$	η_s	$\sigma_s \times 10^3$	$\frac{\Delta p}{\Delta p_o}$	η_s	$\sigma_s \times 10^3$	$\frac{\Delta p}{\Delta p_o}$	η_s
50	2.95	0.60	1.00	.39				0.48	1.00	.13
100	5.9	0.30	1.02	.40	0.25	1.00	.18	0.22	1.00	.16
100	6.8	0.36	1.00	.42	0.17	1.00	.15	0.18	1.00	.11
100	8.8	0.32	1.00	.31						
50	2.95	3.96	1.08	.64				2.11	1.02	.14
100	5.9	1.92	1.08	.50	1.27	1.04	.20	1.11	1.04	.17
100	6.8	2.02	1.12	.56	1.34	1.03	.24	0.90	1.02	.13
100	8.8	1.93	1.07	.45						
50	2.95	7.50	1.25	.71				3.57	1.04	.12
100	5.9	3.55	1.18	.50	2.36	1.10	.24	1.90	1.06	.14
100	6.8	3.72	1.22	.61	2.44	1.09	.19	1.62	1.05	.12
100	8.8	3.67	1.12	.54						
50	2.95	10.90	1.35	.68				5.05	1.08	.12
100	5.9	5.20	1.26	.54	3.45	1.18	.21	2.62	1.10	.13
100	6.8	5.50	1.28	.61	3.48	1.13	.20	2.33	1.08	.12
100	8.8	5.40	1.17	.54						
50	2.95	14.6	1.49	.75				6.85	1.11	.14
100	5.9	6.95	1.34	.54	4.63	1.24	.25	3.44	1.14	.13
100	6.8	7.40	1.37	.68	4.55	1.18	.20	3.16	1.12	.15
100	8.8	7.14	1.22	.50						

Nominal Particle Size (μm)		4				12				26			
Fibre size (μm)	Fibre Reynolds No.	$\bar{k}_2$	η_{si}	η_A	$\bar{k}_1$	$\bar{k}_2$	η_{si}	η_A	$\bar{k}_1$	$\bar{k}_2$	η_{si}	η_A	$\bar{k}_2$
50	2.95	33	.60	.85	18	20	.15	.13	32	15	.14	.09	00
100	5.9	50	.48	.98	19	49	.19	.19	60	38	.16	.13	39
100	6.8	50	.54	1.00	32	37	.17	.17	59	37	.12	.10	33
100	8.8	31											

TABLE 3.10

Influence of Particle Size and Velocity on Filtration of AC Dust with Model Filters.

Face Velocity (ms^{-1})	0.4				1.0							
Nominal particle size (μm) / %Relative humidity	8 ; 47%		28 ; 49%		8 ; 42%		10 ; 45%		19 ; 40%		28 ; 38%	
	Feed load (gms)	η	Feed load (gms)	η	Feed load (gms)	η	Feed load (gms)	η	Feed load (gms)	η	Feed load (gms)	η
	0.09	.77	0.11	.65	0.11	.84	.09	.66	0.11	.55	0.10	.21
	0.20	.82	0.24	.65	0.23	.92	.19	.75	0.21	.39	0.24	.21
	0.49	.88	0.53	.72	0.52	.94	.49	.80	0.56	.43	0.57	.20
	0.69	.92	1.05	.55	1.02	.98	.99	.74	1.08	.39	1.07	.16
	1.95	.95	2.06	.46	2.02	.998	1.98	.74	2.10	.49	2.08	.21
	3.0	.96	3.08	.44	3.03	.997	2.99	.78	3.11	.50	3.09	.12
	5.0	.90	5.03	.37	5.03	.996	4.99	.73	5.11	.54	5.06	.15
			7.04	.31	6.02	.994	7.00	.65			7.08	.14
											12.10	.09

No. of grids = 20 Fibre diameter = 50μm α = 0.03

TABLE 3.11

Influence of Particle Size & Velocity on Filtration of AC Dust with Model Filters.

Face Velocity (ms^{-1})											
0.4 ms^{-1};				1.0 ms^{-1}							
8 μm ; 47%		28 μm ;49%		8 μm ; 42%		10 μm ;45%		19 μm ; 40%		28 μm ;38%	
4.8	.37	5.1	.26	6.3	.46	4.3	.27	4.5	.202	1.5	.060
11.4	.42	11.5	.26	15	.61	9.3	.35	7.5	.124	3.4	.060
30.8	.52	26.6	.34	33.6	.68	26.5	.40	17.3	.142	8.3	.056
63	.61	47.3	.20	69	.90	53	.34	32.2	.124	13.9	.045
133	.72	76	.155	140	1.00	106	.34	75	.170	29.4	.060
205	.75	108	.145	212	1.00	162	.38	111	.175	38.4	.033
347	.91	160	.115	355	1.00	266	.33	190	.195	60	.042
		205	.094	495	1.00	359	.26			81	.040
										113	.024
η_{si}	.33		.28		.40		.25		.18		.06
η_A	.39		.20		.41		.24		.14		.04

TABLE 3.12

Influence of velocity on Filtration of Wide Fractions of AC dust with Model Filters.

Particle Size range (μm)	0-25									
Face Velocity (ms-1)	2.5		3.2		4.3		5.6		7.0	
Feed load (gms)	Δp	η	Δp	η	Δp	η	Δp	η	Δp	η
	100		130		220		360		560	
0.5	140	.74	180	.74	260	.70	420	.60	610	.50
1.0	180	.80	230	.76	320	.70	500	.52	640	.50
2.0	310	.89	320	.83	410	.78	590	.56	700	.39
3.0	500	.84	450	.90	480	.71	630	.63	740	.50
6.0	950	.99	830	.87	820	.80	800	.52	870	.46

Particle Size range (μm)	0-60							
Face Velocity (ms-1)	2.0		2.75		3.7		5.1	
Feed load (gms)	Δp	η	Δp	η	Δp	η	Δp	η
.0	80		110		170		300	
0.5	110	.50	130	.38	210	.25	320	.18
1.0	130	.38	150	.34	250	.22	340	.18
2.0	150	.44	170	.26	270	.18	360	.12
3.0	180	.34	190	.20			370	.06
5.0	230	.38	220	.20	320	.12	390	.06

No. of grids = 30 α = 0.03

d_f = 50μm Relative humidity = 50%

TABLE 3.13

Influence of Velocity on Filtration of Wide Fractions of AC Dust with Model Filters.

Face Velocity (ms^{-1}) ; Fibre Reynolds No.														
2.5 ; 7.4			3.2 ; 9.5			4.3 ; 12.7			5.6 ; 16.5			7.0 ; 20.7		
$\sigma_s' \times 10^3$	$\frac{\Delta p}{\Delta p_o}$	η_s	$\sigma_s' \times 10^3$	$\frac{\Delta p}{\Delta p_o}$	η_s	$\sigma_s' \times 10^3$	$\frac{\Delta p}{\Delta p_o}$	η_s	$\sigma_s' \times 10^3$	$\frac{\Delta p}{\Delta p_o}$	η_s	$\sigma_s' \times 10^3$	$\frac{\Delta p}{\Delta p_o}$	η_s
17	1.40	.22	14	1.39	.22	16	1.18	.20	14	1.17	.15	12	1.09	.12
36	1.80	.27	33	1.77	.25	33	1.45	.20	27	1.39	.12	23	1.14	.12
78	3.10	.37	74	2.46	.30	69	1.87	.26	54	1.64	.14	41	1.25	.08
117	5.00	.31	116	3.45	.37	102	2.18	.21	84	1.75	.17	64	1.32	.12
258	9.50	.73	238	6.40	.34	215	3.83	.27	158	2.22	.12	127	1.55	.10
$\bar{k}_2$	28.0			23.0			12.4			10.9			5.8	
η_{si}	.185			.195			.190			.145			.120	
$\bar{k}_1$	11.5			7.7			2.4			0.			-1.5	

Particle size range = 0-25μm

Face Velocity (ms^{-1})						Fibre Reynolds No.					
2.1 ; 5.9			2.75 ; 8.1			3.7 ; 10.9			5.1 ; 15.1		
$\sigma_s' \times 10^3$	$\frac{\Delta p}{\Delta p_o}$	η_s	$\sigma_s' \times 10^3$	$\frac{\Delta p}{\Delta p_o}$	η_s	$\sigma_s' \times 10^3$	$\frac{\Delta p}{\Delta p_o}$	η_s	$\sigma_s' \times 10^3$	$\frac{\Delta p}{\Delta p_o}$	η_s
12	1.38	.116	8.6	1.18	.080	5.7	1.23	.050	3.8	1.07	.034
20	1.62	.080	16	1.37	.070	11	1.47	.043	7.7	1.13	.034
40	1.88	.100	28	1.55	.051	18	1.59	.034	12	1.20	.022
56	2.25	.070	36	1.73	.038				14	1.23	.010
91	2.87	.082	53	2.00	0.38	34	1.87	.022	18	1.30	.010
$\bar{k}_2$	25.4			20.3			28.2			17.0	
η_{si}	.106			.097			.055			.045	
$\bar{k}_1$	-3.9			-12.7			-18.5			-46.7	

Particle size range = 0-60μm

TABLE 3.14

Influence of Particle Size on Filtration of AC Dust using Model Filters at High Load.

Nominal Particle Size (μm).					
3.8		11.4		40.7	
Feed load (gms)	η	Feed Load (gms)	η	Feed Load (gms)	η
1.13	.68	0.95	.11	0.90	.16
2.25	.70	1.82	.28	1.87	.12
3.26	.76	2.83	.20	2.94	.11
4.27	.78	3.50	.26	3.92	.12
5.23	.84	4.50	.13	4.93	.14
6.23	.86	5.50	.13	7.40	.10
7.20	.78	6.50	.09	14.10	.10
8.20	.77			19.20	.09
9.16	.78			24.40	.10
10.10	.75				
12.25	.67				
15.53	.57				

No. of grids = 20; Fibre size = 50μm

Relative humidity = 50% Face velocity = 3.5 ms^{-1}

TABLE 3.15

Influence of Soot Content on Loading Characteristics.

	Feed load (gms)	U_o = 2.25 ms^{-1} $\Delta p \times 10^2$	η	Feed load (gms)	U_o = 4.75 ms^{-1} $\Delta p \times 10^2$	η
75% soot		5.0				
	0.5	5.4	.68			
	1	6.4	.68			
	2	60.4	.79			
50% soot		5.0			17.7	
	0.5	5.2	.62	0.5	18.5	.54
	1	5.6	.60	1.0	20.1	.46
	1.5	6.4	.56	2.0	48.7	.50
	2.5	64.8	.78	2.7	102.7	.60
25% soot		5.0			17.7	
	0.5	5.2	.46	0.5	18.3	.28
	1	5.4	.50	1	19.1	.38
	2	5.8	.46	2	20.5	.32
	3	7.0	.46	3	25.9	.34
	4	29.2	.56	4	42.3	.39
	4.5	53.8	.70	4.5	42.9	.38
	5	51.8	.74	5	76.5	.50
				6		.56
				7		.54
10% soot		5.0			17.7	
	0.5	5.0	.42	0.5	17.7	.34
	1	5.2	.39	1	17.9	.30
	2	5.4	.39	2	18.1	.25
	3	5.6	.37	3	18.7	.24
	4	6.0	.39	4	19.1	.23
	5	6.4	.39	6	20.1	.22
	7	8.0	.42	8	21.5	.21
	9	19.6	.42	10	22.9	.22
	11	44.6	.39	12	25.3	.23
	13	60.9	.58	14	29.3	.21
	17	91.2	.79	18	44.7	.26
				22	89.3	.26
				24	118.7	.27
				28	149.7	.30
				32	176.2	.30
				42	237.7	.39
				52	272.7	.41
5% soot		5.0			17.7	
	0.5	5.2	.42	0.5	17.9	.30
	1	5.2	.36	1	17.9	.32
	2	5.4	.39	2	18.1	.24
	3	5.4	.35	3	18.3	.22

Feed load (gms)	U_o = 2.25 ms^{-1} $\Delta p \times 10^2$	η	Feed load (gms)	U_o = 4.75 ms^{-1} $\Delta p \times 10^2$	η
4	5.6	.39	4	18.5	.19
6	6.0	.39	6	18.9	.18
8	6.0	.34	8	19.3	.18
10	6.4	.36	10	19.3	.16
14	6.8	.34	14	20.3	.16
18	7.6	.32	18		.15
22	8.8	.30	20	21.5	.14
26	10.8	.32	24	22.3	.14
30	15.8	.30	28	23.3	.16
34	21.4	.33	32	24.5	.16
38	26.2	.36	36	26.3	.18
42	31.4	.36	40	27.9	.15
46	52.6	.37	44	30.5	.17
			48	36.1	.15
			52	39.3	.16
			60	46.9	.15
0% soot 100% AC dust					
-	5.0	-	-	17.7	-
0.5	5.2	.28	0.5	17.7	.18
1	5.4	.28	1	17.9	.14
2	5.4	.29	2	18.1	.18
3	5.5	.25	3	18.3	.15
4	5.5	.26	4	18.3	.15
6	5.6	.25	5	18.5	.14
7	5.6	.22			
10	5.8	.24			
15	6.0	.26			
25	6.8	.20			
50	8.2	.22			

Filter diameter = 0.038m
Filter depth = 0.1m
Filter weight = 349gms
Fibre diameter = 145μm
Fibre properties - woven stainless steel

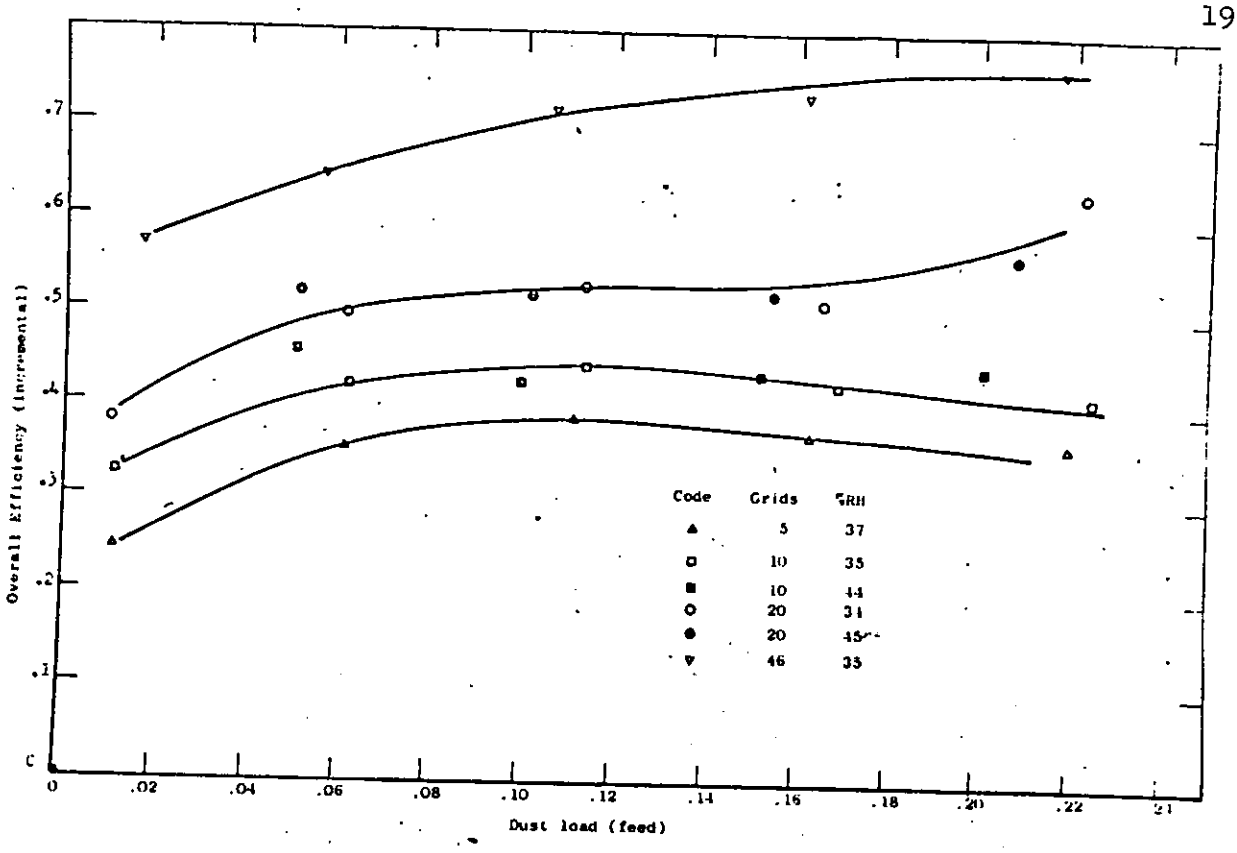
Overall Efficiency (Incremental)
.7
.6
.5
.4
.3
.2
.1
0
.02
.04
.06
.08
.10
.12
.14
.16
.18
.20
.22
Dust load (feed)
Code
Grids
%RH
5
37
10
35
10
44
20
31
20
45
46
35

Fig. 3.1

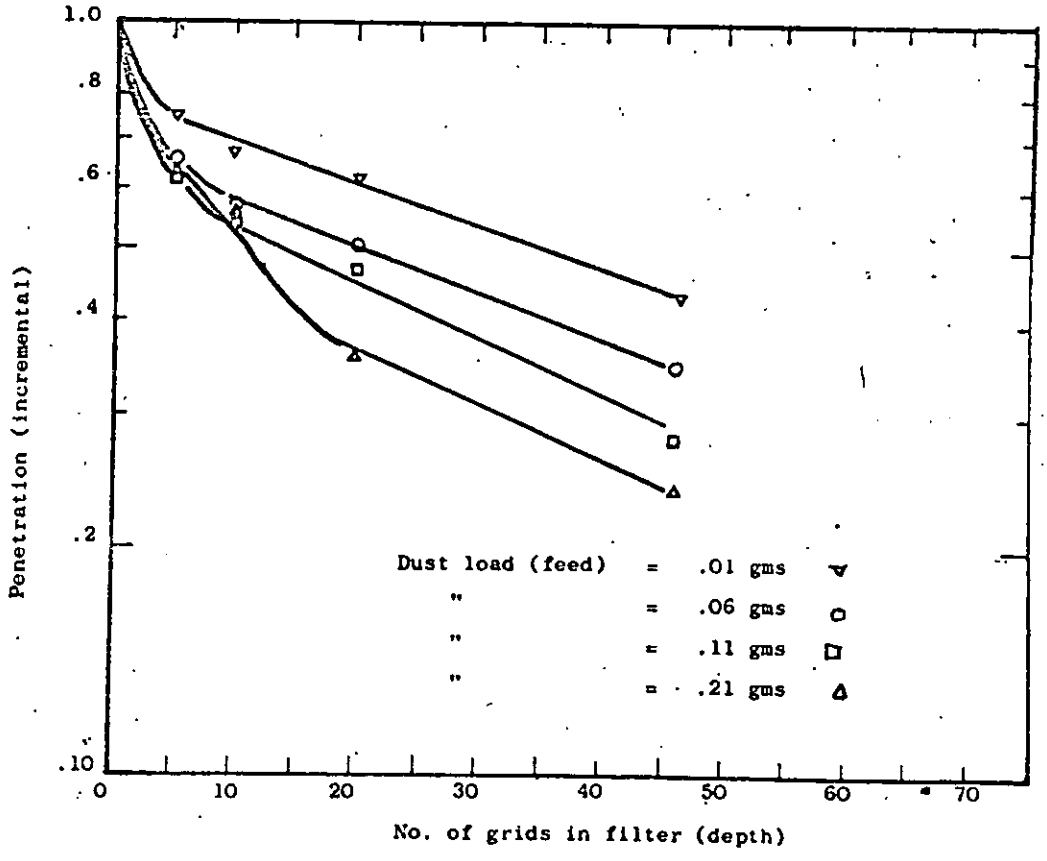
Penetration (incremental)
1.0
.8
.6
.4
.2
.10
0
10
20
30
40
50
60
70
No. of grids in filter (depth)
Dust load (feed) = .01 gms
" = .06 gms
" = .11 gms
" = .21 gms

Fig. 3.2

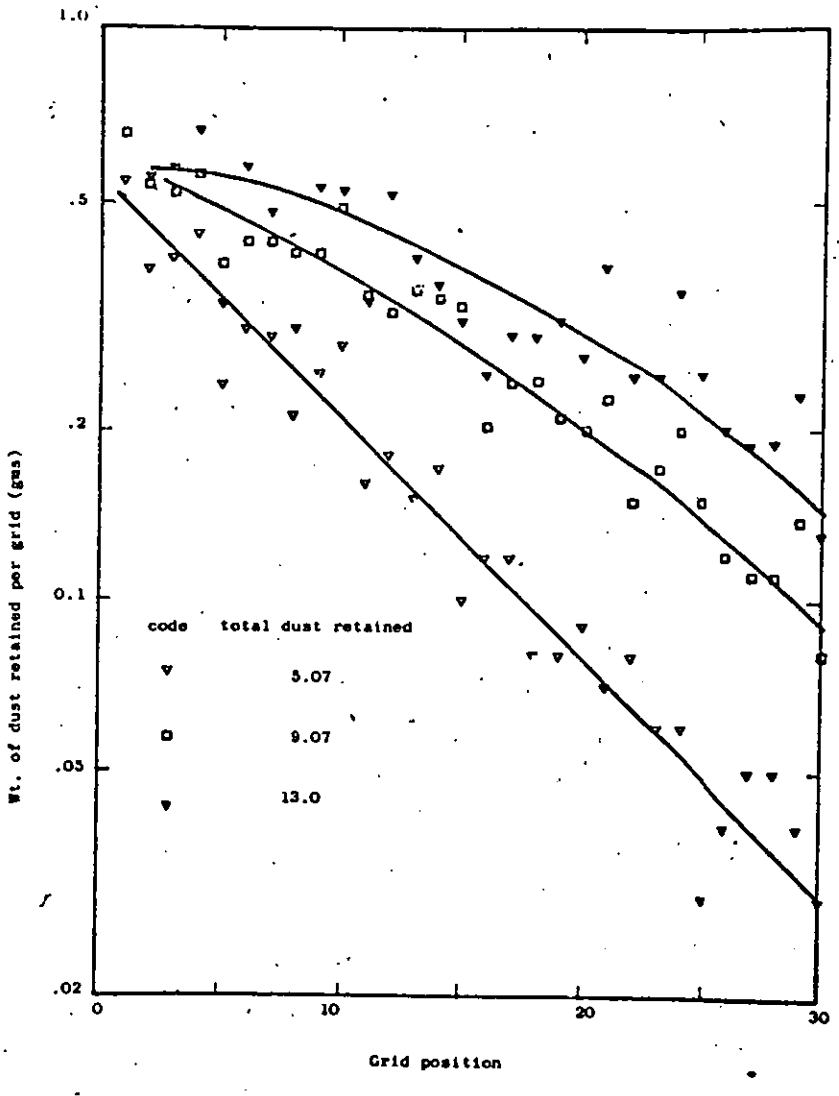
1.0
.5
.2
0.1
.05
.02
0
10
20
30
Wt. of dust retained per grid (gms)
Grid position
code
total dust retained
5.07
9.07
13.0

Fig. 3.3

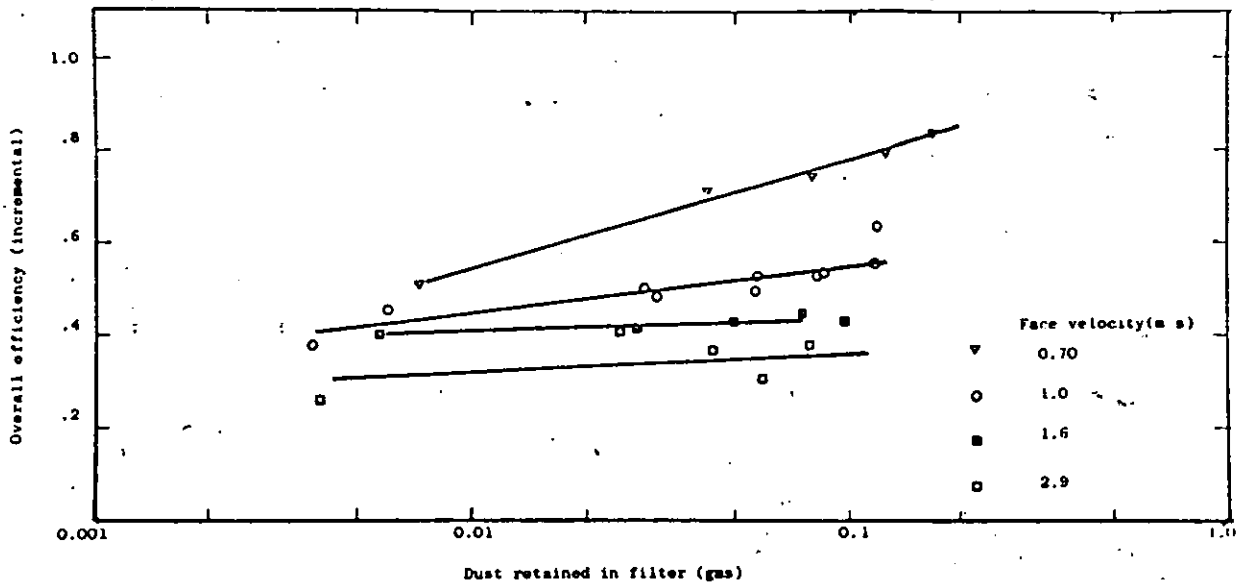

Initial Loading Characteristics of Limestone.
Fig. 3.4

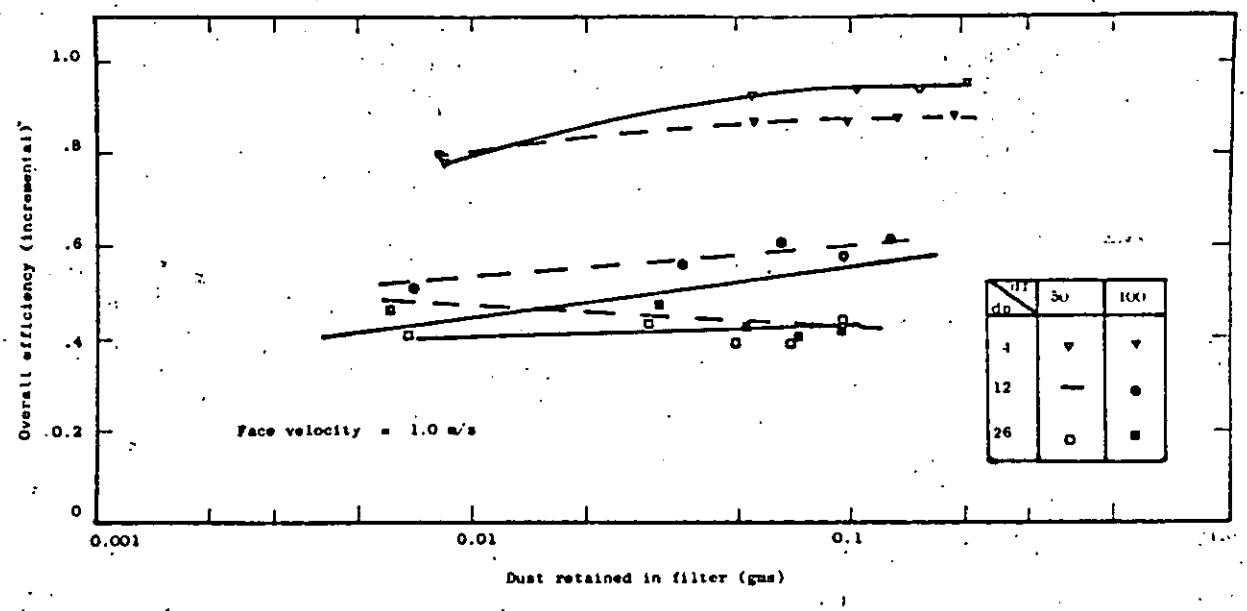

Initial Loading Characteristics of Limestone.
Fig. 3.5

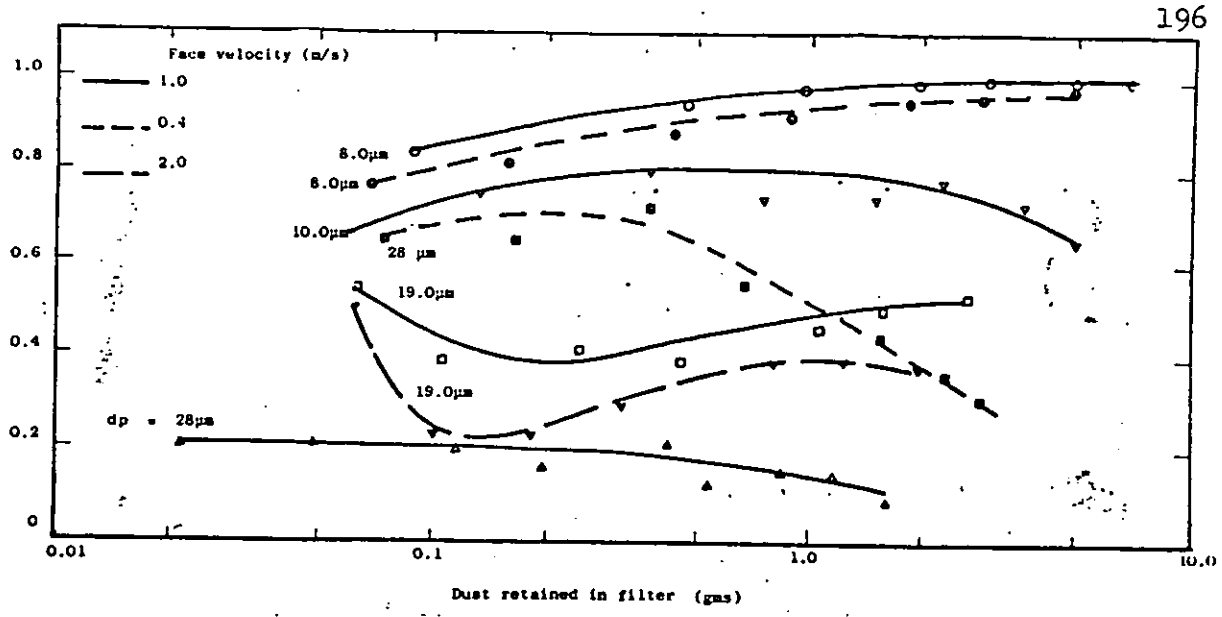

Intermediate Loading Characteristic of AC Dust.

Fig. 3.6

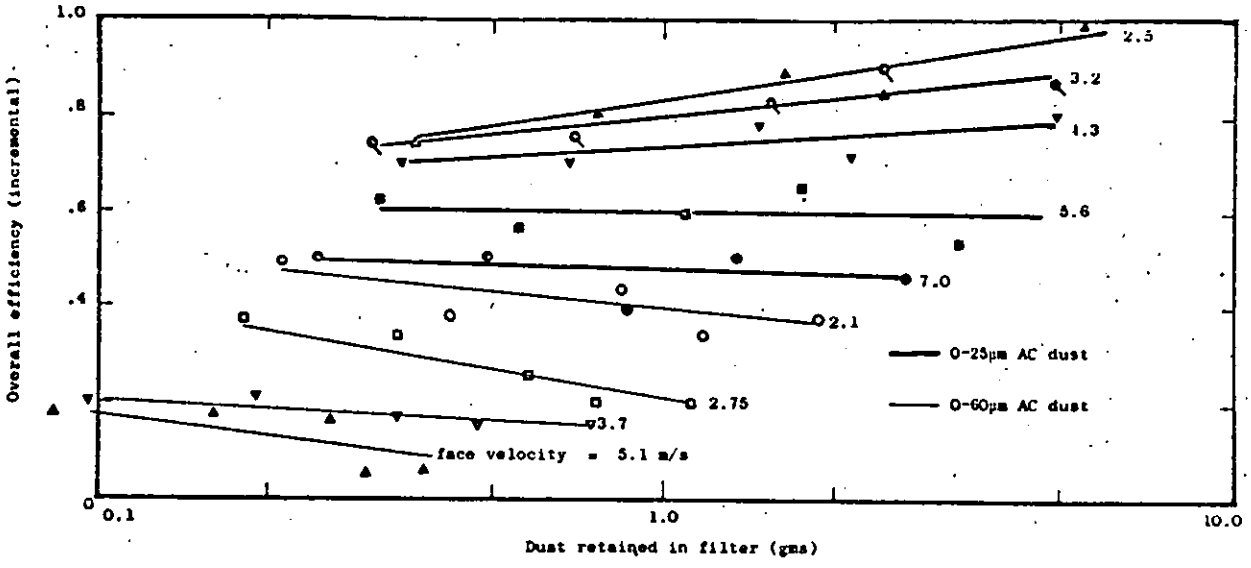

Intermediate Loading characteristic of AC Dust.

Fig. 3.7

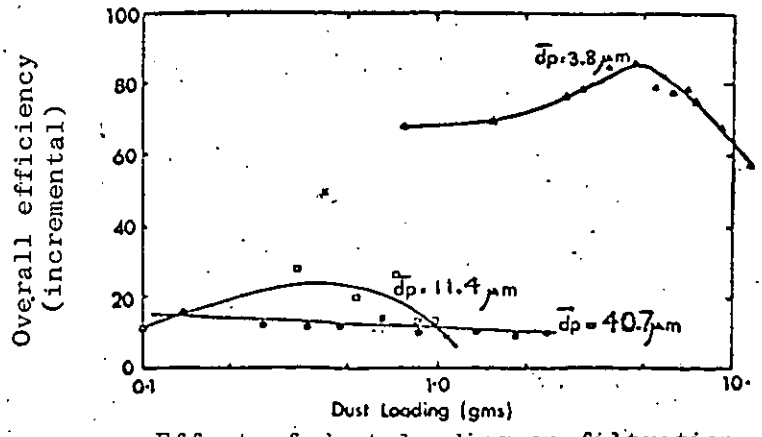

Effect of dust loading on filtration efficiency.

Fig. 3.8

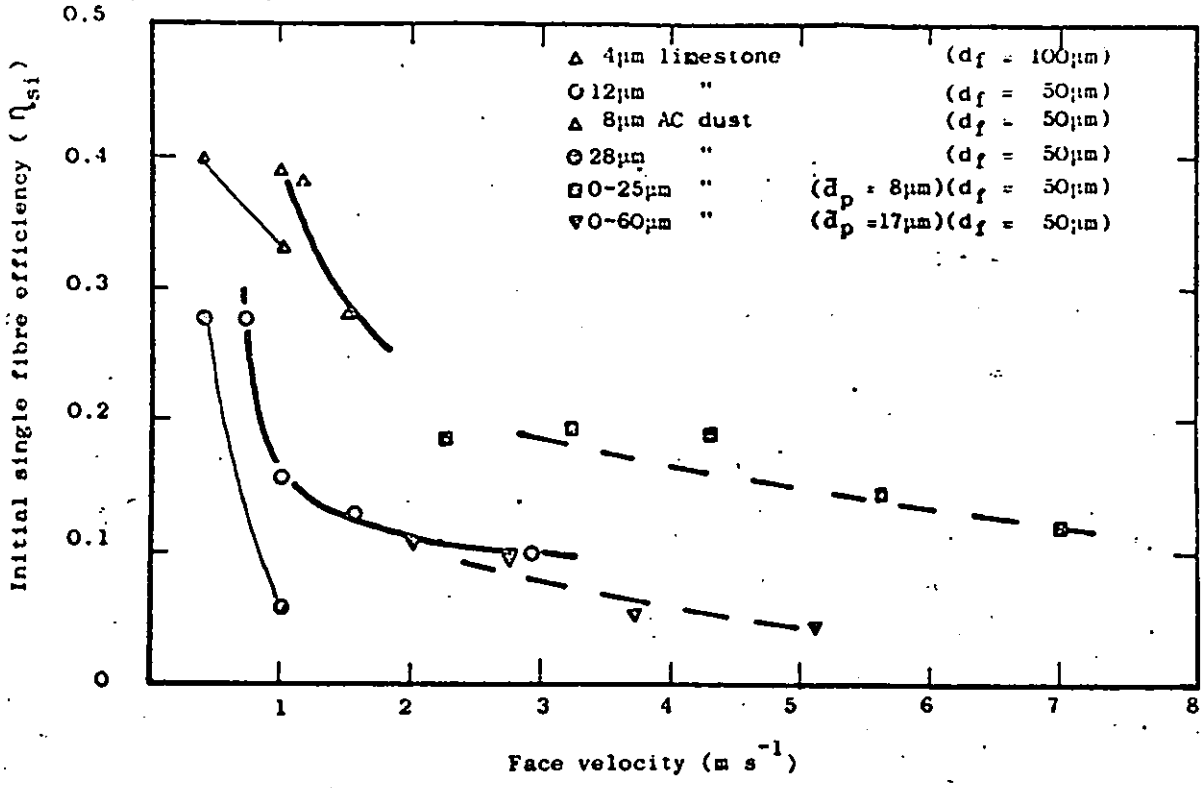

Initial Single Fibre Efficiency,
Fig. 3.9

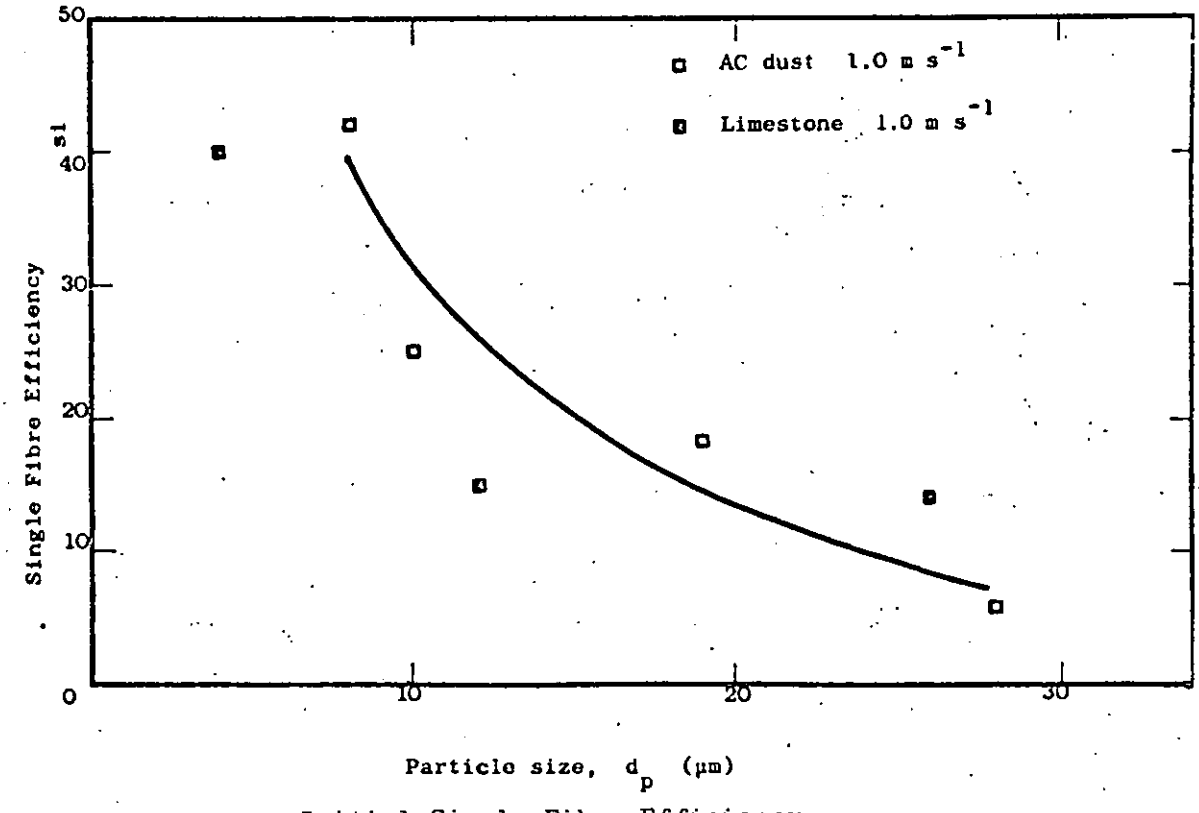

Initial Single Fibre Efficiency,
Fig. 3.10.

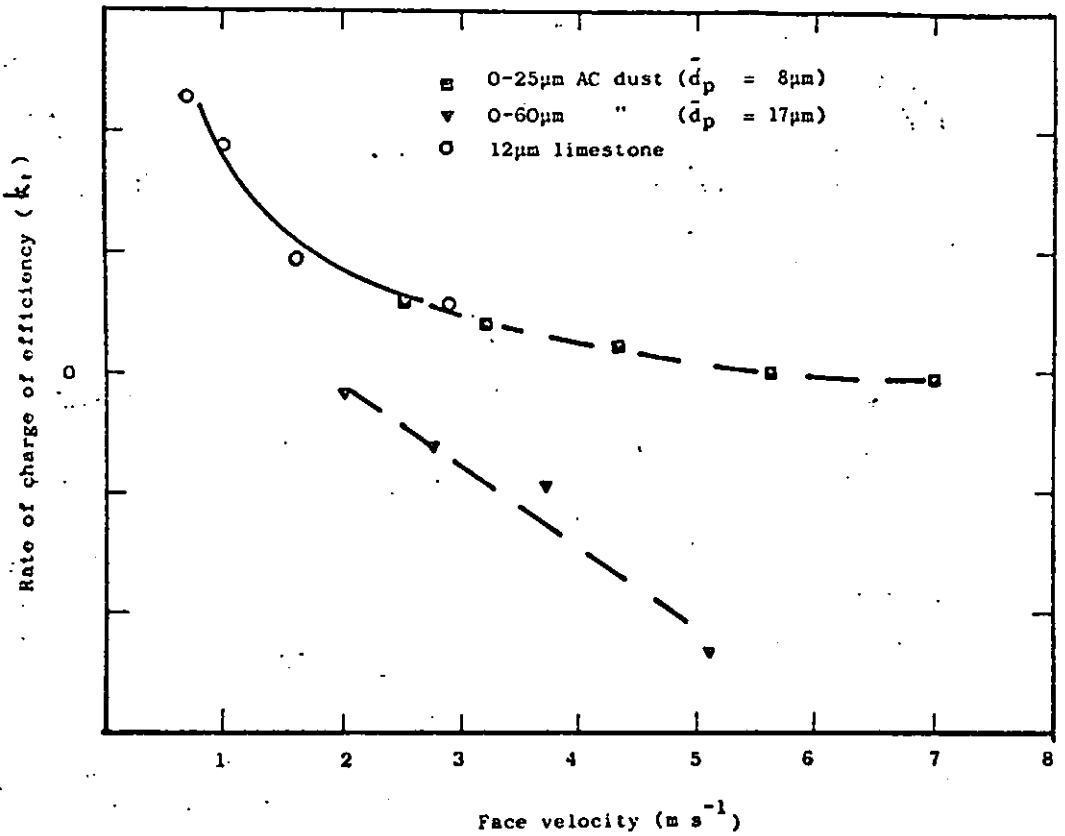

Influence of Face Velocity on

Fig. 3.11

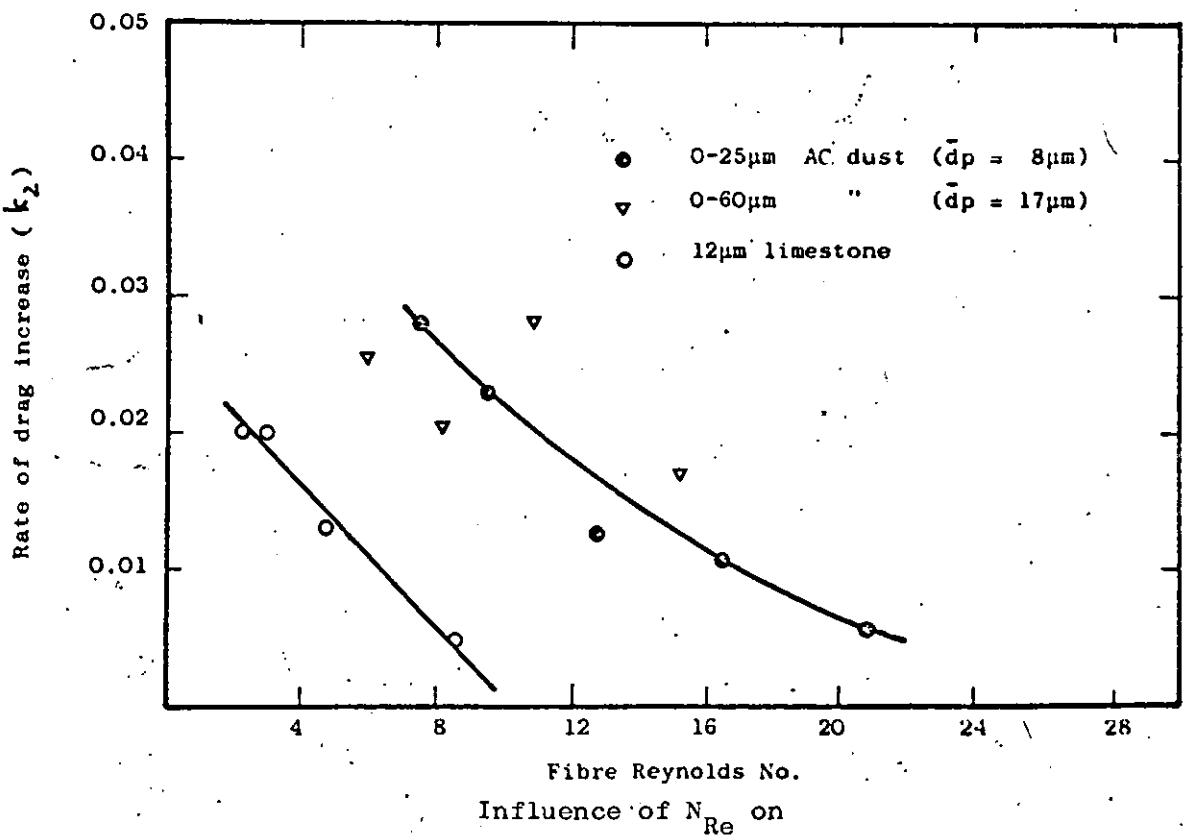

Influence of N_{Re} on

Fig. 3.13

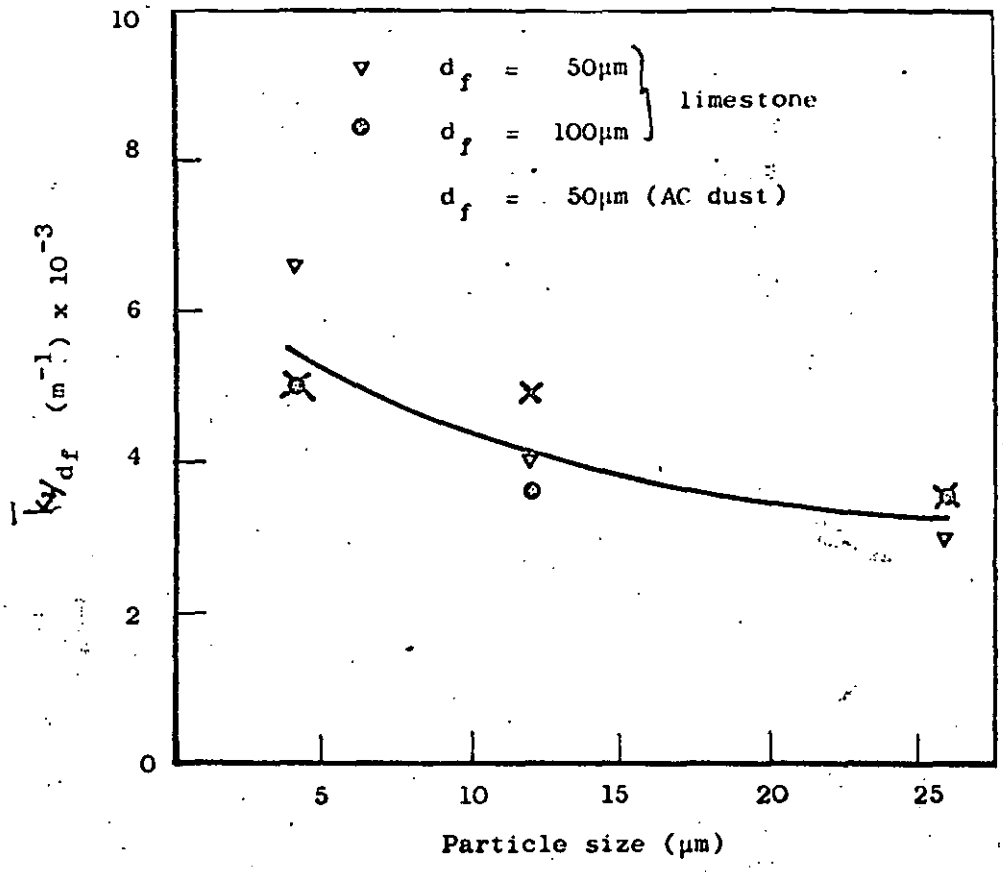

Fig. 3.12

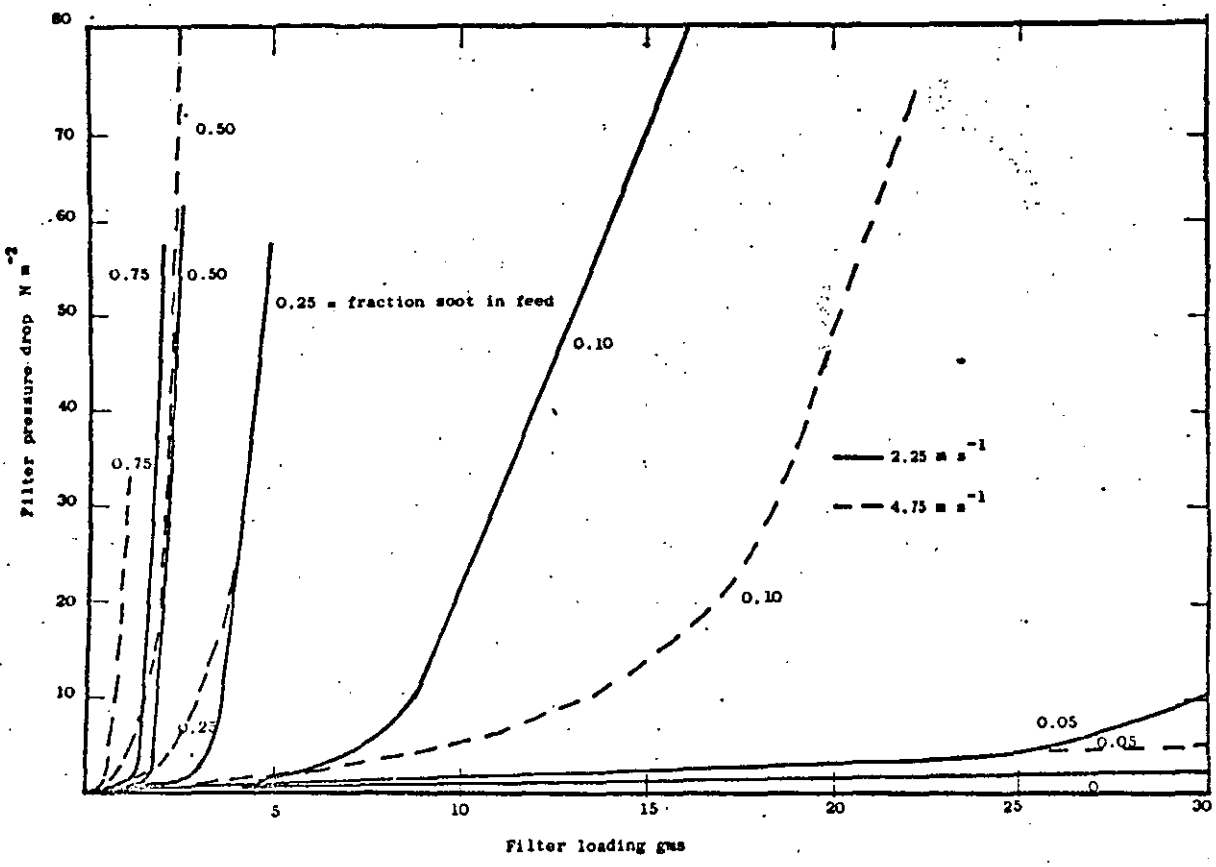

Influence of soot content of test dust on performance of fibrous filter.

Fig. 3.14

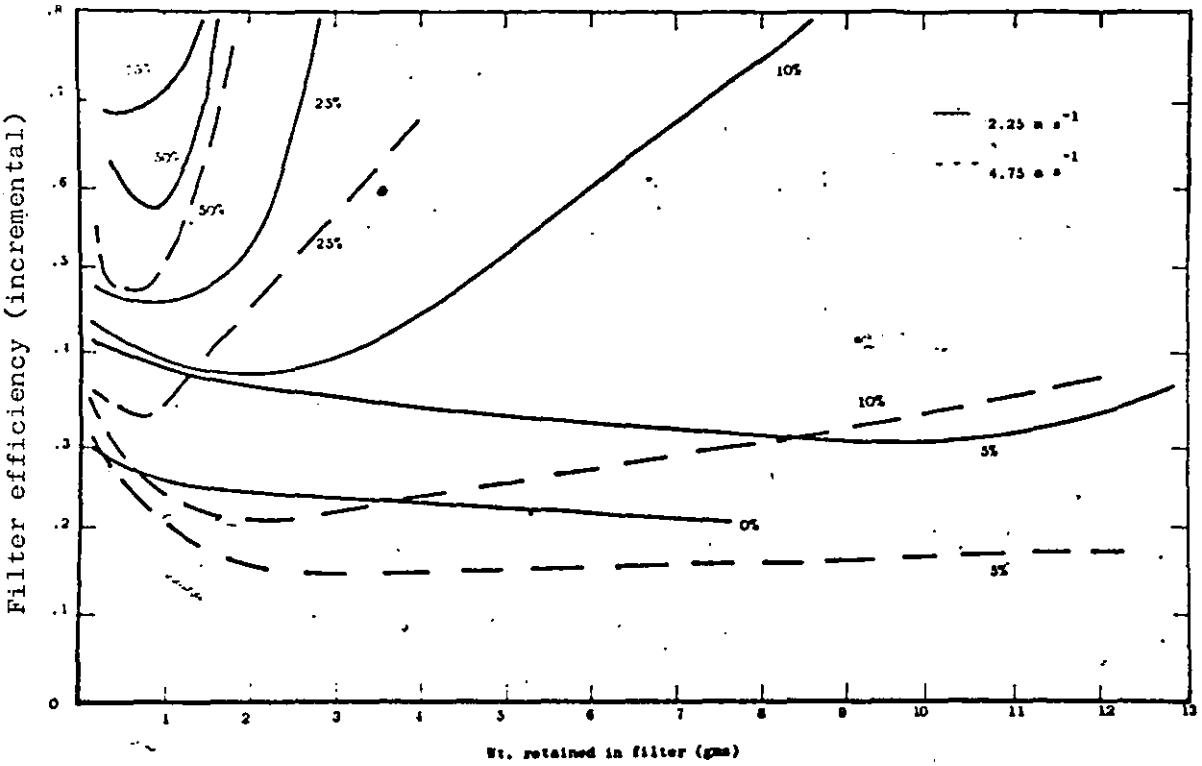

Influence of soot content on test dust on filter performance.

Fig. 3.15

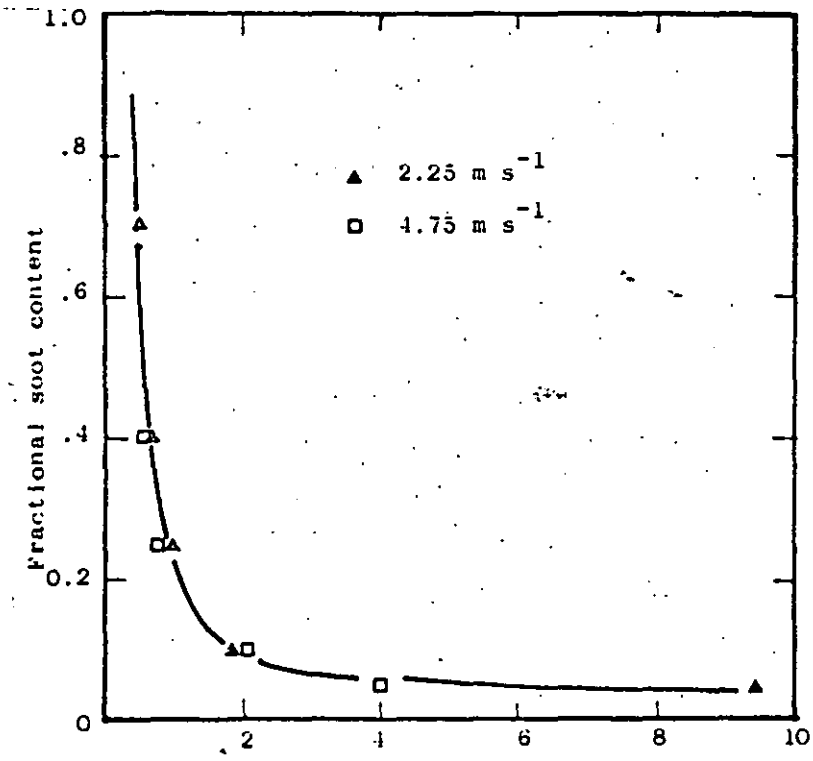

Influence of soot content and velocity on clogging criterion.

Fig. 3.16

CHAPTER 4

Conclusions and Recommendations for Future Work

1. Collision efficiency

1.1 Filter geometry

1.2 Lift Forces

1.3 Electrostatics

2. Retention efficiency

2.1 Critical particle size

2.2 Low adhesion characteristics

2.3 Self cleaning

2.4 Fibre oiling

3. Non-stationary filtration

3.1 High adhesion systems

3.2 Low adhesion systems

4. Experimental techniques

CHAPTER 4

CONCLUSIONS AND RECOMMENDATIONS FOR FUTURE WORK

The conclusions to Chapters 1, 2 and 3 have already been recorded so they will only be briefly summarised here in as much as they affect the recommendations for future work. Although a vast amount of work has been done on the subject of fibrous filtration this has almost exclusively been confined to the classical regions of determining the collision efficiency, normally for an isolated fibre. Many aspects of the subject, some of important practical interest, have received very little attention. Outlined below are some of the topics which in the author's opinion merit further study.

4.1 Collision Efficiency

4.1.1 Filter geometry

The outstanding theoretical problem of fibrous filtration is to describe realistically the fluid flow through the filter. Before this can be accomplished the geometry of the filter must be described. An accurate and realistic description of such a random system and particularly of the flow of a fluid through it has not yet been accomplished. Models such as those of Happel, Kuwabara or Brinkman are idealistic and have severe limitations. However,

they are at present the best descriptions available and the incorporation of a cell size distribution into the theory, although it ignores boundary value problems, allows us to take a step further in synthesizing the flow through a real filter. A significant improvement will be found if both the influence of packing density and fibre Reynolds number can be incorporated in the one model. The similarity of the approximate Lamb and Kuwabara/Happel solutions for the stream functions suggests that this is possible. The external surface boundary conditions in the cellular model are not compatible with the inclusion of a Reynolds number effect but it may be feasible that the inertia terms can be taken into account in an equation of motion similar to that employed by Brinkman. The use of an infinite boundary condition would then allow both factors to be considered.

The method of taking the distribution of fibre spacing into account as described in section 1.8 could be extended to include a study of the behaviour of filters containing a distribution of fibre sizes. The predominant effect of large fibres on the behaviour of fine fibres, within a filter, can be estimated by employing the fine fibre efficiencies within the velocity distribution of the large fibre system. The determination of a value of σ_s presents a major problem. Experimental studies such as that used to obtain the photographs shown in fig. 1.22 provide a useful comparision between the filters. They are capable of showing whether fibres are evenly packed or otherwise and whether the overall density of packing influences the apparent distribution. These photographs serve to remind us of the inadequacy of the present methods of describing a filter, and of the need for a more realistic technique.

4.1.2 Lift Forces

The influence of hydrodynamic lift forces between the particle and fibre requires further investigation. The forces described recently by Goren (129) should be included in the trajectory calculations. It is likely, however, that the results will, as in the case of the lift forces described in Chapter 1, be of marginal importance. The most significant factor in the description of efficiency of inertial interception is the tortuosity of the flow field.

4.1.3 Electrostatics

The possibility of providing a highly efficient, low resistance filter is one which is extremely attractive to industry. Filters constructed of metal fibres which are artificially charged to attract and retain particles have been investigated with most encouraging results. This line of inquiry deserves further investigation.

4.2 Retention Efficiency

4.2.1 Critical particle size

The critical particle size at which adhesion fails should be determined experimentally. This could be performed using a sodium flame detection system* such as that described in reference 4 but the use of salt particles wouldlimit the value of the results. A more fundamental approach would be to drop particles (monosized

*see Appendix II

glass spheres could be used for this purpose) onto flat surfaces and observe their behaviour photographically using stroboscopic illumination. Particle impact velocity could be controlled by altering the pressure of operation and hence the particle terminal velocity. Oblique impact could also be studied using the technique.

4.2.2 Low adhesion characterisitics

A more detailed and extensive experimental study of the influence of the main operating and design parameters in the low adhesion region is required. This, together with theoretical values of collision energies, may permit the development of a theory for the retention efficiency based on the difference between bounce and adhesion energies, and the distribution of adhesion energies, for any given particle size or species. Unfortunately our lack of knowledge of the behaviour of particles during bounce and of the influence of such factors as velocity and impact angle on adhesion forces will severely limit such approaches. A study such as that described in 4.2.1 above would be extremely useful. There is a practical need to remove particles greater than 1 μm from i.e. engine intakes using uncoated fibrous filters. Before such filters can be designed effectively further information is required on the influence of fibre properties on the behaviour. It is hoped that a theoretical approach similar to that described in Chapter 2 will be of use in predicting the influence of fibre physical properties. The influence of sonic and mechanical vibration should also be studied.

4.2.3 Self cleaning

In the use of uncoated fibrous filters, mechanical automatic cleaning is often necessary. There is room for much experimental work on dust removal from fibres.

4.2.4 Fibre oiling

Virtually nothing has been published on the behaviour of coated filters. Work is required to determine whether the increased efficiency is due to viscous dissipation of impact energy or capillary adhesion forces or both.

4.3 Loading.

4.3.1 High adhesion systems

The influence of operating parameters such as particle size, shape, distribution and face velocity on the increase in both resistance and efficiency with loading require further experimental investigation. Filter packing density, and distribution of pore size and fibre sizes must have an important effect on clogging. All these factors require experimental investigation. Theoretically the use of the cellular model should provide an estimate of the influence of filter parameters.

4.3.2. Low Adhesion systems

A cellular model of a filter could be developed which includes the "cohesiveness" of the dust and fibre surfaces. Using such a model (provided the theories of 4.2.2 were available) overall filter performance could be predicted. If this were

successful a series of simplified tests could be designed to characterise any dust with regard to its filterability (i.e. size analysis and cohesiveness).

This appoach is perhaps at the present idealistic. Further information regarding the mechanisms of particle agglomerate dislodgement and behaviour of the agglomerates in their subsequent passage through the filter is first required. This may be accomplished with the use of high speed photography and model filters.

4.4 Experimental Techniques

The advantages of using model filters have already been described and it is logical to use them in situations such as those described above where it is essential to study filter behaviour with depth. However, the infuence of filter structure, fibre size distribution etc. can only be studied using narrow pads of randomly arranged fibres.

The parameters of depth, loading and size distribution are added to those which are normally studied in filtration research. The method of testing must, therefore, be extremely rapid to obtain the very large number of results necessary; a method using polydispersed test dust would be desirable; sampling should be avoided. There are two methods which can be developed to satisfy these conditions:-

(i) The test rig described above suffers from two main disadvantages namely that a sufficiently narrow sized fraction could not be obtained below 7-8 μm and that it was limited in the lower size of feed sample which could

be analysed. The latter restriction was imposed by using model filters. Both of these faults could be obviated by extracting the grids from the model filter and performing a "Coulter count" of the material thus collected. The count thus obtained would then be compared with that on an absolute filter. The sample size required for a conventional Coulter count is much too high but the system could be converted to count all the particles contained in a large sample of fluid (say 250 ccs) instead of the standard 0.5-2 ccs. The method is extremely rapid and reliable with particle sizes down to about 2 μm.

By comparing the particle counts obtained in a knitmesh filter and a cellulose diacetate fibre filter which was used as a master, a grade efficiency curve has been obtained (fig.4.1). 0.1 gms AC dust was fed to the unit and the dust removed from each filter. The dust was dispersed in saline with the help of a dispersant and ultrasonics in the case of the knitmesh filter. The master filter was completely dissolved in acetone to leave only dust; this was then rendered electrically conducting by adding ammonium thiocyanate. The system was not satisfactory for analysing dust below about 10 μm due to evaporation of acetone in the Coulter orifice. This has been rectified by using a recently developed membrane filter as an absolute filter. The dust is easily removed from the surface of such a filter by washing with saline. The method is applicable down to particle sizes of about 2 μm. Some preliminary results obtained using the technique are shown in appendix II.

(ii) Light scattering has frequently been applied to filter testing. However, the normal procedure is to remove a sample before and after filtration, usually of a closely sized aerosol such as D.O.P. Continuous particle counting and sizing in-situ before, after, and within the depth of a filter could be achieved using the method illustrated in fig. 4.2. The principle of light scattering for the in-situ analysis of filter behaviour has already been illustrated by Loffler (78).

A more detailed diagram of the proposed measuring system is shown in Fig.4.2. A very thin beam, or slice, of light will pass into the tube through which the aerosol is passing. The total flux of light scattered in the forward mode is a definitive function of particle size. As at an angle of 40° the effect of variations in refractive index of the particles disappears (131), the intensity of light scattered in a narrow annular cone of 40° should be measured. The use of a light guide and series of stops as shown in fig. 4.3 will ensure that only light from such an annular cone will be detected by a photomultiplier tube. The height of the resulting pulse can be measured and the data stored in one of twenty channels in a commercially available pulse height analyser. As subsequent particles enter the sensing zone they will be similarly sized and counted. In this way a histogram showing the number of particles in each of 20 size ranges will rapidly be built up. A series of such instruments could be operated simultaneously at different depths in the filter as shown in Fig.4.2

Coincidence problems can be minimised by using an

extremely thin beam of light (fig.4.4) less than 100 μm in depth the observed area of which can be altered by adjusting the light stops. The area of the sensing zone used is dependent on the concentration of aerosol and should be adjusted to give a satisfactory count rate commensurate with a low coincidence error.

The proposed sizing and counting technique offers many advantages over previous methods using the same principle. The recent development of very low noise photomultiplier assemblies enables the analyses of the 40° forward narrow cone of scattered light rather than the total flux as is the current practice. The use of a narrow beam of light rather than a focused point as at present, will minimise edge effects. The method works in-situ, a polydispersed dust can be used and it is not restricted to a single aerosol material. It is very rapid being capable electroncially of counting and sizing at least 10^4 particles per second. Agglomerates are not broken up, but are analysed as they pass through the filter. It should be possible to use the system over the size range 0.2 - 100 μm. Such a unit is being designed and constructed by the author (see fig.4.5) and will be used by him in the next stage of the work on fibrous filtration.

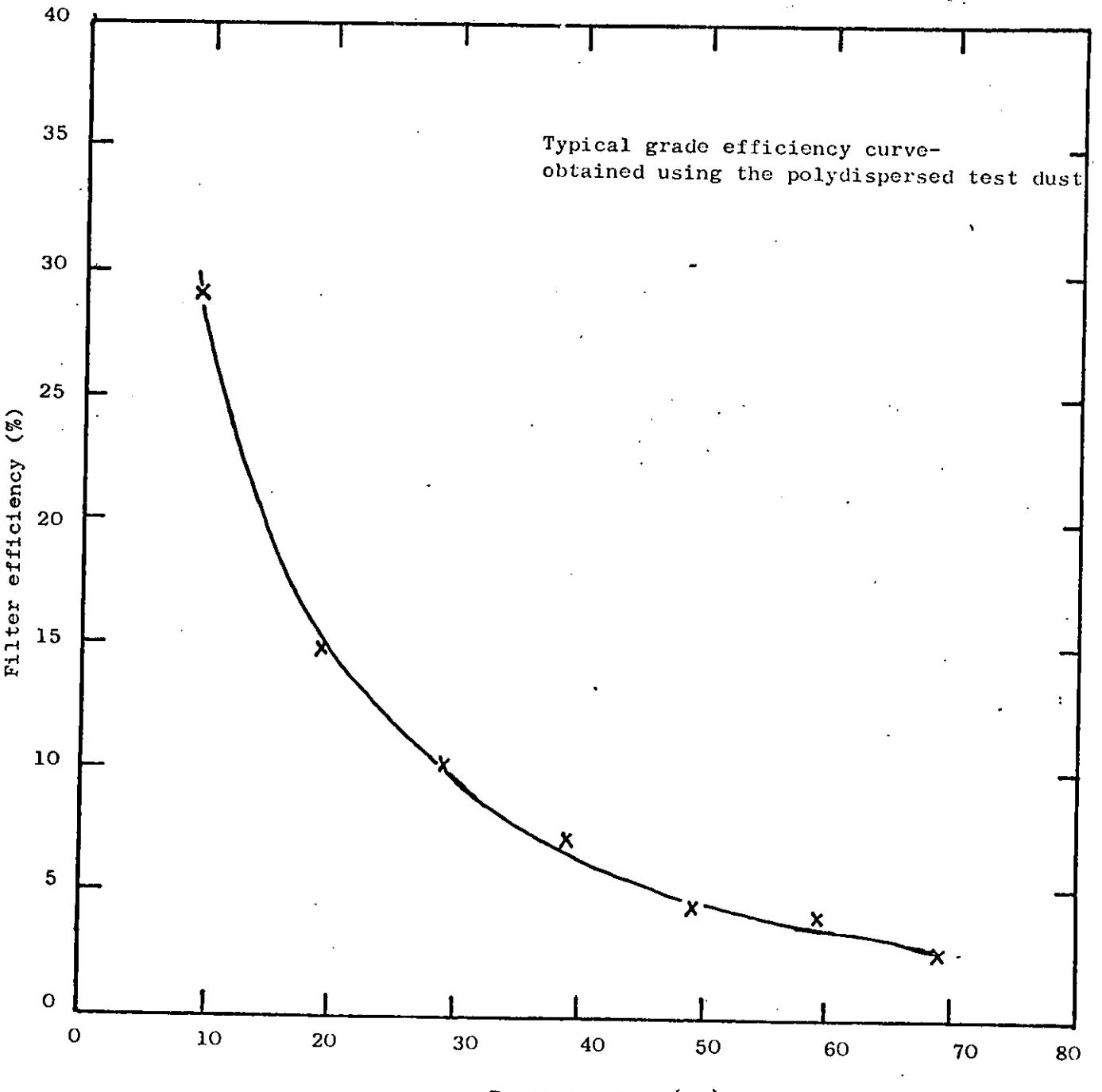
Typical grade efficiency curve-
obtained using the polydispersed test dust
Filter efficiency (%)
0
5
10
15
20
25
30
35
40
0
10
20
30
40
50
60
70
80
Particle size (μm)

Fig.4.1

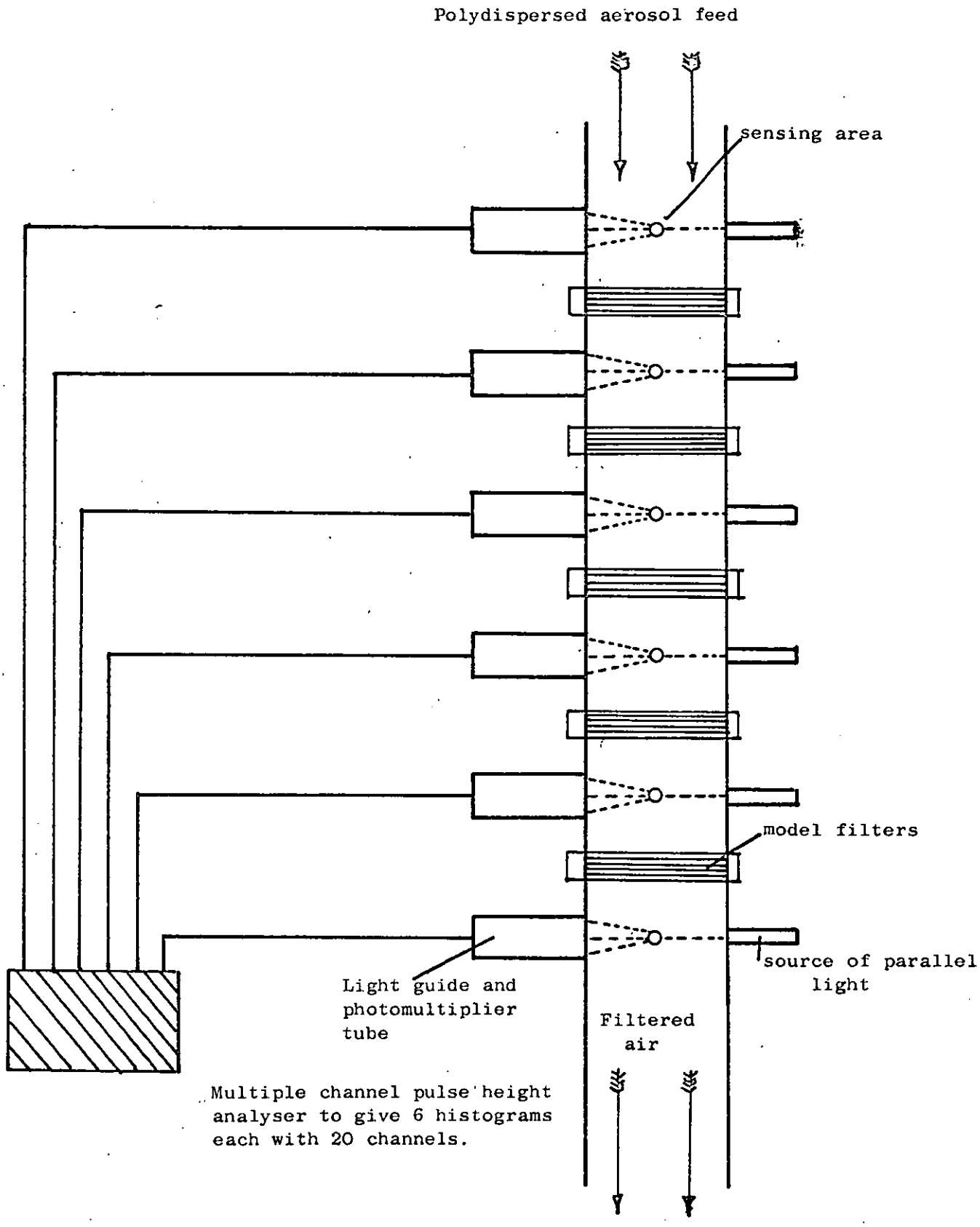

Block diagram of proposed filter test rig.

FIGURE 4.2

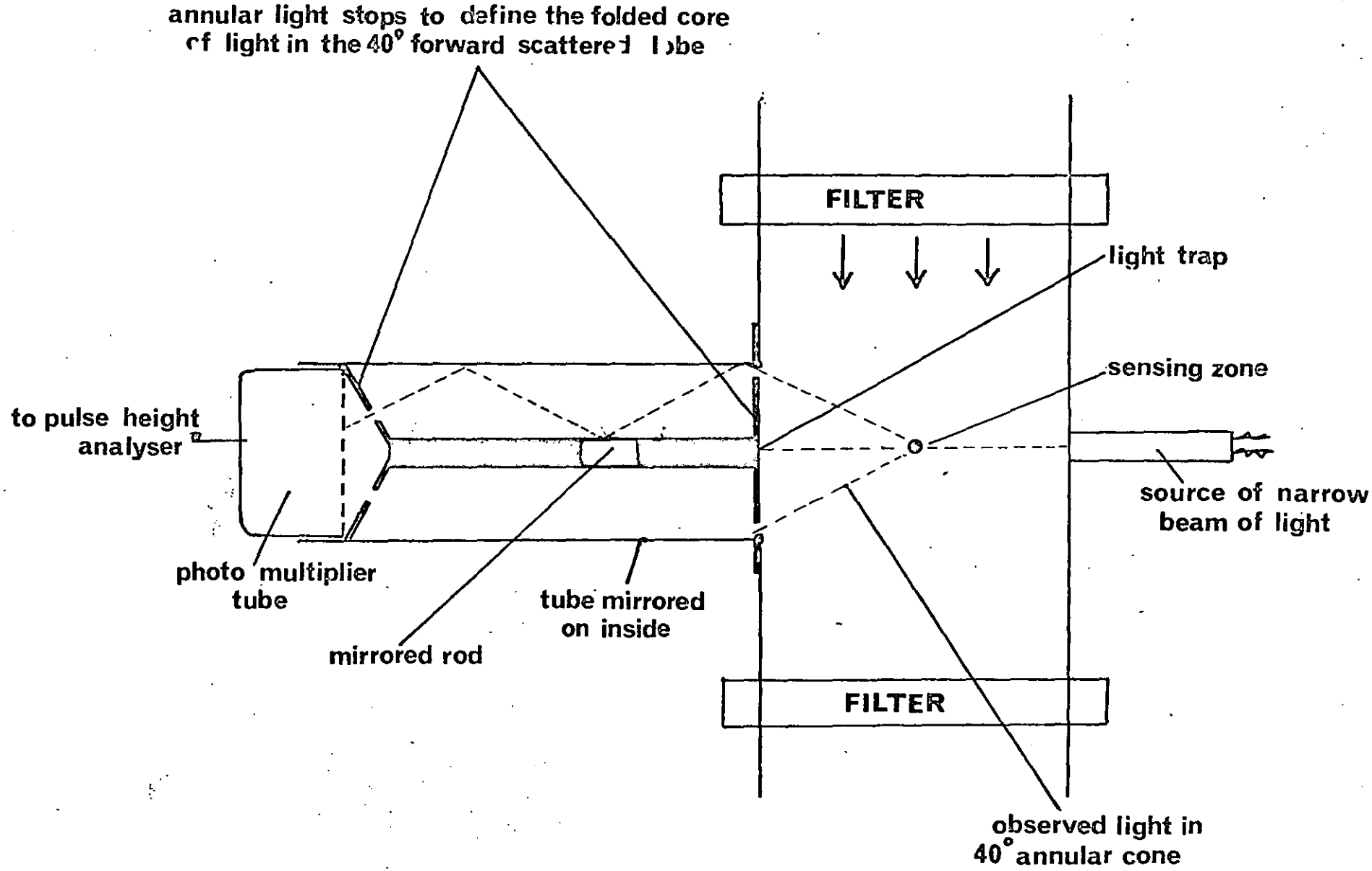

Particle detection system

Figure 4.3

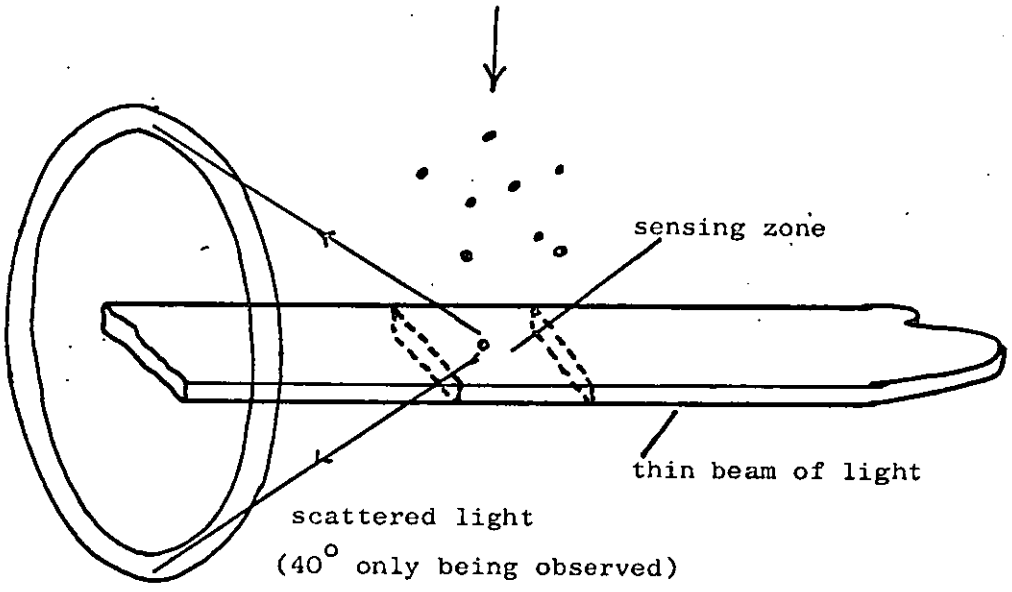

Sensing zone.

Figure 4.4

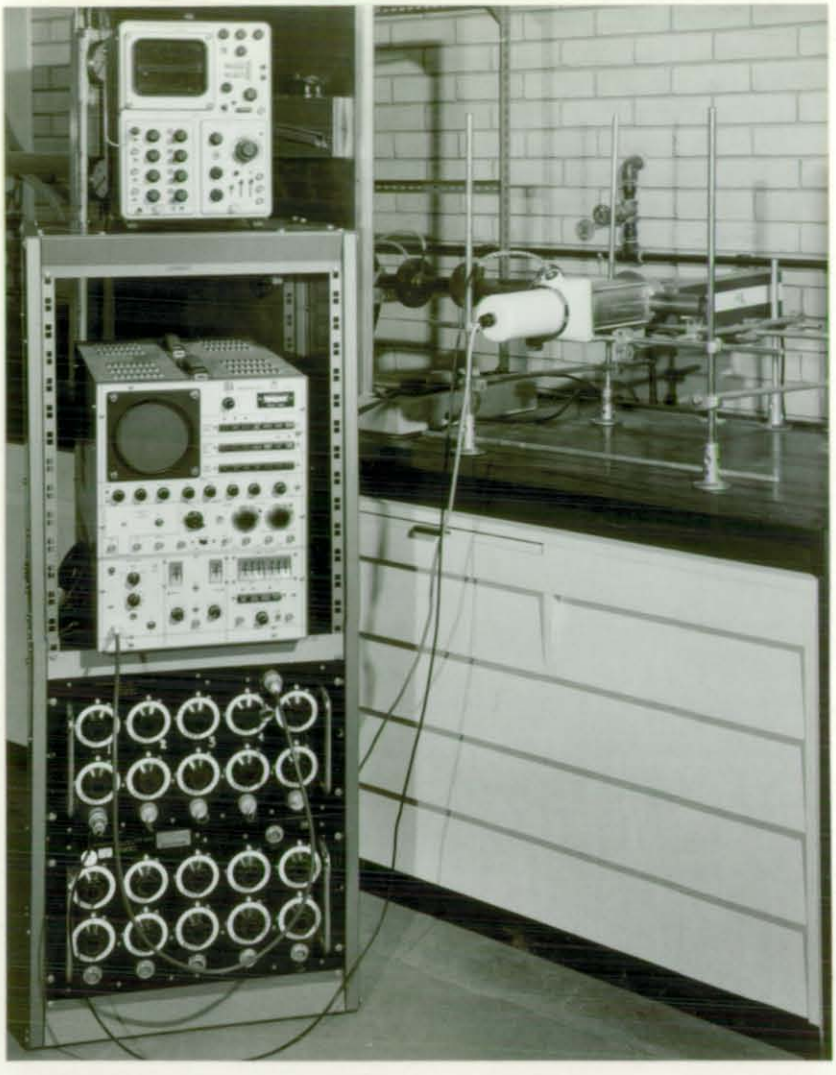

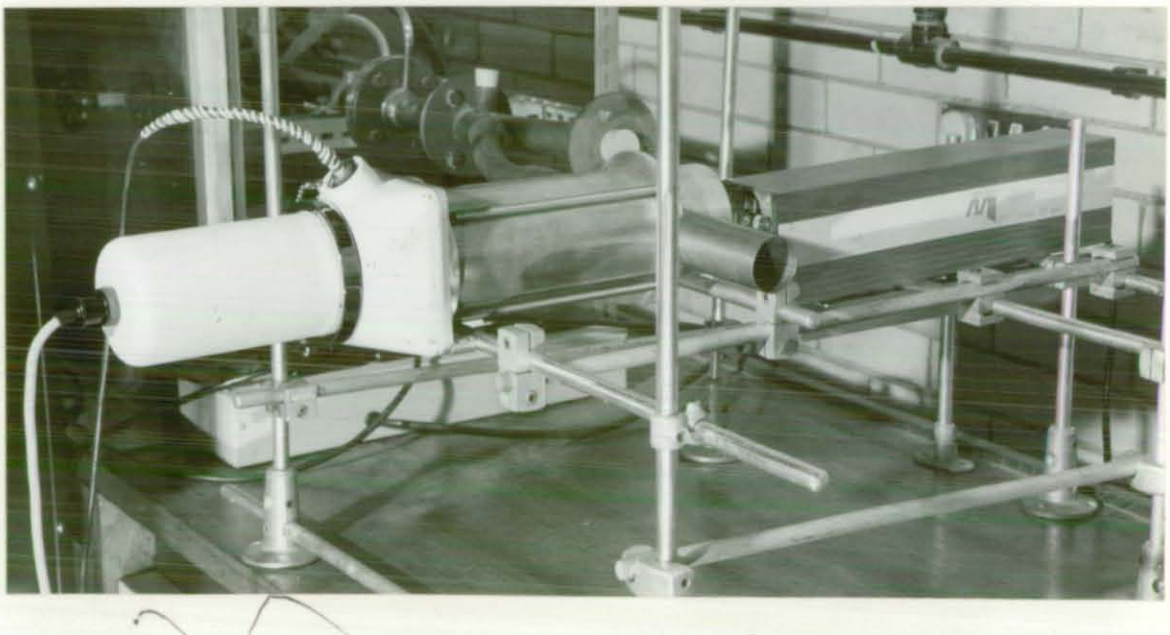

Figure 4.5 General views of light scattering device

ACKNOWLEDGMENTS

The financial assistance of the Science Research Council and the Military Vehicles Experimental Establishment is gratefully acknowledged.

Grateful acknowledgment is given to the following people without whose help this work would not have been completed.

Professor D.C. Freshwater for his help and encouragement and for providing the research facilities.

Members of staff of the Particle Technology Group of the Chemical Engineering Department for their encouragement and useful discussions.

Mr. L. Moore and his workshop staff who constructed most of the experimental apparatus.

Mrs. M. Warren who took the stereoscan photographs.

Mr. R.E. Buxton and his staff for laboratory assistance. Mr. E. Kempson conducted most of the experimental work. Mr. A.G. Perridge constructed the model filters.

Mr. I. Sinclair who is responsible for the electronics in the work described in Chapter 4.

The data used to construct figures 3.8, 3.14-16 and 4.1 were obtained by undergraduate students. The results shown in appendix 11 were obtained by T. Unwin and D. Pinder.

BIBLIOGRAPHY

1. DAVIES, C.N., "Air Filtration" Academic Press,(1973)

2. WONG, J.B., JOHNSTONE, H.F., "Collection of aerosols by fibre mats" Tech. report no.11. Engineering Experimental Station, University of Illinois, (00-1012) (1953).

3. PICH,J., Chapter in "Aerosol Science" ed. by C.N. Davies, Academic Press, (1967).

4. HARROP, J.A., Ph.D., thesis, Loughborough University of Technology (1969).

5. OSEEN,C.W., "Hydrodynamik", Leipzig, (1927).

6. LAMB,H., "Hydrodynamics", Cambridge University Press, (1932).

7. TOMOTIKA,S., AOI,T., Quart.J.Mech. and App.Maths., 3(2), 140, (1950) and 4(4), 401, (1951).

8. DAVIES,C.N., Proc.Phys.Soc., B.63, 288, (1950).

9. NATANSON,G.L., Proc.Acad.Sci., U.S.S.R. 116 (1-6), 587, (1957).

10. PROUDMAN,I., PEARSON,J.R.A., J.Fluid Mech. 2, 237, (1957).

11. KAPLUN,S., J. Mathematics and Mechanics, 6(5), 595, (1957).

12. THOM,A., Proc.Roy.Soc.(london), A141, 651, (1933).

13. KOVASZNAY,L.I.G., Proc.Camb.Phil.Soc., 44, 58, (1948).

14. TAMADA,K., FUJIKAWA,H., Quart.J.Mech.& App. Maths., 10,425, (1957).

15. MIYAGI,T., J. Phys.Soc.Japan, 13(5), 493, (1958).

16. HAPPEL, J., A.I. Chem.E.J., 5(2), 174, (1959).

17. KUWABARA,S., J. Phys.Soc.Japan, 14, 527, (1959).

18. KIRSCH,A.A., & FUCHS,N.A., J. Phys.Soc.Japan, 22(5), 1251, (1967).

19. MASLIYAH,J.H., EPSTEIN,N., Ind.Eng.Chem.Fundam., 10(2), 293, (1971).

20. BRINKMAN,H.C., Appl.Sci.Res., A1(1), 27,(1947).

21. SPIELMAN, L., GOREN,S.L., Environ.Sci.Technol., 2 279, (1968).

22. HASIMOTO, H., J.Fluid.Mech., 5, 317, (1959).

23. EINSTEIN,A., Ann.Phys., 175, 2, (1905).

24. LANGMUIR, I., O.S.R.D. Report No.865, (1949).

25. NATANSON,G.L., Proc.Acad.Sci. U.S.S.R. 112 (1-6), 100, (1957).

26. FUCHS,N.A., STECHKINA,I.B., Ann.Occ.Hyg., 6 27, (1963).

27. ZEBEL,G., J. Colloid Sci., 20(6), 522, (1965).

28. WALKENHORST, W., ZEBEL,G., Staub 24, 444, (1964).

29. WALKENHORST, W., J. Aerosol Sci. 1(3), 225, (1970).

30. KUNKEL, W.B., J. Appl. Phys., 21, 833, (1950).

31. LUNDGREN,D.A., WHITBY, I.T., Ind.Eng.Chem.Proc.Des. Dev., 4(4), 345, (1965).

32. WHITBY, I.T., PETERSON,C.M., Ind.Eng.Chem.Fund., 4(1), 66, (1965).

33. KRAEMER,H.F., JOHNSTONE, H.F., Ind.Eng.Chem., 47, 2426, (1955).

34. NATANSON,G.L., Dokl. Akad. Nank. S.S.S.R. 112, 696, (1957).

35. YOSHIOKA, N., EMI,H., HATTORI,M., TAMORI,I., 32, 815, (1968).

36. CLARENBURG,L.A., VAN DER WAL, J., Ind.Eng.Chem.Proc. Des.Dev., 5(2), 110, (1966).

37. DAVIES,C.N., PEETZ, C.V., Proc.Roy.Soc., A234, 269, (1956).

38. YOSHIOKA, N., EMI,H., FUKUSHIMA,M., Kagaku Kogaku, 31, 157, (1967).

39. LOFFLER, F., MUHR, W., Chemie Ing.Tech., 8, 510, (1972).

40. WHITBY, K.T., A.Soc.Htg. Refrig. & Air Cond.Eng.J., 7, 56, (1965).

41. CHEN,C.Y., Chem.Rev., 55, 595, (1955).

42. DORMAN, R.G., Chapter in "Aerosol Science" ed. by C.N. Davies, Academic Press, (1967).

43. DAVIES, C.N., Proc.Instn. Mech.Engrs. London 1B 185, (1952).

44. HARROP, J.A., STENHOUSE, J.I.T., Chem.Engrg.Sci., 24, 1475, (1969).

45. STENHOUSE, J.I.T., HARROP,J.A., Chem. Engrg.Sci., 25, 1113, (1970).

46. DAWSON, S.V., D.Sc. Thesis, Harvard School of Public Health, (1969).

47. STECHKINA, I.B., KIRSCH, A.A., FUCHS, N.A., Ann.Occ. Hyg. 12, 1, (1969).

48. KIMURA, N., IINOYA, K., Kagaku Kogaku, 29, 538, (1965).

49. GALLILY,I., Ph.D. Thesis, Hebrew University, Jerusalem, (1955).

50. GALLILY,I., J.Coll.Sci., 10, 588, (1955).

51. THOMAS,J.W., RIMBERG,D., MILLER, T.J., J. Aerosol Sci., 2, 31, (1971).

52. NATANSON,G.L., Kolloid. Zh., 24, 52, (1962).

53. VELICHKO,M.V., RADUSHKEVICH,L.V., Doklady Physical Chem., 154(1-6), 43, (1964).

54. PICH,J., J. Colloid & Interface Sci., 37(4), 912, (1971).

55. STERN, S.C., ZELLER, H.W., SCHEKMAN, A.I., J. Colloid Sci., 15, 546, (1960).

56. TORGESON,W.L., "General Mills" Inc. Minneapolis 13, Minnesota, (1961).

57. DORMAN R.G., "Aerodynamic Capture of Particles" Pergamon Press, (1960).

58. CLARENBURG,L.A., PIEKAAR, H.W., Chem.Eng.Sci., 23(7) 765, (1968).

59. CLARENBURG,L.A., SCHIERECK,F.C., Chem.Eng.Sci., 23(7), 773, (1968).

60. CLARENBURG,L.A., WERNER,R.M., Ind.Eng.Chem.Proc.Des. Dev., 4(3), 293, (1965).

61. PIEKAAR,H.W., CLARENBURG,L.A., Chem.Eng.Sci. 22(11), 1399, (1967).

62. PIEKAAR,H.W., CLARENBURG,L.A., Chem.Eng.Sci., 22(12), 1817, (1967).

63. WERNER, R.M., CLARENBURG, L.A., Ind.Eng.Chem.Proc.Des. & Dev. 4(3), 288, (1965).

64. SAFFMAN, P.G., J. Fluid Mech. 22(2), 385, (1965) and ibid 31(3), 624 ( ).

65. EVANS, G.W., Ph.D. Thesis, University of Oxford, (1971).

66. HAPPEL, J., BRENNER,H., "Low Reynolds Number Hydrodynamics", Prentice-Hall, (1965).

67. HERDAN,G., "Small Particle Statistics", Butterworth Scientific Publications, (1960).

68. CORTE,H., Filtration & Separation, 3, 396, (1966).

69. SHIRATO, M., SHIMIZU,S., KAKIZOE,M., Kagaku Kogaku, 31(1), 60, (1967).

70. FUCHS, N.A., KIRSCH, A.A., Ann.Occ.Hyg.10, 23, (1967).

71. KIMURA,N., IINOYZ, K., Kagaku Kogaku 23(12), 792 (1959).

72. BECKER,F., STAUB, 23, 60, (1963).

73. LOFFLER,F., Ph.D. Thesis, University of Karlsruhe,(1965).

74. DAVIES,C.N., Paper presented to symposium on "Filtration in Medical Health Engineering", Filtration Soc. London, (1969).

75. GILLESPIE,T., J. Coll.Sci., 10, 266, (1955).

76. STENHOUSE, J.I.T., Paper presented to meeting of Filtration Soc., London, Dec. (1970), Filtration and Separation.

77. FRESHWATER,D.C., STENHOUSE,J.I.T., Am.Inst., Chem. Engrs.J.

78. LOFFLER,F., STAUB, 31,(2), 51, (1971).

79. DAHNEKE, B., J. Colloid & Interface Sci., 37, (2), 342, (1972).

80. JORDAN, D.W., Brit.J. of Appl. Phys. S194, (1954).

81. LARSEN,R., Am.Ind.Hygiene Assoc. Journal,19, 265, (1958).

82. VIDAL, R.J., J. Aerospace Sci., 1067, (1962).

83. CORN, M., & SILVERMAN, L., Ind.Hyg. Journal, 337,Oct.(1961).

84. GOLDSMITH, W., "Impact : The Theory and Physical Behaviour of Colliding Solids" Arnold (1960).

85. HERTZ, H., J. reine n. augen, 92 (1881).

86. MATSUMOTO, S., SAITO, S., J. of Chem. Eng. of Japan, 3, No. 1, 83 (1970).

87. MUSCHELKNAUTZ, E., FORSCHUNGSHEFT, V.D.I., 476, 18,(1959).

88. RUMPF, H., PROFESSOR DR. ING., Norman Swindin Memorial Lecture, Loughborough University of Technology, (1969).

89. CORN,M., Chapter in 'Aerosol Science' ed. byC.N. Davies, pub. by Pergamon Press Ltd., (1964).

90. ZIMON, A.D., 'Adhesion of Dust and Powder', by Plenum Press, New York-London (1969) translated by M. Corn.

91. HAMAKER, H.C., Physica 4, 1058, (1937).

92. BRADLEY, R.S., Trans. Faraday Soc. 32, 1088, (1936).

93. GREGORY, J., Advan. Colloid Interface Sci., 2, 396,(1969).

94. LIFSHITZ, E.M., J. Exp. Theor. Phys., U.S.S.R., 29, 94, Translation as 'Soviet Physics' J.E.T.P. (1956), 2, 73, (1955) (see also refce.99).

95. TABOR, D., WINTERTON, R.H.S., Proc. Roy. Soc. A312, 435, (1969).

96. LANGBEIN, D., 'Physics of Adhesion', Proc. of Conf. on Adhesion edited by Polke and Hohn p.55 (1969).

97. KRUPP, H., Adv. Colloid InterfaceSci. I, 111-239 (1969).

98. MULHEARN,T.O., TABER,D., J. Inst. Metals 89,7, (1960/1).

99. DERYAGIN,B.V., FIZ KHIM, ZH., 6(10), 1306, (1939).

100. SPERLING,G., DR.ING., Dissertation, Technischen Hochschule, Karlsruhe, (1964).

101. POLKE, "Physics of Adhesion" Proc. Of Conference on Adhesion edited by Polke and Hohn (1969).

102. CHO,A.Y.H., J. Appl. Phys. 35, (1964), 2561.

103. DEFAY,R., PROGIGINE,I., Surface Tension and Adsorption, Longmans (1951).

104. MCFARLANE,J.S., TABOR,D., Proc.Roy.Soc., A202, 224, (1950).

105. KORDECKI,M.C., ORR,C., A.M.A. Arch.Env.Hlth., I, (1960).

106. BOWDEN,F.P., TABOR,D., Proc.Roy.Soc.A169, 391, (1939).

107. TOPPER,J., Ph.D. Thesis, Loughborough University of Technology, (1971).

108. LESCHONSKI,K., Private communication.

109. CROSS,N.L., PICKNETT,R.G., p.383, Conf. on "The Mechanism of Corrosion by Fuel Impurities" - Southampton, May 1963.

110. FUCHES, N.A., "The Physics of Aerosols", Pergamon Press (1964).

111. STENHOUSE,J.I.T., HARROP, J.A., FRESHWATER, D.C., J. of Aerosol Sci., 1, 41, (1970).

112. FUCHES,N.A., STECHKINA, I.B., Am.Occ.Hyg., 6, 27,(1963).

113. RADUSHKEVICH,L.V., KOLGANOV,V.A., Kolloid Zh 27(1), 95, (1965).

114. BOTTERILL, J.S.M. AND AYNSLEY,E., Br.Chem.Engng., 12(10), 1593, (1967)., and ibid., 12(12), 1893, (1967).

115. WALKENHORST, W., Staub-Reinhalt, 32,(6),30, (1972).

116. RADUSHKEVICH, L.V., Bull.Acad. Sci. USSR (3), 367,(1963).

117. LA MER,V.K., DROZIN,V.G., Proc.Second Int.Congress of Surface Activity,111, London, Butterworth 600, (1957).

118. YOSHIOKA,N., SATO,H., Kagaku Kogaku 33, 1013, (1969).

119. RADUSHKEVICH,L.V., Colloid J. USSR 26(2) 194, (1964).

120. YOSHIOKA,N., EMI,H., YASUNAMI,M., Kagaku Kogaku Chem. Eng., Japan, 33(10), 1013, (1969).

121. BLASEWITZ,A.G., et al; Hanford Works, AEC Report, HW-20847,(1951).

122. NITTA,KO., YOSHIKAWA,A., Research Report of Japan Cotton Tech. Inst., No.29 (1958).

123 DAVIES,C.N., J. Aerosol Sci. 1, 35, (1970).

124. KIMURA N & IINOYA K., Kagaku Kogaku 2(2), 136, (1964).

125. JUDA J. & CHROSCIEL S., Staub-Reinhalt Luft 30(5) 196,(1970)

126. LAPPLE, C.E., STASNY, R.J., SRIGHT, T.E., Tech.Report 55-457. Wright-Patterson Air Force Base, Ohio, A.S.T.I.A. Doc.No. AD-142075 (1957).

127. KIMURA,N., FUKUHIRO H., IINOYA,K., Kagaku Kogaku 9(8), 622,(1965).

128. HERZIG,J.P., LECLERC,D.M., P.LEGOFF., "Flow of Suspensions through Porous Media -Application to Deep Filtration". 6th State of the Art Symposium, sponsored by the Ind. and Engng. Chem. and the Divn of Ind. and Engng. Chem. of the Am.Chem.Soc. Washington D.C., June,(1969).

129. GOREN, S.L., O'NEILL,M.E., Chem.Eng.Sci., 26,325, (1971).

130. Standard ASHREA dust test "Method of testing air cleaning devices used in general ventilation for removing particulate matter". Am.Soc. of Heating, Refrigerating and Air-Conditioning Engrs.Inc.

APPENDIX I

Alternative derivation of Equation 1.57

The average volumetric efficiency, $\bar{\lambda}_s$, the fraction of particles removed per unit volume of filter, can be related to the average single fibre efficiency, $\bar{\eta}_s$, using equation 1.52 as follows:-

$$-\frac{dc}{c} = \frac{2\bar{\eta}\bar{\alpha}\,dL}{\pi r_f (1-\bar{\alpha})} = \bar{\lambda}_s\,dL$$

$$\text{so,} \quad \bar{\eta}_s = \frac{\pi r_f (1-\bar{\alpha})\bar{\lambda}_s}{2\bar{\alpha}}; \qquad \eta_s = \frac{\pi r_f (1-\alpha)\lambda_s}{2\alpha} \qquad \text{(i)}$$

Considering a volume V of filter and inlet dust concentration, c, then the particles collected in unit time is given by:-

$$\int_V \lambda c (1-\alpha) U_o \, dV$$

The total particles available for collection in volume V of the filter is

$$c \bar{U}_o V (1-\alpha)$$

Hence

$$\bar{\lambda} = \frac{\int_V (1-\alpha)\lambda c U_o \, dV}{c \bar{U}_o V (1-\bar{\alpha})} = \frac{\int_0^1 (1-\alpha) c U_o V . V(\alpha)\, d\alpha}{c \bar{U}_o V (1-\alpha)} \qquad \text{(ii)}$$

It follows from (i) and (ii) that

$$\bar{\eta}_s = \frac{1}{\bar{\alpha}\bar{U}_o}\int_0^1 \alpha \eta_s U_o V(\alpha)\, d\alpha \qquad 1.57$$

APPENDIX II

Determination of Filtration Efficiency using Coulter and Sodium Flame Techniques

The Coulter technique described in section 4.4 was used to determine the grade efficiency of a knitmesh filter (d_f = 145μm) over a range of velocities. About 0.2 gm AC dust was fed to the filter in each case. The particle size range studied was 3 - 17μm diameter. To obtain a sufficiently reproducible Coulter count it was necessary to perform the analysis in a Faraday cage. The high reproducibility of the method is shown in fig. (i) where two individual runs, each performed at a velocity of 1.2ms^{-1}, are compared. The results are shown in fig. (ii).

The knitmesh filter was thoroughly washed in carbon tetrachloride to remove traces of oil or grease from the fibre surface before use. The grade efficiency curves of "dry" knitmesh filters shown in references 76 and 77 show maxima at much higher particle sizes than shown here. These filters were not washed in carbon tetrachloride and new knitmesh was used for each test - the presence of a small amount of grease on the surface caused an increase in the adhesion forces.

The sodium flame technique as described in references 4 and 111 was used to measure the efficiency of model filters over a range of particle sizes and velocities. A diagram of the rig is shown in fig.(iii). A mono dispersed aerosol of sodium chloride particles (geometric standard deviation = 1.15) is produced using a spinning top genarator and the efficiency of removal of these particles determined using flame photometry. The stability of the galvanometer was increased by including a large capacitance in

the circuit. This enables the range of variables to be increased to 1.4 ms^{-1} velocity and 5.5μm particle diameter. To ensure that a maximum was observed grids constructed of small (25μm diameter) stainless steel fibres were used in the model filter. Each of the 9 grids had a packing density of 0.03 and was cleaned with carbon tetrachloride frequently. The relative humidity was in the range 35-40%. The results of tests with 3 particle sizes are shown in figure iv. A maximum in the efficiency curve was not observed when larger fibres (50μm and 100μm) were used in the test. The positions of the maxima found in figure (iv) are compared with other values in figure (v).

The values of d_{pcrit} shown in fig. (v) are much higher than any theoretical predictions. The order of magnitude of the results is in agreement with the findings of Harrop and Loffler, however, the results reported here for sodium chloride particles indicate higher values of d_{pcrit} than reported by Harrop. A maximum could not be found in curves obtained using 50μm and 100μm fibre model filters. The reason for this discrepancy is not known.

Several factors may be responsible for the discrepancy between theoretical and experimental values of d_{pcrit}. The calculation of contact area during oblique impact may be widely in error, the adhesion force may be significantly increased due to surface moisture, impact will be much more complex than that imagined using the simple model (rolling may occur or multiple contact between the particle and already deposited particles).

The experimental results agree with the predicted relationship between d_{pcrit} and U_o.

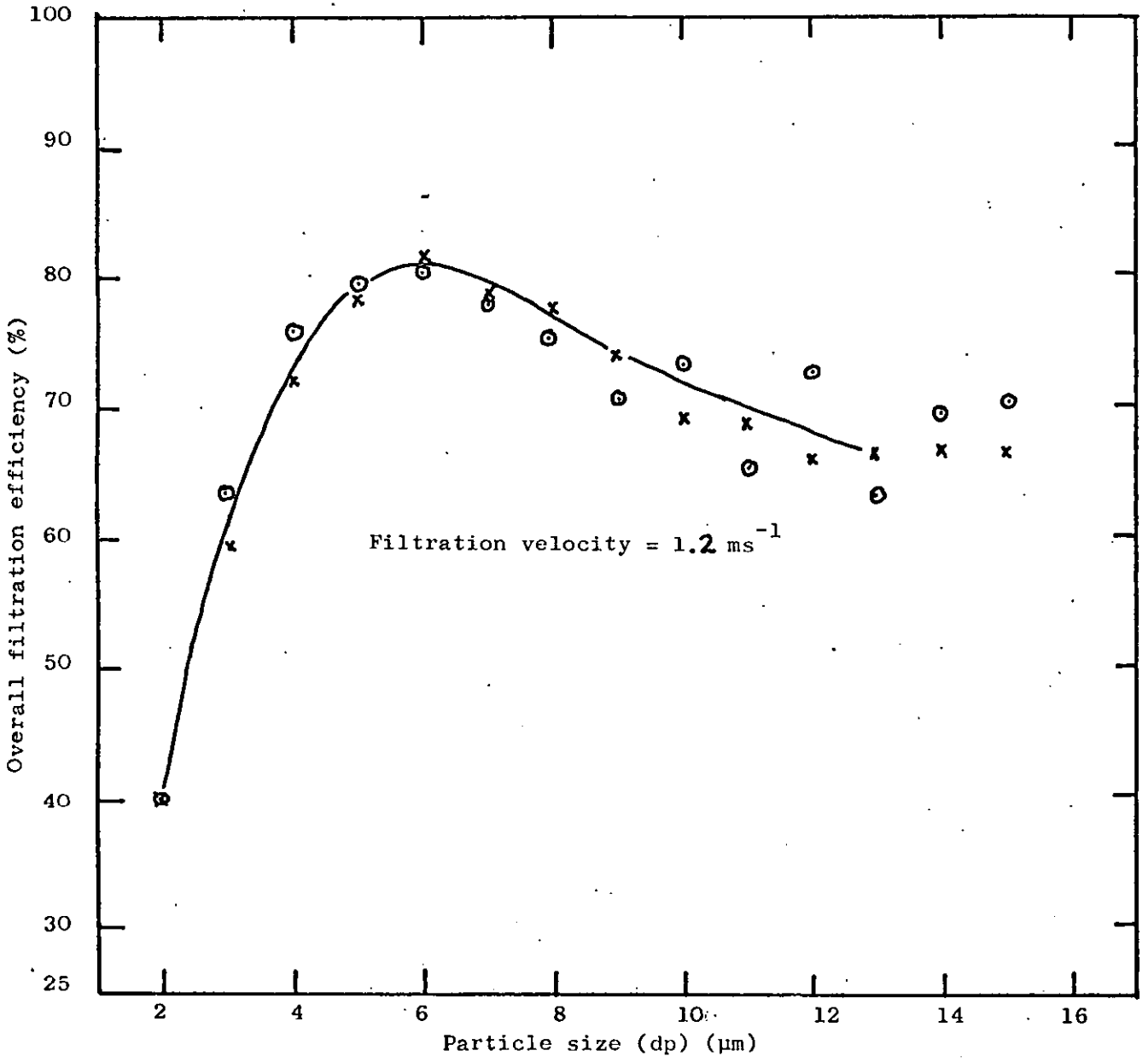

Fig. (i) Filtration of AC dust by knitmesh filter (df = 145 μm) - reproducibility test.

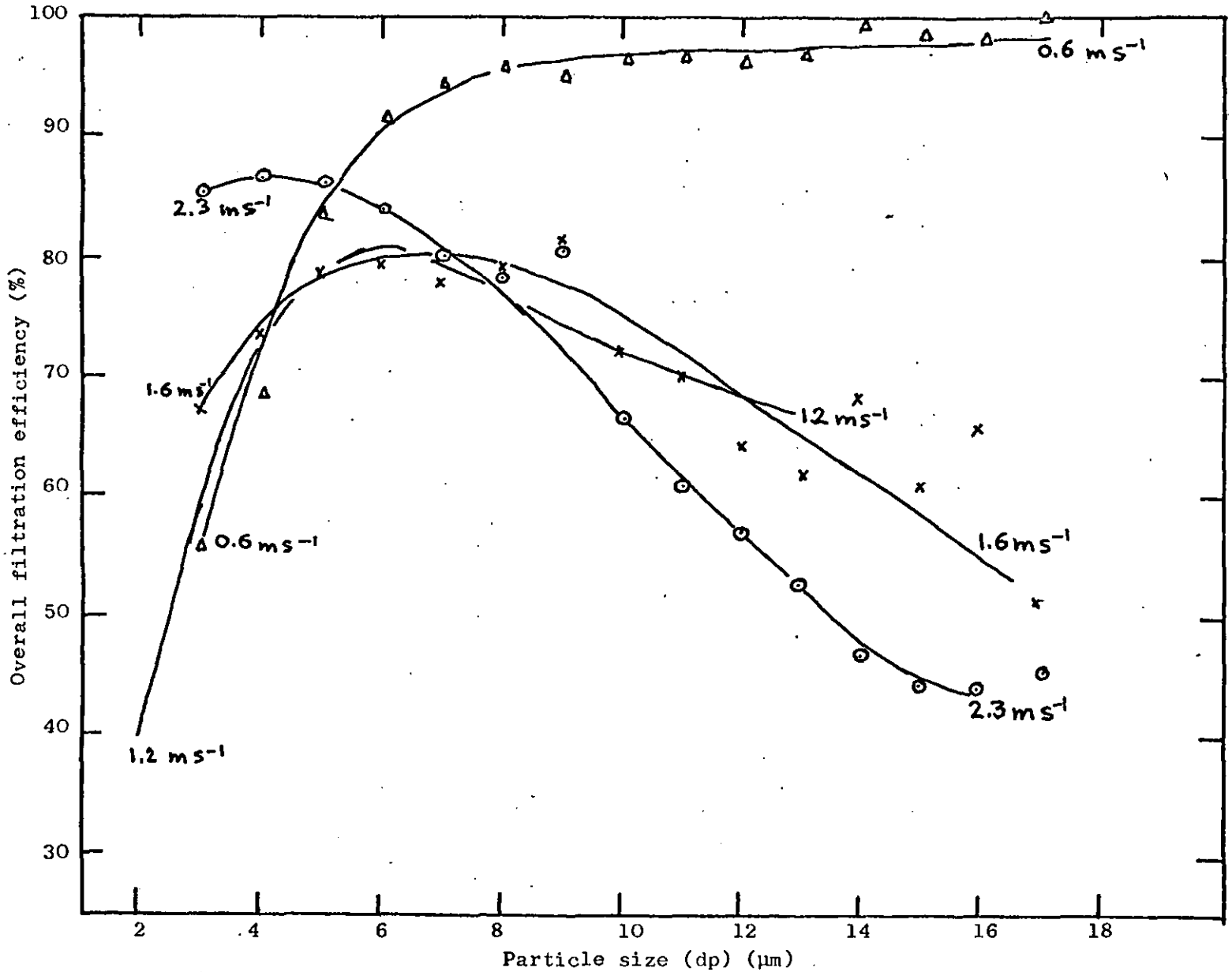

Figure (ii) Filtration of AC dust by knitmesh filter (df=145µm) - influence of filtration velocity.

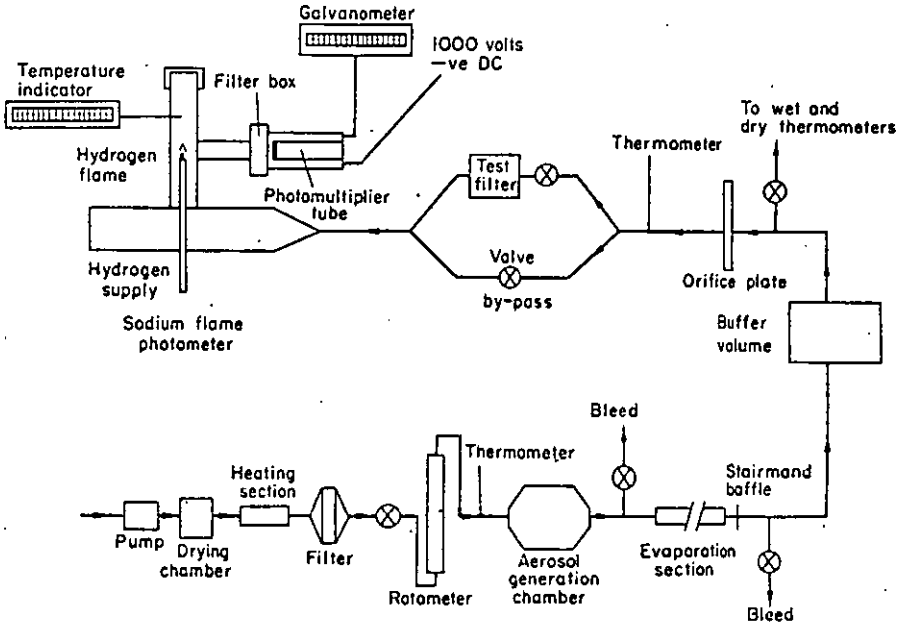

FIG. iii Experimental apparatus.

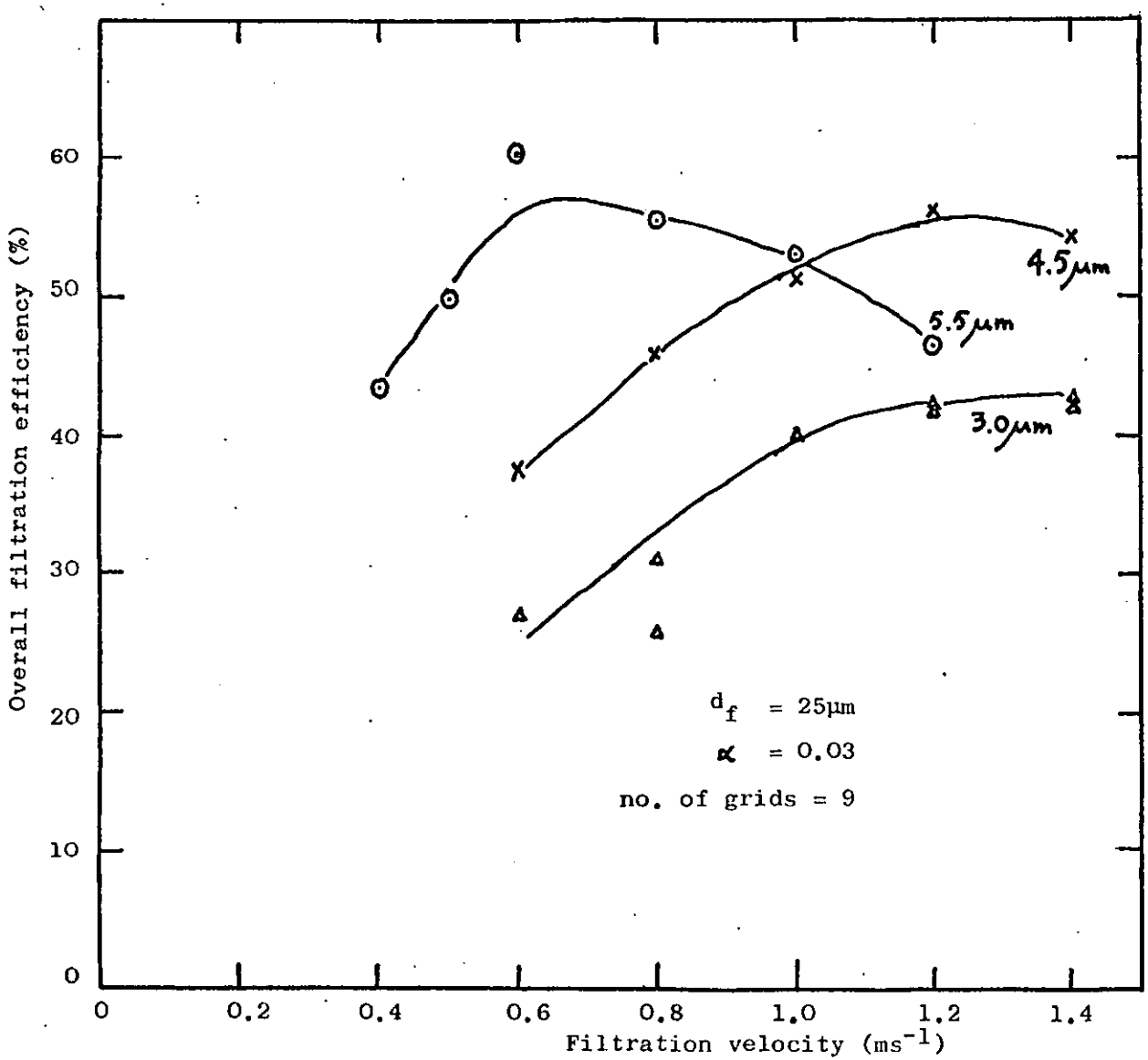

Figure (iv) Efficiency of collection of monosized salt particles on model filters.

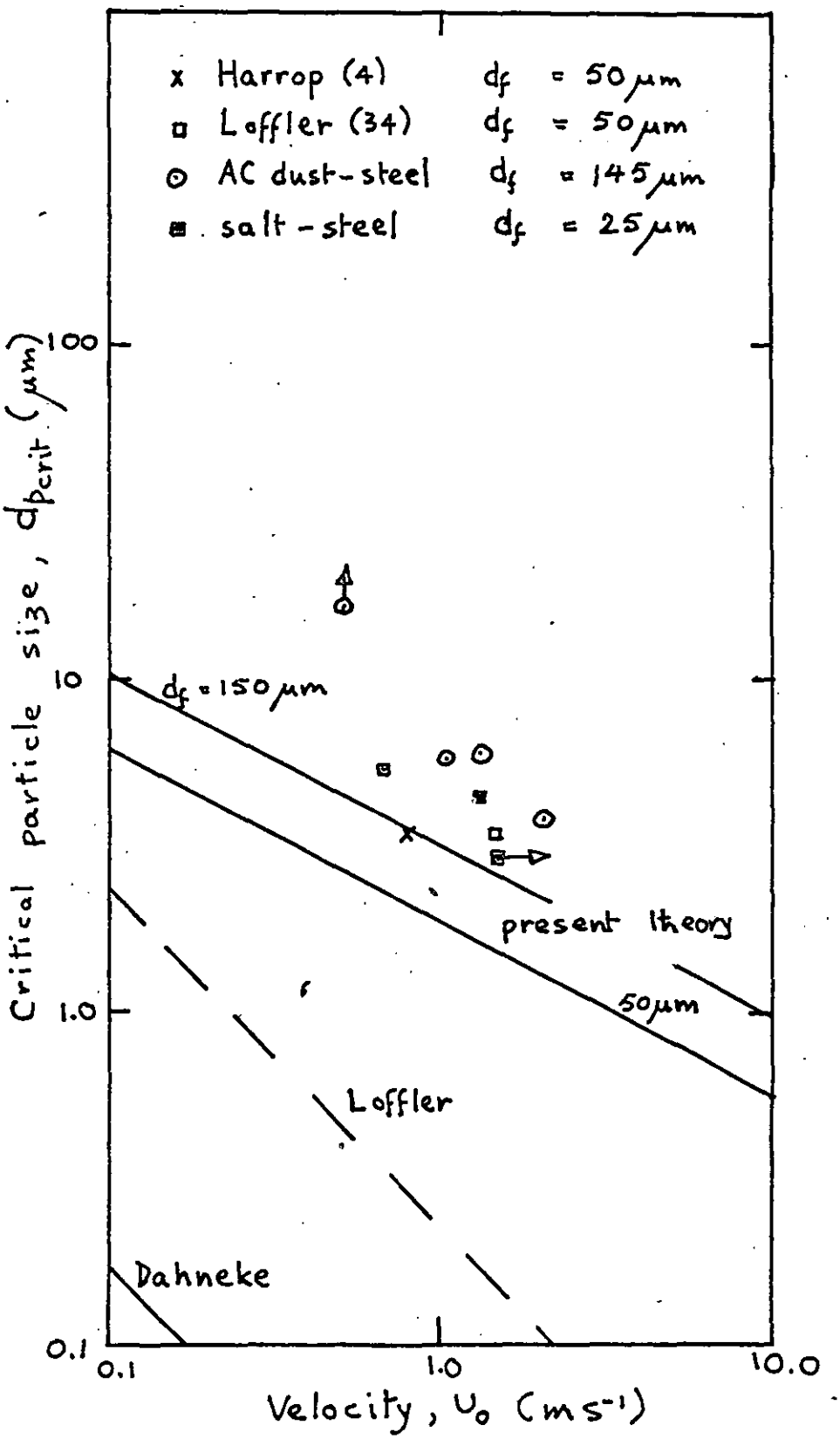

Figure (V) Critical particle size

comparison of theory and experiment